Title
Determination of p-y Curves by Direct Use of Cone Penetration Test (CPT) Data

Author
ARIANNIA, SHAWN SHAHRIAR

Publication Date
2015

Peer reviewed|Thesis/dissertation

UNIVERSITY OF CALIFORNIA

Los Angeles

Determination of *p-y* Curves by Direct Use of Cone Penetration Test (CPT) Data

A dissertation submitted in partial satisfaction of the requirement

for the degree Doctor of Philosophy

in Civil Engineering

By

Shawn S. Ariannia

2015

ABSTRACT OF THE DISSERTATION

The current best practice in geotechnical engineering in determining lateral capacity of piles is to replace the soil reaction with a series of independent springs. Basically, the model uses beam theory to represent the pile and uncoupled, non-linear load transfer functions, called *p-y* curves to represent the soil.

Most of the existing methods for determining *p-y* curves are highly empirical, based on a limited number of cases of laterally loaded piles, which were instrumented, enabling to measure the pile deflection in discrete depth intervals subject to different lateral load (i.e. Matlock 1970, Reese 1975). In essence, these methods have their own limitations, and are mainly applicable for the conditions similar to the tested conditions.

Although later, more detailed investigations by different people addressed some of the problems, still the basis of the existing design programs such as LPILE, or procedures introduced in applicable codes such as API (American Petroleum Institute), is the same original recommendations made by Matlock and Reese during seventies.

In recent era, demand in employment of in-situ direct-pushed based methods using multi-measurement in-situ devices, such as the seismic cone penetration test with pore water measurement (SCPTu) and Seismic Flat Dilatometer Test (SDMT) is significantly increased.

The main objective of this research is to introduce a unified CPT-based approach for determining *p-y* curves and pile responses to lateral loads. The suggested approach will provide explicit and defined steps/criteria to develop *p-y* curves for piles subjected to lateral loads using CPT data. CPT data will be used to determine soil strength parameters. Recent developments in relating

CPT data to soil basic parameters using Critical State Soil Mechanics (CSSM) framework will be implemented in the suggested model.

In all current common models, pre-determination of the soil behavior and the model to be used (e.g. Matlock clay, 1970 or Reese sand, 1975), will become warranted even before commencement of the analysis. On the contrary, in the proposed model, the need for the said pre-determination of soil behavior is eliminated. As discussed in Section 2.3.5, soil behavior in the model is being classified into four broad and general groups: drained-dilative, drained-contractive, undrained-dilative and undrained-contractive

The main factor driving the suggested analytical approach is Soil Behavior Type Index, I_c. In the proposed approach, the SBT index, I_c, will be used to determine the in-situ characteristics and behavior of the soil. Based on the value of I_c calculated from CPT data, it could be determined that the soil behaves as a sand-like or a clay-like soil, and during the shearing would behave in undrained or drained condition. The measured shear wave velocity during field test using seismic cone penetration test or other methods such as SASW (Spectral Analysis of Surface Waves) or Cross-Hole logging, may be used to determine the small strain shear modulus, G_0, which corresponds to the initial stiffness of the linear part of the *p-y* curve.

In this research, the proposed model will be verified using collected case histories of laterally loaded piles with available CPT data at the same site. The *p-y* curves, and pile force-head displacements determined from the model will be compared to the field-resulted *p-y* curves and pile head displacement measurements available from the case histories.

The dissertation of Shawn S. Ariannia is approved.

Anne Lemnitzer

Jonathan P. Stewart

Ertugrul Taciroglu

Scott J. Brandenberg, Committe Chair

University of California, Los Angeles

2015

TABLE OF CONTENTS

ACKNOWLEDGEMENTS

During past five years, I have had the privilege of working with Professor Brandenberg, who taught me how to think and research, and always stay patient and determined. I not only learned technical approaches and topics during my working years with Professor Brandenberg, but also I learned how to look at the technical tasks from different angels. Professor Brandenberg showed me the way and helped me in achieving one of the largest lifetime goals I had. I admire him and am grateful of him for the rest of my life.

VITA

1982	Bachelor Degree in Civil Engineering Tehran University, Tehran, Iran
1984	Master Degree in Civil Engineering Tehran University, Tehran, Iran

1. Introduction

1.1. General

Site-specific soil investigations are required for the analysis and design of all major projects such as multi-story buildings foundations, highway bridge foundations, embankments, retaining walls, slopes, excavations, and pavements. A sound site-specific investigative program should include a reasonable combination of field exploration, field testing and laboratory testing. The optimal point of the balance of each component is widely dependent on the judgment and experience of the geotechnical engineer in charge of the project, the structure type and importance, budget limitations and other constraints applicable to the project.

In the majority of geotechnical engineering projects, a complete set of essential properties and engineering parameters of the soil materials is never well known with a high degree of accuracy or reliability. This is because of the natural variability of geomaterials, as well as other limitations imposed on the projects such as the budget constraints restricting the numbers of field borings, laboratory tests and undisturbed samples that can be obtained on a project. Furthermore, extensive series of laboratory tests are required for the discrete determination of selected parameters, at great expense for high-quality sampling, specimen preparation, and long test durations.

Sampling and testing an adequate number of "undisturbed" samples to fully characterize a site is not feasible, so in-situ tests must also be utilized to provide the stratification and quick assessment of soil properties during the site exploration. This is not to express that laboratory testing is in competition with field testing, but that the two are actually complementary to each other. There are some basic differences that necessitate both laboratory and field testing. In the laboratory, we can fully control boundary conditions, strain rates, and drainage conditions to

measure specific engineering properties of the soil, but we must account for the effects of unavoidable sample disturbance. On the other hand, in-situ testing offers immediate (in the case of cone penetration testing) profiling of the subsurface materials and some good preliminary evaluations of soil strength properties, but engineering properties must be correlated with penetration resistance measurements and drainage conditions cannot be carefully controlled during an in-situ test. In-situ properties can be used immediately by the engineer and for the purpose of preliminary design.

Some engineers in practice unfortunately rely solely on soil test borings and Standard Penetration Test (SPT) blow counts to provide almost all of the necessary geotechnical data for their evaluations and analyses, and possibly they supplement these data with a few laboratory tests. Furthermore, common practice in southern California is to utilize non-standard samplers, such as the modified California sampler, which provides an erroneous blow count (since the sampler is a different size from the standard penetration test sampler) and a highly disturbed sample (since the sampler is a thick-walled split spoon sampler that is driven with a hammer). Nevertheless, southern California geotechnical engineers often rely upon both blow counts and laboratory tests from modified California samples. Reliance on SPT measurements alone, even when performed correctly, is problematic as stated by Mayne (2000):"it is quite unrealistic to believe that the one-number from the standard penetration test (SPT), i.e. the blow count, can provide all of the adequate and reliable information for analysis." Figure 1 depicts the skeptical wish-list thinking and over-reliance on SPT measurements in the state-of-practice. Essentially a single N-value obtained using ASTM D-1586 guidelines (or using non-standard samplers that violate ASTM D-1586), and possibly is corrected to 60 percent energy efficiency (ASTM D-4633) (note that energy measurements are rarely made, in which case energy corrections are

based on hammer type), is often utilized via empirical correlations to determine a number of geotechnical parameters.

Another problem is that the sampling interval for SPT blow counts is often from 3 to 5 feet or more, which can be too large to identify important geologic features such as thin compressible layers. The over-reliance on the SPT-N value therefore often results in mischaracterization of site stratigraphy and soil properties, which can be either uneconomical or unsafe/under-conservative for design of foundations, slopes, and other geotechnical works. More sophisticated computer software (finite difference, discrete element, and finite elements) that is becoming more commonly used in design demands higher quality input parameters. While the standard penetration test will remain an important feature of geotechnical site investigations, other in-situ tests may provide important independent information that can significantly improve site characterization.

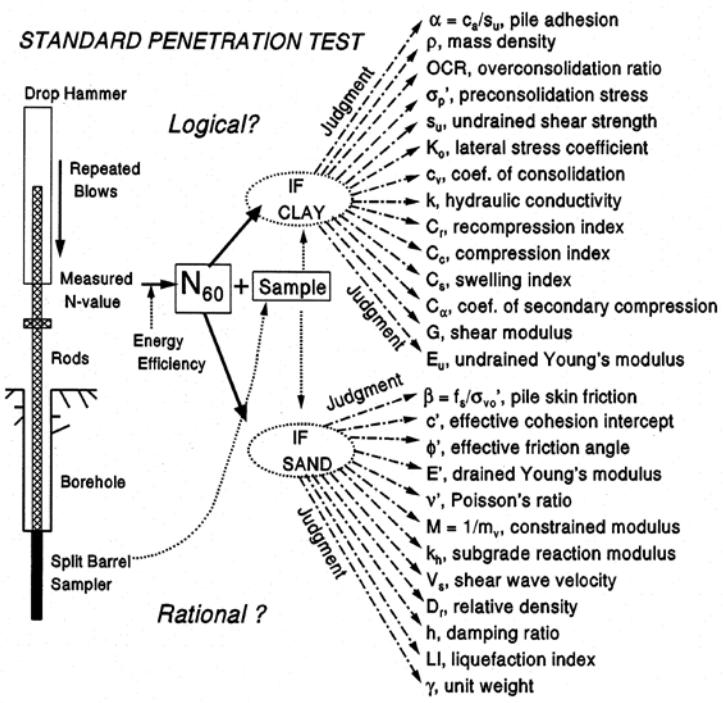

Figure 1.1: *Over Reliance on SPT-N Values for Interpretation of Geotechnical Parameters (Mayne, 2000)*

During the recent decades and as a complement to (or in some cases, as a replacement for) soil borings with SPT *N*-values, the Cone Penetration Test (CPT) has been vastly used. The CPT provides a continuous profile of the substrata, rather than a discrete set of information, which helps to better define the interface between layers, thicknesses, and relative consistencies of each stratum. The CPT is a quick, cost effective way of determining very useful information about the site soil profile. In recent years, creating of reliable correlations between the results of CPT sounding and soils characteristic and strength parameters has been a focal point of research studies. Some recent developments are direct application of CPT sounding into the design of foundations and piles under axial loads, which the behavior of the latter is somehow analogous to the pushing of the cone and the utilized resistance thereto. Several methods of determining pile axial capacity using CPT soundings have been developed by different researchers. In past decade some researches have been focused on centrifuge modeling and determining of pile lateral

capacity using CPT data and the CPT sounding was performed in centrifuge set up by smaller cones such as 6mm diameter cones. However, and to the best of my awareness, evaluation of the lateral capacity of piles by direct implementation of CPT data, which is the focal point of this research, is not yet being addressed and discussed by others.

1.2. Cone Penetration Test; History and Introduction

The cone penetration test (CPT) is a method used to determine the geotechnical engineering properties of soils and delineating soil stratigraphy. This method was initially developed in the 1950s at the Dutch Laboratory for Soil Mechanics in Delft to investigate soft soils. Therefore and based on this history it has also been called the "Dutch cone test". Today, the CPT is one of the most frequent used and accepted in-situ soil testing methods for soil investigation worldwide.

The early application of CPT was mainly to determine the bearing capacity of the soil. The first Dutch cone penetrometer tests were made in 1932 in Holland. The original cone penetrometers involved simple mechanical measurements of the total penetration resistance to pushing a tool with a conical tip into the soil. Different methods were employed to separate the total measured resistance into components generated by the conical tip (the "tip friction") and friction generated by the rod string. A friction sleeve was added to quantify this component of the friction and aid in determining soil cohesive strength in the 1960s. Although mechanical cone penetrometers go back to more than a half century ago, still they are being used. Electronic measurements began in 1948 and were improved further in the early 1970s. In electric cones, the signals are transmitted to the ground surface through an installed cable inside the hollow rod. The main difference between mechanical and electric cone is that by using electric cones possible error due to friction between inner rod and outer tube is eliminated, and a more continuous testing with more reliable electrical measurements become possible. In this type of cones, very sensitive load cells can be

used that result in more accurate readings. Most modern electric CPT cones now also employ a pressure transducer with a filter to gather pore water pressure data. During the 1970's, Schmertmann was the first person to recognize the importance of pore water pressure measurement for the interpretation of CPT data, especially in saturated clays. The pore water pressure filter can be located on the cone tip (the so-called u_1 position), immediately behind the cone tip (the most common u_2 position) or behind the friction sleeve (u_3 position), as depicted on Figure 1.3. Porewater pressure data aids determining stratigraphy and is used to correct tip resistance and friction values. CPT testing which also gathers this piezometer data is called CPTu testing. The modern version of seismic cone was developed at the University of British Columbia (Robertson, 1986).

The test method consists of pushing an instrumented cone, with the tip facing down, into the ground at a controlled rate between 1.5 -2.5 cm/s. The resolution of the CPT in delineating stratigraphic layers is related to the size of the cone tip, with typical cone tips having a cross-sectional area of either 10 or 15 cm², corresponding to diameters of 3.6 and 4.4 cm. The schematic of the test and a detailed depiction of the cone are presented in Figure 1.2a and 1.2b.

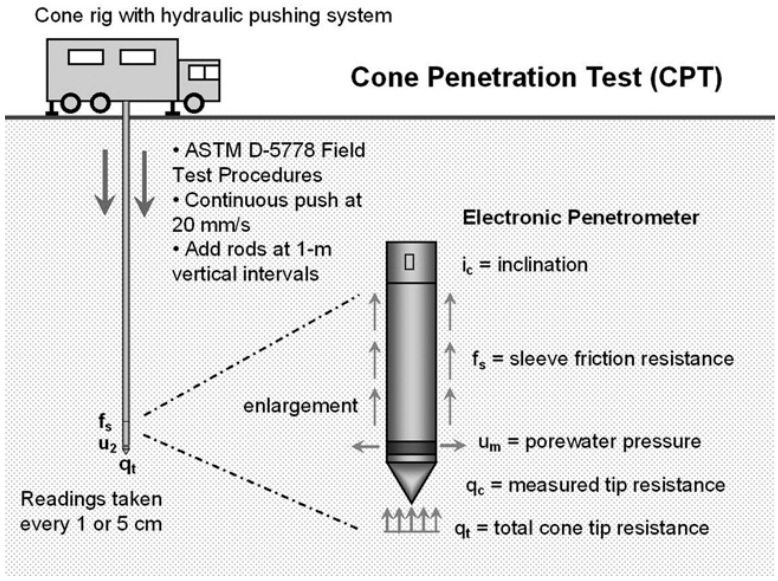

Figure 1.2a: *Schematic of Cone Penetration Test (Mayne 2007, NCHRP Synthesis 368)*

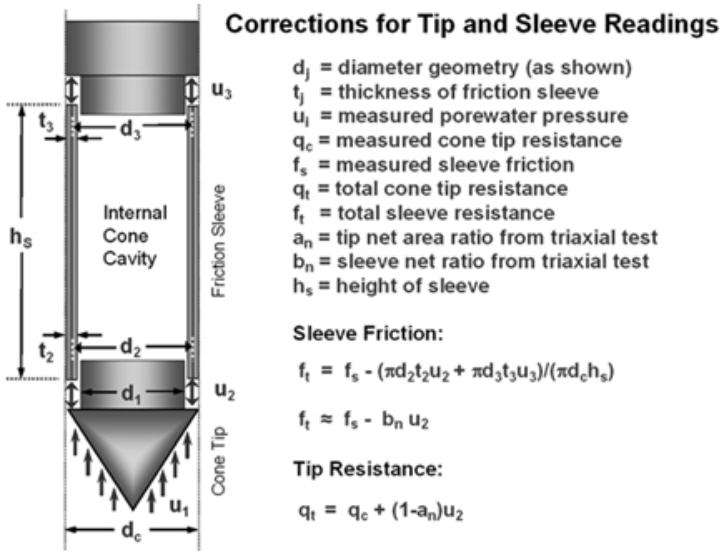

Figure 1.2b: *Schematic of Cone Penetration Test (Mayne 2007, NCHRP Synthesis 368)*

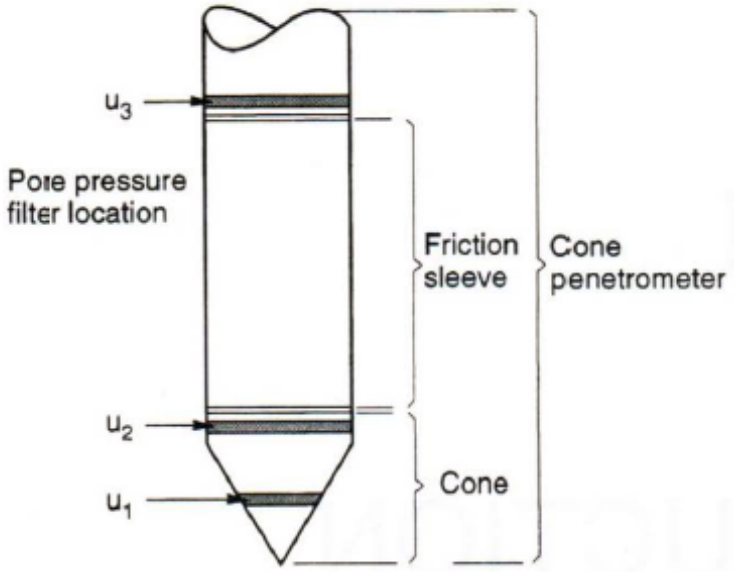

Figure 1.3: *The cone components (Robertson et al., 1997)*

CPT and CPTu testing equipment generally advances the cone using hydraulic rams mounted on either a heavily ballasted vehicle or using screwed-in anchors as a counter-force. Two advantages of CPT over the Standard Penetration Test, SPT, are (1) a more continuous profile of soil parameters, with CPT data recorded typically at 2 cm intervals and (2) a significant reduction in possibility of operator error (hammer energy, non-standard sampling, etc.).

Geophones or accelerometers are often housed within the cone tip to gather seismic shear wave and compression wave velocities using the downhole method. A source of seismic energy is generated at the surface, typically by using a sledgehammer to strike a steel plate on which the truck rests, and the resulting downward propagating wave is measured by the geophones. Travel time picks are made from the recorded waveforms, and the average shear wave velocity is computed as the travel distance divided by the travel time. The process is repeated at different depths to obtain a shear wave velocity profile. This data helps determine the shear modulus and Poisson's ratio (in unsaturated soils only) at intervals through the soil column, which can be used for settlement analysis, dynamic problems, and soil liquefaction analysis.

Under certain circumstances, the tip and sleeve readings alone can suffice to produce a basic cone sounding that serves well for delineating soil stratigraphy and testing natural sands, sandy fills, and soils with deep water tables. Generally, this is accomplished using an Electric Cone Penetration Test (ECPT), with readings taken at 2 cm (0.8 in.) or 5 cm (2.0 in.), although a system for Mechanical Cone Penetration Testing (MCPT) is also available that is less prone to damage, but that is advanced slower and provides coarser resolutions using an incremental vertical step of 20-cm (8-in.) intervals. With piezocone penetration testing (CPTu), transducers obtain readings of penetration porewater pressures that can help identify hydrostatic or steady-state pore pressures in free-draining materials, and changes in pore pressure due to increased total stress and shear in less permeable materials such as silt and clay. The porewater pressures at the shoulder position (u_2) are required for correcting the measured q_c to the total cone tip resistance, designated q_t. This is especially important in the post-processing phase when determining the engineering properties of soils, for which the pore pressure correction may prove important. Additional sensors can be provided to increase the numbers and types of measurements taken.

With CPT, results are immediately available on the computer for assessment in real time by the field engineer or geologist. A 10-m (30-ft) sounding can be completed in approximately 15 to 20 min, in comparison with a conventional soil boring that may take between 60 and 90 min. No spoil is generated during the CPT; thus, the method is less disruptive than drilling operations. Therefore, CPTs are especially advantageous when investigating environmentally sensitive areas and/or potentially contaminated sites, because the workers are exposed to a minimal amount of hazardous material. CPTs can be advanced into most soil types, ranging from soft clays and firm silts to dense sands and hard over- consolidated clays, but are not well suited to gravels, cobbles, or rock. Soil samples are not normally obtained during routine CPT and therefore may be a

disadvantage to those who rely strictly on laboratory testing for specifications and state code requirements. However, soil samples can be obtained using a special sampler that can thread on to the cone rods. Nevertheless, a large amount of high-quality in situ digital data can be recorded directly by CPT in a relatively short time in the field. These data can subsequently be post-processed to provide a quick profile of subsurface conditions, including layering, soil types, and geotechnical engineering parameters, as well as both direct and indirect evaluations of foundation systems, including shallow footings, driven pilings, drilled shafts, and ground modification.

For geotechnical investigations in recent era, CPT's increased accuracy, speed of deployment, more continuous soil profile and reduced cost over other soil testing methods, makes it a more in demand method. The ability to advance additional in situ testing tools using the CPT direct push drilling rig, including the seismic tools described above, are advantageous as well.

1.3. Pile Lateral Design; History

Pile foundations are often used to support heavy structures such as tall buildings, industrial structures, bridges, and off-shore platforms. Different sources of lateral loadings such as wind, earthquake, waves (in offshore condition), decking of the ships, etc.., create demands on the structures that must be accommodated in design of the foundations.

Development of methods for design of piles for lateral loads has been perhaps most significantly motivated by installation of offshore platforms in the Gulf of Mexico. Design of piles for lateral loads became more critical when for the first time offshore platforms were built in the Gulf of Mexico. One of the first publications describing that a pile subjected to lateral load behaves as a beam was written by Hetenyi (1946). In the early fifties, the oil companies planned and started to install offshore platforms. The piles for the platforms were subject to large magnitude lateral loads and designing the piles for the lateral loads was vital. Two different design approaches, i.e.

using Hetenyi's framework, and limited equilibrium analysis, were implemented to obtain the reaction of soft clay in Gulf of Mexico on piles supporting the offshore platform and the answers obtained from solutions varied widely, triggering a comprehensive research program initiated by Shell Oil Company. The other companies later participated in the research activities, which lead to the development of the idea of p-y modeling of soil-pile interaction. The *p-y* method, in which discrete soil "springs" representing the soil response to lateral pile movement are distributed along the length of the pile, is the most common approach to analyzing laterally loaded piles today. Although a lot of researches have been so far conducted, the complexity of the interactional behavior of the soils and piles warrants more research works to come, and research is continuing.

1.4. CPT and Pile Design; History

The Determination of pile axial capacity is one of the earliest applications of CPT data which goes back to the 1970's. The method of pile installation has a significant influence on pile response. The way the pile disturbs/affects the perimeter soil could result in change in densification of the soils in granular materials, or change in pore water pressure and time-related strength of the saturated soils.

The act of pushing CPT cone into the ground is somehow analogous to driving a pile. Several methods suggested by Nottingham (1975), Schmertmann (1978), Price and Wardle(1982), and Bustamante and Gianeselli (1982), also known as LCPC method, used direct CPT readings, i.e. cone tip resistance, to determine the axial capacity of a single pile. In the research conducted by Robertson et al. (1988a), 13 different methods previously introduced by different researchers were used and compared. One of the first attempts to design a laterally loaded pile by directly using the results of in-situ tests, was the use of a driven pressuremeter by Robertson et al (1983).

Mayne and Schneider (2009) suggested using seismic cone results in evaluating axial capacity of drilled shafts. The determination of pile lateral capacity using CPT was not a concerned area of work for the researchers until a decade ago, when some works started. Recently and using centrifuge test, Lehane et al. published two papers (2014a and 2014b) on determining CPT-based *p-y* curves for sands and clays.

1.5. Research Objective

The response of an isolated, single pile to lateral loading is a typical soil-structure interaction problem, meaning that the deflection of the pile depends on the reaction in the soil, and the reaction in the soil depends on the deflection of the pile. The current best practice in geotechnical engineering in determining lateral capacity of piles is to replace the soil reaction with a series of independent springs. Basically, the model uses beam theory to represent the pile and uncoupled, non-linear load transfer functions, called p-y curves to represent the soil.

Most of the existing methods for determining p-y curves are highly empirical, based on a limited number of cases of laterally loaded piles, which were instrumented, enabling to measure the pile deflection in discrete depth intervals subject to different lateral load (i.e. Matlock 1975, Reese 1975). In essence, these methods have their own limitations, and are mainly applicable for the conditions similar to the tested conditions. Some of the main conceptual issues using these models are:

1. The p-y curve for clays is initially tangent to y-axis, corresponding to an infinite initial stiffness (Matlock, 1970, API, 2011).
2. Soil stratum tested is homogeneous and uniform, i.e. soft clay, stiff clay or sand.
3. No or little consideration is taken of the method of pile installation.

4. The different models suggested by different people use different tests to evaluate the undrained strength of clays, such as vane shear, triaxial UU test, or unconfined compression test, which creates major difference between strength results for the same soils.
5. Evaluation of p-y curves is based on a number of limited strength tests, applied to a number of uncoupled/discrete non-linear springs.

Although later, more detailed investigations by different people addressed some of the problems, still the basis of the existing design programs such as LPILE, or procedures introduced in applicable codes such as API, is the same original recommendations made by Matlock and Reese during seventies.

In recent era, two major thought processes has been entered into the geotechnical engineering field;

1. The need for an interpretative framework to assess the results of tests and assign parameters and/or properties based on the measured response.
2. Increasing demand and usage in employment of in-situ direct-pushed based methods using multi-measurement in-situ devices, such as the seismic cone penetration test with pore water measurement (SCPTu) and Seismic Flat Dilatometer Test (SDMT).

The main objective of this research is to evaluate and eventually suggest a method for determining p-y curves by implementing the two above-mentioned concepts into the suggested criteria. In this regards, the soil in-situ behavior determined by using of cone penetration test,

will be a focal point of the research. Basically and in general sense, soil behavior can be considered as one of the following conditions: drained-dilative, drained-contractive, undrained-dilative, and undrained-contractive. The main conceptual steps to be taken as a part of my research are:

- First, the SBT index, I_c, will be used to determine the in-situ characteristics and behavior of the soil. Based on the determined value of I_c, it could be determined that the soil is more of a coarse grained or a fine grained soil, and during the shearing would behave as in undrained or drained condition. Then;

For the soils with sand-like behavior (drained shearing):

- The concept of critical state soils mechanics (CSSM) will be used to determine the in-situ mechanical characteristics of the soils. It has been proven that the state parameter, ψ, reflects the in-situ character of the granular soils and corresponds to the state of the soils, being contractive or dilative.
- The recent developments have suggested ways of determining the peak friction angle of the coarse grained soils from the state parameter calculated by using of the in-situ CPT soundings (Wride et al 2000, Jefferies and Been 2006, Robertson 2010).
- By having the peak friction angle, φ, the soil ultimate lateral resistance will be determined.

For the soils with clay-like behavior (undrained shearing):

- The undrained shear strength of the soil s_u could be obtained from the CPT sounding.

- Having the undrained shear strength of the soil, s_u, soil ultimate lateral resistance will be determined

In the proposed model, the initial stiffness of the *p-y* curves is computed from a shear wave velocity, V_s, profile, which ideally is measured using a geophysical survey, or will be determined by using CPT-based correlations.

Afterwards, two obtained boundaries of the p-y curve, i.e. initial slope and ultimate resistance boundary will be used to create the p-y curve. The curve backbone shape of the p-y curve will be modeled using a recently developed curve shape (Brandenberg et al., 2013) which is believed to overcome some of the shortages of previously used curves.

Eventually, the suggested model will be evaluated using some collected data of laterally loaded instrumented piles with available CPT results at the same site. The *p-y* curves will be measured versus the field-measured p-y curves available from the tested piles.

2. Literature Review

2.1. Introduction

The selected research topic requires a deep understanding of the basic geotechnical concepts, especially behavior of piles under lateral loads. Also appropriate understanding of the interpretation and use of CPT field testing in the current standard of practice, as well as recent developments in use of CPT results in design of foundations, especially deep foundations, becomes warranted. Therefore, the following topics, which will be discussed in the ensuing sections, were the subject of my study and literature review:

I. Single pile behavior under lateral loading
    - Limited Equilibrium Approach
    - Elastic Continuum Approach
    - Discrete Load-Transfer Approach (*p-y* curves)
    - Different practically used/common p-y models
    - Evaluation and comparison of different *p-y* models

II. CPT Soundings; mechanism, understanding of results, obtaining soils characteristics and parameters from correlations

III. Current practice in using CPT sounding in pile design

IV. New framework in Geotechnical Engineering; Critical State Soil Mechanics (CSSM)

V. Recent developments in applying CPT: CSSM framework

VI. Recent developments in CPT-based methods for determining soils characteristics and its application in pile design, specifically for piles subject to lateral loads

To accomplish my goal, I performed an extensive research on the published literatures related to each of the above-mentioned categories. The ensuing sections of this chapter are devoted to the above-mentioned topics, where each topic/subject is introduced and discussed briefly.

2.2. Single Pile Subject to Lateral Loads

The analytical approach to single piles subjected to lateral loads could vary from the most simplified approach of limited equilibrium, to continuum approach, or the most acceptable approach in current practice, called discrete load transfer or *p-y* curves. Each of these approaches is introduced in the forthcoming sections.

2.2.1. Limited Equilibrium Approach

Conventional Static Approach: The simplest method to estimate the ultimate lateral resistance of a pile is to consider the statics of a pile, as shown in Figure 2.1 below:

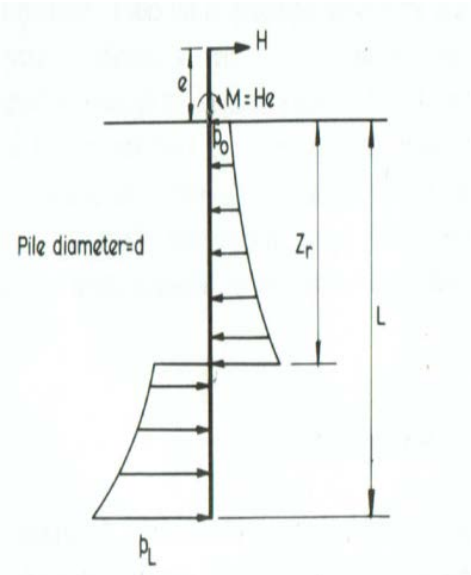

Figure 2.1: *Unrestrained Laterally-Loaded Pile (Poulos, 1980)*

For a free-head pile subject to horizontal load, H, and a moment,M, the ultimate soil pressure, p_u at any depth Z, and assuming that the pile is rigid, the limiting combination of H and M , i.e. H_u

and M_u, to cause failure by mobilizing the ultimate soil resistance along the pile can be obtained by simply applying force and moment equilibrium:

$$H_u = \int_0^{z_r} p_u \, B dz - \int_{z_r}^{L} p_u \, B dz \tag{2.1}$$

$$M_u = H_u e = -\int_0^{z_r} p_u \, BZ dz + \int_{z_r}^{L} p_u \, BZ dz \tag{2.2}$$

For a uniform soil resistance distribution along the length of the pile, the solution of the above equilibrium condition equations yield the following design chart:

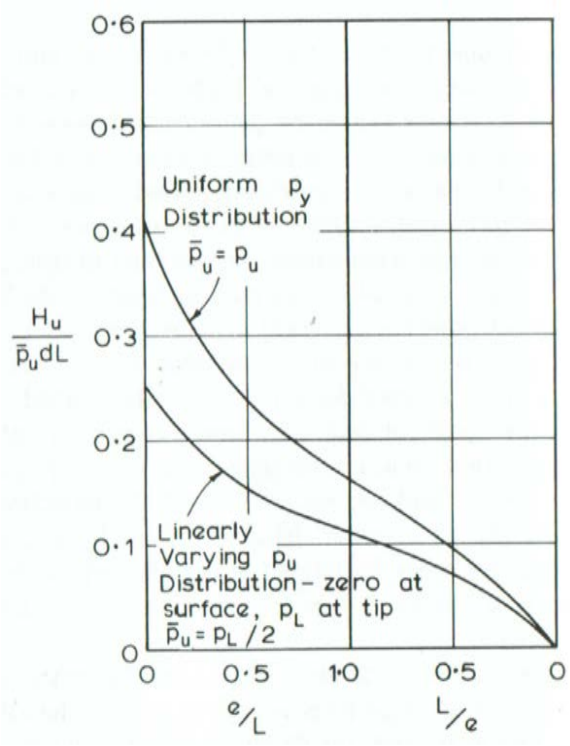

Figure 2.2: *Ultimate Lateral Resistance of Unrestrained Rigid Pile (Poulos, 1980)*

Broms Method: Restricting his work to driven piles, Broms (1964a, 1964b) presented methods for the design of laterally loaded piles in uniform soil profiles consisting of cohesive and cohesionless earth material, and for unrestrained (free-head) and restrained (fixed-head) pile-head conditions.

In doing so, failure modes involving either the pile (formation of plastic hinges) or the soil (mobilization of ultimate lateral resistance) were proposed for short and long piles. For cohesive soils, as shown on Figure 2.3, Broms suggested a simplified distribution of soil resistance as being zero from the ground surface to a depth of 1.5*d* and a constant value of $9s_u$ (c_u in Figure 2.3) below this depth, where *d* is the diameter of the pile.

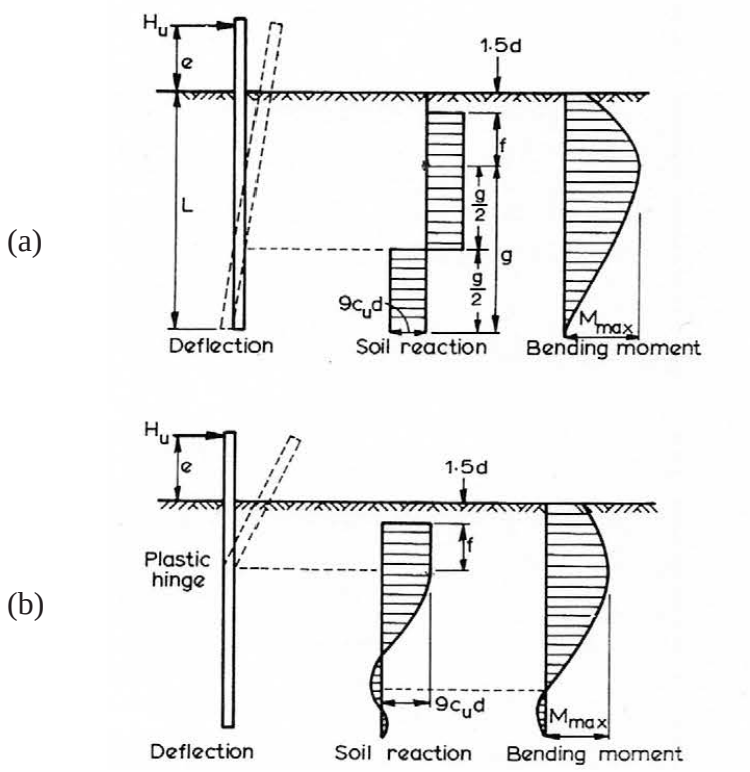

Figure 2.3: *Failure mechanism for Piles in Cohesive Soils (a) Short rigid pile (b) Long Pile (Broms, 1964a)*

For cohesionless soils, the following simplified assumptions are made by Broms (1964b):

1. The active earth-pressure acting on the back of the pile is neglected.
2. The distribution of passive pressure along the front of the pile is equal to three times the Rankin passive pressure.
3. The shape of the pile has no influence on the distribution of the ultimate soils pressure.

4. The full lateral resistance is being mobilized at the movement considered.

Figure 2.4 depicts the distribution of the soil pressure on both short and long free-head piles;

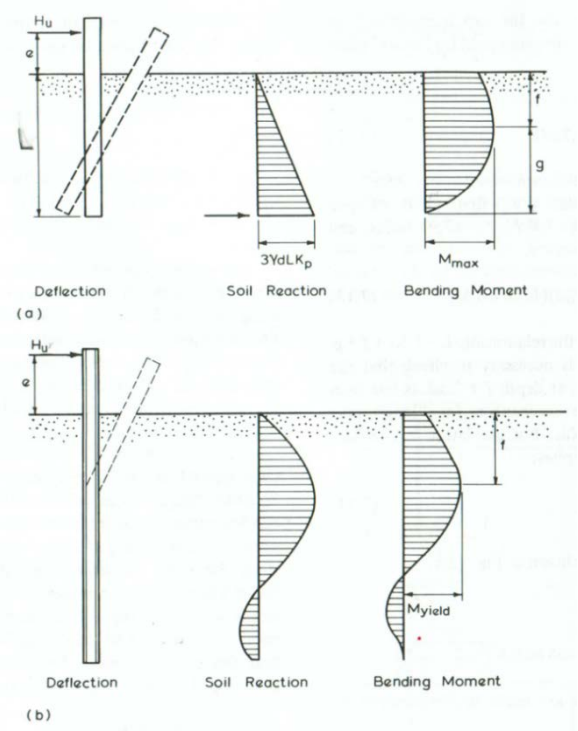

Figure 2.4: *Free-Head Pile in Cohesionless Soils: (a) Short Pile (b) Long Pile (after Broms, 1964b)*

Based on the above-mentioned assumptions on soil pressure distribution along the pile length, Broms suggested different design charts which can be used for determining pile lateral resistance for both conditions of cohesive and cohesionless soils. Examples of the design graphs proposed by Broms are shown in Figures 2.5 and 2.6 below:

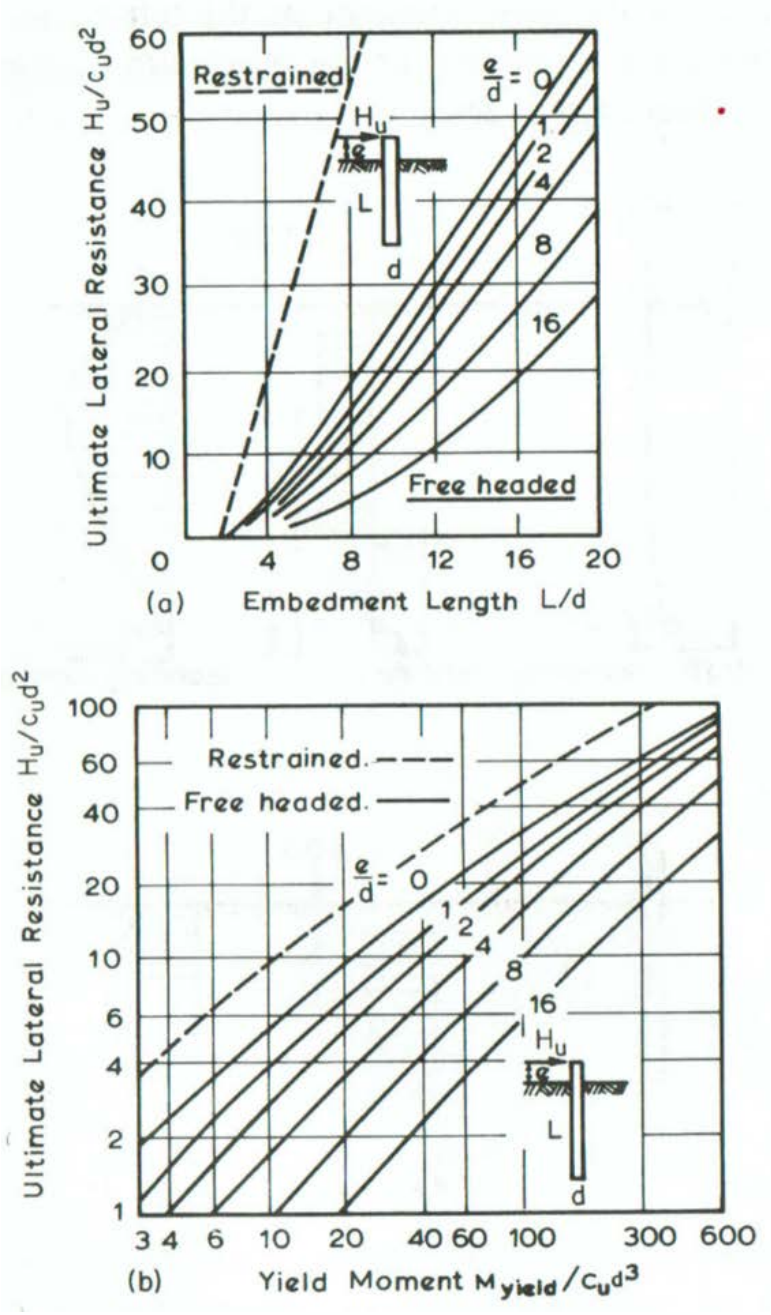

Figure 2.5: *Ultimate lateral resistance in cohesive soils: (a) short piles; (b) long piles (after Broms, 1964a)*

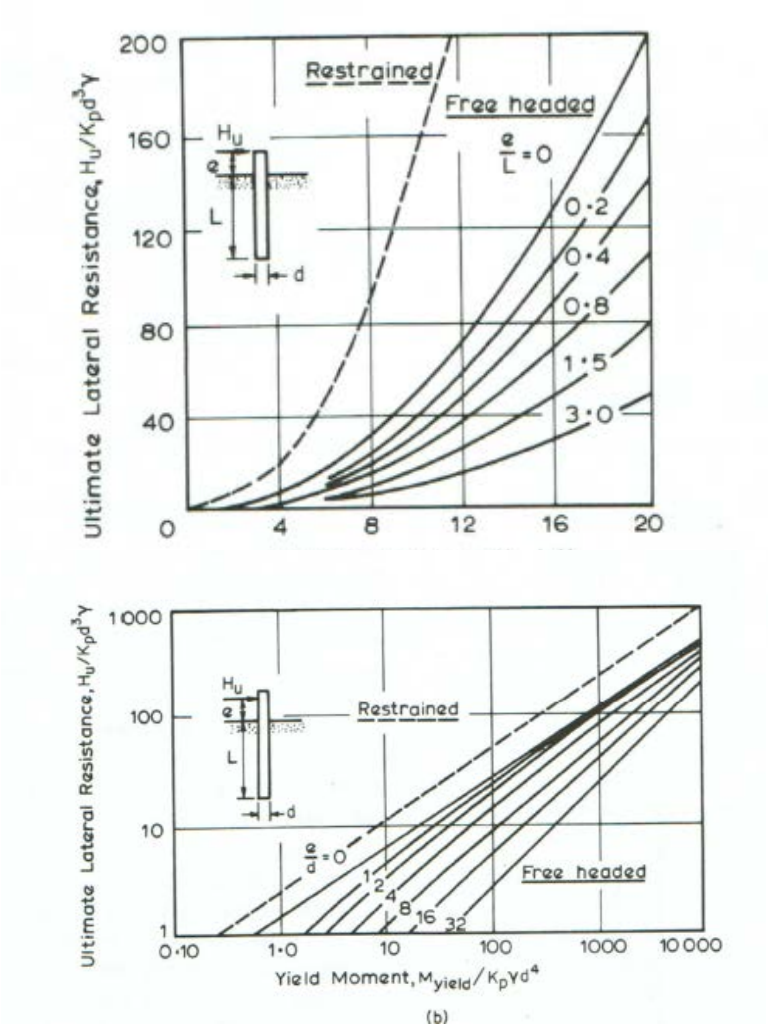

Figure 2.6: *Ultimate lateral resistance in cohesionless soils: (a) short piles; (b) long piles (after Broms1964b)*

Brinch-Hansen Method: This method basically follows the limited equilibrium approach and can be used to predict the ultimate lateral resistance of short rigid piles. One of the advantages of this method to *Broms* method is its applicability to layered soils. It can also be used for the first approximation design of the longer semi-rigid piles. The basics of this method are depicted on Figure 2.7.

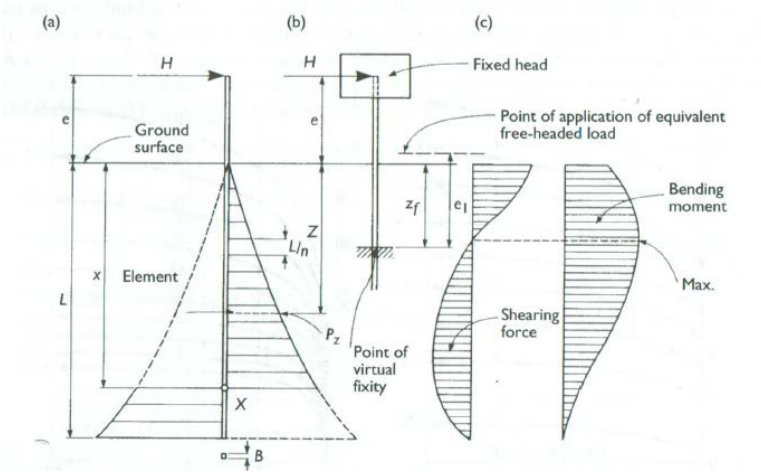

Figure 2.7: *Brinch Hansen's method for calculating ultimate lateral resistance of short piles: (a) Soil reactions (b) Shearing force diagram (c) Bending moment diagram (Tomlinson, 2008)*

The unit passive resistance of an element at a depth z below the ground surface is given by:

$$P_z = p_{oz}\, K_{qz} + C\, K_{cz} \qquad (2.3)$$

Where p_{oz} is the effective overburden pressure, and C is the soil's cohesion at depth Z. Also K_{qz} and K_{cz} are respectively the frictional and cohesive passive pressure components at depth z, which can be obtained by the plots provided by Hanson, shown in Figure 2.8.

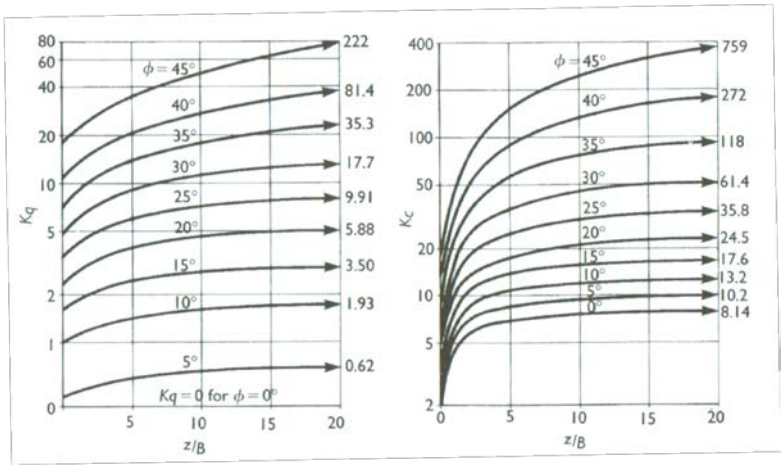

Figure 2.8: *Brinch Hanson's coefficients of K_{qz} and K_{cz} (Tomlinson, 2008)*

This type of approach which represents a limit analysis is confined to ultimate (failure) conditions where reasonable assumptions of lateral soil pressures can be made and solutions readily found by use of the equations of statics.

2.2.2. Elastic Continuum Approach

Analysis in which the soil has been considered as an elastic continuum has been previously described by Douglas and Davis (1964) and others. Continuum approaches, comprise an assortment of solution techniques utilizing either the theory of elasticity alone or both the theory of elasticity and plasticity. These include fully three-dimensional analyses and simplifications using two- dimensional analyses (plane strain or plane stress). Three-dimensional analyses offer the most realistic approach to assessing pile-soil interaction, and are divided into integral equation (or boundary element) method and differential method analysis categories.

Poulos and Davis (1980) chose a somewhat crude approach, starting with the depiction of a pile as a thin rectangular vertical strip of width equal to the pile diameter (d), and a length (L) and constant flexibility *(E_p I_p).* For simplifying the analysis, Poulos assumed developed shear stress between the soil and the sides of the pile equals to zero. The soil assumed to be an ideal, homogenous, isotropic, semi-infinite elastic material with a Young's modulus of E_s, and Poisson's ratio of υ. The pile was divided to n+1elements, where each element is acted upon a uniform horizontal stress p, assumed to be constant across the width of the pile.

By assuming purely elastic behavior is prevailing within the soil, the horizontal displacement of soil and pile are equal. Poulos performed a rigorous analysis by using the differential equation for bending a thin beam, which is:

$$E_p I_p \frac{d^4 y}{d\, Z^4} = -pB \qquad (2.4)$$

Where p is the pressure, y is the deflection, B is the pile diameter, and E_p and I_p are the pile modulus of elasticity and moment of inertia.

By re-writing the equation 2.4 in finite-difference form for the pile's n+1 elements, implementing the boundary conditions and solving the resulting matrix form equations, solutions for the free-head floating pile loaded by a horizontal load of *H* at an eccentricity of e above the ground was obtained. The solutions are expressed in the following forms:

$$y = \frac{\frac{H}{E_S L}\left(I_{yH} + \frac{e}{L} I_{yM}\right)}{F_y} \tag{2.5}$$

$$\theta = \frac{\frac{H}{E_S L^2}\left(I_{\theta H} + \frac{e}{L} I_{\theta M}\right)}{F_\theta} \tag{2.6}$$

Where; H = Horizontal Load

e = Load eccentricity

$M = e.H$; Applied moment at ground lever

$I_{yH}\ and\ I_{yM}$: Elastic influence factor for displacement caused by horizontal load and moment

$I_{\theta H}\ and\ I_{\theta M}$:Elastic influence factor for rotation caused by horizontal load and moment

$F_y\ and\ F_\theta$: Are yield displacements and yield rotations factors, i.e. ratio of pile displacement/rotation in elastic soil to the displacement/rotation yielding soil.

The values for I_{yH}, I_{yM} and I_{yH}, I_{yM} are provided by Poulos in the graphic form as presented in the Figures 2.9, 2.10 and 2.11.

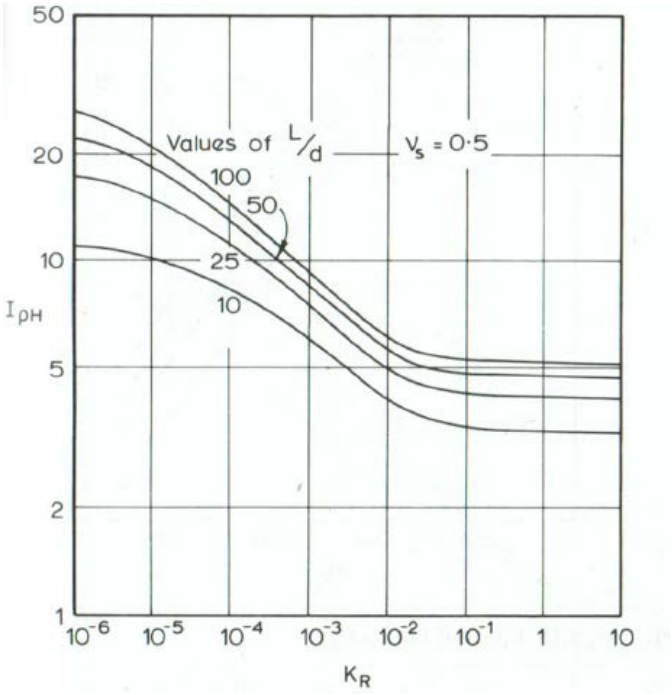

Figure 2.9: *Values of $I_{\rho h}$-free-head floating pile, constant soil modulus (Poulos et al., 1980)*

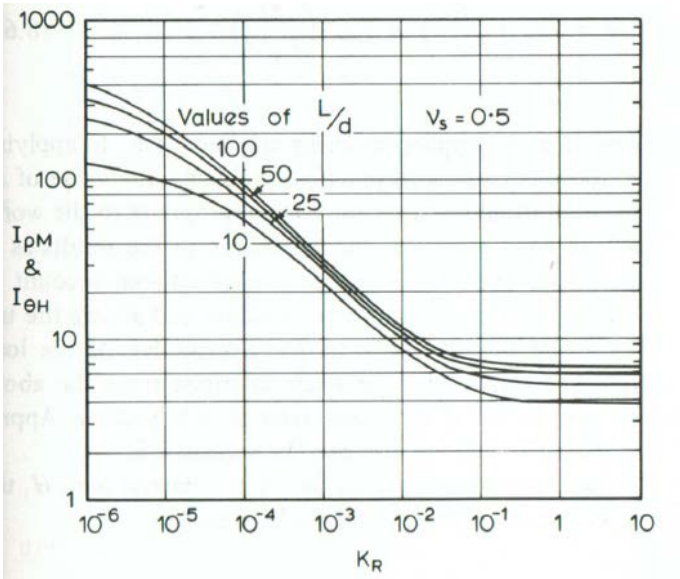

Figure 2.10: *Values of $I_{\rho M}$ and $I_{\rho h}$-free-head floating pile, constant soil modulus (Poulos et al., 1980)*

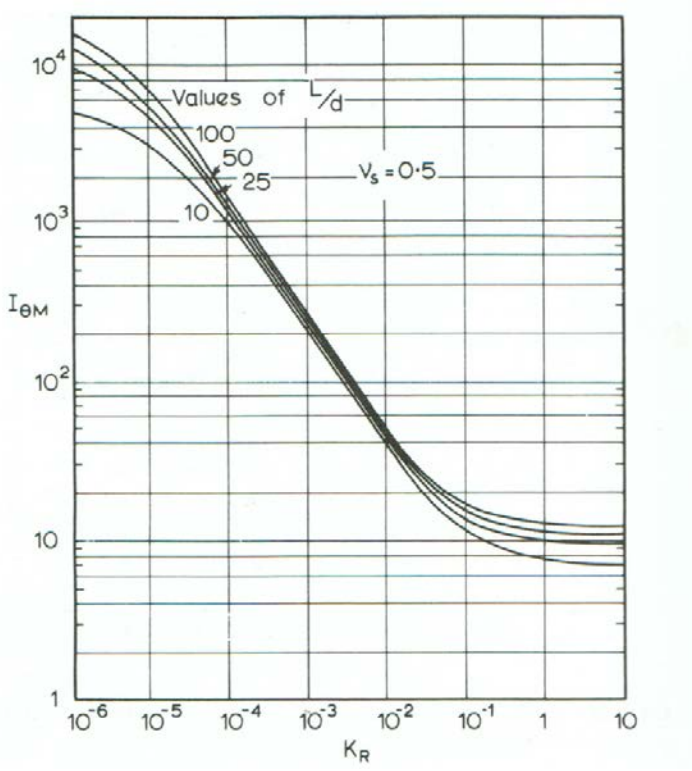

Figure 2.11: *Value of $I_{\theta M}$ -free-head floating pile, constant soil modulus (Poulos et al., 1980)*

Similar type of solution has been provided by Poulos for other conditions of pile top and tip, and corresponding design graphs have been produced.

2.2.3. Discrete Load-Transfer Approach (p-y Curve method)

Lateral capacity of piles in different types of structures such as bridges, tall buildings, off-shore platforms and transmission tower structures, where the lateral loads are predominant, is a key element to design. The analytical methods discussed are applicable only to the deflection of piles which are within the range of elastic compression of soil caused by lateral loading on the piles. However, the analytical methods can be extend beyond the elastic range of soil's behavior by employing of artifice *p-y* curves which represent soil deformation at any given depth for a range of horizontally applied loads on the piles.

Pile lateral capacity is a soil-structure interaction problem. Basically, soil-structure interaction exists in every problem in foundation engineering, but in some cases of considerably stiff structures, a solution can be developed assuming non-linear behavior of the soil and no change in the shape of the structural unit. This could not be the case for piles subject to lateral loading, where any suggested solution should account for the deformation of both pile and the soil. The deflection of the pile and the lateral resistance of the soil are interdependent, i.e. the pile deflection mobilizes the soil resistance, and the soil resistance influences the pile's lateral deformation.

p-y curves, which represent the load-deformation characteristics of the soil at any specific depth for a range of loads from zero to the failure/yield of the soil in ultimate shear, are independent of the shape and stiffness of the pile and represent the deformation of a discrete vertical area of the soil that is unaffected by loading above and below it. In present practice laterally loaded piles are often analyzed using a finite difference model. The model uses beam theory to represent the pile, and uncoupled, non-linear load transfer function, called *p-y* curves, to represent the soil. Therefore, to better understand of the application of *p-y* curve method, it becomes necessary to perform a review on the theory of beam on elastic foundation. Then in the proceeding sections, a brief review of all credible *p-y* models will be conducted and finally the advantages and problems of each one of the addressed *p-y* models will be discussed.

2.2.3.1. Linear Subgrade Reaction Theory

The response of an isolated, single pile to lateral loading is a typical soil-structure interaction problem, meaning that the deflection of the pile depends on the reaction in the soil, and the reaction in the soil depends on the deflection of the pile. The basic need to consider the properties

of both the soil and pile combined is being characterized by the classical beam-on-elastic-foundation problem as illustrated in Figure 2.12.

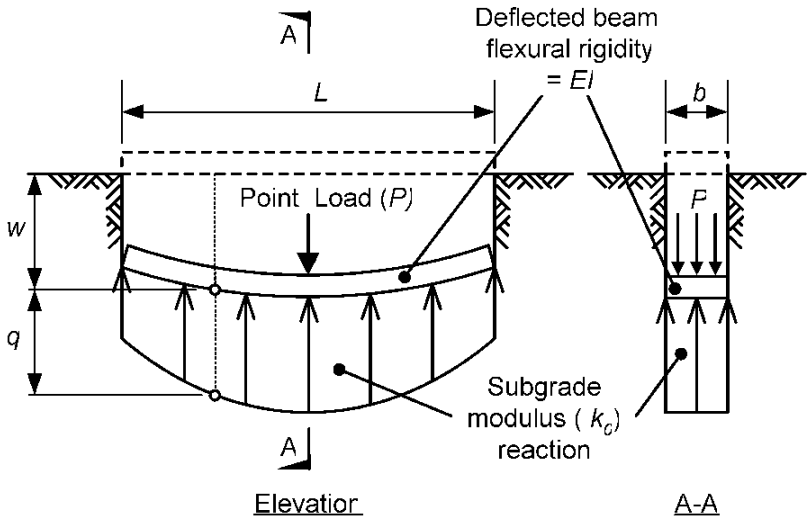

Figure 2.12: *Beam-on-elastic-foundation problem (after Terzaghi, 1955)*

The concept of subgrade reaction was first introduced into applied soil mechanics by Winkler (1867). By idealizing the soil foundation as a Winkler foundation, consisting of a bed of infinitely closely spaced, independent springs each possessing a linear vertical pressure q per unit area versus vertical deflection w, the following relationship will be obtained;

$$\frac{q}{w} = k_o \ or \ \frac{qb}{w} = k \qquad (2.7)$$

Where k_o is the subgrade modulus ($^{force}/_{L^3}$), w is the deflection, b is the beam width, and k is the subgrade modulus of the beam ($^{force}/_{L^2}$).

and the general solution would be:

$$w = (C_1 \cos \lambda x + C_2 \sin \lambda x)e^{\lambda x} + (C_3 \cos \lambda x + C_4 \sin \lambda x)e^{-\lambda x} \qquad (2.8)$$

Where C_1 through C_4 are constant. The parameter λ depends on the properties of both the "soil" and beam, and its reciprocal represents a characteristic length of the soil-beam system. The parameter λ defines the interaction of the soil and beam. If the beam is very stiff compared to the soil then the characteristic length is large and a load applied to the beam will cause vertical deflections of the soil for a considerable distance from the point of load application; conversely, a beam that is very soft compared with the soil (i.e. a very stiff soil) will result in a small characteristic length and only cause vertical deflections in the immediate vicinity of the point load (Scott, 1981). Although use of subgrade reaction theory to depict soil is far removed from real soil behavior, identification of λ as an interactive measure dependent on the relative stiffness of the soil and structure, and in turn the dependency of behavior on such a measure, is a fundamental aspect of soil-structure interaction.

The dependence of behavior of laterally loaded piles on relative stiffness has resulted in the need to distinguish between "short" (rigid) and "long" (flexible) piles. These definitions acknowledge a somewhat intuitive sense of pile behavior whereby a very short and relatively stiff pile would be expected to deflect in a rigid manner when laterally loaded, whereas a very long pile in the same situation would be expected to exhibit a different type of behavior due to the increased embedment and accompanying fixity that this implies. There are many inter-related factors influencing the behavior of laterally loaded piles. One of the dominant factors is the pile stiffness which affects the deflection and determines whether the pile behaves as a short pile, corresponding to rotational mechanism failure, or behaves as a long pile, failing due to failure in flexural bending.

Reese (1986) discussed this dependence of lateral behavior on pile length, noting that short piles can deflect a large amount at the ground line given movement of the pile tip, but with increasing

depth of penetration the soil resistance at the pile tip increases until a point is reached at which ground line deflection reaches a limiting value.

A pile subject to a small axial load, a moment and a lateral force at the top was analyzed under the condition of constant loading, constant cross section and an initial length in the long pile range. Then, the length was reduced in relatively small increments and the calculations were repeated and the ground line deflection vs. the pile depth was plotted, as shown in Figure 2.13. As shown, a so called "critical length" l_c exists, beyond which any additional pile length has no further influence on the pile head response.

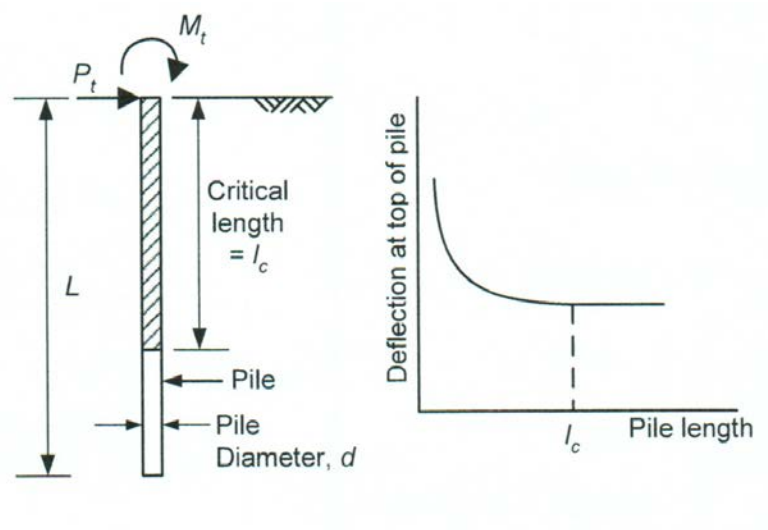

Figure 2.13: *Critical Length of Laterally Loaded Pile (Reese at al., 2006)*

Thus a flexible pile is defined as a pile whose length equals or exceeds its critical length. In subgrade reaction terms such critical lengths have been established for the case of a horizontal subgrade modulus (k_h) that is constant with depth (as in Figure 2.11), in which case:

$$l_c = \frac{\lambda}{4} \tag{2.9}$$

Where $\lambda = \sqrt[4]{\frac{k_h}{4\ E_p I_p}}$ (2.10)

k_h : Subgrade modulus for pile, ($^{force}/_{L^2}$)

E_p : Pile Young's modulus

I_p : Second moment of inertia for pile

And for the case of a subgrade modulus linearly increasing with depth,

$$l_c = 4\,T \tag{2.11}$$

Where, $\lambda = \sqrt[5]{\frac{E_p I_p}{n_h}}$ (2.12)

n_h = constant of horizontal subgrade reaction, ($^{force}/_{L^3}$)

$$k_h = n_h . z \quad (^{force}/_{L^2}) \tag{2.13}$$

Where z is the depth.

The concept of a critical length is nevertheless of general validity and acknowledges the dependence of lateral behavior on a certain mobilized depth of soil that may or may not extend the entire length of the pile.

The selection of an appropriate subgrade modulus is a real challenge in solution of pile lateral capacity analysis. Terzaghi (1955) expressed such concern as the basic limitations involved with subgrade reaction theory, and the difficulty of obtaining an appropriate value for the subgrade modulus. Terzaghi (1955) stated that the theory was only approximately valid for pile-soil contact pressures less than about one-half the ultimate bearing capacity of the soil under lateral load. He also emphasized the importance of soil type and the dimensions of the pile, as shown schematically

in Figure 2.14., where stiff (overconsolidated) clay and sand subgrade characteristics were idealized by constant and linearly increasing subgrade reaction models respectively, and as shown pile dimensions were utilizing differing horizontal pressure bulbs mobilized by different pile widths. The issue of flexural rigidity of a structure, such as a pile, and its effect on the subgrade modulus was only briefly mentioned by Terzaghi (1955), and only then in the context of theoretical work.

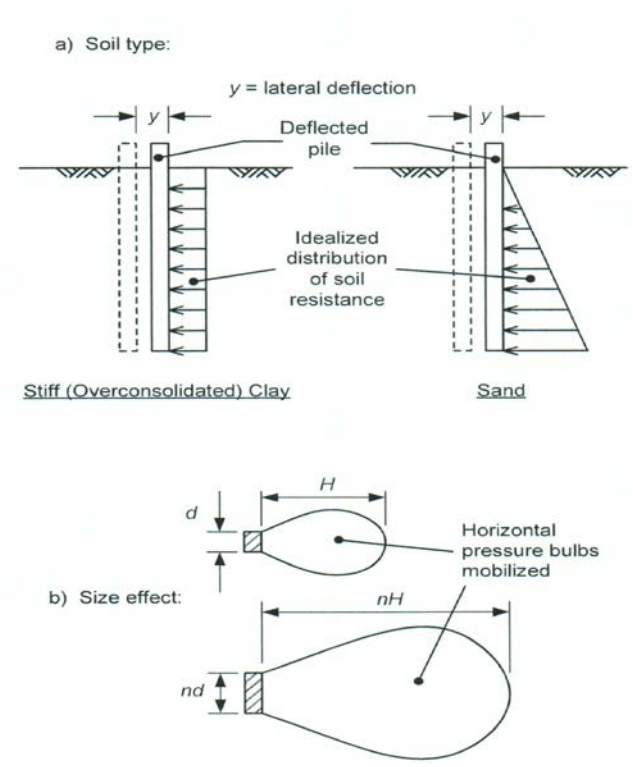

Figure 2.14: *Soil type and size effect (after Terzagi, 1955)*

That subgrade reaction theory is limited from both a physical and theoretical point of view is a fact that has long been recognized: Terzaghi himself expressed reservations in publishing his 1955 paper and only did so after numerous requests (Reese, 1986). Jamiolkowski and Garassino (1977) acknowledged this limitation in their review of soil moduli for laterally loaded piles, noting the important observation made earlier by McClelland and Focht (1958a) that the subgrade modulus is

not a property exclusively of the soil, but simply a convenient mathematical parameter that expresses the ratio of soil reaction to pile deflection. In doing so, such a parameter depends on the characteristics of the pile (i.e. pile geometry, flexural rigidity, boundary conditions at the top and bottom of the pile, etc.), the soil, and the manner in which the pile and soil characteristics change with the level of lateral loading applied.

In response to this complex concerns, two general categories of design approaches for single piles have developed: a) Those that retain the basic qualities of subgrade reaction theory in the form of discrete, nonlinear load-transfer mechanisms along the pile length depicting the soil reaction to pile deflection relationship; and b) those that represent the soil as a continuum. These approaches will be referred to here as the Discrete Load-Transfer and Continuum approaches, respectively.

2.2.3.2. *p-y* Models

As discussed in section 2.2.2, in present practice laterally loaded piles are often analyzed using a finite difference model. The model uses beam theory to represent the pile, and uncoupled, non-linear load transfer function, called *p-y* curves, to represent the soil. The Winkler Method was the attempt of using the Discrete Load Transfer approach, with the assumption of a linear load transfer function for the soil, which assumes the pressure p and the deflection y at any discrete point along the pile are related through a modulus of subgrade reaction. The following section is dedicated to the description of the Winkler method, ensuing by sections to discuss the non-linear models of pressure/deflection relation, called *p-y* curves.

2.2.3.3. Winkler Model

The most basic soil-structure interaction analysis approach for the response of the piles to lateral loading is called subgrade reaction approach, or Winkler idealization of the soil (Figure 2.15). In

the Winkler method, the pressure *p* and deflection y at a point are assumed to be related through a modulus of subgrade reaction. Thus;

$$p = k_h y \quad (k_h in\ units\ of\ {}^{force}/_{L^3}) \tag{2.14}$$

or could be restated as;

$$P = K.y \tag{2.15}$$

Where K is the subgrade modulus, $K = k_h.B$, in units of $({}^{force}/_{L^2})$

B = Pile diameter

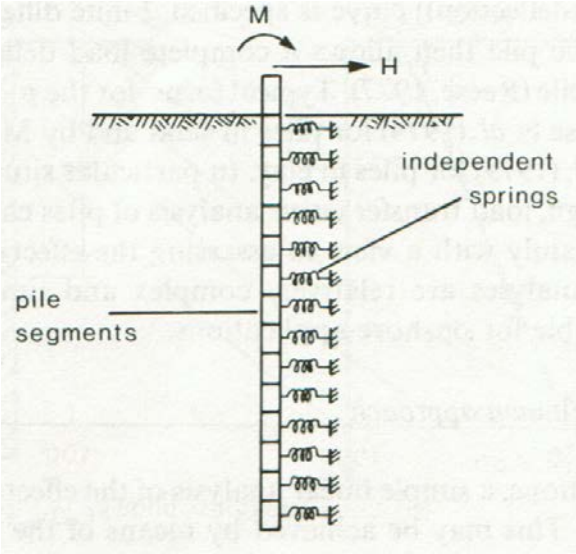

Figure 2.15: *Subgrade reaction model of soil around pile (Fleming at al., 1985)*

It should be known that the soil subgrade modulus is not a soil property but instead is a function of pile deflection, depth below the surface, as well as soil properties.

As stated by Poulos (1980), the pile subjected to lateral loading is usually assumed to act as a thin strip whose behavior is governed by beam equation:

$$E_p I_p \frac{d_y^4}{dx^4} + p.B = 0 \quad (2.16)$$

or

$$E_p I_p \frac{d_y^4}{dx^4} + kh.B\, y = 0 \quad (2.17)$$

As in the simple theory of bending, the effect of axial load in the pile is ignored. This in most cases has relatively little influence on bending moment and the resultant deflection thereafter.

In some cases the axial load is needed to be utilized into the derivation. The derivation for differential equation for the beam-column on an elastic foundation was provided by Hetenyi (1964), and is shown as below:

$$\frac{dM}{dx} + Px \frac{dy}{dx} - V_v = 0 \quad (2.18)$$

and by differentiating equation 2.18 with respect to x, we will obtain:

$$\frac{d_M^2}{dx^2} + Px \frac{d2y}{dx^2} - \frac{dVv}{dx} = 0 \quad (2.19)$$

knowing the following basic equations from the strength of materials:

$$\frac{d^2M}{dx^2} = E_p I_p \frac{d_y^4}{dx^4} \quad (2.20)$$

$$dV_v / dx = p \quad (2.21)$$

$$p = E_{py}.y \quad (2.22)$$

and substitute them into equation 2.19; the following equation will be obtained:

$$E_p I_p \frac{d_y^4}{dx^4} + Px \frac{d2y}{dx^2} - p = 0 \quad (2.23)$$

Where,

$P =$ axial load on pile,

$y =$ lateral deflection of pile at depth x,

$p =$ soil resistance per unit length of pile,

$Ep.Ip =$ Flexural stiffness of the pile,

The following Figure 2.16 depicts the forces on an element of beam column and clarifies the mentioned equations:

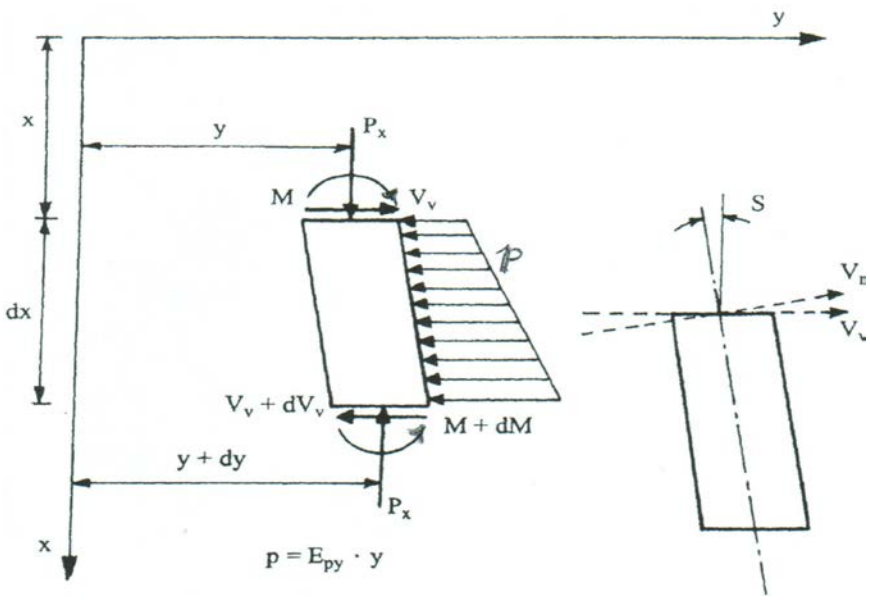

Figure 2.16: *Element from a beam-column (after Hetenyi, 1946)*

It is viable to determine the bending moments, shearing forces and deformed shapes of a pile over its full length for any working load condition assuming the pile behaves as an elastic beam on an elastic foundation, i.e. series of elastic springs representing the soil. The solution of the equation (2.23) by Reese and Matlock (1956) for normally consolidated and cohesionless soils for which the elastic modulus of the soil *Es* is assumed to increase from zero at the ground surface in direct proportion to the depth, resulted is a set of curves such as shown in Figure 2.17.

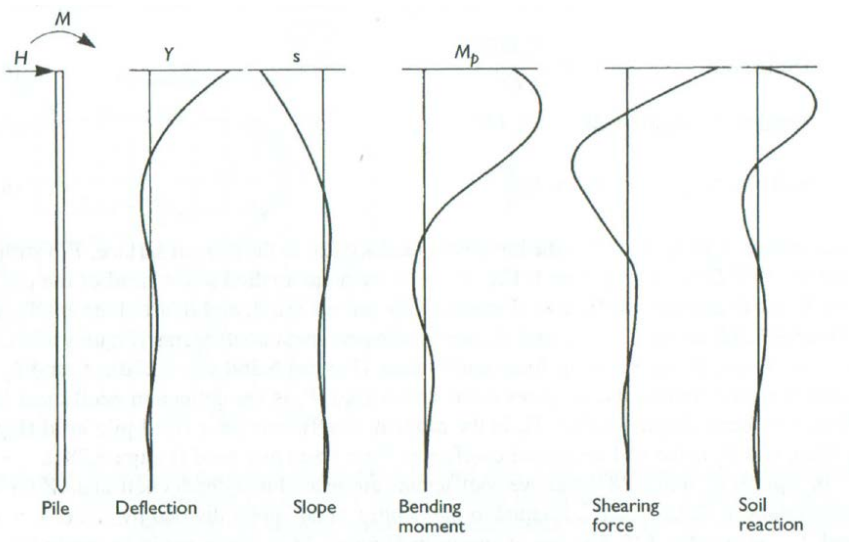

Figure 2.17: *Deflections, slopes, bending moments, shearing forces and soil reactions for elastic condition (after Reese and Matlock, 1956)*

They solutions for each of the curves for a free pile condition are given as the following formulas, where the introduced constants A, could be obtained from the curves provided by Reese and Matlock (1956), presented as Figure 2.18:

Deflection, $y = y_A + y_B = \frac{A_y H T^3}{EI} + \frac{B_y M_t T^2}{EI}$ (2.24)

Slope $= S_A + y_B = \frac{A_s H T^2}{EI} + \frac{B_s M_t T}{EI}$ (2.25)

Bending moment $= M_A + M_B = A_m H T + B_m M_t$ (2.26)

Shearing Force $= V_A + V_B = A_v H + \frac{B_v M_t}{T}$ (2.27)

Soil Reaction $= P_A + P_B = \frac{A_p H}{T} + \frac{B_p M_t}{T^2}$ (2.28)

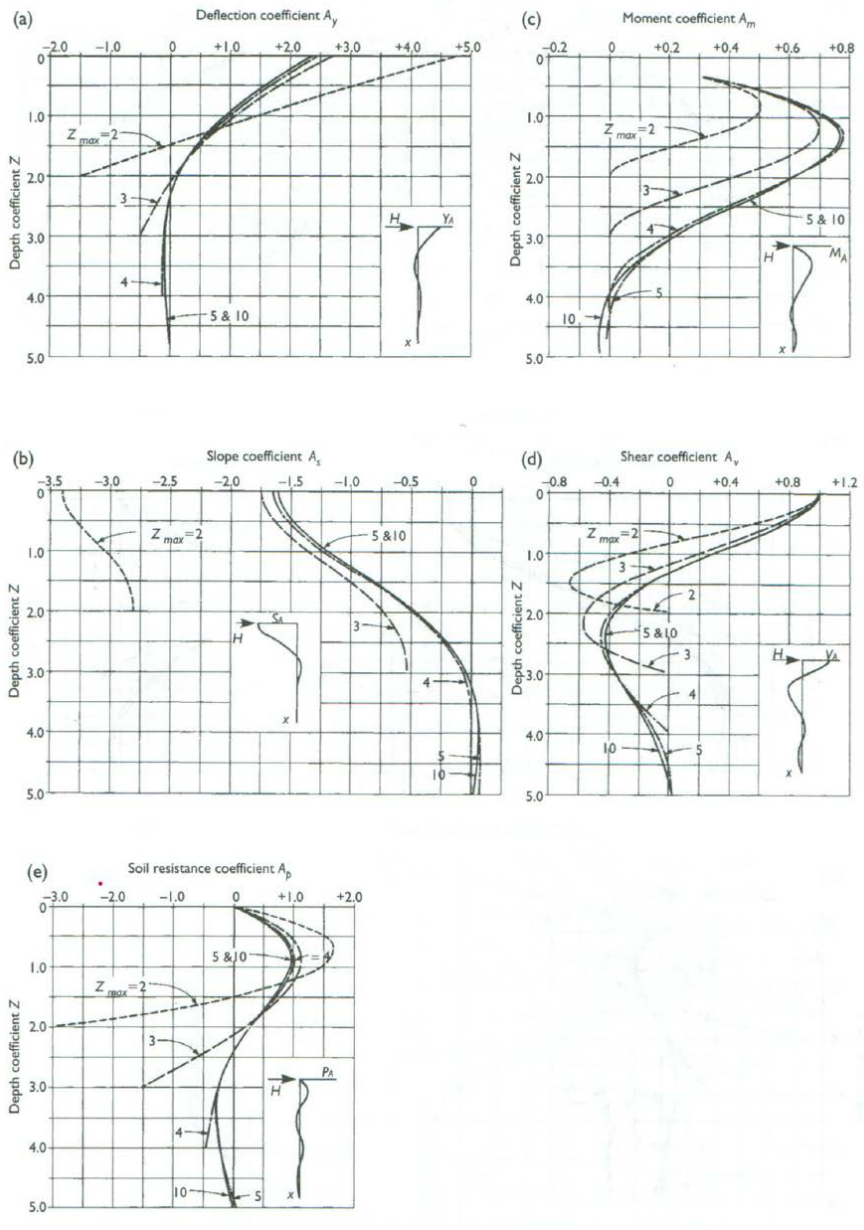

Figure 2.18*: Coefficients for laterally loaded free-head piles in soils with linearly increasing modulus (after Reese and Matlock, 1956)*

2.2.3.4. Different Established P-Y Criteria – Cohesive Soils

In current practice the method to analyze laterally loaded piles is comprised of using beam theory to represent the pile and an uncoupled, non-linear load transfer function, called "*p-y* Curves" to

represent the soils. The basic ascribed models used to define *p-y* curves for cohesive soils are presented in the following table:

p-y Model/Criteria	Applicability	Test Site Location	G.W.T. Condition
Matlock (1970)	Soft Clay	Lake Austin and Sabin River, TX	Free Water
Reese and Welch (1975)	Stiff Clay	Huston, TX	Below Ground Level
Gazioglu and O'Neill (1984)	All Clays	N/A (Database)	Not Defined
API (2011)	All Clays	N/A (Database)	Not Defined

TABLE 3.1-*Different p-y models for cohesive soils*

The above-introduced criteria are discussed in the forthcoming sections.

Matlock (1970) Criteria: The Matlock Criteria was first developed based on a research program on laterally loaded piles for offshore structures. The program included field test on an instrumented pile, laboratory model testing, and development of correlations. The test site representing the condition for offshore piles embedded in soft clay, i.e. below mud line, was selected in two locations of Lake Austin and Sabine River, in Texas. The soils at Lake Austin consist of clays and silts deposited during the recent century behind the Lake Austin dam. The upper portions have been subjected to desiccation and the clays were somewhat fissured and jointed. The van shear test resulted in about 800 psf in average. The Sabine site clay appeared to be a more typical of slightly over-consolidated marine deposits, with average Vane shear strength of about 300 psf for the upper zone.

The summary data on the field test piles installed at Sabine River site are:

- The tested pile is a driven steel tube (open-ended) with 12.75 inches diameter

- 35 pairs of electric resistance strain gages were installed in the upper 42 feet embedded portion
- Gage spacing varied from 6 inches at top to 4 feet at the lower part of the pile

The arrangement of testing assembly for restrained head test is shown on Figure 2.19 below:

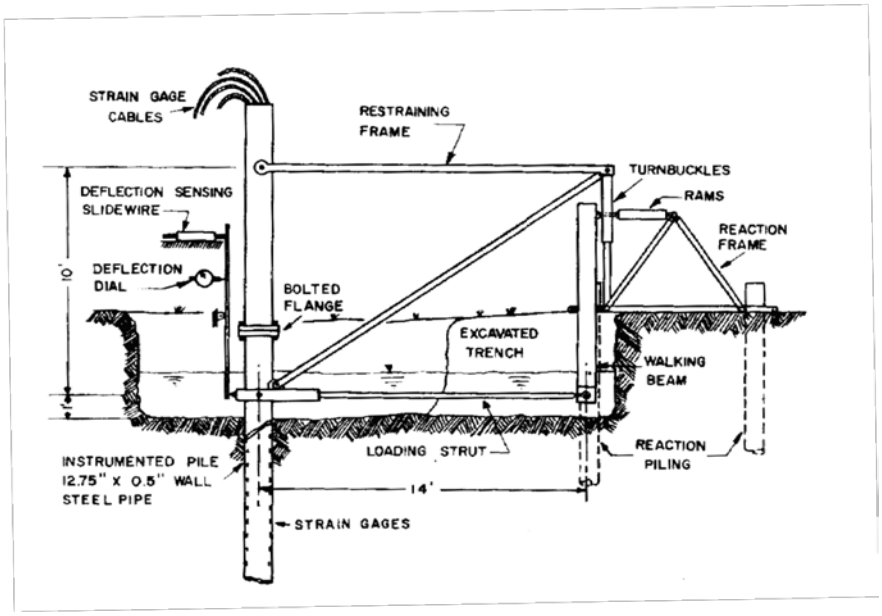

Figure 2.19: *Arrangements for field tests at Sabine using restrained head lateral loading (Matlock, 1970)*

The following steps were taken to determine the correlations between soils resistance and the pile's lateral deflection:

- Application of a lateral force, *P*
- Precise determination of the bending moments by use of readings of strain gages at each sections
- Obtaining distribution of soil reaction by differentiation of the moments
- Obtaining deflections along the pile by integration of the moments
- Repeat the steps for different lateral loads, *p*

- At each section, plot variation of *p* (lateral load) vs. resulted *y* (deflection), to obtain *p-y* curve for that depth

In summary, and as a result of his research program, Matlock proposed the following *p-y* curve for short-term static loading;

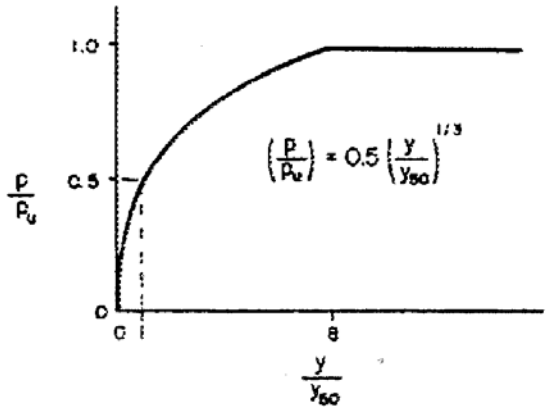

Figure 2.20: *Short-term p-y curve construction criteria (Matlock, 1970)*

As verification to his suggested criteria, Matlock produced a family of predicted curves using his model, which is shown in Figure 2.21. Then, the *p-y* curves from Figure 2.20 were used as input data for computer simulation of pile-soil system in condition corresponding to the Sabine loading. The resultant solutions for bending moments were compared with the field experimental results. Figure 2.20 presents one of the comparisons made by Matlock (1970).

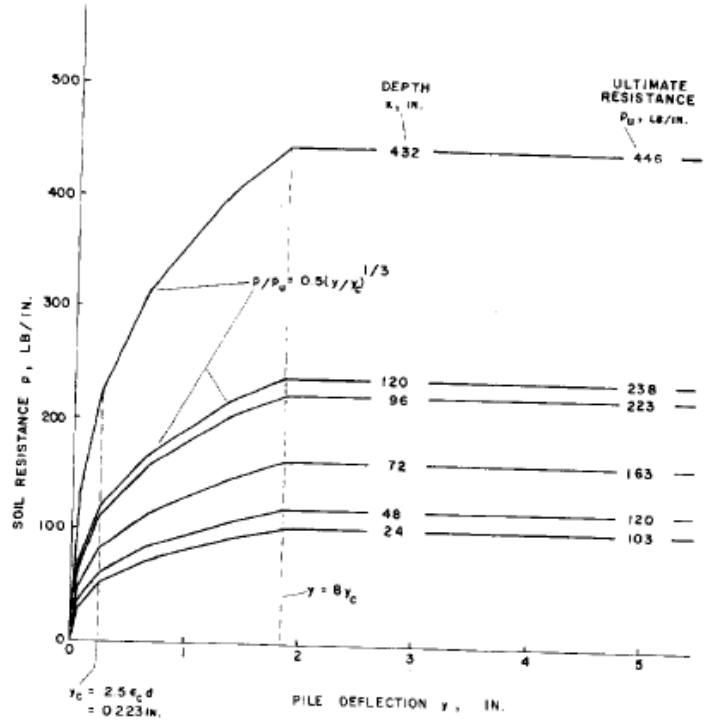

Figure 2.21: *Family of p-y curves for Sabine Clay for short-time static loading (Matlock, 1970)*

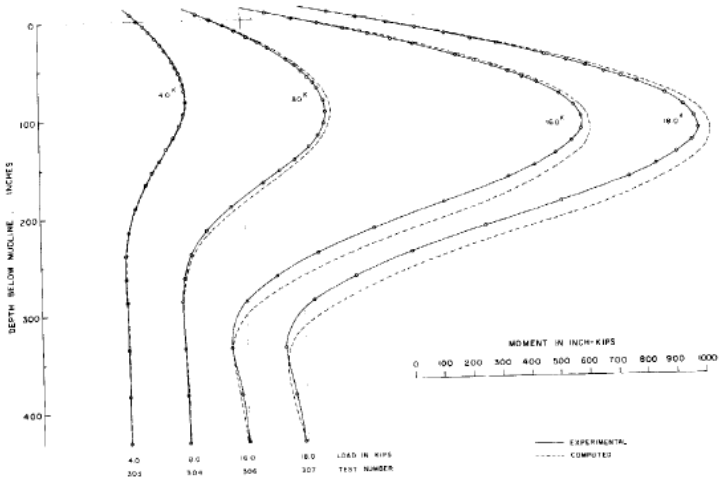

Figure 2.22: *Predicted bending moments for Sabine free-head static loadings, compared with experimental results (Matlock, 1970)*

For construction of the non-dimensional curve, as Matlock suggested in Figure 2.20, the following are suggested to be used:

$$y_c(y_{50}) = 2.5\ \epsilon_c\ B \quad (2.29)$$

$$Pu = Np\ Su\ B \quad (2.30)$$

Where:

$$Np = min\ \{\ (3 + \frac{\gamma x}{S_u} + 0.5\ \frac{x}{B}) \text{ and } 9\} \quad (2.31)$$

Where;

ϵ_c: is the strain at one-half of the maximum stress on a laboratory UU triaxial strain-stress curve

y_c: is the deflection at point C, corresponding to the resistance of 0.5 Pu

Pu: is the ultimate soils resistance per unit length of pile

Np: is a non-dimensional coefficient, varying from 3 at surface to a maximum of 9 at the depth

$$x_r = \frac{6\ B}{\frac{\gamma\ B}{Su} + J} \quad (2.32)$$

S_u: is undrained shear strength

B: is pile diameter

As stated in his paper, the outlined method is applicable for submerged clay of naturally consolidated or slightly over-consolidated. Also no allowance was made for possible increase in soils strength because of lateral consolidation due to the driving of displacement pile

Reese and Welch (1975) Criteria: The experimental and research program conducted by Reese and Welch was to propose a criteria for prediction of the behavior of stiff clay around a deep foundation subjected to short-term static or cyclic loading. The test site was located in Houston, Texas, near the intersection of State Highway 225 and Old South Loop East. The near surface soil

is Pleistocene age, locally named as Beaumont Clay. The soils strata consisted of 28 feet of stiff to very stiff red clay; 2 feet inter-bedded thin layers of silt and clay, underlain by very stiff tan silty clay extending to a depth of 42 feet. At the time of testing, the water level was at about 18 feet below the ground surface.

The average value of undrained shear strength for the upper 20 feet measured by performing UU (unconsolidated undrained) triaxial test was about 1.1 tsf (110 Kpa).

The summary data on the field test piles installed at Sabine River site are:

- Drilled shaft, poured in place concrete, with 30 inches diameter
- A 10.75-inch diameter steel tube was installed inside the shat, in a co-center condition. The pipe had a 1/4 inch thick wall.
- Gages were spaced at 15-inch for the top two-third of the shaft and 30-inch intervals within the lower one-third.

The arrangement of testing assembly for restrained head test is shown on Figure 2.23 below:

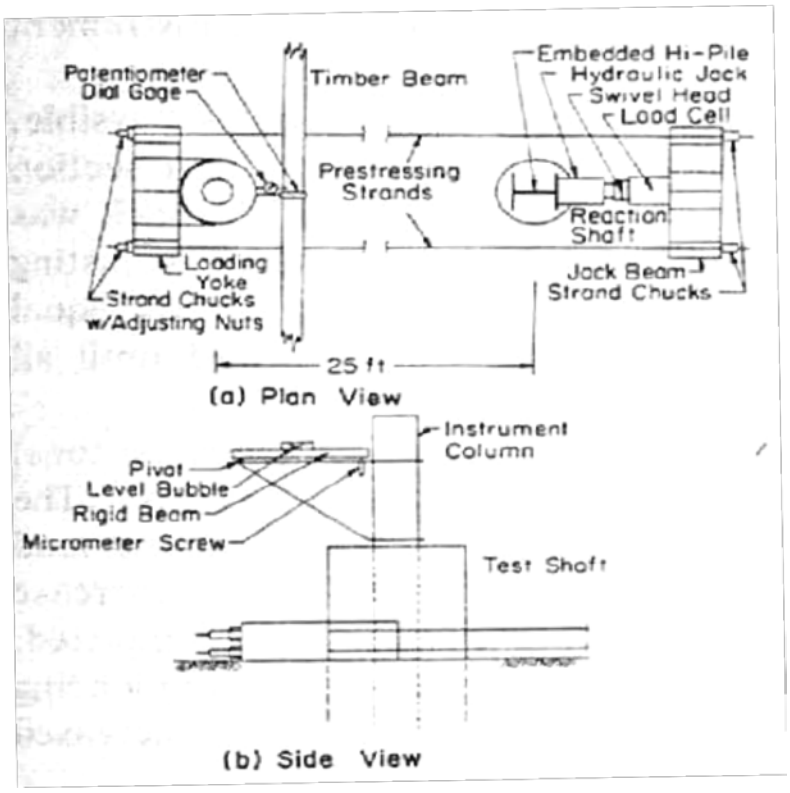

Figure 2.23: *Arrangements for field tests for free head lateral loading (Reese and Welch, 1975)*

The following is the proposed criteria for construction of *p-y* curves for stiff clay subject to short-term static loading;

a) Obtain the best possible estimate of soils parameters, i.e. the variation of shear strength and unit weight with depth, and the value of ϵ_{50}. If no value for ϵ_{50} is available, a value of 0.005 or 0.010 may be used.

b) Calculate the ultimate soil resistance per unit length of the shaft, Pu, using the smaller values given by equations Matlock(1970)

c) Calculate y_{50} by using equation (2-33), as :

$$y_{50} = 2.5\, B\, \epsilon_{50} \qquad (2.33)$$

d) P-y curve points may be computed by using the following equation:

$$\frac{P}{Pu} = 0.50(\frac{y}{y_{50}})^{0.25} \quad (2.34)$$

e) And ; $P = P_u$ for beyond $y = 16\ y_{50}$ (2.35)

The general configuration of the resultant p-y curve is shown below;

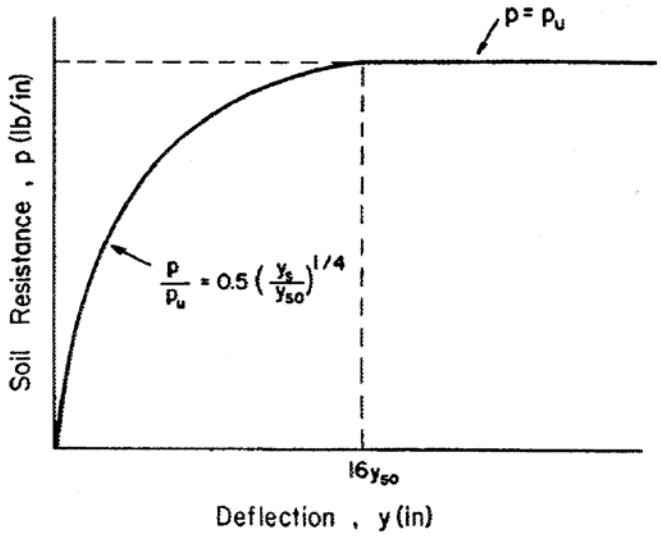

Figure 2.24: *Short-term p-y curve construction criteria, (Reese and Welch, 1975)*

Gazioglu and O'Neill (1984): Criteria: In their paper published in 1984, Gazioglu and O' Neil introduced a method that integrates relative pile-soil stiffness and soil degradability effects to represent the response of all cohesive soils, i.e. soft and stiff, in a consistent manner. They used a relatively broad data base to compare their model to the soft clay model (Matlock, 1970) and stiff clay model (Reese et al, 1975). Their proposed p-y model is called "Integrated Clay Method", was developed in order to address several concerns:

- Preference of having only one unified method for all clays which includes factors such as soil ductility into the model, rather than being only based on consistency of the soil

- Consider non-linear relation between reference deflection, y_c, and the pile diameter, as addressed by Stevens and Audibert (1979), rather than linear relation used in previous methods
- Implement the continuum effects into the model

The proposed model is a semi-empirical method applicable to all clays. The model includes empirical terms to reflect soil ductility, non-linear relation on pile diameter, and relative pile-soil stiffness.

The proposed method is summarized as below:

1. Determine the critical pile length, L_c:

$$L_C = 3(\frac{EI}{E_S.B^{0.5}})^{0.286} \quad (2.36)$$

Where EI is the flexural stiffness of the pile, E_s is the secant young's modulus of the soil at 50% of deviator stress at failure in undrained triaxial test, and B is the pile diameter.

2. Determine Reference Deflection, y_c:

$$y_C = A'\varepsilon_c B^{0.5}(\frac{EI}{E_S.})^{0.125} \quad (2.37)$$

Where: E_s is the value of soil modulus at the depth of interest, and A' is a constant factor

Equation (3.36) was derived by assuming that y_c could be expressed in the form:

$$y_C = A'\varepsilon_c B\ K_r^n \quad (2.38)$$

Where K_r is a relative stiffness that implements the continuum effect and is defined as:

$$K_r = (\frac{EI}{E_S})L_C^4 \quad (2.39)$$

The factor A′was determined through an optimization technique based on modeling seven well documented, full scale static and cyclic load tests. Based on the data available and their judgment, the authors recommend a value of 0.8 for A′.

In their paper, Gazioglu and O'Neill provided values of E_s for different values of undrained shear strengths of clays.

3. Calculating Ultimate Soil Resistance:

The ultimate soil resistance is determined using equation (2.40):

$$P_u = FN_pS_uB \tag{2.40}$$

Where F is a reduction factor based on ductility and form of loading, i.e. static or cyclic.

The factor F is related to the soil ductility and is provided in the following Table 2.2:

Factor	Loading Condition	UU Triaxial Compression Failure Strain		
		<0.02	0.02-0.06	>0.06
Fs	Static	0.5	0.75	1.00
Fc	Cyclic	0.33	0.67	1.00

Table 2.2: *Soil Degradation Factor, F*

The parameter N_p has the following variation with depth:

$$N_p = 3 + 6\left(\frac{X}{X_{cr}}\right) \leq 9 \tag{2.41}$$

And

$$X_{cr} = \frac{L_c}{4} \tag{2.42}$$

It is important to notice that the definition of X_{cr} follows the logic addressed by *Briaud et al*.(1983*)* based on pressuremeter data, which X_{cr} depends on relative pile-soil stiffness. This is not the same principal used in soft and stiff clay criteria discussed before, which do not consider relative stiffness. The explained approach results in smaller values of X_{cr} for a given pile as the soil becomes stronger, while the soft clay method (Matlock 1970) and stiff clay method (Reese 1975) produce larger values of X_{cr} with increasing soil strength.

API Criteria: The API criterion is somehow the modified version of soft clay (Matlock, 1970) and stiff clay (Reese 1975) criteria. The suggested method distinguishes soft clays from stiff clays with introducing boundary shear strength of s_u equal to 100 KPa (2000 psf). The soil ultimate resistance for static loads is obtained from the aforementioned equations (2.30) to (2.31). The *p-y* curve used by API is the curve previously presented as Figure 2.18.

2.2.3.5. Different Established p-y Criteria – Cohesionless Soils

The basic ascribed models used to define P-Y curves for cohesionless soils studied as a part of my literature review are presented in the following table:

P-Y Model/Criteria	Applicability	Test Site Location	G.W.T. Condition
Reese, Cox and Koop (1974)	Clean fine sand to silty fine sand	Mustang Island, Texas	Free Water
Murchison and O'Neill (1984)	Very loose to dense very dense sand	N/A (Database)	Not Defined
API (2011)	All sands	N/A	Not Defined

Table 2.3: *p-y models for coheisonless soils*

The above-introduced criteria are discussed in the forthcoming sections.

Reese, Cox and Koop (1974) Criteria: Their paper published in 1974, Reese and Cox used the data obtained from the lateral loading of two 24-inch diameter piles installed at the site where the soil consisted of clean fine sand to silty fine sand. The tests were performed under two types of static and cyclic loadings and the families of *p-y* curves where developed. Then, the authors suggested a semi-empirical method for predicting *p-y* curves based on the properties of the sand and the pile diameter.

The test site was located in the Mustang Island, Texas. The water level was maintained above the ground level to simulate an offshore condition, i.e. free water presence for the pile. A series of lateral loads were applied and a bending moment curve was obtained for each loading. Laboratory tests were performed on the undisturbed samples, resulting in the internal angle of friction of 39^{o}.

The typical family of *p-y* curves for the proposed criteria is shown in Figure 2.25.

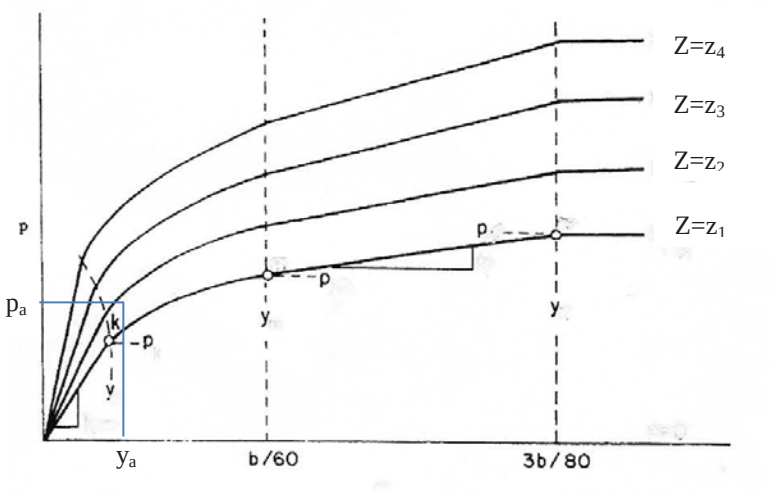

Figure 2.25: *Typical Family of p-y curves in sand (Reese, Cox and Koop, 1974)*

The authors proposed the following equations to construct a *p-y* curve;

$$P_{ct} = \gamma H[\frac{K_o H\ tan\emptyset\ sin\beta}{\tan(\beta-\emptyset)cos\alpha} + \frac{\tan\beta}{\tan(\beta-\emptyset)}(B + H\ tan\beta\ tan\alpha) + K_o H\ tan\beta\ (tan\alpha\ sin\beta - tan\alpha) -$$

$$K_a B] \quad (2.43)$$

$$P_{cd} = K_a B\gamma H(tan^8\beta - 1) + K_o B\gamma H\ tan\emptyset\ tan^4\beta \quad (2.44)$$

Where P_{ct} and P_{cd} are ultimate resistance of the soil near ground surface and well below ground surface, respectively.

In their proposed typical p-y curve, Figure 2.23, the curve is being comprised of four regions:

- A straight line from the origin to point "a"
- A parabola connecting point "a "to point "b" at the deflection of $\frac{B}{60}$
- A linear part between point "b" and point "c" with coordinates of $P_u and\ \frac{3B}{80}$
- And a straight line representing the plastic/ultimate state of the soil behavior

A step by step procedure to compute and obtain p-y curves is provided in their paper (Reese, Cox, Koop, 1974).

Murchison and O'Neill (1984) Criteria: In their paper published in 1984, the authors discussed four semi-empirical procedures for construction of *p-y* curves in cohesionless soils. The relative accuracy of each method was studied by applying each method to a variety of conditions defined in a database containing results of full scale laterally loaded piles in very loose to very dense sand. The four methods discussed/compared in their paper consisted of: a) API RP2A (1982); b) Bogard and Matlock (1980); c) Scott (1980); and d); their proposed method.

This method was originally formulated by Parker (1970) from his study of small-diameter pipe piles, and was reformulated by O'Neill and Murchison (1984).

The suggested equation for *p-y* curve in the model is:

$$P = \eta A P_u \tanh[\left(\frac{KZ}{A\eta P_u}\right) y] \quad (2.45)$$

Where P_u is the unmodified ultimate soil resistance from the formulas given in the API method. The empirical adjustment factor suggested by the authors was:

$A = 0.9$ for cyclic loads and $A = 3 - 0.8\ \frac{Z}{D}$ for static loading.

η: is the pile shape factor, equal to 1.5 for uniformly taperd piles such as timber and *H* piles, and 1.0 for circular, prismatic piles.

The general shape a group of p-y curves determined by the proposed model is presented in Figure 2.26.

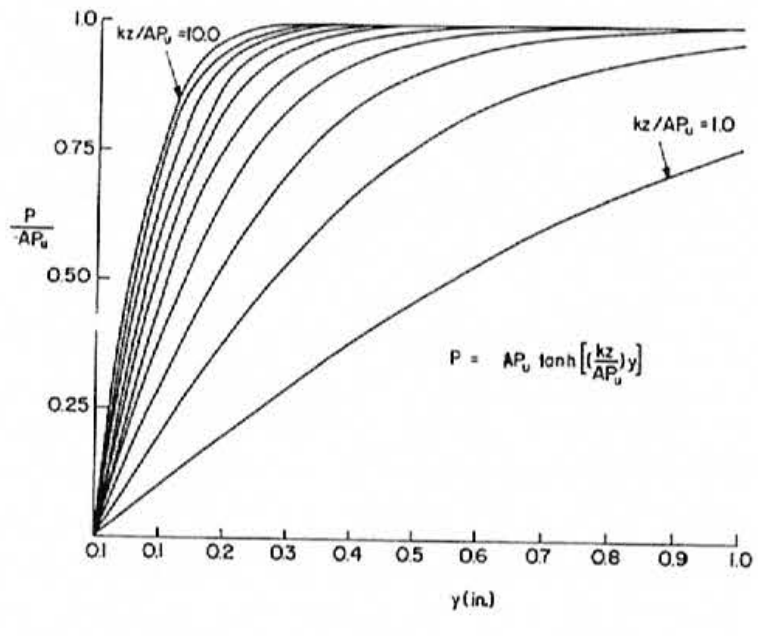

Figure 2.26: *A group of p-y curves (Murchison and O'Neill, 1984)*

The database used in Murchison and O' Neill research was small, and they concluded that the small database had some influence on the numerical error computations they did. However, they

concluded that their proposed method provided the most accurate results for the database used, in comparison to the three other models.

API Criteria: The latest editions of API provide the same approach proposed by Bogard and Matlock (1980). The ultimate lateral capacity for sands at a given depth is the smallest value of P_u from equations (2.46) and (2.47):

$$P_u = (C_1\, Z + C_2\, B)\gamma' Z \tag{2.46}$$

$$P_u = C_3\, B\gamma' Z \tag{2.47}$$

Where

P_u: ultimate resistance $\left(\frac{force}{unit\ length}\right)$

γ': submerged unit weigth

$\emptyset'$: angle of internal friction of sand

B : pile diameter

And $C_1, C_2\ and\ C_3$ are the coefficients which are the functions of $\emptyset'$, being calculated from the following equations:

$$C_1 = \frac{(\tan\beta)^2\ \tan\alpha}{\tan(\beta-\emptyset')} + K_0\ [\frac{\tan\emptyset'\sin\beta}{\cos\alpha\ \tan(\beta-\emptyset')} + \tan\beta\ (\tan\emptyset'\ \sin\beta - \tan\alpha)] \tag{2.48}$$

$$C_2 = \frac{\tan\beta}{\tan(\beta-\emptyset')} - K_a \tag{2.49}$$

$$C_3 = K_a\ [(\tan\beta)^8 - 1) + K_o\ \tan\emptyset'\,(\tan\beta)^4 \tag{2.50}$$

Where:

$$\alpha = \frac{\emptyset'}{2}, \beta = 45 + \frac{\emptyset'}{2}, K_0 = 0.4, and\ K_a = \frac{1-\sin\emptyset'}{1+\sin\emptyset'} \quad (2.51)$$

API suggests the use of the same equation (2.45) introduced by Murchison and O' Neill, which is:

$$P = \eta A P_u \tanh[\left(\frac{KZ}{A\eta P_u}\right) y] \quad (2.52)$$

2.2.4. Existing p-y Models; Weaknesses

There are limitations associated with each and any of the basic models discussed. Some *p-y* model were based on the field test measurements on instrumented piles installed and tested in a specific site/ground condition, while some other models are semi-empirical, based on works done on databases of number of laterally loaded piles. The most commonly used *p-y* models were introduced during 1960's and 1970's. As explained before, API model, which is one of the most widely used model in current practice, is mainly based on the works performed by Matlock (1970), Reese (1975) and Bogard and Matlock (1980). The main shortages and issues these models have, is briefly discussed hereafter.

Generalization of Site Specific Conclusions: Each one of the models has been prescribed for a specific type of soil, and based on the tests performed at a specific site and testing condition. Most of the commonly used models were not validated for different conditions such as wide range of soil types, different loading conditions or pile types. For example, a Matlock (1970) criterion is only applicable for submerged clay of naturally consolidated or slightly over-consolidated, while Reese and Welch (1975) approach is applicable to stiff clays.

Pile Diameter Effect: The models consider the *p-y* characteristics, i.e. subgrade modulus, independent of pile diameter. Evidence that laterally loaded pile response appears to become stiffer with increasing diameter has been reported in several cases. The works performed to

incorporate the effect of diameter dependency in characteristics of *p-y* curves has resulted in various suggestions for determination of characteristic deflection values in clays, such as:

$$y_c = 8.9\,\epsilon_{50}\,d^{0.5} \qquad \text{(Stevens and Audibert, 1979)} \qquad (2.53)$$

$$y_c = 0.8\,\epsilon_{50}\,d^{0.5}\,(\frac{E_p I_p}{E_s})^{0.125} \qquad \text{(Gaziouglu and O' Neill, 1984)} \qquad (2.54)$$

Soil Strength Change: Due to installation effects, the soil around a pile experiences physical changes. The current common models being used in practice ignore this fact. Broms (1964a, 1964b) stated that driven piles affected the soil within a distance of about 1 x pile diameter from the pile surface. The installation effect could result in increase in the relative density of cohesionless soils, and time-dependent changes in stiffness and strength of cohesive soils. Recent researches by Hwang et al., (2001) are indicative of larger disturbed distances around the piles, reported as up to 4% of pile diameter displacement at a distance of about 3 x pile diameter.

Definition of Undrained-Strength for Clays: The undrained shear strengths obtained from laboratory tests on collected samples for each one of the tests were either of or combination of; In-situ vane-shear, Miniature van-shear, unconfined compressive test (in conservative side), confined compressive test. It should be noted that undrained shear strength of clayey soils,s_u, is not a property of soils and widely depends on the test method. Actually, the in-situ undrained strength, s_u, depends on the mode of failure, soil anisotropy, strain rate and stress history. The following table retrieved from the paper published by Mayne et al. (2009), indicates versatility of s_u in relation with the laboratory test method applied:

Test Method/Mode	$S = (s_u/\sigma_{vo}')_{NC}$
Plane strain compression (PSC)	*0.34*
Triaxial compression (CK_0UC)	*0.33*
Iso-consolidated triaxial compression (CIUC)	*0.32*
Iso-consolidated triaxial extension (CIUE)	*0.24*
Direct simple shear (DSS)	*0.20*
Plane strain extension (PSE)	*0.19*
Unconsolidated Undrained (UU)	*0.185*
Triaxial extension (CK_0UE)	*0.16*
Unconfined compression (UC)	*0.14*

Figure 2.27: *Undrained strength ratios (S) for normally-consolidated Boston Blue Clay (Data from Ladd et al, 1980; Ladd & Lamb, 1963)*

Initial Stiffness of the p-y curve: The initial stiffness of *p-y* curve, i.e. the slope of linear part, in Matlock (1970) is infinity, corresponding to a stiffness of ∞. The initial stiffness of *p-y* curves for sands demonstrated by Reese et al (1975), Boagard and Matlock (1980) and API sand model, is represented by a constant rate increase, η, that specifies linearly increase of subgrade modulus reaction with depth. As stated by Brandenberg et al., (2013), values of η suggested in the API relations are based on the smallest measurable displacements from the field test, which are likely large enough to induce non-linear response in soil.

Non-linear behavior of soil begins at very small strains, about 0.001 to 0.002%, which is way smaller than the measurable displacements during filed tests. The more reasonable approach seems to be the measurement of shear wave velocity at the site and determine the initial stiffness characteristics of the soil.

Ultimate Capacity: Each of the common models discussed, suggest different equations for determining ultimate capacity/resistance of the soil around piles subject to lateral loadings.

For cohesionless soils, Broms (1964) has suggested that the ultimate capacity per unit length of pile P_u, is given by:

$$P_u = 3\, K_p\, \sigma_v'\, d \tag{2.55}$$

Reese et al (1974) suggested that the variation of $P_u$in shallower depths is initially proportional to K_p, but at greater depths is proportional to ${K_p}^3$. An intermediate approach suggested (Fleming, 1985) is:

$$P_u = {K_p}^2\, \sigma_v'\, d \tag{2.56}$$

Figure 2.28 depicts the comparison of three discussed ultimate resistances, with data points from Borton's (1982) model pile loaded laterally in a centrifuge.

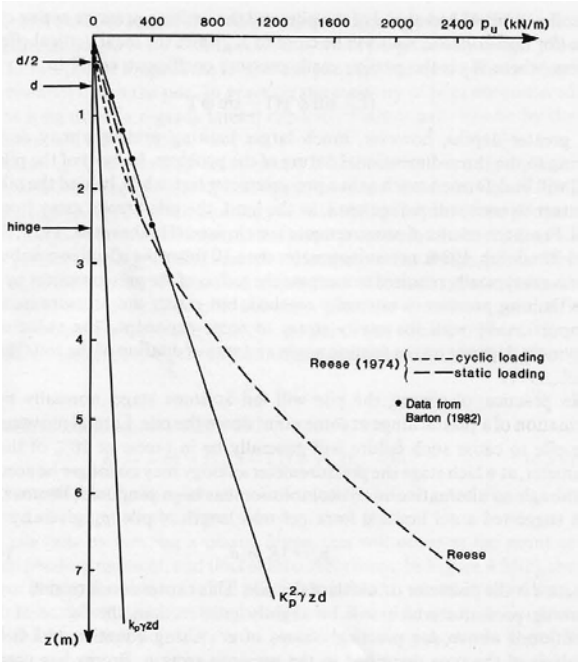

Figure 2.28: *Variation with depth of measured ultimate force down laterally loaded pule (Fleming et al., 1885)*

Shape of *p-y* curve backbone curve: Recent research has shown that there might be some problems in the conventional shape of *p-y* curves. For instance, Varun (2010) stated that the API sand curve is too linear at small strains. Brandenberg et at. (2013) demonstrated that for dynamic loads API sand backbone curve is dependent of intensity of shaking, indicating that the API functional form is not capturing the proper nonlinear backbone shape. Choi et al. (2015) suggested a uniaxial plasticity model of the nonlinear force-displacement response between laterally loaded piles and soil based on general principals of bounding surface plasticity, which overcomes some of shortcomings of *p-y* backbone curve. This model constitutes the curve portion of *p-y* relations in the proposed model. Further discussion of this curve shape used in the proposed model will be provided in the forthcoming section 3.2.5.

2.3. CPT-Based Approach

In recent era, two major thought processes have been entered into the geotechnical engineering field;

A. The need for an interpretative framework to assess the results of tests and assign parameters and/or properties based on the measured response.
B. Increasing demand and usage in employment of in-situ direct-pushed based methods using multi-measurement in-situ devices, such as the seismic cone penetration test with pore water measurement (SCPTu) and Seismic Flat Dilatometer Test (SDMT).

The first theory offering the principals of what currently is a common ground to identify the comprehensive and interpretive framework was first suggested by Schofield and Worth (1968), addressed as the critical state approach.

The basics of the "Critical State Soils Mechanics (CSSM)", to the extent which is relevant to this research, will be explained hereafter followed by the recent developments in interpretation of CPT soundings in terms of CSSM.

2.3.1. Critical State of Soil as a Framework for Behavior of Soils

The in-situ state of coarse-grained soils in geotechnical engineering practice used to be and is already being captured by relative density of the soils, *Dr*. Any particular soil can exist across a wide range of densities and it seems unreasonable to treat any particular density as having its own properties. For example, the same geological material may have a friction angle of 32^o in loose condition, when the same soil will have a larger friction angle, for instance 38^o, when compacted. The traditional geotechnical practice takes into account the density and assigns different properties to the soil according to whether it is loose or dense. In this approach, no suggestion is being made between the soil density and its behavior, as if each density of the same geological material is being treated as a different material whose properties must be established by testing.

In their theoretical approach, Schofield and Worth (1968) captured the density of soil as a state variable, rather than a soil property, and thus accounted for volume changes during shearing, was the framework that became known as the critical state soil mechanics. Simply said, the critical state of a soil is the ultimate state the soil reaches if we keep deforming (shearing) the soil. In 1936 Casagrande found out that during direct shear text, loose sand in the shear box contracted and dense sand dilated until for both sands approximately the same void ratio was approached at large strain. This is graphically shown in Figure 2.29. The reached void ratio was called the critical void ratio (e_c), and anything looser than this state ($e > e_c$) was always contractive.

The critical void ratio changes by variation in mean effective stress, becoming smaller when the mean stress increases. The relationship between critical void ratio and mean effective stress is called the critical state locus, CSL.

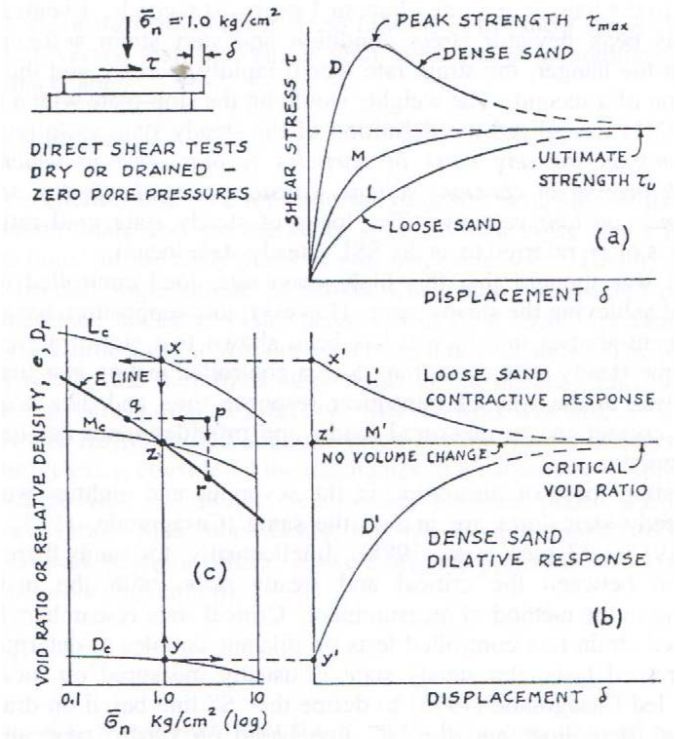

Figure 2.29: *Early hypothesis of critical void ratio by Casagrande, 1975 (Jefferies and Been, 2006)*

As concluded by Casagrande, sands dilate or contract when they are sheared until they reach the same void ratio, i.e. the critical state. The further the soil's state is from the final critical state, the faster contraction or dilation happens. The state parameter ψ, is a measure of the mentioned deviation as shown in Figure 2.30 below:

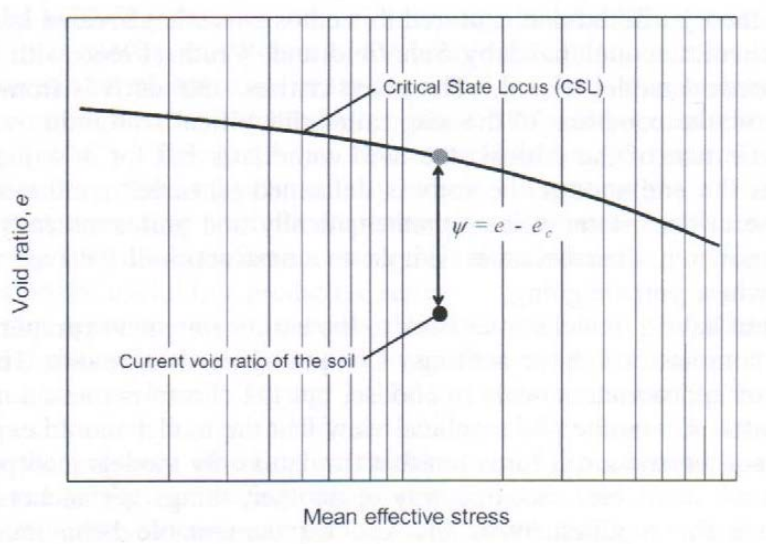

Figure 2.30: *Definition of State Parameter ψ (Jefferies and Been, 2006)*

Confining stress affects the shearing behavior of the sands. The definition of state parameter takes into consideration the stress level and it could be said that it is the magnitude of dilation that determines strength, not the void ratio or density at which dilation occurs. As Been and Jefferies (2006) stated, the state parameter, ψ, is a normalizing index for soil behavior irrespective of stress level or material type.

The critical void ratio is the void ratio of the state at which shear deformation occurs indefinitely at constant volume change, i.e. $\frac{\Delta V}{V} = 0$, and occurrence of this state of shearing is associated with the friction angle called constant volume friction angle φ_{cv} , or critical friction angle, φ_c.

Figure 2.31 (a) and (b) depicts the critical state line (CSL). As it is seen, at the critical state, there is a unique relationship between the normal effective stress, the voids ratio and the shear stress. Figure 2.31 (c) is the same re-plot of (b), with normal effective stress being plotted on a logarithmic scale.

The critical state line is defined by:

$$\tau_f' = \sigma_f' \tan \varphi_c' \quad (2.57)$$

$$e_f = e_c - C_c \log \sigma_f' \quad (2.58)$$

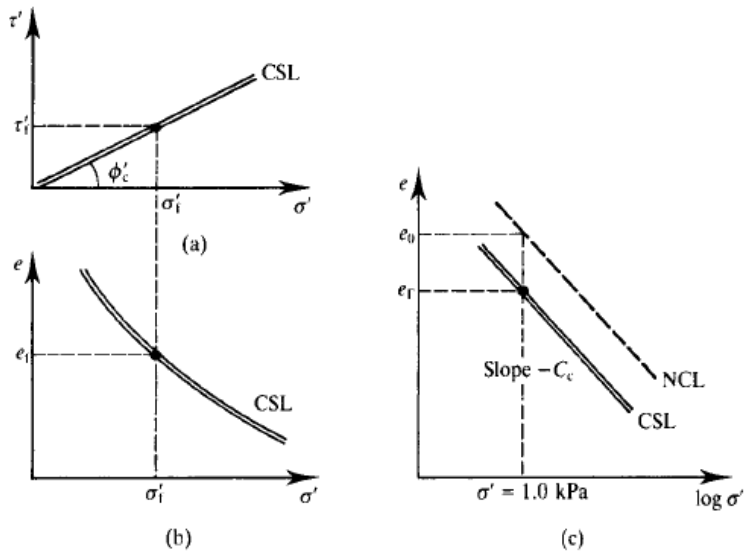

Figure 2.31: *Critical State of soils (Atkinson, 2006)*

Normal Consolidation Line (NCL) is parallel to CSL and is shown in Figure 2.31. The parameter e_c and e_0 are the points on the CSL and NCL, respectively, for a given effective stress. It should be again re-emphasize that the soil continues to deform and continue experiencing ongoing shear strain without any change in shear or effective stress or void ratio, i.e. shearing at constant rate. Due to the critical state's independency of the initial state, parametersφ_c', e_c and C_c are only related to the nature of the grains, and they are real material properties.

In Figure 2.32 (a) and (b), Atkinson (2007) re-presented the same Figure (a) and (b). Figure (c) is made by combining Figures (a) and (b), showing the relation between the void ratio and critical shear stress at failure. In saturated soils, it could be said that the void ration is simply related to the water content as shown in equation 2.59, there is a unique relationship between critical state

strength and water content. As stated by Atkinson (2007), quote: “This is the essence of the undrained strength: it is the strength of soil tested or loaded without any change in water content”.

$$e = w.G \tag{2.59}$$

Since undrained strength of the soil changes with changing void ratio, it is not considered as a material property, it is a state-dependent parameter.

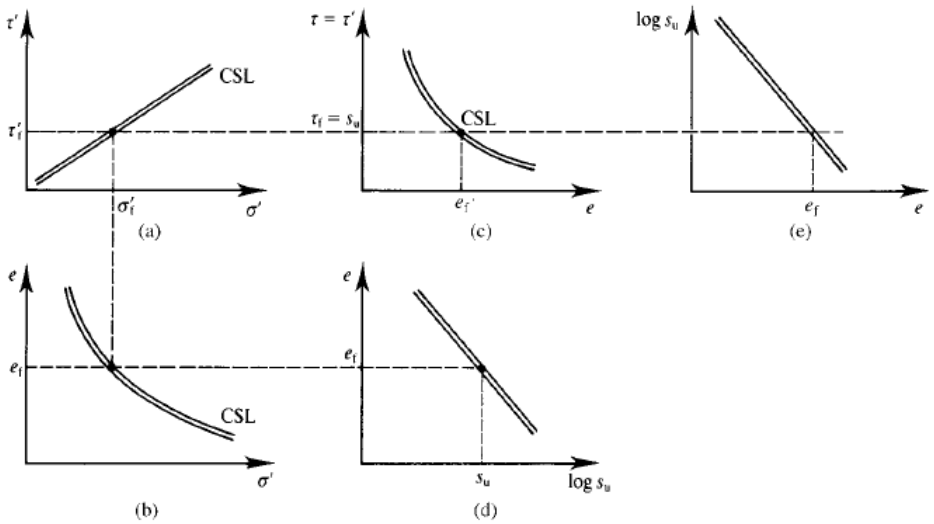

Figure 2.32: *Undrained strength of soils (Atkinson, 2007)*

As a summary, the CSSM states that regardless of the initial state of the soil, being contractive or dilative, any shearing will tend towards and eventually reach the critical state line (CSL). In the $\tau' - \sigma'$ space, the CSL is the same as effective frictional envelope defined by φ'. In the $e - \log \sigma'$ space, the CSL is parallel to the NCL given by Cc, and on the left of NCL, as shown in Figure offset to the left, as shown by the (red) dashed line in Figure 2.33.

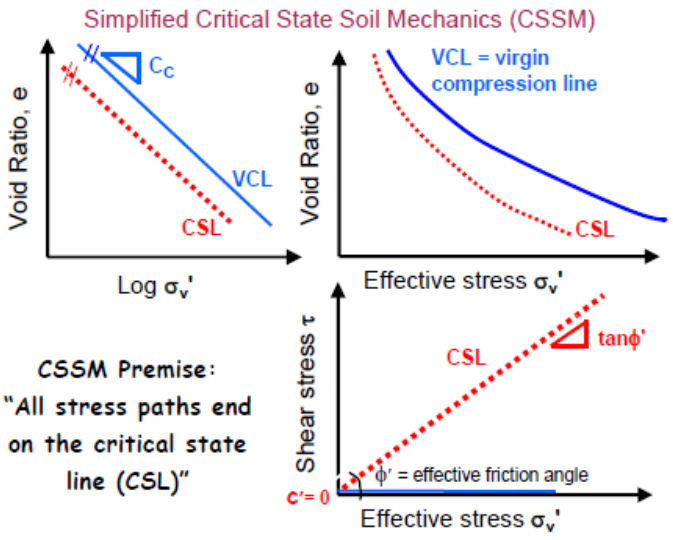

Figure 2.33: *State spaces for NC soil using simplified CSSM (Mayne, 2009)*

2.3.2. Soil Classification vs. Soils Behavior

Douglas and Olsen (1981) performed a comprehensive work on soils classification using electric CPT. Their suggested correlation was based on extensive data collected from western United States. They concluded that CPT classifications charts cannot be expected to provide accurate prediction of soil type based on grain-size distribution, but provide a guide to soil behavior type. Later, Robertson et al., (1986) and Robertson (1990) suggested use of the CPT-based charts in predicting soil behavior and mentioned that the CPT-based charts can be used in prediction soil behavior, and introduced the term Soil Behavior Type (SBT), because the cone responds to the in-situ mechanical behavior of the soil such as strength, stiffness and compressibility, and not directly to conventional soil classification criteria such as what is outlined by Unified Soil Classification System, USCS, which mainly use grain-size and plasticity. Although grain-size distribution and Atterberg limits are measured on disturbed soil samples, soil classification criteria based on grain-size distribution and plasticity often relates reasonably well to in-situ soil

behavior. Therefore, always there is often a good agreement based on USCS-based soil type and CPT-based SBT.

However, several examples might be found when classifications based on USCS and CPT is different. For instance, a soil with 60% sand and 40% fines may be classified as ‘silty sand or ‘clayey sand, using the USCS classification system. The soil behavior then will depend on the plasticity characteristics of the fines. If the fines are mostly clay with high plasticity, the soil behavior will likely be more controlled by the clay and the CPT-based SBT will reflect this behavior by predicting a more clay-like behavior, and the soil will probably will fall within the limits of Zone 4, Figure 2.35 such as ‘silt mixtures - clayey silt to silty clay. On the contrary, if the fines are non-plastic, soil behavior will be controlled more by the sand, resulting CPT-based SBT prediction of a more sand-like soil type, such as ‘sand mixtures - silty sand to sandy silt’, and the soil will probably will fall within the limits of Zone 5, Figure 2.35. As another example, very stiff, highly over-consolidated fine-grained soils will usually behave like a coarse-grained soil; they are dilatant, and can have high undrained shear strength compared to their drained strength, and CPT-based SBT for these soils can fall in either zone 4 or 5. These examples indicate that the CPT-based SBT may not always be in agreement with traditional USCS-based soil class. Especially, the majority of disagreements are likely to occur for intermediate/mixed soils region.

Availability of more data in recent years has resulted in improvements in soils classification charts. Also research has illustrated the importance of cone design and the effect of water pressure on measured cone resistance and sleeve friction. The results of recent studies also concluded that the measurement of sleeve friction (*fs*) is often less accurate and less reliable than the measurement for cone resistance, q_c (Lunne *et al*., 1986). Experience has shown that more

reliable soil classification can be made using all three in-situ measured parameters, i.e.q_t, f_s and u. In 1986, a classification approach using all three pieces of information was suggested by Robertson et. al., and is shown as Figure 2.34 below:

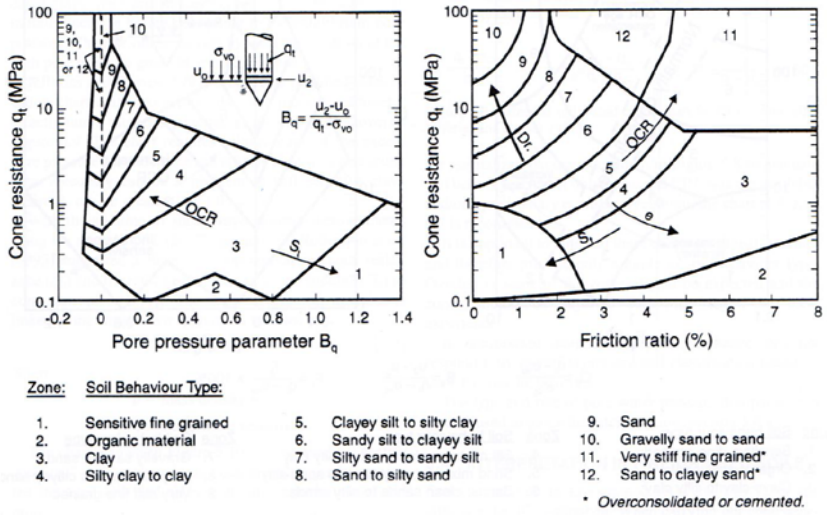

Figure 2.34: *Proposed soil behavior type classification system from CPTU (Robertson et al. 1986)*

Later, it was recognized that soils classification charts using (q_t) and (R_f), may become less accurate when due to the depth increase in the same soil, the overburden stress increases, resulting in increase in cone resistance (q_t), pore pressure (u) and friction (f_s) , which causes changes in apparent classification of the soil. The later developed approach of using charts developed based on normalized cone data resolved the issue. The two charts shown in Figure 2.35 are examples of normalized charts being widely used in soil classification.

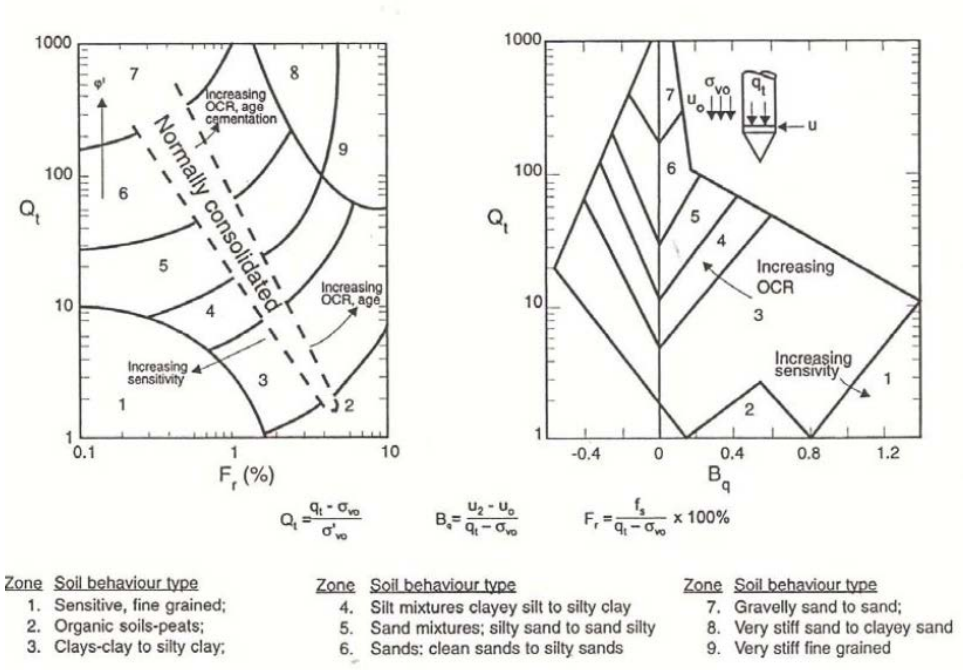

Figure 2.35: *Soil behavior type classification chart based on normalized CPT/CPTU (after Robertson, 1990)*

The most commonly used CPT soil behavior type (SBT) chart was suggested by Robertson et al. (1986) and an updated, dimensionless version (Robertson, 2010) is shown in Figure 2.36.

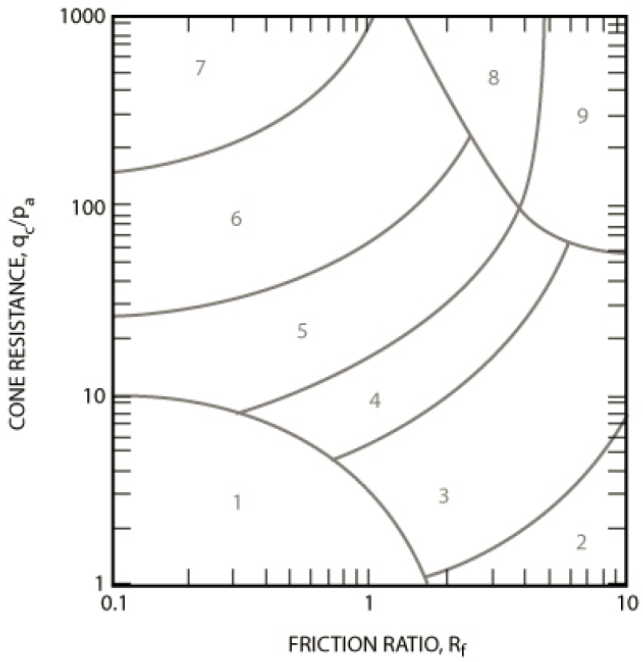

Zone	*Soil Behavior Type*
1	*Sensitive, fine grained*
2	*Organic soils - clay*
3	*Clay – silty clay to clay*
4	*Silt mixtures – clayey silt to silty clay*
5	*Sand mixtures – silty sand to sandy silt*
6	*Sands – clean sand to silty sand*
7	*Gravelly sand to dense sand*
8	*Very stiff sand to clayey sand**
9	*Very stiff fine grained**

** Heavily overconsolidated or cemented*

Figure 2.36: *CPT Soil Behavior Type (SBT) chart (Robertson et al., 1986, updated by Robertson 2010)*

The parameter Ic defined by Jefferies and Davis (1993), called Soil Behavior Type Index, later modified by Robertson and Wride (1998), and basically is the radius of concentric circles that defines the boundaries of soil type. The equation for Ic is:

$$I_c = ((3.47 - \log Q_t)^2 + (\log F_t + 1.22)^2)^{0.5} \quad (2.60)$$

Contours of Ic are shown on the normalized CPT chart in Figure 2.37 below:

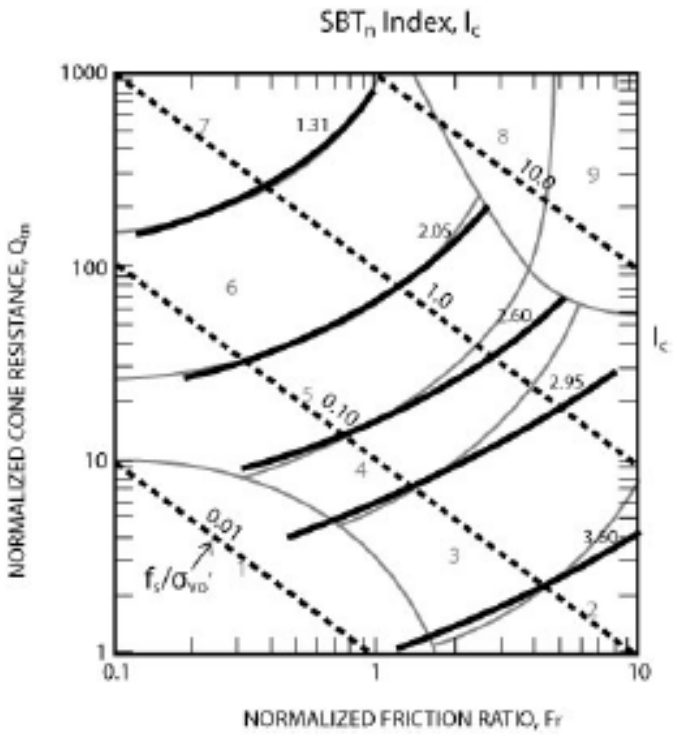

Figure 2.37: *Contours of Soil Behavior Type index, I_c on normalized SBT$_n$ Q_{tn}-F_r chart (Robertson, 1990)*

Work of Robertson and Wride (1998), later updated by Zhang et al. (2002), suggested the following normalized cone penetrometer using normalization with a variable stress exponent, n, as:

$$Q_{tn} = [\frac{(q_t - \sigma_v)}{p_a}] [\frac{p_a}{\sigma_v}]^n \quad (2.61)$$

Recently, Robertson (2009) suggested the following updated approach to allow for a variation of the stress exponent with both SBT I_c index and stress level:

Where: $= 0.381(Ic) + 0.05\ (\frac{\sigma'_v}{p_a})$)-0.15, $n \leq 1.0$ (2.62)

As stated in his paper, the above stress exponent would capture the correct in-situ state for soils at high stress level and that this would also avoid any additional stress level correction for liquefaction analyses in silica-based soils.

2.3.3. Estimating in-situ State Parameter and Friction Angle of Sandy soils from CPT

In a recent paper by Robertson (2010), the relation between state parameter ψ, and equivalent clean sand normalized cone resistance ($Q_{tn,cs}$) was evaluated with the purpose of developing a simplified method enabling to estimate state parameter and peak friction angle for sandy soils from CPT data.

As stated before, in 1998, Robertson and Wride, and as later updated by Zhang et al (2002), suggested a normalized cone parameter based procedure to evaluate soil liquefaction. The suggested normalized cone parameters included a variable stress exponent, and is:

$$Q_{tn} = \left(\frac{Q_t - \sigma_v}{p_a}\right)\left(\frac{p_a}{\sigma_v'}\right)^n \qquad (2.63)$$

Where:

$\left(\frac{Q_t - \sigma_v}{p_a}\right)$: dimensionless net cone resistance

$\left(\frac{p_a}{\sigma_v'}\right)^n$: Stress normalization factor

Later in 2009, Robertson suggested an updated approach which introduces the stress exponent as a function of both SBT I_c (soil type) and stress level:

$$n = 0.381(I_c) + 0.05\left(\frac{\sigma_v'}{p_a}\right) - 0.15 \quad where\ n \leq 1.0 \qquad (2.64)$$

Also, based on their suggestion in 1998, the equivalent clean sands value of normalized cone resistance may be found using the following:

$$Q_{tn,cs} = K_c Q_{tn} \qquad (2.65)$$

For: $Ic \leq 1.64,\ k_c = 1.0$

When: $Ic > 1.64, k_c = 5.581{I_C}^3 - 0.403{I_C}^4 - 21.63{I_C}^2 + 33.75I_C - 17.88$ (2.66)

Figure 2.38 below, depicts contours of equivalent clean sand cone resistance, $Q_{tn,cs}$ on the updated SBT chart.

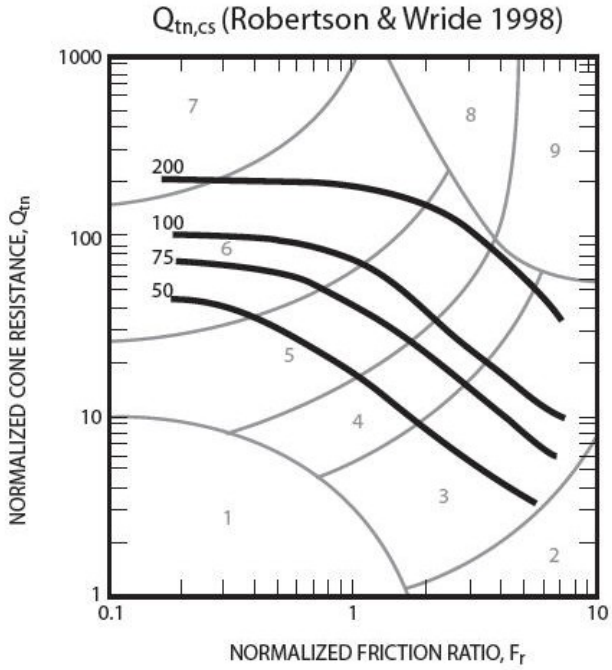

Figure 2.38: *Contours of clean sand equivalent normalized cone resistance (Robertson, 2010)*

Also in the following Figure 2.39 developed by Robertson (2009), contours of state parameter (ψ) are plotted on the updated SBTn chart.

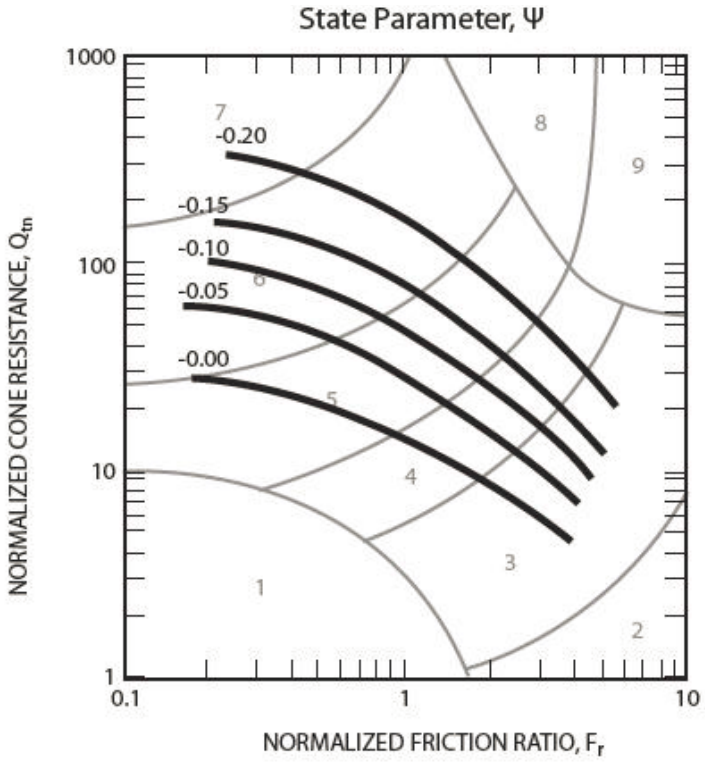

Figure 2.39: *Contours of state parameter (Robertson, 2009)*

By considering the similarity between the contours of ψ and $Q_{tn,cs}$, and based on Figures2.36 and 2.37, the following simplified relationship can be developed between ψ and $Q_{tn,cs}$:

$$\psi = 0.56 - 0.33 \log(Q_{tn,cs}) \quad (2.67)$$

In 2006, Jefferies and Been introduced a strong relation between ψ and the peak friction angle φ, suggesting the following equation derived from Figure 2.40:

$$\varphi' = \varphi_{cv}(1 - \frac{5}{3}\psi) \quad (2.68)$$

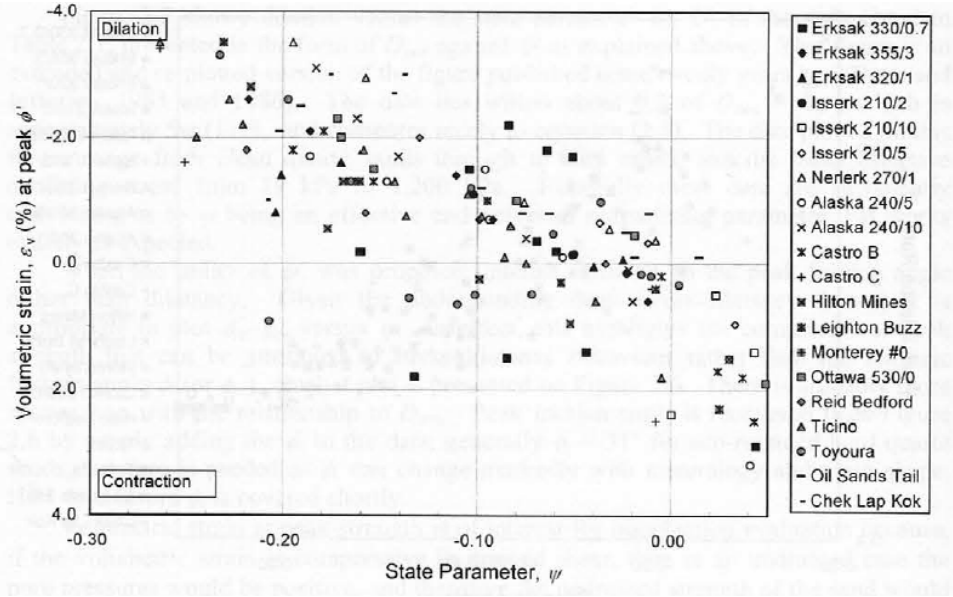

Figure 2.40: *Volumetric starin at peak stress for drained triaxial compression tests on 20 sands (Jefferies and Been, 2006)*

and by using the suggested link, Robertson(2010) suggested the following:

$$\varphi' = \varphi_{cv} - 48\,\psi \tag{2.69}$$

or

$$\varphi' = \varphi_{cv} + 15.84\,(\log Q_{tn,cs}) - 26.88 \tag{2.70}$$

Where φ_{cv} is the constant volume (critical state) friction angle of the soil.

2.3.4. Estimating in-situ Over Consolidation Ratio (OCR) and Undrained Shear Strength (Su) for fine-grained soils from CPT

For fine-grained soils, in-situ state is usually defined in terms of overconsolidation ratio (OCR).

In 1990, Kulhawy and Mayne suggested a simple relationship to find OCR from cone resistance:

$$OCR = k\left(\frac{q_t - \sigma_v}{\sigma'_v}\right) = k\,Q_{t1} \tag{2.71}$$

Where k is the preconsolidation cone factor.

Kulhawy and Mayne showed that with an expected range of 0.2 to 0.5, an average value of 0.33 can be assumed. In clays, the peak undrained shear strength, Su, and OCR are generally related. Based on SHANSEP concept, Ladd and Foott (1974) developed the following relationship:

$$\frac{S_u}{\sigma'_{v0}} = \left(\frac{S_u}{\sigma'_{v0}}\right)_{NC} (OCR)^m = S.(OCR)^m \quad (2.72)$$

Ladd and DeGroot (2003) recommended $S = 0.25$ and $m = 0.8$ for most soils.

The well-known CPT correlation, equations 2.73 and 2.74, are usually used to estimate the undrained shear strength of the clay from corrected cone resistance data:

$$S_u = \frac{(q_t - \sigma_{v0})}{N_{kt}} \quad (2.73)$$

And:

$$N_{kt} = 10.5 + 7\ \log(F_r) \quad (2.74)$$

Equations 2.73 and 2.74 should be used with utmost care and cautious, and site specific calibration should be performed when field and laboratory data for the intended site is available.

2.3.5. CSSM Framework and the CPT-based SBT Classification

As mentioned, the concept of critical void ratio was first recognized by Casagrande (1936), which later led to the first theory capturing this principal, published by Schofield and Worth (1968). It is apparent that density affects the behavior of all soils. Any particular soil under different density condition would have different properties. For example, the same quartz sand could have different friction angle while has different densities, and is not reasonable to treat each soil as a number of different soils with different properties. The needs for a framework to separate the description of soil into true properties which do not vary with density have been recognized as a long time and real need.

The CSSM based approach has in recent years found its way to the new researches using CPT in-situ tests. Mayne (1991) suggested a new approach which combined cavity expansion theory and critical state theory, and provided a CPT-based correlation to determine OCR.

Coarse-grained soils tend to respond drained during most static loading, while fine-grained soils tend to respond undrained during most loading. Soils can be dilative or contractive during shear. In general, soil behavior can be classified into four broad and general groups: drained-dilative, drained contractive, undrained-dilative and undrained contractive. Hence, it is helpful if any in-situ test can identify these broad behavior types. Although there are a large number of potential geotechnical parameters and properties, the major ones used most in practice are in general terms: in-situ state, strength, stiffness, compressibility and conductivity. In-situ state represents quantification of the density and compactness of the soil, as well as factors such as cementation.

For most soils, in-situ state is captured in terms of either relative density (*Dr*) or state parameter (ψ) for coarse-grained soils and over-consolidation ratio (*OCR*) for fine-grained soils. These 'state' parameters essentially identify if soils will be either dilative or contractive in shear. Sands with a negative state parameter (i.e. 'dense') and clays with high OCR ($OCR > 4$) will generally dilate at large strains in shear, whereas sands with a positive state parameter (i.e. 'loose') and normally to lightly over-consolidated clays *(OCR < 2)* will generally contract in shear at large strains. The tendency of a soil to either dilate or contract in shear often defines if the key design parameters will be either the drained shear strength (φ') or the undrained shear strength (s_u).

Robertson (2010) suggested superimposing of the solid line shown in Figure 2.41, here called Behavior Boundary Line (BBL), onto the following SBT_n chart. Basically, the soils location above the BBL will dilate during shearing, and the soils below the BBL will contract.

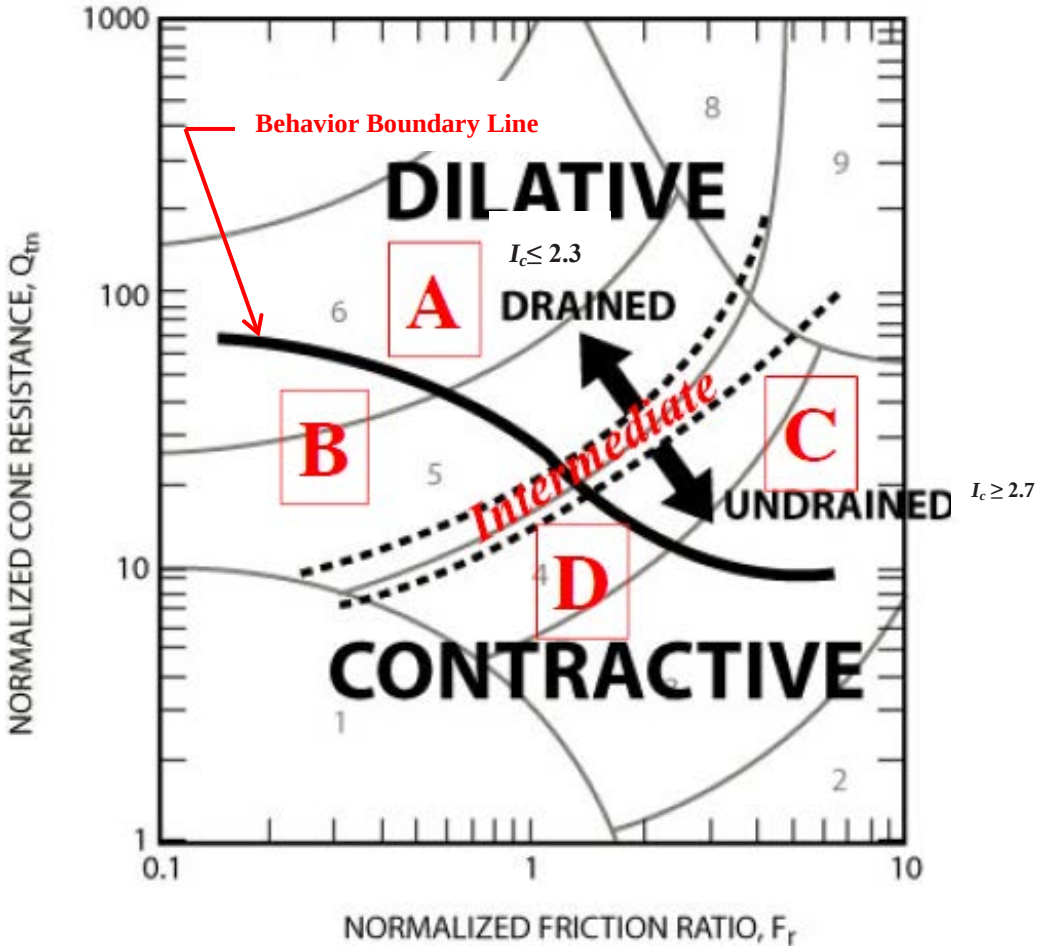

Figure 2.41: *Soil Behavior Zones on Normalized SBTn Chart (Robertson, 2010)*

Two dashed-line I_c contours shown on the chart correspond to two different regions. As suggested by Robertson, for I_c values smaller than 2.3, the soil generally responds drained as CPT penetration, while for I_c values larger than 2.7, the soil generally behaves undrained while for CPT penetration. Therefore, four explicit areas could be distinguished on the chart as:

- Zone A: Drained-Dilative soils
- Zone B: Drained-Contractive soils
- Zone C: Undrained-Dilative soils
- Zone D: Undrained-Contractive soils

2.3.6. Estimating Shear Wave Velocity from CPT-based correlations

Findings in geotechnical research over the past two decades have established that the originally-defined dynamic shear modulus *(G_{dyn})* is actually a fundamental stiffness at nondestructive strains *(G_{max})* that applies to static, cyclic, and dynamic loading, as well as to both drained and undrained conditions, also called as G_0. Therefore, G_0 is a state parameter. It is determined from the shear wave velocity *(Vs)* and total mass density ρ_t using either or both laboratory or field tests:

$$G_0 = G_{max} = \rho_t V_s$$

As a fundamental property of earth materials the shear wave velocity, V_s, is representative of the nondestructive response at very small strains. The measurement of V_s in soils can be done by using laboratory and/or field tests and these are illustrated in Figure 2.42. Different laboratory tests include the resonant column, torsional shear, bender elements. Field measurement methods include cross-hole test, downhole test, spectral analysis of surface waves, seismic cone penetration test, seismic refraction, and suspension logging technique. The stiffness of materials at small strains is finite and denoted by the low-strain shear modulus G_{max} *(G_0)*. Researches have shown that the value of G_{max} in soils is the same for both static (monotonic) and dynamic loading conditions (Jamiolkowski, et al. 1994). The magnitude of G_0 is also independent of drainage because the strains are too small to cause excess porewater pressures, and thus applies to both drained and undrained conditions.

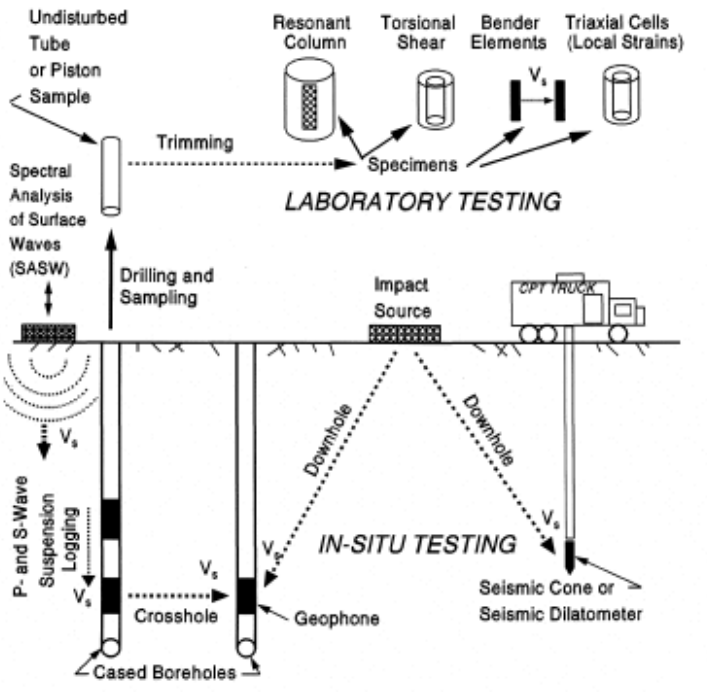

Figure 2.42: *Laboratory and field measurements for determination of shear wave velocity (VS) and small-strain stiffness, $G_0 = G_{mac} = \rho_t V_s$ (Mayne, 2000)*

The report published by the Pacific Earthquake Engineering Research Center (PEER), PEER 2012/08 dated December 2012, (Wair B.R. et al, 2012) reviews some existing correlations between V_s and field tests such as SPT and CPT. Summary of work of various researchers who studied the correlations between CPT and V_s are presented in the following tables 2.4 and 2.5.

Study	Location	# Sites	Geologic Age	Deposition	Method of V_S Measurement
Sykora (1983)	United States	9	----	----	Crosshole
Baldi et al. (1989)	Italy	2	Holocene	----	----
Hegazy & Mayne (1995)	Worldwide	61	Quaternary	Glacial, Marine, Deltaic,	Crosshole, Downhole, SCPT, SASW
Mayne & Rix (1995)	Worldwide	31	Quaternary	Glacial, Marine, Deltaic,	Crosshole, Downhole, SCPT, SASW
Piratheepan (2002)	California, Japan, Canada,	----	Holocene, Pleistocene	----	----
Mayne (2006)	Worldwide	----	Quaternary	Glacial, Marine, Deltaic,	Crosshole, Downhole, SCPT, SASW
Andrus et al. (2007)	California, Japan, South Carolina	----	Holocene, Pleistocene, Tertiary	----	SCPT, Downhole, Suspension
Robertson (2009)	Worldwide	----	Quaternary	-----	SCPT

Table 2.4: *Summary of studies between the Cone Penetration Test and V_s (Wair et al., 2012)*

Soil Type	Study	Geologic Age	Number of Data Pairs	r^2	V_S (m/s)	(Eq #)
All Soils	Hegazy & Mayne (1995)	Quaternary	323	0.70	$(10.1 \log(q_c) - 11.4)^{1.67} (100 f_s/q_c)^{0.3}$	(5.6)
	Mayne (2006)	Quaternary	161	0.82	$118.8 \log(f_s) + 18.5$	(5.7)
	Piratheepan (2002)	Holocene	60	0.73	$32.3\ q_c^{0.089} f_s^{0.121} D^{0.215}$	(5.8)
	Andrus et al. (2007)	Holocene & Pleistocene	185	(H) 0.71 (P) 0.43	$2.62\ q_R^{0.395} I_C^{0.912} D^{0.124} SF^a$	(5.9)
	Robertson (2009)	Quaternary	1,035	----	$[(10^{(0.55I_c+1.68)}) (q_t - \sigma_v) / p_a]^{0.5}$	(5.10)
Sand	Sykora & Stokoe (1983)	----	256	0.61	$134.1 + 0.0052\ q_c$	(5.11)
	Baldi et al. (1989)	Holocene	----	----	$17.48\ q_c^{0.13} \sigma'^{0.27}_v$	(5.12)
	Hegazy & Mayne (1995)	Quaternary	133	0.68	$13.18\ q_c^{0.192} \sigma'^{0.179}_v$	(5.13)
	Hegazy & Mayne (1995)	Quaternary	92	0.57	$12.02\ q_c^{0.319} f_s^{-0.0466}$	(5.14)
	Piratheepan (2002)	Holocene	25	0.74	$25.3\ q_c^{0.163} f_s^{0.029} D^{0.155}$	(5.15)
Clay	Hegazy & Mayne (1995)	Quaternary	406	0.89	$14.13\ q_c^{0.359} e_0^{-0.473}$	(5.16)
	Hegazy & Mayne (1995)	Quaternary	229	0.78	$3.18\ q_c^{0.549} f_s^{0.025}$	(5.17)
	Mayne & Rix (1995)	Quaternary	339	0.83	$9.44\ q_c^{0.435} e_0^{-0.552}$	(5.18)
	Mayne & Rix (1995)	Quaternary	481	0.74	$1.75\ q_c^{0.627}$	(5.19)
	Piratheepan (2002)	Holocene	20	0.91	$11.9\ q_c^{0.269} f_s^{0.108} D^{0.127}$	(5.20)

Units: q_c, q_t, f_s, σ_v, and σ'_v are measured in kilopascals (kPa), and depth (D) is measured in meters (m). p_a = 100 kPa.
[a]SF = 0.92 for Holocene and 1.12 for Pleistocene

Table 2.5: *Summary of studies between the Cone Penetration Test and V_s (Wair et al., 2012)*

2.3.7. Recent CPT-Based *p-y* Curve Models

Lehane and Truong (2014), and Lehane and Suryasentana (2014), suggested numerically derived CPT-bases formulations for p-y curves in soft clays and sands, respectively.

In their work for soft clay case (Lehane and Truong, 2014) they conducted numerical analysis using Plaxis 3D, the 3D FEA program, on six models of a pile with length to diameter ratio of 11.8 with a lateral load applied to the pile at 1.5 pile diameter above the ground surface. The regression analyses of all cases resulted in the following two equations:

$$\frac{p}{p_u} = tanh\left[(0.26\, I_r + 3.98)\left(\frac{y}{D}\right)^{0.85}\left(\frac{Z}{D}\right)^{-0.5}\right] \qquad \text{for: } 0 < \frac{Z}{D} < 3 \qquad (2.76)$$

$$\frac{p}{p_u} = tanh\left[(0.15\, I_r + 2.3)\left(\frac{y}{D}\right)^{0.85}\right] \qquad \text{for: } \frac{Z}{D} \geq 3 \qquad (2.77)$$

According to their work, the *p-y* curves can be directly derived from CPT, q_{net} profiles, but an additional assumption shall be made to determine the value of I_r, which is defined in the following equation:

$$I_r = \frac{1}{3}\left(\frac{E}{q_{net}}\right) N_{kt} = \frac{1}{3\epsilon_c} \qquad (2.78)$$

As a part pf their work for sands Lehane and Suryasentana (2014) proposed the following equation:

$$\frac{p}{\gamma z D} = 2.4\left(\frac{q_c}{\gamma z}\right)^{0.67}\left(\frac{z}{D}\right)^{0.75}(1 - \exp(-0.62\left(\frac{z}{D}\right)^{-1.2}\left(\frac{y}{D}\right)^{0.89}) \qquad (2.79)$$

My focus in this research is to work with real data rather than using data and models based on centrifuge test, or mini CPT in the laboratory condition. However, for one of the cases presented in the forthcoming Chapter 4, the model suggested by Lehane et al (2014) is compared with the field data and the model this research suggests.

3. Technical Approach: Calculation of p-y Material Properties from CPT Data

This section presents the methodology utilized to compute p-y material properties from CPT data. The p-y material model utilized for this work is presented first, followed by calculation of the input parameters for the p-y model based on: (1) CPT data, (2) pile properties, and (3) any available geophysical data and/or strength measurements. The input parameters to the p-y model include: ultimate capacity, initial stiffness, yield force, and a backbone shape constant. A method for interpolating the p-y properties at nodal locations for a beam on nonlinear Winkler foundation (BNWF) analysis is also presented since the number of data points in a CPT sounding typically significantly exceeds the number of nodes desired for a BNWF analysis.

3.1. *PySimple3* Material Model

Choi et al. (2015) developed a p-y material model based on bounding surface plasticity theory called *PySimple3*, which is implemented in OpenSees. Inputs to the model include the elastic stiffness, k_e, the ultimate capacity, p_u, the yield force, p_y, and a backbone shape parameter, C. The plastic modulus, k_p, is defined in Eq. 3.1, where $\dot{y}$ is the displacement rate, and p_{in} is the value of p at the start of the current plastic loading cycle.

$$k_p = C.k_e\left(\frac{p_u - p.sign(\dot{y})}{|p - p_{in}|}\right) \tag{3.1}$$

The value of p_{in} must be updated as an internal variable when a change in the direction of plastic loading occurs. Note that k_p is zero when the ultimate capacity is mobilized [i.e., when $p_u = p\ sign(\dot{y})$], resulting in a condition where p approaches p_u asymptotically as y increases. Furthermore, k_p is infinite at the start of the current plastic loading cycle (i.e., when $p = p_{in}$), resulting in the elasto-plastic tangent modulus, k, being equal to k_{max} at the beginning of plastic

loading thereby resulting in a smooth load-displacement relationship. The value of k is computed using Eq. 3.2.

$$k = \frac{dp}{dy} = \frac{k_p.k_e}{k_p+k_e} \tag{3.2}$$

Values for k_e and p_u can be readily obtained from established literature, as summarized in the literature review section of this dissertation. However, the values of p_y and C require special attention as guidance for selecting these parameters is not directly available in published literature. The following Figure 3.1 depicts the discussed components on a schematic *p-y* curve, and the ensuing sections presents the methods utilized to obtain the input parameters for the PySimple3 material model.

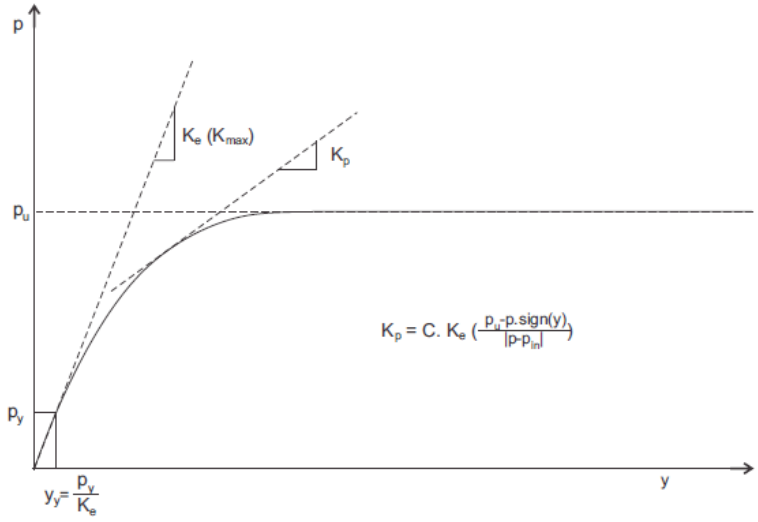

Figure 3.1: *Example p-y curve, PySimple3 model*

3.2. Computing PySimple3 Input Parameters Based on CPT Measurements

This section presents methods for using CPT data, and any other available strength data and/or geophysical data, to compute input parameters, p_u, p_y, k_e, and C, for the *PySimple3* material model. A flow chart illustrating the approach is shown in Fig. 3.2. The flow chart is divided into

four separate categories: 1. Stiffness, 2. Capacity, 3. Yield, and 4. Shape, for which the outputs are k_e, p_u, p_y, and C, respectively. Each category is discussed in detail in the sections that follow.

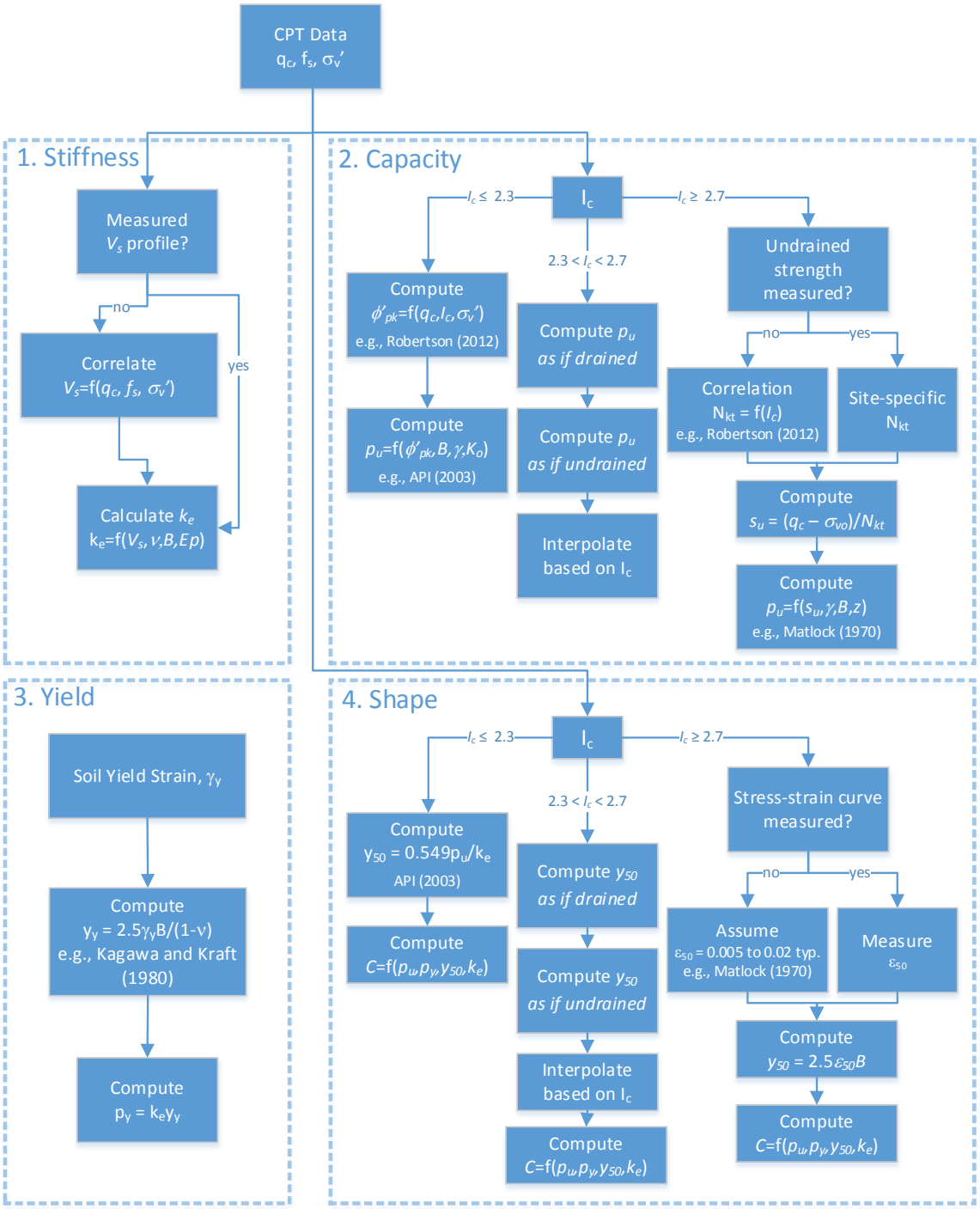

Figure 3.2: *Flow diagram of the proposed model*

3.2.1. Stiffness (Calculation of k_e)

In the proposed model, the initial stiffness of the *p-y* curves is computed from a shear wave velocity, V_s, profile, which ideally is measured using a geophysical survey. The seismic CPT approach is a natural option since CPT data are already a required input, but other methods can also be utilized. In general, methods that provide a direct measure of V_s at a specific depth (e.g., suspension logging, SCPT, cross-hole) are preferred over methods that involve significant averaging, poor resolution at depth (SASW, MASW). Non-uniqueness in the inversion of surface wave methods introduces significant potential for error in measurement of V_s at a specific depth.

While direct measurement of V_s is the recommended approach, sometimes such measurements are not available and cannot reasonably be obtained for a specific project. In these cases, a crude approximation of V_s can be obtained by correlation with CPT measurements. These correlations are generally quite poor because factors that strongly influence soil stiffness do not necessarily exert a similar influence on cone penetration resistance. For example, light cementation can significantly increase V_s, but may have little influence on cone penetration resistance.

A number of researchers have proposed correlations between CPT measurements and *Vs*, as discussed in aforementioned Section 2.3.6. In the proposed model correlations suggested by Robertson (2009), Hegazy and Mayne (1995), Mayne and Rix (1995), and Baldi et al (1989) are implemented. Robertson (2009) is for all types of soils, while the other three mentioned correlations are combined to cover the entire spectra of all types of soils. These three correlations are provided in Mayne, 2007, and for the purpose of this research and within this document will be designated as Mayne (2007) correlations.

Robertson (2009) suggested the following equation 3.3. Parameter α_{vs} called as “the shear wave velocity cone factor” is determined based on the SBT index, I_c from equation 3.4.

$$Vs = \left[\alpha_{vs}\left(\frac{q_t - \sigma_v}{p_a}\right)\right]^{0.5} \quad \textit{(m/sec)} \quad (3.3)$$

$$\alpha_{vs} = 10^{(0.55I_c + 1.68)} \quad \textit{(m/sec)}^2 \quad (3.4)$$

Robertson (2009) suggests that the provided equation may be used for all soils. As another alternative in the model, the following equations 3.5., 3.6, and 3.7, applicable to clays, sands and intermediate soils respectively, have been bundled together and used to determine V_S.

Mayne and Rix (1995) suggested the following equations 3.5 for clays.

$$Vs = 1.75\ {q_t}^{0.627} \quad (SI\ units) \quad (3.5\text{-a})$$

Where: $(q_t\ in\ KPa\ and\ V_s\ in\ {}^{m}/_{s})$

$$Vs = 100\ {q_t}^{0.627} \quad (\text{Imp. units}) \quad (3.5\text{-b})$$

where: $(q_t\ in\ tsf\ and\ V_s\ in\ {}^{ft}/_{s})$

Equation 3.6 has been suggested by Baldi et al (1989) may be used for sands.

$$Vs = 277\ {q_t}^{0.13}\ (\sigma'_{v0})^{0.27} \quad (SI\ units) \quad (3.6\text{-a})$$

where: $(q_t\ and\ \sigma'_{v0}\ in\ MPa\ and\ V_s\ in\ {}^{m}/_{s})$

$$Vs = 355\ {q_t}^{0.13}\ (\sigma'_{v0})^{0.27} \quad (Imp.units), \quad (3.6\text{-b})$$

where: $(q_t\ and\ \sigma'_{v0} in\ tsf\ and\ V_s\ in\ {}^{ft}/_{s})$

For intermediate soils the following equation 3.7, suggested by Hegazy and Mayne (1995) has been used.

$$Vs = [10.1\ log\ q_t - 11.4]^{1.67}[100\tfrac{f_s}{q_t}]^{0.3} \quad (SI\ units) \quad (3.7\text{-a})$$

where: $(q_t\ and\ f_s\ in\ KPa\ and\ V_s\ in\ {}^{m}/_{s})$

$$Vs = [21.67\, log\, q_t + 15.62]^{1.67}[100\,\tfrac{f_s}{q_t}]^{0.3} \quad (Imp.units) \qquad (3.7\text{-b})$$

where: $(q_t \; and \; f_s \; in \; tsf \; and \; V_s \; in \; {ft}/{s})$

AS a summary, the equations provided in Table 3.1 are used in this research for determination of V_s when site measurements are not available. Apparently, based on each site's specific geologic condition, other equations may be employed to determine V_S.

Studied by	Soil Type	V_S (m/s)
Hegazy and Mayne (1995)	All Soils	$Vs = [10.1\ \log q_c - 11.4]^{1.67}\left[100\,\frac{f_s}{q_t}\right]^{0.3}$ $(SI\ units)$
Mayne and Rix (1995)	Clays	$Vs = 1.75\ {q_t}^{0.627}$ $(SI\ units)$
Baldi et al. (1989)	Sands	$Vs = 277\ {q_t}^{0.13}\ (\sigma'_{v0})^{0.27}$ $(SI\ units)$
Robertson (2009)	All Soils	$Vs = \left[\left(\left(10^{(0.55I_c+1.68)}\right)\frac{q_t-\sigma_v}{p_a}\right)\right]^{0.5}$ $(SI\ units)$

Table 3.1: *Correlations used to determine V_s from the Cone Penetration Test*

The initial horizontal interaction between a laterally-loaded pile and soil does not induce nonlinearity in the pile or soil. Although the nonlinear pySimple3 model we use is linear only for very small displacements [on the order of y/B of $2x10^{-5}$ for sand (after Choi et al. 2015) and $2x10^{-6}$ for clay], the elastic slope has a significant impact on the shape of the p-y curve and the resulting tangent stiffness and hysteresis. Hence, it is important to make an accurate estimate of *Ke* in order to capture nonlinear behavior at larger strains.

Existing *p-y* relationships such as the widely-used API (1993) curve for sand and Matlock's (1970) curves for clay were derived by fitting equations that have a functional form based on theory to the results of full-scale load tests. While load tests may provide a reasonable estimate of the ultimate lateral soil resistance p_{ult}, the instrumentation used to measure strain in the pile in the

original tests was not capable of accurately measuring small enough deformations to capture the truly elastic soil behavior. Since E_s can be related to the small-strain shear modulus measured using geophysical methods, and since geophysical tests are an increasingly common part of site investigations for projects in seismic regions, a more attractive approach would relate the soil elastic Young's modulus E_s directly to the initial stiffness of the *p-y* curve K_e. Soil shear modulus *G*, shear wave velocity V_S, and Young's modulus are related through:

$$G = \rho V_S^{\,2} \tag{3.8}$$

$$E_s = 2G(1+\nu) \tag{3.9}$$

Where ν and ρ are the soil Poisson's ratio and mass density, respectively.

Several researchers performing elastic pile KSSI analyses have quantified a Winkler spring coefficient δ (sometimes called the "Winkler modulus"), where the linear-elastic Winkler spring stiffness is defined as the product of the dimensionless parameter δ and the soil modulus *Es*:

$$K_e = \delta E_s \tag{3.10}$$

In other words, δ is the ratio of the *p-y* curve elastic stiffness to the soil elastic stiffness.

Values and equations for δ for fixed- versus free-head piles and various soil properties (homogeneous, layered, stiffness increasing linearly with depth, etc.) have been proposed by many researchers including Kagawa and Kraft (1980), Roesset (1980), Dobry et al. (1982), Gazetas and Dobry (1984), Kavvadas and Gazetas (1993), Mylonakis (2001), and Syngros (2004). In these studies, a single value of δ was applied over the length of the pile in an elastic BDWF model, and the value of δ was adjusted until the pile head displacement matched the displacement computed with finite-element or boundary-element solutions under the same applied lateral force at the pile head. These values of δ were therefore not derived based on the

fundamental mechanics governing lateral soil-pile interaction during kinematic excitation. A more rigorous derivation of δ based on theory and rigorous numerical modeling is a future research need.

Syngros (2004) derived separate equations for fixed- and free-head values of δ for soil profiles with both constant stiffness (i.e., homogeneous) and linearly increasing stiffness with depth. The equations are:

$$\delta = 2.0\left(\frac{E_p}{E_s}\right)^{-0.075} \tag{3.11}$$

for a fixed-head pile in a homogeneous half-space, where Ep is the pile material Young's modulus,

$$\delta = 3.5\left(\frac{E_p}{E_s}\right)^{-0.11} \tag{3.12}$$

for a free-head pile in a homogeneous half-space,

$$\delta = 3.0\left(\frac{E_p}{E_s}\right)^{-0.08} \tag{3.13}$$

for a fixed-head pile in a soil profile with linearly increasing stiffness versus depth, and

$$\delta = 5.8\left(\frac{E_p}{E_s}\right)^{-0.13} \tag{3.14}$$

for a free-head pile in a soil profile with linearly increasing stiffness versus depth.

Dobry et al. (1982) derived the following equation for a fixed-head pile in homogeneous soil:

$$\delta = 1.67\left(\frac{E_p}{E_s}\right)^{-0.053} \tag{3.15}$$

Equations 3.11 through 3.15 are compared in Figure 3.3. Anoyatis et al. (2013) showed that the commonly-used value of δ=1.2, initially proposed by Roesset (1980) for inertial interaction cases where loading is applied at the pile head rather than from free-field seismic excitement, does not provide a good match to finite-element solutions for kinematic loading for certain pile and soil stiffness combinations. The remaining expressions for δ presented in Figure 3.3 were also derived for inertial interaction cases where loading was applied at the pile head. The difference between δ values for fixed- and free-head piles in 3 clearly shows that pile rotation or the lack thereof has a significant influence on the magnitude of the mobilized soil resistance. Near the head of a free-head pile where rotation is significant, the pile encounters greater soil resistance than a fixed-head pile because pile rotation mobilizes soil shear resistance in addition to the predominantly compressive stress induced by translation. Ideally, *p-y* curves should be formulated as *p-y-θ* curves, where θ is pile rotation. This is a future research need and will not be addressed in the current study.

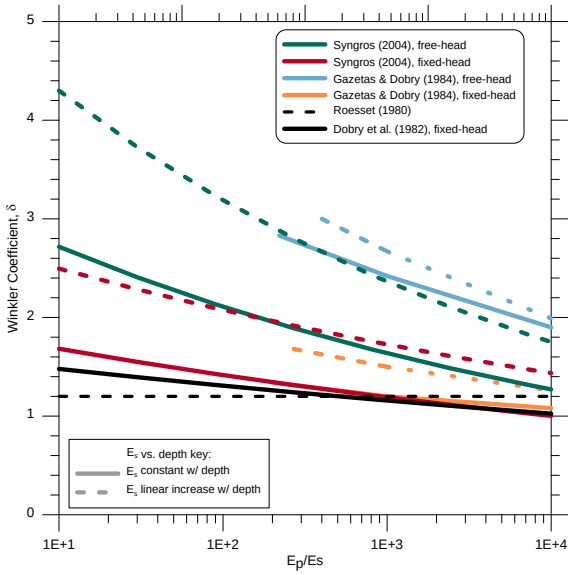

Figure 3.3: *Values of Winkler coefficient δ proposed by various researchers (prepared by Benjamin Turner, ongoing Doctoral research, UCLA-2015)*

The initial stiffness of the *p-y* curves, k_e, is related to the Young's modulus of soil, E_s, using a functional form $k_e = \delta \cdot E_s$, where δ is a constant that depends on the relative pile-to-soil stiffness (E_p/E_s), depth, and head fixity condition (k_e is generally higher for free-head than for fixed-head piles due to the influence of pile rotation). For the purpose of this study, the following equations (3.16-a) or (3-16-b) have been used for the free-head pile condition:

$$k_e = 1.6 \left(\frac{E_p}{E_s}\right)^{-0.137} E_s \qquad \text{(Gazetas and Dobry, 1984)} \qquad (3.16\text{-a})$$

$$k_e = 1.6 \left(\frac{Z}{B}\right)^{-0.13} E_s \qquad \text{(Gazetas et al., 2005)} \qquad (3.16\text{-b})$$

And for a fixed-head pile, the following equation 3.17 is being considered:

$$k_e = 0.66 \left(\frac{E_p}{E_s}\right)^{0.35} B\, E_s \qquad \text{(Gazetas et al., 1983)} \qquad (3.17)$$

Where E_p is elastic stiffness of pile and E_s is elastic stiffness of soil.

In the study by Gazetas et al. (1983), it is noticed that, with the exception of very short and rigid piles *(L/d* < 5, *Ep/Es* > 10^4), static pile stiffness are quite insensitive to variations in *L/d,* but tend to increase substantially with increasing *Ep/Es* (Gazetas et al., 1983).

The elastic stiffness of soil will be determined by the following basic equation:

$$G_0 = \rho\, (V_s)^2 \qquad (3.18)$$

$$E_0 = 2G_0(1 + \nu) \qquad (3.19)$$

3.2.2 Capacity (calculation of p_u)

Published equations for computing p_u are generally different for different soil types. For example, Matlock's (1970) equations for clay, Reese (1975) equation for stiff clay, Gazioglu and O'Neill (1984) equations for clays, Murchison and O'Neill (1984) for cohesionless soils, Reese, Cox and Koop (1974) and API equations for sand are commonly used in geotechnical engineering practice.

Such categorizations require users to pick a specific equation for the soil encountered at a specific site, which is often not a simple task. For example, are Matlock's equations applicable to unsaturated clay that may exhibit a partially drained response? What about low-plasticity fine grained soils that clearly lie between sand-like and clay-like behavior? In this dissertation, such problems are directly addressed using the soil behavior type index, I_c, as an indicator of whether the soil is behaving in a drained or undrained manner during CPT testing. Matlock's clay equations are conceptualized as corresponding to undrained loading conditions, assumed to occur when $I_c \geq 2.7$, and the API sand equations are conceptualized as corresponding to drained loading conditions, assumed to occur when $I_c \leq 2.3$. For intermediate soils with $2.3 < I_c < 2.7$, values of p_u are computed using both Matlock and API equations, and the resulting value of p_u is interpolated based on I_c.

3.2.2.1 Sand-Like/Drained Behavior ($I_c < 2.3$)

For the soils with sand-like behavior ($I_c < 2.3$), a critical state soils mechanics (CSSM) framework is utilized to compute the peak friction angle, which is then input to the API sand equations to compute p_u. The state parameter, $\psi = e - e_c$, is related to dilatancy, which in turn is related to the difference between the peak friction angle, ϕ', and critical state friction angle, ϕ'_c. As discussed in Chapter 2, Robertson (2009, 2010) developed a procedure to compute the difference between peak and critical state friction angles based on CPT data following the work of Wride et al. (2000) and Jefferies and Been (2006). The dilation angle is computed as a function of the clean-sand equivalent over-burden corrected cone tip resistance, $Q_{tn,cs}$ using Eq. 3.20:

$$\psi = 0.56 - 0.33 \log(Q_{tn,cs}) \quad \text{(Robertson, 2010)} \quad (3.20)$$

The peak friction angle is then computed from the state parameter using Eq. 3.21:

$$\varphi' = \varphi_{cv} - 48\,\psi \quad \text{(Robertson, 2010)} \quad (3.21)$$

To determine the friction angle, φ' from the equation introduced by Robertson (2010), the value of $Q_{tn,cs}$, the equivalent clean sands normalized cone resistance is to be determined from the following CPT equations:

$$q_t = q_c + (1 - a)\, u_2 \tag{3.22}$$

$$Q_{t1} = \frac{(q_t - \sigma_v)}{\sigma'_v} \tag{3.23}$$

$$Q_{tn} = \left[\frac{(q_t - \sigma_v)}{p_a}\right] \left[\frac{p_a}{\sigma_v}\right]^n \tag{3.24}$$

$$Q_{tn,cs} = k_c . Q_{tn} \quad \text{(Robertson, 1998)} \tag{3.25}$$

Where; for $I_c \leq 1.64, k_c = 1.0$,

and for $I_c > 1.64$: $k_c = 5.581{I_c}^3 - 0.403{I_c}^4 - 21.63{I_c}^2 + 33.75I_c - 17.88$

The range of critical state friction angle for quartz sand generally lies in the range of φ'_{cv} = 32° to 34° (e.g., Bolton 1986), and sands with significant feldspar content may have significantly higher critical state friction angle. A value of 32° is selected here based on the observations that the sands encountered in the analyzed load tests are quartzitic. Therefore, the peak friction angle was computed as max (32°, 32° - 48ψ).

And as outlined in API (2001), the ultimate soil resistance of the soil is:

$$p_u = Min(P_{us}\ and\ P_{ud}) \tag{3.26}$$

Where: $p_{us} = (C_1 z + C_2 B)\gamma z$ (3.27)

and $p_{ud} = C_3 B \gamma z$ (3.28)

$C_1, C_2\ and\ C_3$ are the coefficients determined from the equations given in API (2011):

$$C_1 = \frac{(\tan\beta).\tan\alpha}{\tan(\beta - \varphi')} + k_0\left[\frac{\tan\emptyset' \sin\beta}{\cos\alpha\ \tan(\beta - \varphi')} + \tan\beta\,.(\tan\varphi' \sin\beta - \tan\alpha\right] \tag{3.29}$$

$$C_2 = \frac{\tan\beta}{\tan(\beta - \varphi')} - k_a \tag{3.30}$$

$$C_3 = k_a[(\tan\beta)^8 - 1] + k_a \tan\varphi' . (\tan\beta)^4 \quad (3.31)$$

3.2.2.2. Clay-Like/Undrained Behavior (I_c > 2.7)

For the soils with clay-like behavior, (i.e., $Ic \geq 2.7$), the undrained shear strength of the in-situ soils is computed from the CPT tip resistance using equation 3.32, which is the re-written/modified version of the basic bearing capacity theory equation introduced by Terzaghi (1943):

$$s_u = \frac{(q_t - \sigma_v)}{N_{kt}} \quad (3.32)$$

Ideally, the cone factor, N_{kt}, is calibrated on a site-specific basis by measuring undrained strength independently using laboratory strength tests on "undisturbed" samples (e.g., Shelby tubes or Pitcher barrel samples, not driven split spoon samplers such as the Modified California sampler), or from in-situ vane shear measurements. However, N_{kt} is often selected based on experience with previous field measurements. The value of N_{kt} generally varies between about 10 and 20, with an average of 15 commonly used in the absence of site-specific calibration. Robertson proposed a relationship in which Nkt is related to the dimensionless sleeve friction resistance as:

$$F_r = 100 \left[\frac{f_s}{(q_t - \sigma_v)}\right] \ \% \quad (3.33)$$

$$N_{kt} = 10.5 + 7log(F_r) \quad \text{(Robertson, 2012)} \quad (3.34)$$

After estimating the undrained strength based on CPT measurements, the value of p_u can be computed. Matlock (1970) developed equations for computing p_u (Eq. 3.35). The first term in Eq. 3.18 corresponds to a wedge mechanism in which significant vertical soil movement is associated with the plastic soil failure mechanism at shallow depths due to proximity of the ground surface. The second term is associated with a flow-around mechanism in which the ground surface does not significantly alter the failure mechanism formation.

$$P_u = \left(3 + \gamma' \frac{z}{S_u} + J \frac{z}{B}\right) S_u B \leq 9 S_u B \qquad \text{(Matlock, 1970)} \qquad (3.35)$$

Where a value of $J = 0.5$ is suggested by Matlock (1970).

3.2.2.3 Intermediate Soils ($2.3 \leq I_c \leq 2.7$)

Having discussed separate CPT-based procedures to evaluate p_u for drained and undrained conditions, intermediate soils within the range of $2.3 < I_c < 2.7$ are now addressed. Intermediate soils tend to be partially drained during CPT testing. Hence the measured tip resistance cannot directly be related to a peak friction angle or undrained shear strength because the drainage boundary conditions contribute to the measured penetration resistance. Jaeger et al. (2010) demonstrate that varying the rate of cone penetration resistance can produce either drained or undrained conditions in intermediate soils (Fig. 3.4). Furthermore, they show that cone tip resistance increases as the loading rate transitions from undrained to drained loading. The increase in loading rate is caused by an increase in effective stress due to dissipation of excess pore pressures that develop during loading.

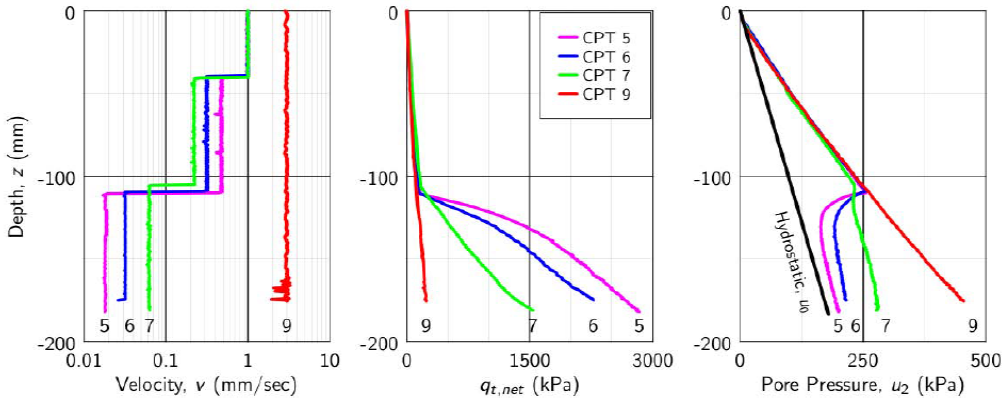

Figure 3.4: *Results of variable rate cone penetration testing in an intermediate soil (Jaeger et al. 2010)*

Jaeger et al. indicate that the drainage conditions can be related to a normalized velocity parameter, $V = v \cdot d/c_v$, where v is the penetration rate, d is the cone diameter, and c_v is the vertical coefficient of consolidation. Drained loading occurs when $V < 0.1$, and undrained loading occurs when $V > 2$, with a transition occurring between these values (Fig. 3.5).

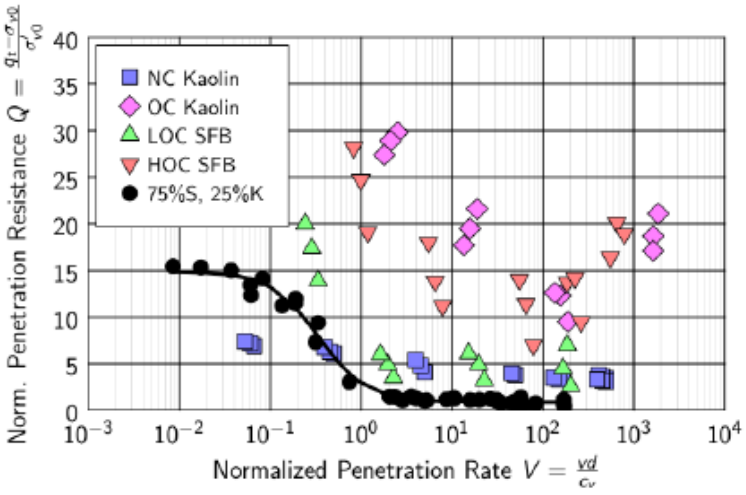

Figure 3.5: *Relation between normalize cone tip resistance and normalized penetration rate (Jaeger et al. 2010)*

The dimensionless velocity directly captures parameters pertinent to the problem, but typically the value of c_v is not known. Dissipation tests can be utilized to measure V, but dissipation tests are generally not performed at every depth where a p-y curve may be desired. Utilizing soil behavior type index as a proxy is therefore useful. Robertson (2012) indicates that the transition from drained to undrained loading occurs for values of I_c from 2.3 to 2.7, respectively.

The transition of cone tip resistance is related to two fundamental issues: (1) whether a soil is initially loose or dense of critical state, and (2) the stress path associated with cone penetration testing. Regarding (1), consider a laboratory strength test with a vertical total stress path conducted on isotropically consolidated soil that is (i) initially dense of critical ($\psi < 0$), and (ii) initially loose of critical ($\psi > 0$). Figure 3.6 illustrates the drained and undrained stress paths for

these soils in a schematic manner. The drained stress paths are illustrated with blue lines, and undrained with red lines. The soil with $\psi < 0$ is dilative, and the void ratio increases as shear strain increases in drained shearing. As a result, a peak is mobilized at the time when $de/d\varepsilon_q$ is maximum. Suppression of the dilative tendency in undrained loading causes p' to increase during shearing. Since p' at failure is higher for the undrained stress path, the undrained shear strength is higher than the drained shear strength in this case. By contrast, the soil with $\psi > 0$ is contractive, and the void ratio decreases during shearing. Suppression of the contractive tendency in undrained loading is manifested as a decrease in p'. Since p' at failure is lower for undrained loading, the undrained strength is lower than the drained strength in this case. Soil initially at the critical state void ratio would exhibit identical drained and undrained shear strengths for a vertical total stress path.

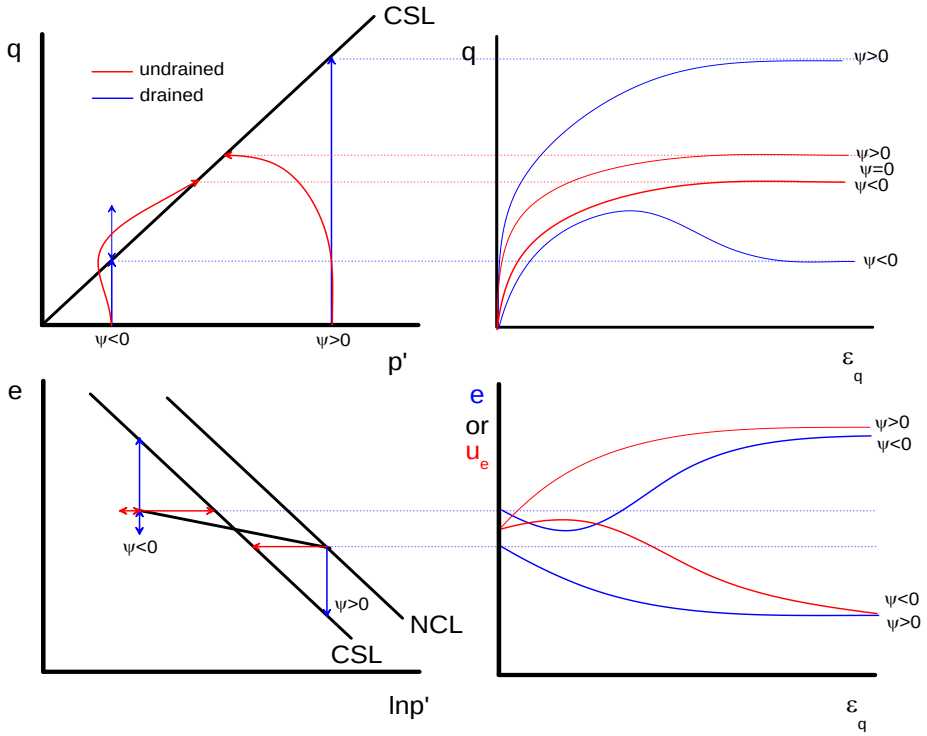

Figure 3.6: *Schematic drained and undrained stress paths for soil initially loose (ψ>0) and dense (ψ<0) of critical state. Total stress path is vertical in q-p' space.*

If the laboratory strength tests were conducted under partially drained conditions, the shear strength would be expected to lie somewhere between the drained and undraind stress paths. Figure 3.7 illustrates how drained strength transitions to undrained strength as I_c increases.

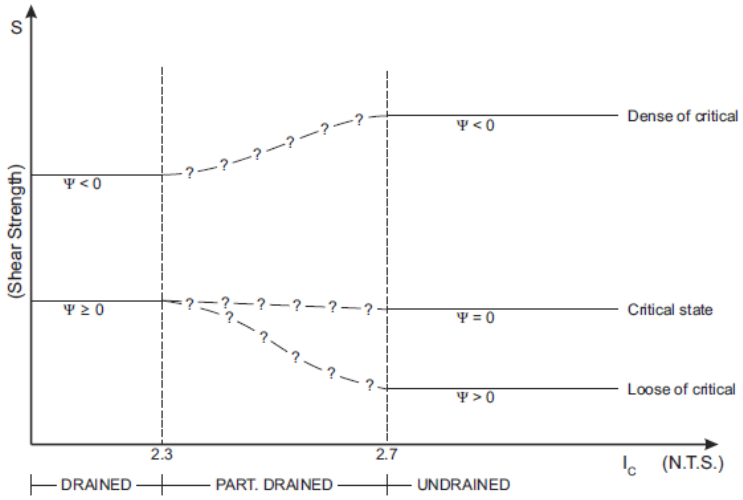

Figure 3.7: *Transition from drained to undrained strength as I_c increases.*

A vertical total stress path was selected to discuss the relation between drained and undrained shear strength in Figs. 3.6 and 3.7 because this stress path is very easy to interpret since the effective stress at failure is equal to the initial effective stress for drained loading, and because pore pressure generation is attributed entirely to shear and there is no contribution from total stress change. However, the total stress path in the soil surrounding the tip of a CPT probe is not well-represented by a vertical stress path. Rather, immediately beneath the center of the cone tip, the vertical and horizontal total stresses both increase significantly as the probe is advanced. As a result, drained loading involves a significant increase in effective stress compared to the initial condition, while undrained loading involves a significant increase in pore pressure. This stress path is illustrated schematically in Fig. 3.8. Note that the stress path varies spatially in the vicinity of the cone tip, and Fig. 3.8 is intended primarily for illustrative purposes.

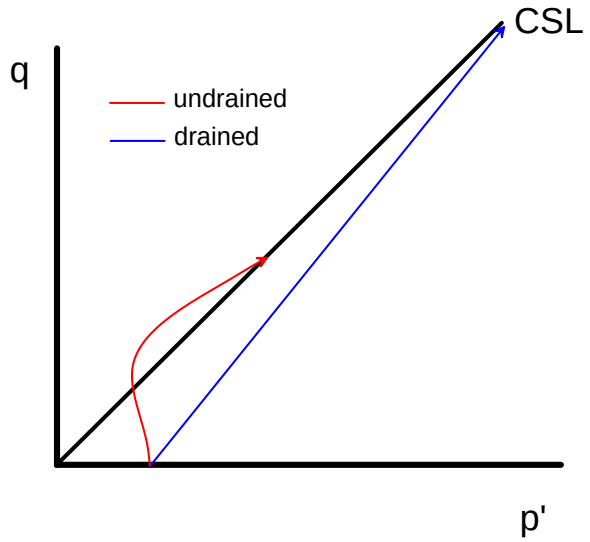

Figure 3.8: *Schematic stress path for soil immediately beneath cone tip.*

The stress path mobilized beneath a cone tip is reflected in the bearing factors that are commonly used to compute pile tip resistance (e.g., Fig. 3.9) or interpret cone penetration resistance measurements to compute undrained shear strength or drained friction angle. The bearing equation is $q_u = cN_c + qN_q$, where q_u is the ultimate resistance, c is cohesion (or undrained shear strength), q is the initial vertical effective stress at the pile tip elevation, and N_c and N_q are bearing factors that depend on friction angle. The friction angle in Fig. 3.9 corresponds to a total stress friction angle (i.e., ϕ rather than ϕ'), therefore $\phi = 0$ for undrained loading, in which case $N_q = 0$, and N_c is in the range from about 8 to 10 depending on the bearing depth ratio. For drained loading with ϕ =30°, these values increase to N_q = 30 to 60 and N_c = 50 to 100 depending on bearing depth ratio. This increase is caused by the increase in effective stress beneath the cone (or pile) tip during drained loading.

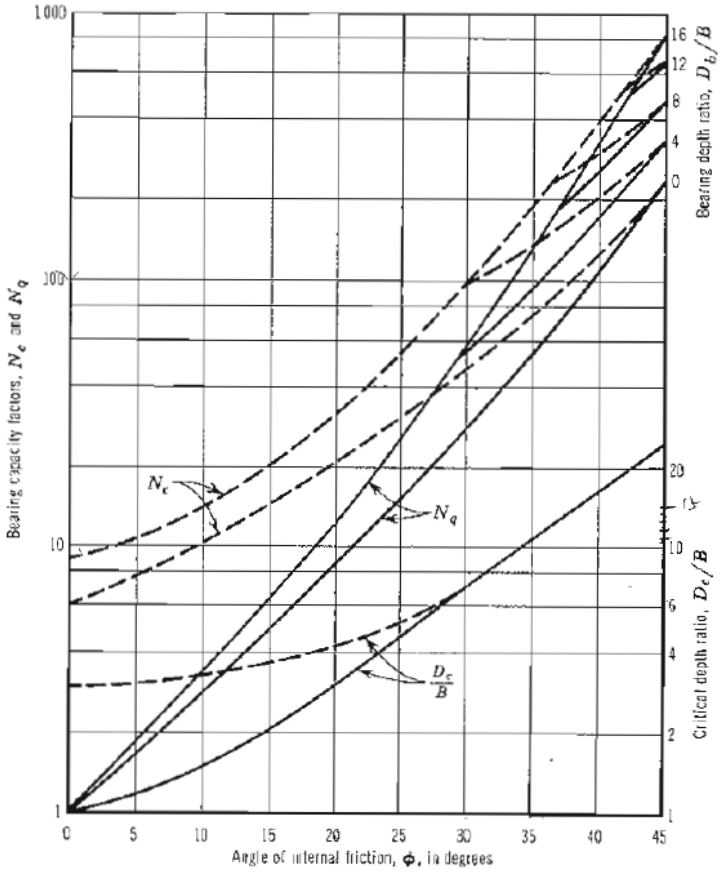

Figure 3.9: Bearing factors for pile end bearing resistance (Meyerhof 1976).

The transition from undrained to drained loading is associated with an increase in the total stress friction angle, and an associated increase in N_c and N_q. This trend is illustrated schematically in Fig. 3.10.

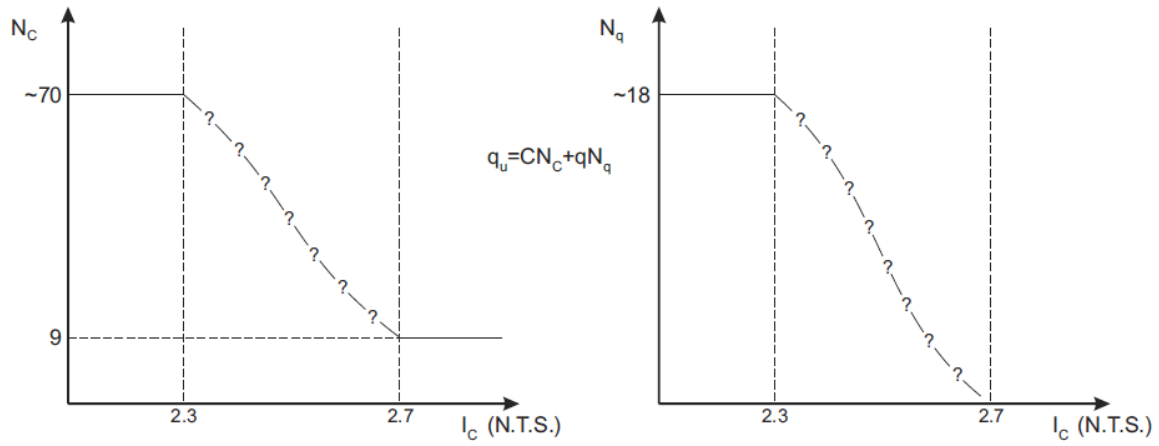

Figure 3.10: Variation of lateral pile bearing factors with I_C.

By combining the shear strength trend in Fig. 3.7 with the bearing factor trend in Fig. 3.10, the variation in cone tip resistance with I_c is illustrated schematically in Fig. 3.11. Drained strengths are always higher than undrained strengths in this figure because the influence of bearing factor (due to stress path) overwhelms the trends in shear strength. The transition from drained to undrained loading as I_c increases is not precisely known. For simplicity, it is assumed to transition linearly from the drained to the undrained tip resistance within the I_c range from 2.3 to 2.7.

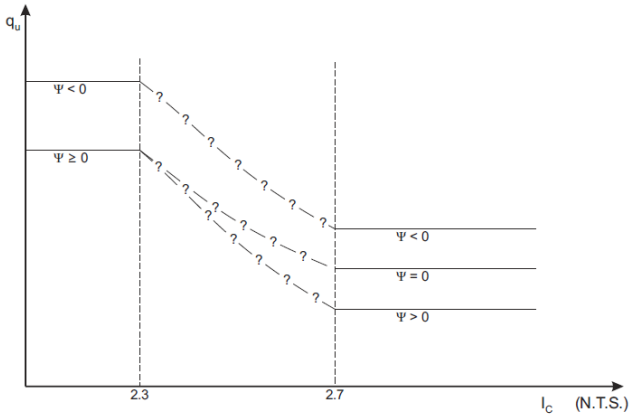

Figure 3.11: Variation of cone tip resistance with I_c

Having discussed the manner in which partial drainage influences cone penetration resistance, I now turn my attention to extending this to pile lateral loading. For simplicity, drainage conditions

encountered during CPT testing are assumed to be the same as those encountered during pile load testing. The approach adopted herein for soil with $2.3 < I_c < 2.7$ is to treat the soil as though it is drained, and compute a friction angle from the measured tip resistance, then treat the soil as though it is undrained and compute an undrained shear strength. These parameters are then input to the p-y relations to compute values of $p_{u,drained}$ and $p_{u,undrained}$. The resulting value of pu is then linearly interpolated based on I_c using Eq. 3.36.

$$p_u = p_{u,drained} + (p_{u,undrained} - p_{u,drained}) \frac{(I_C - 2.3)}{0.4} \quad (3.36)$$

This equation is considered to be a crude approximation, and should not be interpreted as rigorous in a soil mechanics context. Future research in this area may shed light on improved procedures for characterizing the properties of intermediate soils.

3.2.3. Yield (calculation of p_y)

Soil is known to exhibit nonlinear behavior at very small strains. The strain at which soil yields, γ_y, depends on soil type, plasticity index (e.g., Vucetic and Dobry 1991), and confining pressure. Figure 3.12 Influence of plasticity index, *PI* (left, Vucetic and Dobry 1991) and mean effective stress, σ'_m (right, Ishibashi 1992) on modulus reduction versus cyclic shear strain relationships. The yield strain generally varies from 0.0001% to 0.01%, increasing with increasing PI and increasing confining pressure. Nonlinear lateral pile behavior should therefore be anticipated at very small displacements because the onset of soil yielding creates nonlinearity in the soil-pile interaction response.

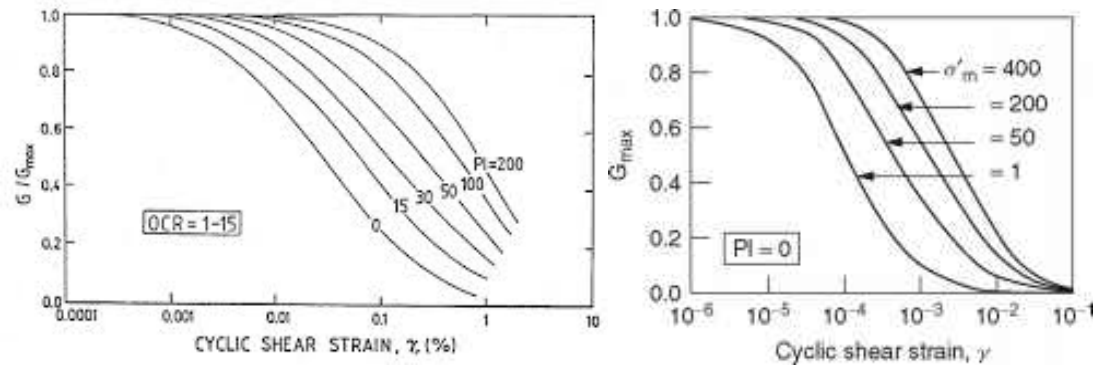

Figure 3.12: *Shear strain versus Shear modulus*

Kagawa and Kraft (1980) extended a relation by Matlock (1970) to define the maximum shear strain in the soil around a pile to the relative displacement as $\gamma_{max} = (y/B)(1+\nu)/2.5$, where ν is the Poisson ratio. The pile displacement at which soil yielding occurs can therefore be written as $y_y = 2.5\gamma_y B/(1+\nu)$

To compute p_y, the soil yield shear strain is assumed to be γ_y = 0.001% (i.e., 0.00001), and the yield displacement is computed as $y_y = 2.5(0.00001)\,B/(1+\nu)$. The value of p_y is then computed as $p_y = k_e y_y$. Assuming γ_y to be a constant value neglects the influence of plasticity index and confining pressure on soil yield strain. However, yielding occurs at a very small load regardless of the selection of γ_y, and adjusting the size of the elastic range has very little influence on monotonic pile load test behavior like the cases analyzed herein. More careful selection of p_y might be warranted for problems where the small-strain behavior is important (e.g., machine vibrations, or earthquake loading conditions).

3.2.4 Shape (calculation of *C*)

Commonly used *p-y* curves exhibit problems known to violate key principles of soil mechanics. For example, the parabolic *p-y* curve recommended by Matlock (1970) has an initial stiffness that

is infinite, whereas soil exhibits a finite elastic stiffness. The hyperbolic tangent function utilized in the API relation exhibits a very large region where the p-y behavior is essentially linear elastic, but soil is known to exhibit significant small-strain nonlinearity (e.g., Choi et al. 2015). The *PySimple3* functional form overcomes these problems by explicitly including a finite elastic stiffness and small-strain nonlinearity. However, this desired feature of behavior comes at the expense of an additional input parameter, *C*, that controls the shape of the *p-y* relation. Figure 3.13 schematically shows the effect of variations of *C* on the shape of the *p-y* curve. As *C* decreases, the *p-y* relation becomes softer. As *C* increases, the *p-y* relation becomes more elastic-perfectly plastic.

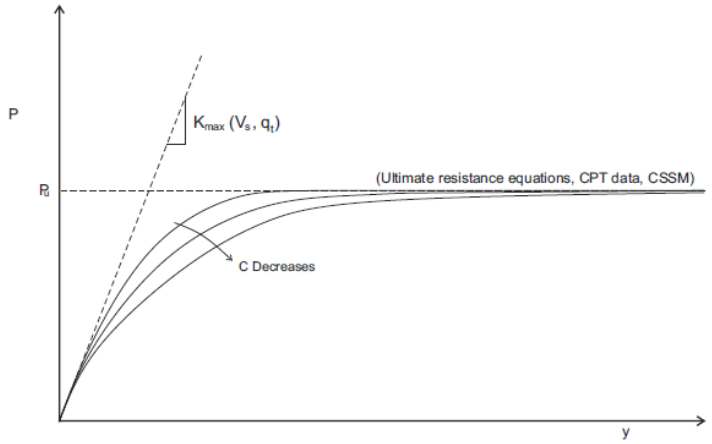

Figure 3.13: *Schematic presentation of p-y curves from the "Model"*

The approach adopted here is to set *C* to match a desired value of y_{50} (i.e., the value of *y* when $p = 0.5p_u$) computed from published *p-y* relations. The backbone behavior for post-yield monotonic virgin loading can be computed by separating variables in 3.2 and integrating as shown in Eq. 3.37, where *p'* and *y'* are dummy variables for integration.

$$\int_{p_y}^{p} \frac{k_p + k_e}{k_p} dp' = \int_{y_y}^{y} k_e dy' \tag{3.37}$$

Substituting 3.1 into 3.37, and noting that $p_{in} = p_y$ at the outset of virgin monotonic plastic loading, the integral in 3.37 simplifies to the implicit expression given by 3.38.

$$(p - p_y)(C - 1) - (p_u - p_y)\left[ln(p_u - p) - ln(p_u - p_y)\right] = Ck_e(y - y_y) \quad (3.38)$$

Substituting $p = 0.5p_u$ and $y = y_{50}$, and solving for C results in Eq. 3.39:

$$C = \frac{p_y - 0.5p_u + (p_u - p_y)\ln(p_u - p_y) - (p_u - p_y)ln(0.5p_u)}{k_e.y_{50} - 0.5p_u} \quad (3.39)$$

For clay like-behavior, (i.e. $I_c \geq 2.7$), Matlock (1970) recommended computing the value of y_{50} using the following equation:

$$y_{50} = 2.5\ \varepsilon_{50}\ B \quad (3.40)$$

The parameter ε_{50} is the axial strain at which 50% of the soil capacity is mobilized in a triaxial compression test. Matlock (1970) suggests a range from 0.005 to 0.02 for ε_{50} for different clays, with an intermediate value of 0.01 being satisfactory for all clays. Ideally, ε_{50} would be measured for a particular soil type, but more commonly a reasonable average value of 0.01 is assumed.

For sand-like behavior, (i.e. $I_c \leq 2.3$, the API (2003) hyperbolic functional form is used to compute a value of y_{50}. The hyperbolic function is defined as:

$$p = p_u \tanh\left(\frac{k_e y}{p_u}\right) \quad (3.41)$$

Note that the API formulation multiplies p_u by a depth-dependent variable, A, that adjusts the load transfer curves to match field measurements. The A variable is omitted here because p_u is taken to be the true ultimate capacity. Substituting $p = 0.5p_u$, and $y = y_{50}$, the resulting value of y_{50} is:

$$y_{50} = 0.549\ \frac{p_u}{k_e} \quad (3.42)$$

For intermediate soils with 2.3 < I_c < 2.7, the value of y_{50} is linearly interpolated between the values for sand-like and clay like behavior. The resulting equation is:

$$y_{50} = 2.5\,\varepsilon_{50}\,B + \left(0.549\frac{P_u}{K_{max}} - 2.5\,\varepsilon_{50}\,B\right)\left(\frac{I_c - 2.3}{2.7 - 2.3}\right) \quad (3.43)$$

3.3. Layering Effects

The influence of layer interfaces on p-y behavior has long been recognized as an important issue. For example, when a pile is pushed into a profile consisting of a stiff layer over a soft layer, the stress conditions in both soil layers are altered from what would exist if the pile were pushed into a uniform profile of either layer. Georgiadis (1983) developed a procedure to approximate layering effects that uses the concept of an "equivalent depth". This procedure is implemented in LPile, so is worth discussing here in some detail. For a layer 1 of thickness H_1 overlying layer 2, the procedure operates by first computing the integral of p_u over the thickness of layer 1:

$$F_1 = \int_0^{H_1} p_{u1}(z)dz \quad (3.44)$$

Then an "equivalent thickness" H_2* of the layer 2 soil is solved such that the integral of p_u based on the layer 2 material properties is equal to F_1:

$$F_1 = \int_0^{H_2^*} p_{u2}(z)dz \quad (3.45)$$

If a function $p_{u2}(z)$ is a known integrable function, H_2* can be solved analytically. The values of pu in layer 2 are then computed by assuming that the soil profile consists of the material properties for layer 2 with the top of the layer at a height of H_2* above the layer interface. This procedure is then repeated for all of the layers in the profile. The method adjusts the properties of

an underlying layer to account for the influence of the overlying layer, but the inverse is not true; overlying layers are not adjusted to account for the presence of underlying layers.

Yang and Jeremic (2002) performed three-dimensional finite element simulations of piles in layered soil profiles consisting of two sand layers (φ =37.1°, γ = 14.5 kN/m3) with a clay layer (S_u = 21.7 KPa, γ = 13.7 kN/m3) sandwiched in between, and two clay layers with a sand layer sandwiched in between. The pile material was elastic with the Young's modulus of aluminum for their study, and the pile section consisted of a square with side length of 0.429m. The piles were also analyzed with uniform clay and uniform sand properties for comparison with the layered cases. By comparing subgrade reaction loads in the layered profiles with those in the uniform profiles, they found that the stronger sand layer exerted little influence on the mobilized subgrade reaction loads in the clay, but that the weaker clay layer had a significant influence on the mobilized subgrade reaction loads in the stronger sand. Figure 3.14 shows the mobilized subgrade reaction distribution for a profile with a layer of clay sandwiched between layers of sand. In the upper sand layer, the subgrade reaction increases to a depth of approximately 1.3 m, then decreases below that depth until it reaches the interface between the sand and clay at about 1.72m. The zone of influence is therefore approximately one pile diameter. The mobilized subgrade reactions in the clay are very similar to those that were mobilized at the same pile displacements for the uniform clay profile, though they are slightly higher in a very limited range near the layer interfaces. Subgrade reactions in the lower sand layer are large at the interface, and decrease with depth because the pile displacement is not large enough to mobilize the soil capacity. The key lessons learned from the Yang and Jeremic study are: (1) soft/weak layers introduce a softening effect on stiff/strong layers, whereas stiff/strong layers exert little influence on subgrade reaction

of soft/weak layers, and (2) the zone of influence of a soft/weak layer on a stiff/strong layer is approximately 1 pile diameter.

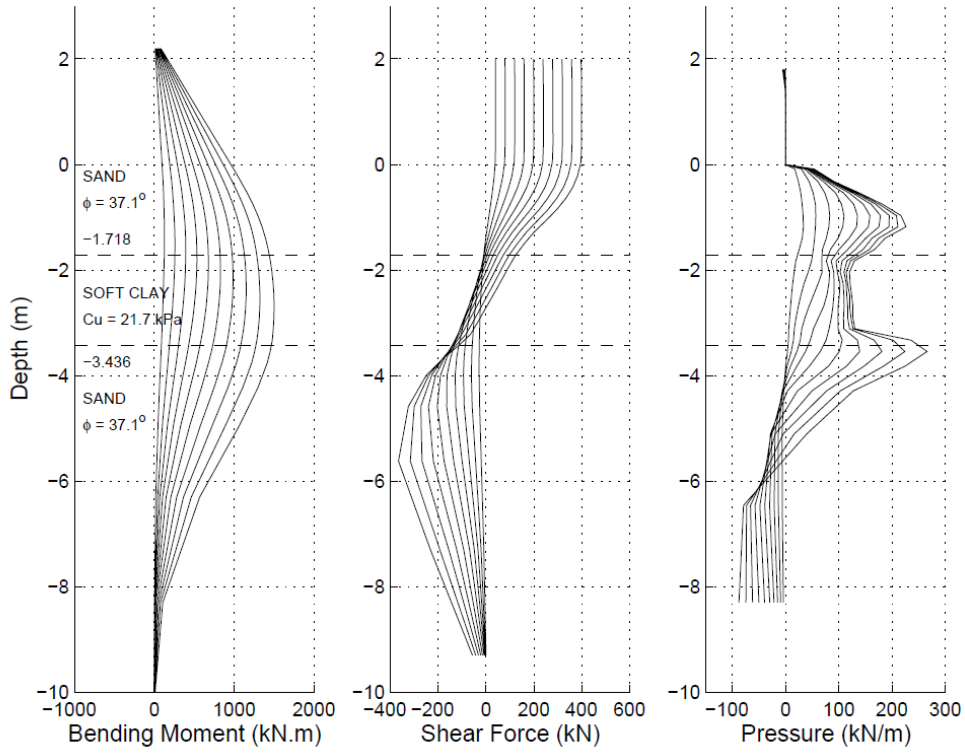

Figure 3.14: *The mobilized subgrade reaction distribution for a profile with a layer of clay sandwiched between layers of sand (Yang and Jeremic, 2002)*

Implementing these findings in a simple profile consisting of only a few layers is a relatively straightforward task; the values of p_u can simply be linearly interpolated in the stiff/strong layer over a thickness of one pile diameter from the layer interface. However, implementing these findings for a CPT profile in which the values of pu change significantly over short distances is more challenging. The procedure adopted herein is to utilize Gaussian weighting functions with the standard deviation equal to half of a pile diameter. The weighting function at a particular depth k for a value of p_u at a depth of j is defined in equation 3.46, where *dnorm*((x, μ, σ) is the

probability density at point x for a normally distributed random variable with mean μ and standard deviation σ.

$$w_{k,j} = \frac{dnorm(depth_k, depth_j, 0.5B)}{\sum_k dnorm(depth_k, depth_j, 0.5B)} \tag{3.46}$$

Applying these weights directly to a profile of p_u would result in the strong layers exerting more influence on the value of p_u than the weak layers. For this reason, the weights are applied to the inverse values of p_u to obtain a profile that accounts for layering effects denoted p_{ul}:

$$\frac{1}{p_{ul_j}} = \sum_k \frac{1}{p_{u_k}} w_{k,j} \tag{3.47}$$

The resulting interpolation scheme is shown in Figure 3.15 using the profile from Yang and Jeremic (2002) with clay sandwiched between two sand layers. Values of p_u were computed using API sand (2011) for the sand layers and Matlock (1970) for clay. The depth is truncated at 4m to focus on the layer interface behavior. The depth sampling interval is 0.001m, and the resulting weighting function at the upper interface between the sand and clay is plotted in 3.15a. The values of $1/p_u$ are then plotted in Figure 3.15b, along with the weighted values obtained by multiplying $1/p_u$ by the weights in Figure 3.15a. The weighted values are then summed, and the value of $1/p_{ul}$ is plotted at the layer interface as a red circle in Figure 3.15b. This process was repeated at every depth to obtain the layer-corrected profile p_{ul} in Figure 3.15c. This relatively simple algorithm reproduces the key aspects observed by Yang and Jeremic, including a significant reduction in the strength of the sand layers near the interfaces, and a mild increase in p_u in the clay near these interfaces. Furthermore, the zone of influence is approximately one pile diameter.

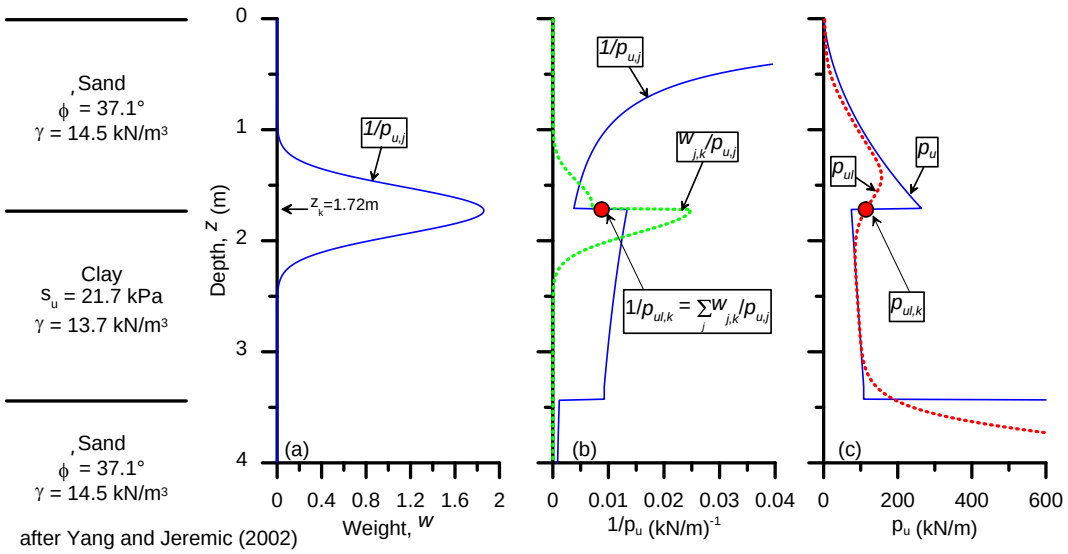

Figure 3.15: *Illustration of weighting scheme adopted to account for layer interface effects.*

3.4. Example Calculations

This section presents an example calculation of the inputs to the *PySimple3* material model for drained conditions with $I_c \leq 2.3$, undrained conditions with $I_c \geq 2.7$, and an intermediate case with $2.3 < I_c < 2.7$. The example calculation is performed at a single depth (i.e., for a single q_c, f_s, σ'_v) for each of the three cases and the resulting *p-y* curve is plotted for each. Values of V_s and S_u are assumed to be known from independent or correlations. The influence of uncertainty in V_s parameters is studied in Chapter 4.

Example 1; Calculation for $I_c \leq 2.3$: The following step by step calculations follows the aforementioned procedures. At a selected depth, the CPT data and calculated values are:

q_t (tsf)	fs (tsf)	σ_v (tsf)	σ'_v (tsf)	I_c	Q_{tn}	$Q_{tn,cs}$
176.23	1.58	0.664	0.664	1.64	210.1	209.7

Using the equations provided in section 3.2.2.1, the followings are determined:

ψ	φ' (degree)	p_{us} (ton/1-ft length of plile)	p_{ud} (ton/1-ft length of plile)	p_u (ton/1-ft length of plile)	V_s (ft/sec)	$k_e(k_{max})$ (tsf)	y_{50} (inch)
-.021	41.9	41.983	94.45	41.98	871.8	2749	0.125

By using equation 3.39, the value of *C* is calculated as 3.81.

The inputs to determine a p-y curve using PySimple3 model then are:

p_u =41.98 (ton/1-ft L. of pile) = 6.99 (kips/1-inch L. of pile)

$k_e(k_{max})$ =2749 (tsf) = 38.18 (kips/in2)

And: *C*=3.81

The resultant *p-y* curve is shown in Figure 3.16.

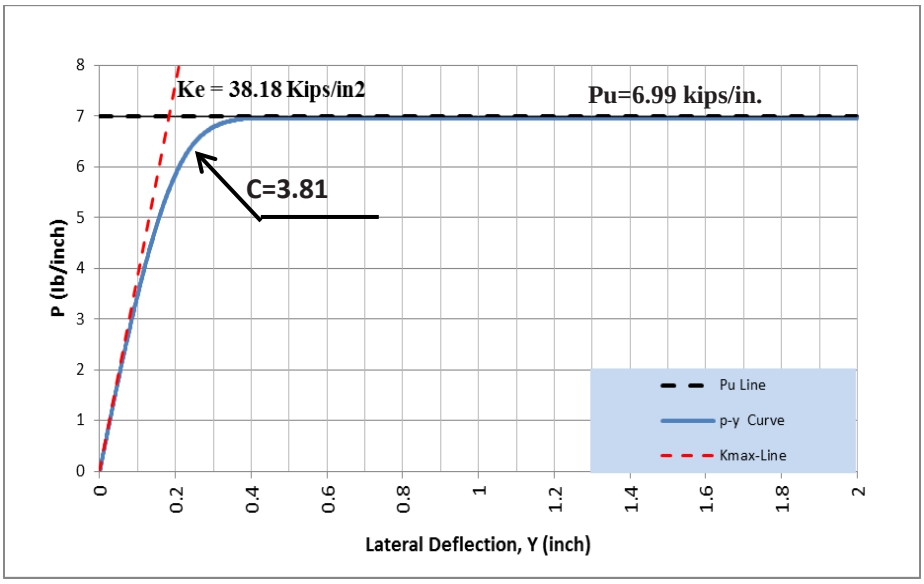

Figure 3.16: *Example 1, p-y curve for sand-like behavior (drained condition),*

Example 2; Calculation for $I_c \geq 2.7$:

At a selected depth, the CPT data and calculated values are:

q_t (tsf)	fs (tsf)	σ_v (tsf)	σ'_v (tsf)	I_c	Q_{tn}	$Q_{tn,cs}$
2.89	0.11	0.89	0.38	3.38	5.29	63.12

Using the equations provided in section 3.2.2.1, the followings are determined:

N_{kt}	S_u (psf)	p_u (ton/1-ft length of plile)	V_s (ft/sec)	$k_e(k_{max})$ (tsf)	y_{50} (inch)
15.7	255.2	1.59	265	1319.6	0.6

By using equation 3.39, the value of *C* is calculated as 0.033.

The inputs to determine a *p-y* curve using PySimple3 model then are:

p_u =1.59 (ton/1-ft L. of pile) = 265 (lb/1-inch L. of pile)

$k_e(k_{max})$ =1319.6 (tsf) = 18330 (lb/in2)

And: C=0.033. The resultant *p-y* curve is shown in Figure 3.17.

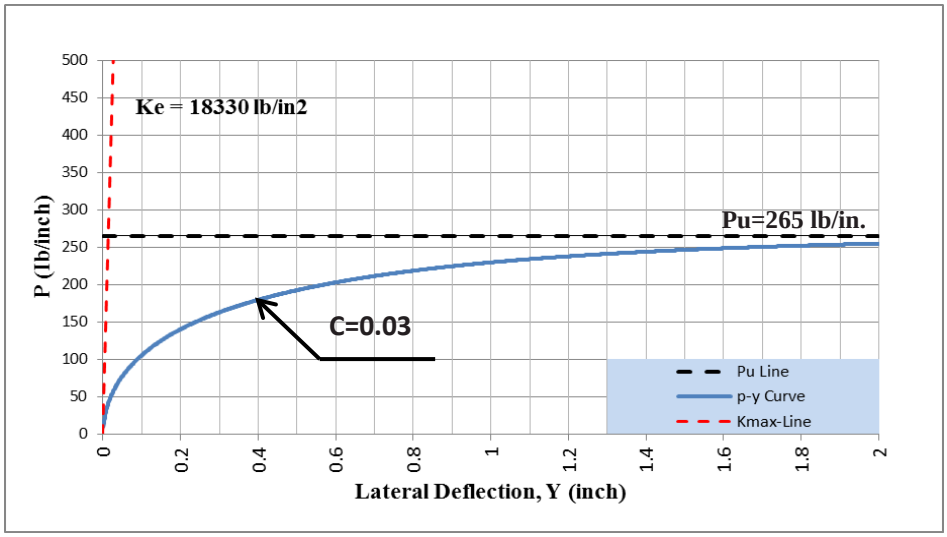

Figure 3.17: *Example 1, p-y curve for clay-like behavior (undrained condition),*

Example 3; Calculation for 2.3 < I_c < 2.7:

At a selected depth, the CPT data and calculated values are:

q_t (tsf)	fs (tsf)	σ_v (tsf)	σ'_v (tsf)	I_c	Q_{tn}	$Q_{tn,cs}$
24.53	0.55	0.63	0.63	2.497	34.59	95.41

Using the equations provided in section 3.2.2.1, the followings are determined:

φ' (degree)	p_{u-sand} (ton/1-ft length of plile)	N_{kt}	S_u (ksf)	p_{u-clay} (ton/1-ft length of plile)	p_u (ton/1-ft length of plile)	V_s (ft/sec)	$k_e(k_{max})$ (tsf)	y_{50} (inch)
36.5	27.20	13.1	3.66	13.05	17.98	526	3749	0.31

By using equation 3.39, the value of *C* is calculated as 0.058.

The inputs to determine a *p-y* curve using PySimple3 model then are:

p_u =17.98 (ton/1-ft L. of pile) = 2.99 (Kips/1-inch L. of pile)

$k_e(k_{max})$ =37496 (tsf) = 52.08 (Kips/in^2)

And: *C*=0.058. The resultant *p-y* curve is shown in Figure 3.18.

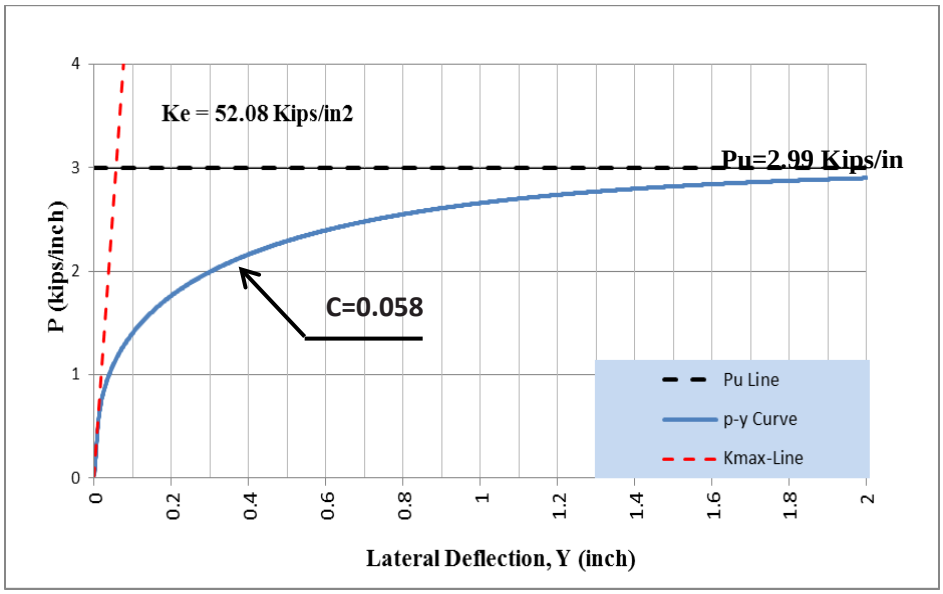

Figure 3.18: *Example 1, p-y curve for partially drained soils*

4. Description of Filed Data and Analysis Results

This chapter includes the available data for five different case histories and the results of analysis for each case by the suggested model. A total of more than twenty pile load test case histories were investigated. Table 4.2 presents list and general information of the studied cases. Five cases were selected for analysis because cone penetration test data were also available at the site for the pile load test. The five sites are summarized in Table 4.1:

SITE	PREDOMINANT SOIL TYPE	LOAD TEST MEASUREMENTS	REFERENCES
Oakland California, Site 2	Soft Saturated Clay, San Francisco Bay Mud	Load-Displacement at pile head, pile slope, and back-calculated p-y relations	Lemke (1997)
Oakland California, Site 4	Soft Saturated Clay, San Francisco Bay Mud	Load-Displacement at pile head, pile slope, and back-calculated p-y relations	Lemke (1997)
Hawthorne California	Stiff Unsaturated Sandy Clay	Load-Displacement at pile head, bending moment along pile, inferred p-y relations	Lemnitzer et al (2010), Khalili Tehrani (2014)
Los Angeles International Airport	Sandy Fill	Load-Displacement at pile head	Diaz Yourman Associates, personal communications (2015)
University of British Columbia	Soft Clay	Load-Displacement at pile head	Davies (1987)

Table 4.1: *Summary Information of Analyzed Case Histories*

The predominant soil types for the selected sites range from soft saturated bay mud to stiff dry sand, and include some "intermediate" materials for which the CPT test is partially drained. All of these soil conditions are analyzed using a single framework for relating CPT measurements to *p-y* behavior, therefore having a range of soil conditions in the available lateral load test database was important.

This chapter presents details of each of the case histories, including a brief introduction of the site, geological and soils condition at the site, explanation of any available laboratory data and/or

geophysical data, plots of cone penetration test results, lateral load testing results, and the results of analysis by the “Model” is presented for each case, compared with available field data on tested piles for each case.

DOCUMENT	PUBLISHER/AUTHOR/YEAR	SITE LOCATION	PILE TYPE	TEST TYPE	SOIL CONDITION	AVAILABLE DATA FROM FIELD AND LAB MEASUREMENT							
						CPT	CPTU	SCPT	SPT	Su	Φ	HEAD F-D	P-Y CURVE
Nonlinear Load Deflection Behavior of Reinfored Concrete Drilled Piles In Stiff Clay	P. Khalili-Tehrani, J.P.Stewart, J. Wallace, E. Taciroglu, A. Lemnitzer/2012	Hawthorne, CA	CIDH-C	C	Stiff Clay	Y	N	N	Y	Y	N/A	Y	Y
Correlations for Design of Laterally Loaded Piles in Soft Clay	Hudson Matlock/1970	Lake Austin, TX	DRIVEN-SP	S+C	Soft Clay	N	N	N	N	Y (INDIRECT)	N/A	N	Y
Analysis of Laterally Loaded Piles in Sand	Lymon Reese, W. Cox, /Offshore Technology Conference/1974	Mustang Island, TX	DRIVEN-SP	S	Sand	N	N	N	N	N/A	Y	Y	Y
Static and Cyclic Lateral Loading of an Instrumented Pile	Shell Oil Company / H.Matlock / 1956	Lake Austin, TX	DRIVEN-SP	S+C	Soft Clay	N	N	N		Y (VS, UC AND TX-CU)	N/A	Y	N
Lateral Pile Load Test Report, I-880 Replacement Project-Site 1	Delta Geotechnical Services/For Caltrans/1997	Oakland, CA	DRIVEN-SP (FILLED WITH	S+C	11.5' med. Dense to dense SC over30.5' very dense SM	N	N	N	Y	N	Y	Y	Y
Lateral Pile Load Test Report, I-880 Replacement Project-Site 2	Delta Geotechnical Services/For Caltrans/1997	Oakland, CA	DRIVEN-SP (FILLED WITH	S+C	16.5' soft CL over alternate dense/hard sand/CL	Y	N	N	Y	Y	Y	Y	Y
Lateral Pile Load Test Report, I-880 Replacement Project-Site 3	Delta Geotechnical Services/For Caltrans/1997	Oakland, CA	DRIVEN-SP (FILLED WITH	S+C	25' dense Sand over 35 stiff CL over dense/hard alternate Sand/CL	N	N	N	Y	Y (UC , TX-UU)	Y	Y	Y
Lateral Pile Load Test Report, I-880 Replacement Project-Site 4	Delta Geotechnical Services/For Caltrans/1997	Oakland, CA	DRIVEN-SP (FILLED WITH	S+C	30' soft CL over 24' Stiff CL over 8' dense Sand	Y	N	N	N	Y (UC , TX-UU)	N	Y	Y
Predicting Axially and Laterally Loaded Pile Behavior using In-Situ Testing Methods	The University of British Columbia/M.Davis/1987	British Columbia, Canada	DRIVEN-SP (FILLED WITH	S+C	~4 m of sand over silty clay to -15m over NC clayey silt to -60 bgs	Y	N	Y	N	NT	NT	Y	N
Analysis of Load Data from filed test	Dep. of Civil. Master thesis, Utha Univesity	Utha University test site	DRIVEN-SP (FILLED WITH	S	~8 feet of clay/silty clay, over ~25 feet sensitive fine grained soils, underlain by	Y	N	N	N	N	N/A	Y	N
Understanding of monopiles in granular marine soils	Pars Co./Hokmabadi et al./2012	Asalouyeh, Iran	DRIVEN-SP	S	Sand, gravely sand	N	N	N	Y	N/A	Y	Y	N
Investigation of Lateral Resistance within a Pile Group	?/Rollins et al./2005	San Fransico, CA	DRIVEN-SP	S+C	Sand	N	N		Y	N/A	Y	Y	N
Investigation of dynamic soil-water-pile interaction and determination of the dynamic characteristics of the whole	Peer Website/Deiz et al/2012	LaMirabello Harbor, Italy	DRIVEN-SP	C	mud and clayey silt	Y	Y	N	N	Y (VS)	n/a	N	N
Influence on lateral rigidity of offshore piles using proposed p-y curves	Ocean Engineering/Jeong et al./2011	South Korea	DRIVEN-SP	S+C	Clay	N	N	N	N	Y (TX-UU)	N/A	N	Y

Nomenculator:

PILE TYPE

CIDH-C :	Cast In Drilled Hole Concrete Pile
DRIVEN-SP :	Driven Steel Pipe(open ended)

LATERAL LOADING TEST TYPE

S :	Static
C :	Cyclic
S+C :	Static +Cyclic

LABORATORY TEST TYPE

VS	Van Shear
TX-CU	Triaxial-Consolidated Undrained
TX-UU	Triaxial-Unconsolidated Undrained
UC	Unconfined Compression
NT	Not Tested

Table 4.2: *Summary Information of reviewed case histories*

DOCUMENT	PUBLISHER/AUTHOR/YEAR	SITE LOCATION	PILE TYPE	TEST TYPE	SOIL CONDITION	AVAILABLE DATA FROM FIELD AND LAB MEASUREMENT							
						CPT	CPTU	SCPT	SPT	Su	Φ	HEAD F-D	P-Y CURVE
Lateral load test on large scale pile	Hokmabadi et al./2012 (PEER Database)	Asalouyeh, Iran	DRIVEN-SP	S	Sand, Gravelly Sand, Sanstone	N	N	N	Y	N/A	Y	Y	N
Lateral load test on large scale pile	Kraner/1991 (PEER Database)	Washington, USA	DRIVEN-SP	S+C	Silt	N	N	N	Y	N/A	N/A	Y	N
Investigation of dynamic soil-water-pile interaction	Dezi et al./2012	Mirabello Harbor, Italy	DRIVEN-SP	D	Clay	Y	N	N	Y	Y	N/A	N	N
Experimental p-y model for submerged stiff clay	Dunnavant, T.W., & O'Niellll, M.W./ASCE Journal of Geotech./1989	University of Huston Site, Texas, USA	DRIVEN-SP	S+C	Clay	Y*	N	N	N	N	N/A	Y	N

Nomenculator:

PILE TYPE

CIDH-C :	Cast In Drilled Hole Concrete Pile
DRIVEN-SP :	Driven Steel Pipe(open ended)

LATERAL LOADING TEST TYPE

S :	Static
C :	Cyclic
S+C :	Static +Cyclic
D	Dynamic

LABORATORY TEST TYPE

VS	Van Shear
TX-CU	Triaxial-Consolidated Undrained
TX-UU	Triaxial-Unconsolidated Undrained
UC	Unconfined Compression
NT	Not Tested
Y*	Test done, data not available

Table 4.2-(Continued…)

4.1. Site 2 – Oakland, California

The following information is from a Caltrans report explaining a lateral pile load testing program conducted in the 1990's (Lemke, 1997). The pile testing was accomplished at four different test sites as part of a comprehensive indicator pile test program for the I-880 Replacement Project. The mentioned sites are located between the 980 South Connector Overcrossing and the San Francisco Oakland Bay Bridge Toll Plaza located in Oakland, California. Site 2, as one of the mentioned four sites is located to the northwest of Wood Street in the Southern Pacific Railroad Desert Yard as shown on Figure 4.1.

Figure 4.1: *Site 2, Oakland Vicinity Plan (Lemke, 1997)*

4.1.1. Soil Condition

Pile load tests at Site 2 were conducted in an excavation with a planar dimension of about 39 by 82 feet. A schematic cross section of the excavated test pit is shown as Figure 4.2. Also a layout of the pile test area is shown in Figure 4.13. One soil boring, B-16, was completed by Caltrans on July 28, 1993 within the plan area of the excavation at Site 2. The boring log and summary of field and laboratory tests performed are shown as Figure 4.3 and 4.4.

In addition, three CPT soundings designated as B-2, B-5, and B-6 were completed in the vicinity of Site 2, with B-6 being the closest one to the test location. The CPT tests were conducted during the year 2000 from the original surface at elevation of about +7.7.

As it is seen in boring B-16, the upper subsurface soil consisted of very dense sand with silt and some gravel extending from the pre-excavation ground surface at elevation +7.7 feet down to an elevation of about -1.5 feet. The upper sandy layer was underlain by soft clay extending to an elevation of about -16.5 feet. Results of Atterberg limits tests indicate liquid limit in the range of 71% to 96% and plasticity index values in the range from 40 to 58. Also three unconfined compression tests performed on samples in this layer indicate undrained shear strengths between 330 to 540 psf. The soft clay layer was underlain by alternate layers of very dense silty sand and very stiff to hard clay layers, to the maximum depth explored. A groundwater level was established in boring B-16 at an elevation of about 0.1 feet on July 28, 1993.

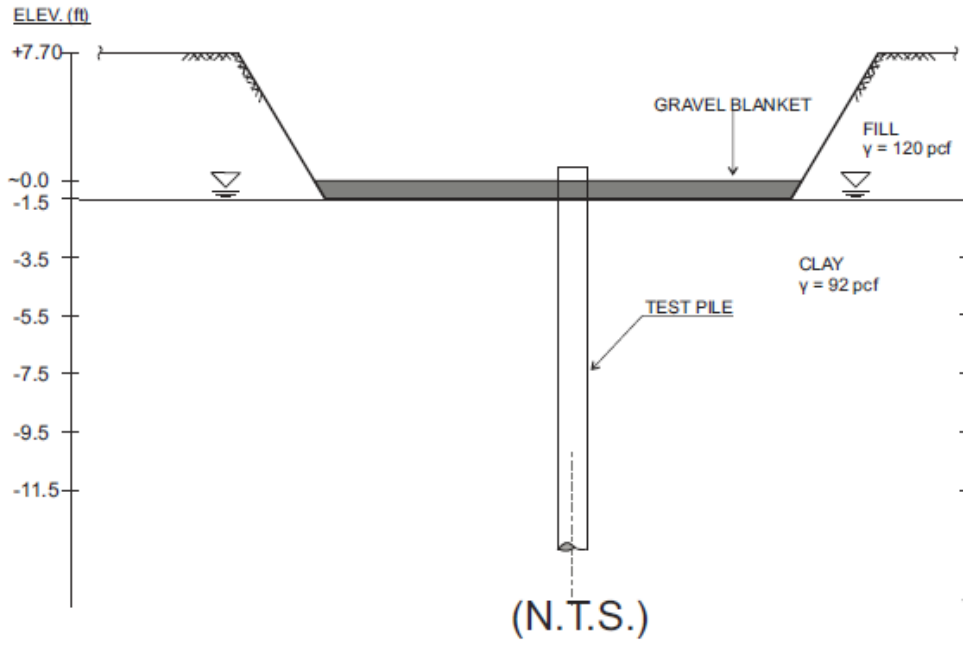

Figure 4.2: *Schematic Cross Section of piles test pit at Site 2, Oakland*

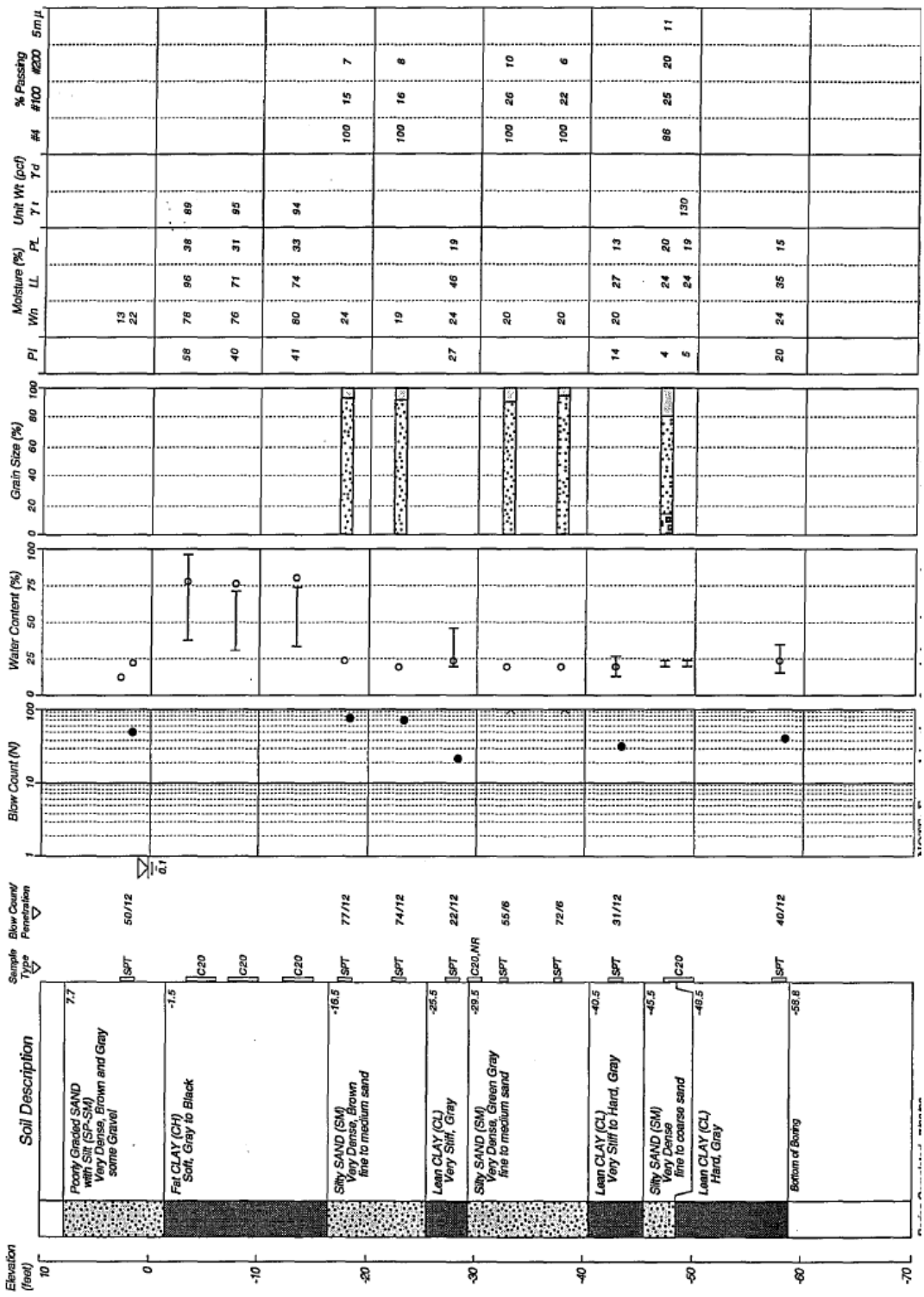

Figure 4.3: *Boring Log – B-16, Site 2 – Oakland (Lemke, 1997)*

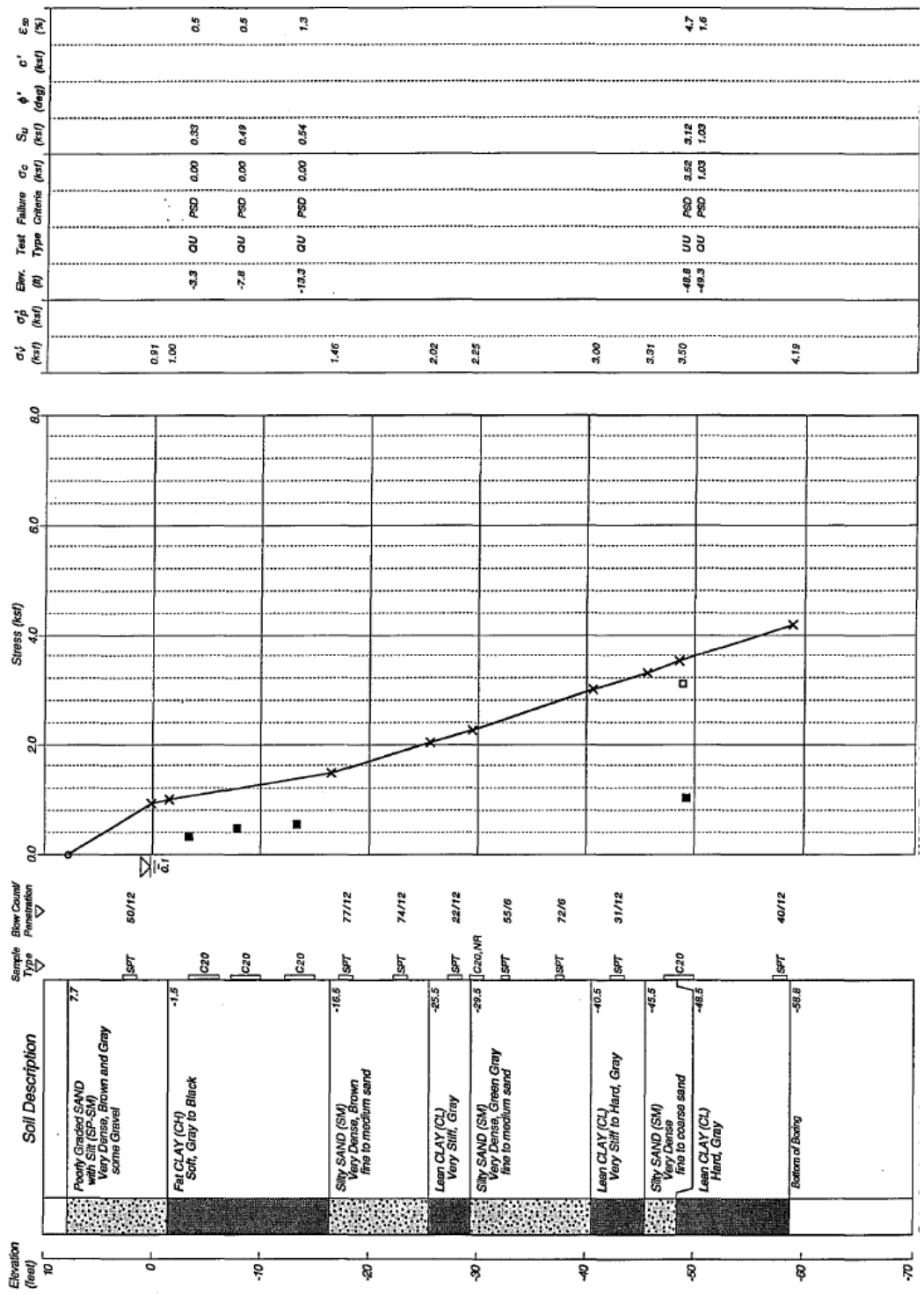

Figure 4.4: *Boring Log – B-16, Site 2, Oakland (Lemke, 1997)*

By utilizing the available CPT field data into the ”CPTeT-IT” software, the regular and normalized plots of cone resistance, friction ratio, Soil Behavior Type index (SBT) and stratification of the site soils at test location are obtained and depicted as Figures 4.5 and 4.6. As shown on Figure 4.2, the ground elevation prior to test was about +7.7 feet, and top of the clay layer and the bottom of the test pit excavation was at elevation of about -1.5 feet. The CPT plots presented conclude the same elevation for the soft clay layer, extending from elevation of about -1.5 to about -16.5 feet. Within the soft clay layer, I_c is higher than 3, indicating that the undrained/Clay-Like behavior of the soft clay layer prevails.

Shawn Ariannia
Civil & Environmental Engineering Department
UCLA

Project: **UCT54-Site 2**
Location: **Oakland**

CPT: CPT-01
Total depth: 43.62 ft, Date: 8/22/2015
Surface Elevation: 0.00 ft
Coords: X:0.00, Y:0.00

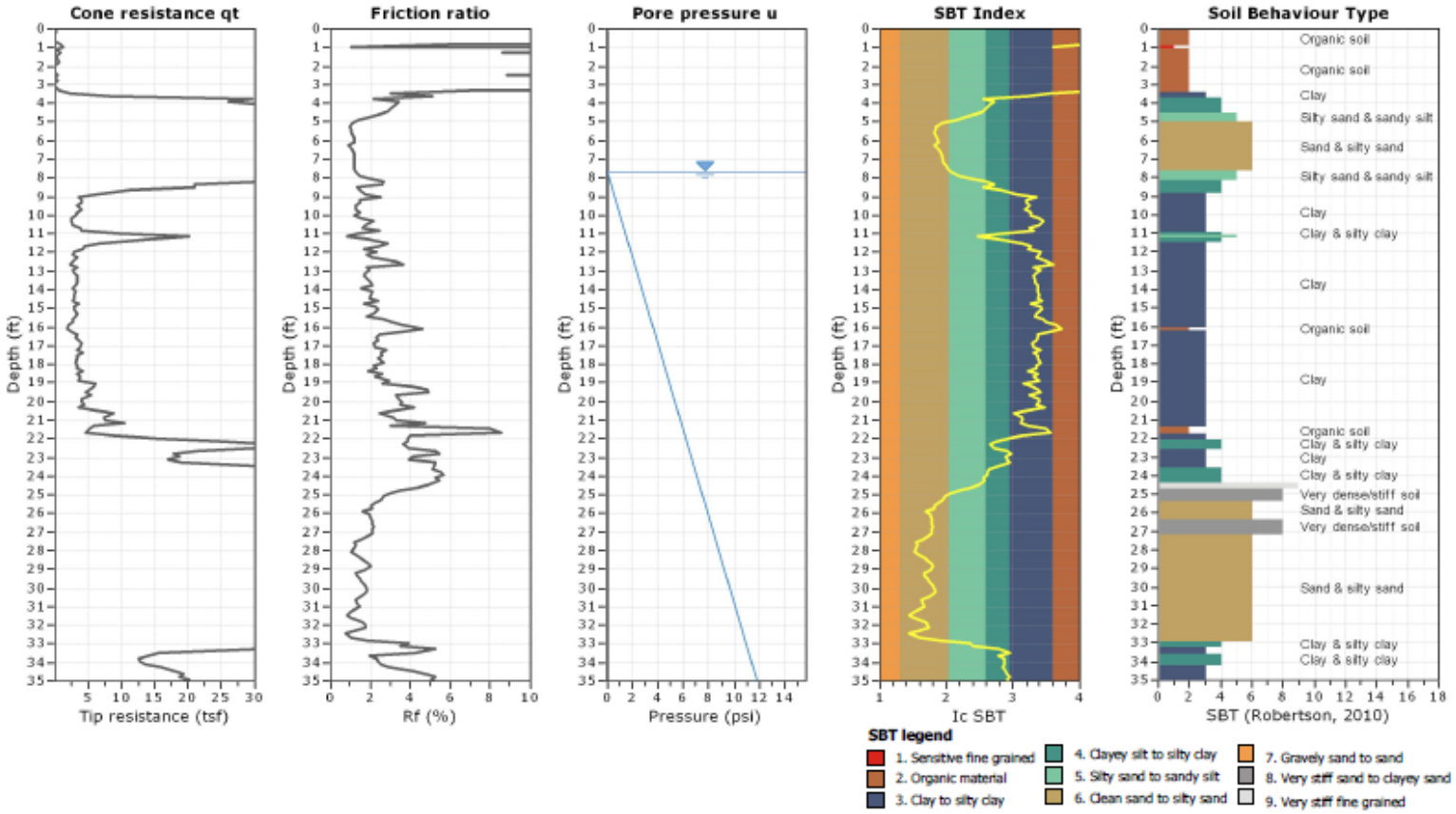

Figure 4.5: *CPT basic plots for Site 2, Oakland*

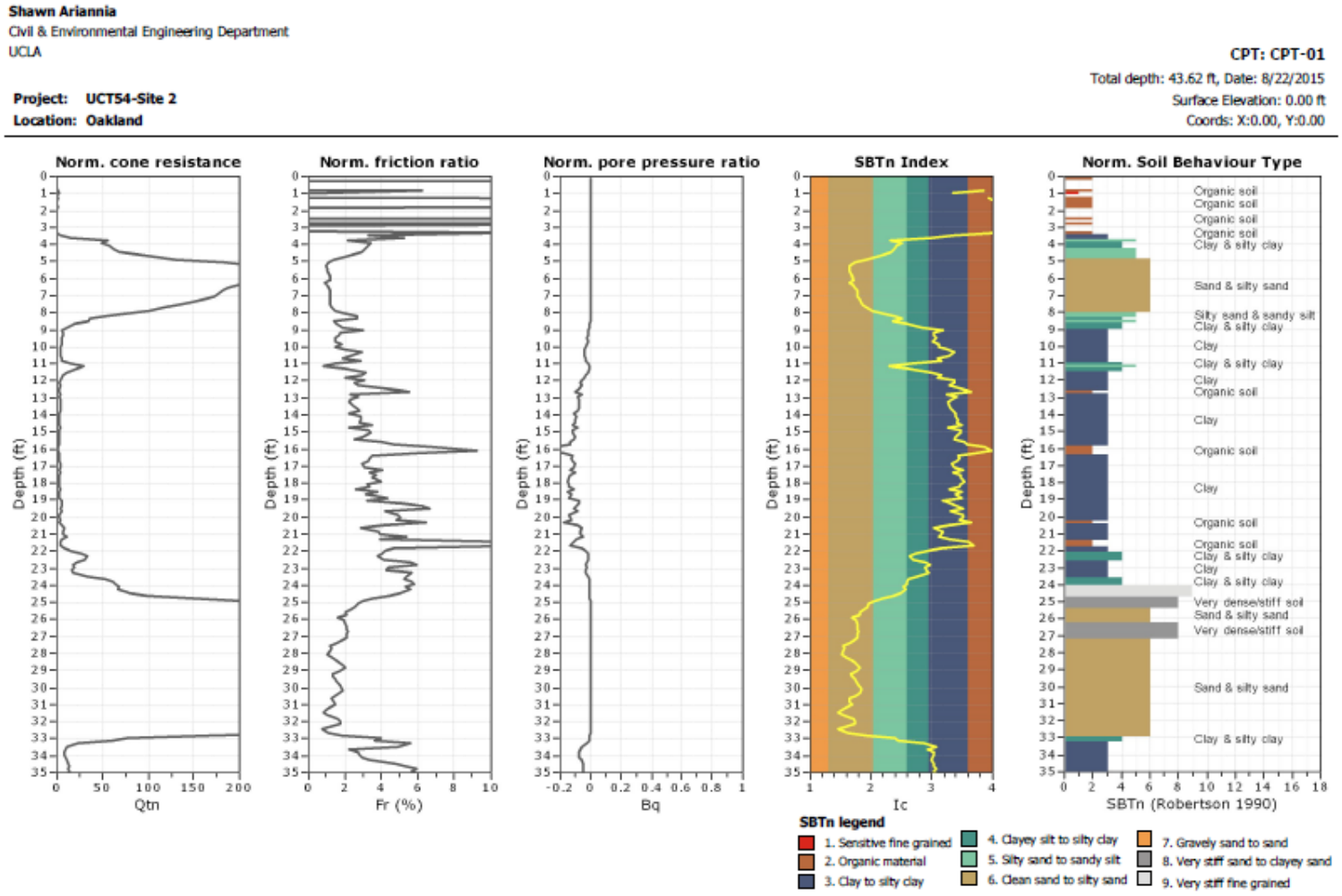

Figure 4.6: *CPT basic plots for Site 2, Oakland*

As discussed, three unconfined compression tests were performed on the samples obtained from the soft clay layer, indicating undrained shear strengths varies between 330 to 540 psf. The following undrained shear strength profile is obtained by using equation $s_u = \frac{(q_t - \sigma_v)}{N_{kt}}$, simulation between the condition in which CPT test was performed versus the condition during the lateral test, and by utilizing the field specific calibrated value of N_{kt}=14 in the CPT data.

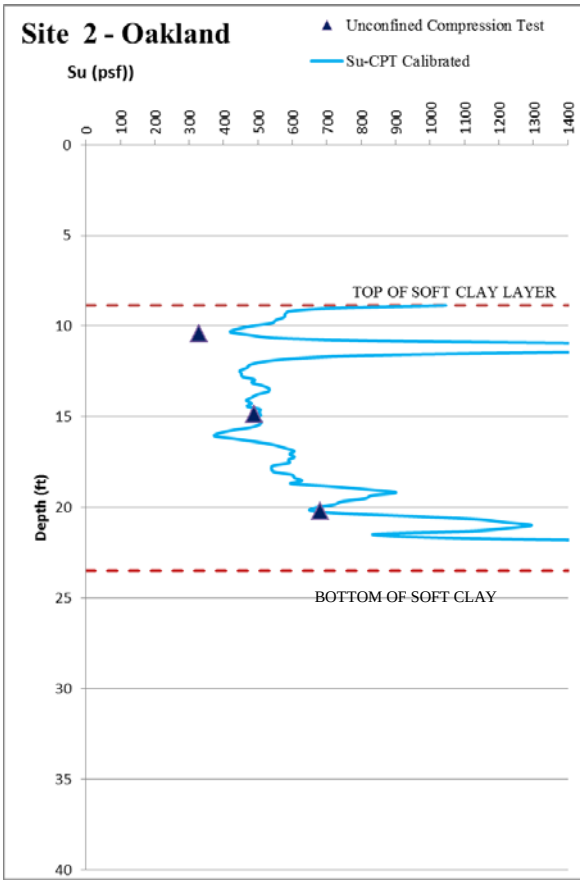

Figure 4.7: *Calibrated S_u profile for the site*

For determination of s_u at the subject site from CPT data, and to account for the effect of excavation in which the piles were tested, an in depth review of the test condition performed. In July 1993, the test area was excavated in to the elevation of -1.5 feet. After excavation, piles were driven, and mobilization for pile load testing occurred. Due to the elapsed time between the

excavation and commencement of testing, heave of clay soils had occurred. Consequent to removal of the soils, overburden pressure below the bottom of excavation decreased, resulting in increase in OCR, and decrease in the shear strength. Therefore, the shear strength during the test time was a lower value compared to the shear strength at the same depth before the excavation. On the other note, CPT was performed from the original grade, elevation +7.7 feet, and the shear strength obtained from CPT corresponds to the values before excavation, which is higher than the shear strength values within the clay layer during the test. This important notion was considered and implemented into the model and determination of the calibrated shear strength profile, shown on Figure 4.7. More detailed provided of the approach is explained hereafter.

Figure 4.8 depicts profile of the excavation. The overburden profiles for during the CPT time and during pile testing, i.e. after excavation, are shown as well. The OCR profile is determined using Ladd, 1991. For example, at elevation -9.5 feet, we have:

σ'_{v0-1} (Overburden pressure during CPT time) = 1,341 psf

σ'_{v0-1} (Overburden pressure during pile test time) = 237 psf

$OCR=\frac{1341}{237}=5.7$

The soft clay layer is normally consolidated, with the ratio of shear strength to effective pressure, $\frac{s_u}{\sigma'_{v0}}$, approximately equal to 0.3. Shear strength at the CPT time is determined as follows:

$s_{u1} = 0.3\ \sigma'_{v0-1} = 0.3\ (1341) = 402$ psf

Therefore, shear strength at each depth may be calculated by using the following equation 4.1, suggested by Ladd (1991):

$$\left(\frac{s_u}{\sigma_v'}\right) = \left(\frac{s_u}{\sigma_v'}\right)_{NC} OCR^{0.8} = 0.3\ (OCR)^{0.8} \quad (4.1)$$

And for the discussed elevation of-9.5 feet;

$s_{u2} = 237(0.3)\ 5.7^{0.8}$ = 286 psf

The two shear strength profiles for during CPT time and pile test time, s_{u1} and s_{u2}, are shown in Figure 4.8. The reduction ratio of shear strength, i.e. the ratio of $\frac{s_{u2}}{s_{u1}}$ at this depth is 0.71. Therefore, to simulate to test condition, the shear strength obtained from CPT at this depth shall be reduced by multiplying to 0.71. This approach has been extended to the entire depth and shear strengths from CPT have been reduced to correspond to the pile test time strength values. The shear strength profile shown in Figure 4.7 is determined by implementing the discussed reduction.

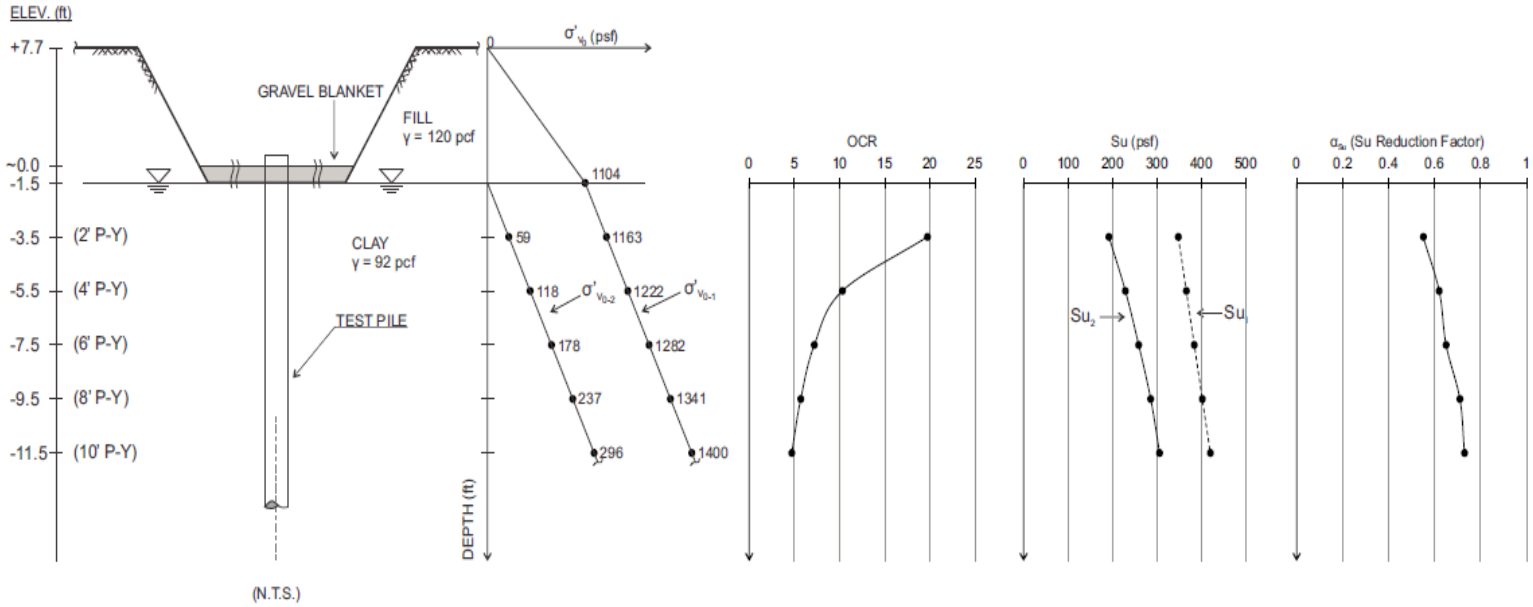

PILE TEST PROFILE FOR OAKLAND - SITE 2

σ'_{v0-1}: EFFECTIVE OVERBURDEN STRESS (CPT TIME)
σ'_{v0-2}: EFFECTIVE OVERBURDEN STRESS (PILE TEST TIME)
Su_1: UNDRAINED SHEAR STRENGTH (CPT TIME)
Su_2: UNDRAINED SHEAR STRENGTH (PILE TEST TIME)

Figure 4.8: *Effect of excavation on shear strength - Site 2, Oakland*

Also, the sensitivity results versus the depth, obtained from CPT correlations is plotted on Figure 4.9., indicating that sensitivity within the soft clay layer at site 2 is higher than 2, varying between 3 to 6 for the upper part of the clay layer.

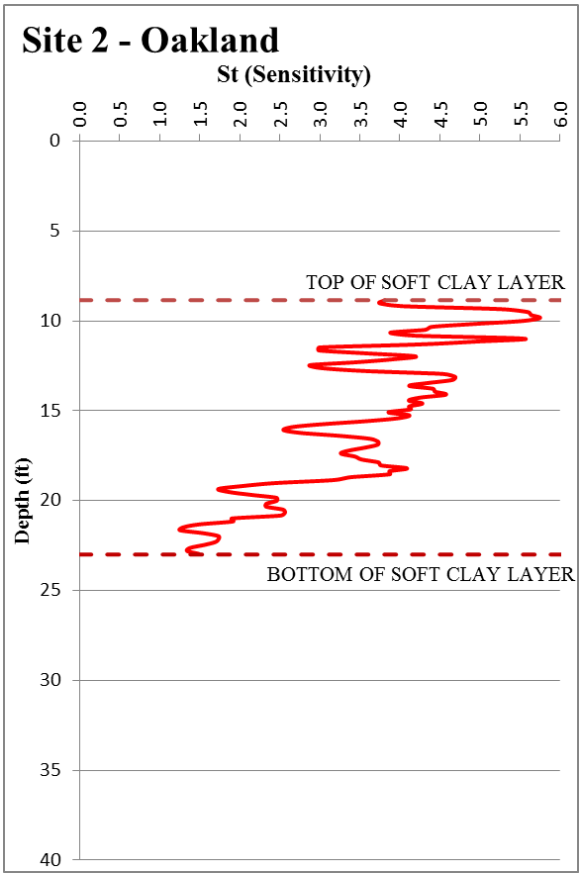

Figure 4.9: *Sensitivity profile for the clay layer using CPT - based correlations*

Shear wave velocity was not measured at this site. Therefore, CPT-based correlations have been used to determine shear wave velocity profile. Shear wave velocity profile may be determined by using equations 3.27 and 3.28 (Robertson, 2009) and equations 3.29, 3.30 (Mayne, 2007). The profiles plotted on Figure 4.10 indicate that the V_s within the soft clay layer obtained from Mayne (2007) varies between about 260 to 400 ft/sec, while by using Roberson (2009), the shear wave velocity is somewhere between 300 to 450 ft/sec.

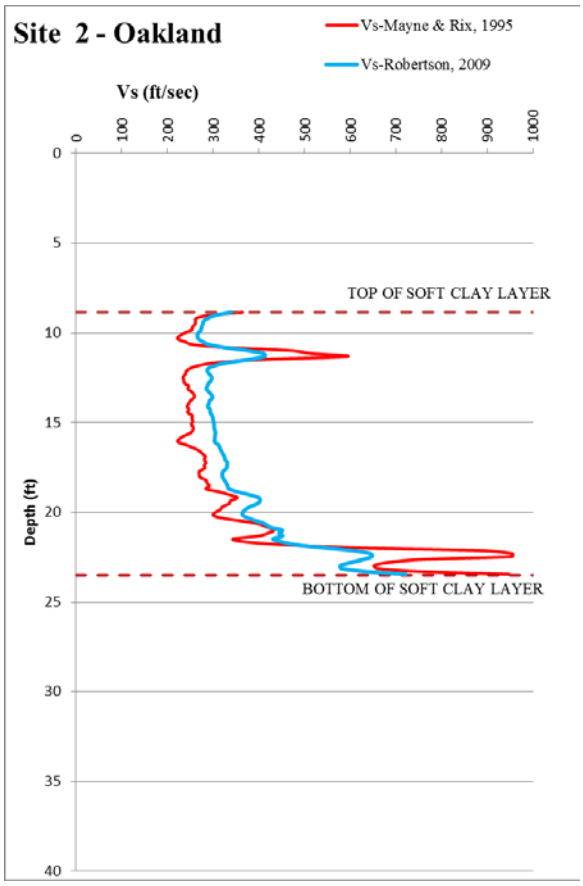

Figure 4.10: *Comparison of shear wave velocity obtained from CPT data using different correlations - Site 2*

The correlation equations to determine *Vs*, as discussed in aforementioned section 3.2.1, are approximate in nature, and should be replaced with site specific values of V_s measured when available for each site. These type of correlations should only be used when no site measurement of V_s is available. In a research published by Brandenberg et al. (2010), regression was performed for sand, silt and clay soils and regression parameters were reported. Based on the results of the said study, a value of $\sigma = 0.35$ is utilized and the plots for $Vs, Vs + \sigma,$ and $Vs - \sigma$ are obtained and depicted on the following Figure 4.11.

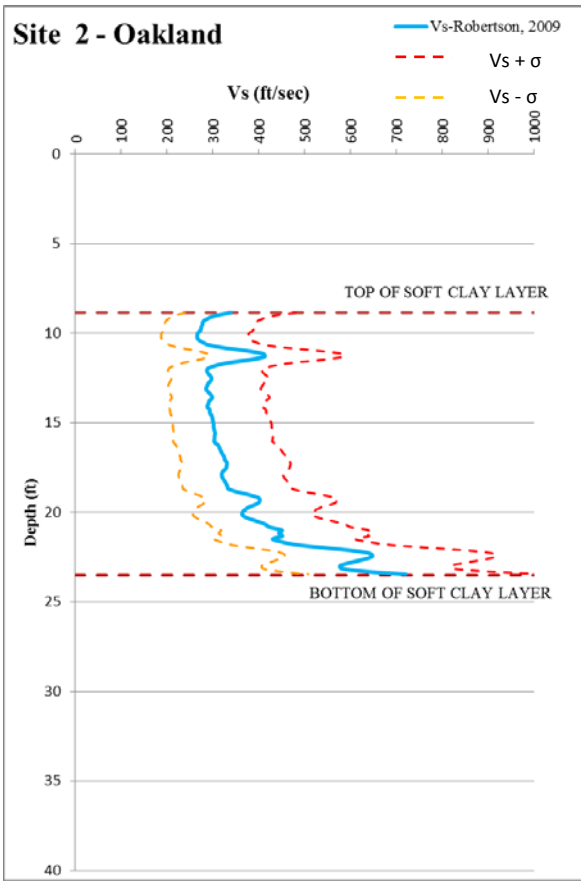

Figure 4.11: *Shear wave velocity obtained from CPT data using Robertson (2009) and +/– σ (+/-one standard deviation) Plots - Site 2*

4.1.2. Pile Properties and Load Test Description

Lateral pile load tests were conducted by simultaneously forcing of piles in pairs by jacking two piles together with two high strength threadbars connected to the piles and two hydraulic jacks. Figure 4.12 depicts plan and profile view of test set up for both sites 2 and 4, in Oakland.

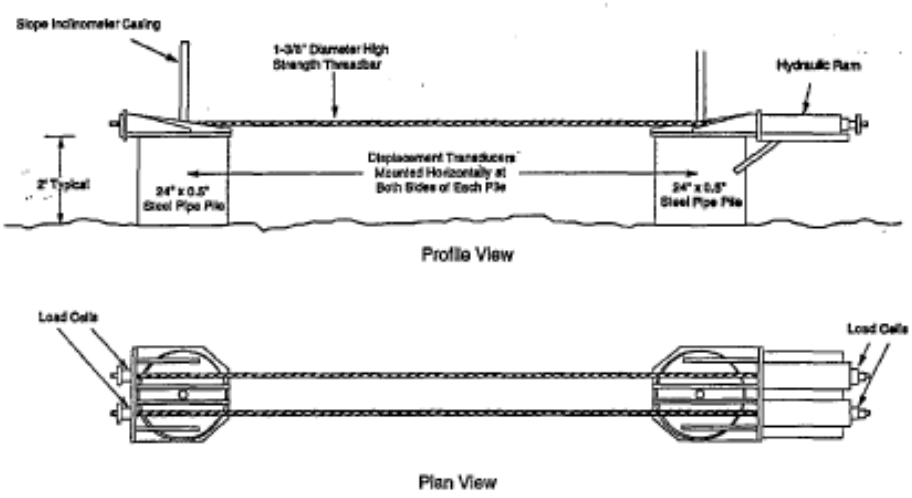

Figure 4.12: *Lateral Load Application set-up for the Oakland Site tests (Lemke, 1997)*

Pile load tests at Site 2 were conducted in an excavation with a planar dimension of about 39 by 82 feet. A plan view of the pile load test layout is shown on Figure 4.13. Prior to installation of the test piles, soil was excavated from its original elevation of about +7.7 to an elevation of about -1.5 feet. The schematic profile shown as Figure 4.12 demonstrates the elevation of the excavated pit for the test area, and the ground surface prior to excavation.

At Site 2, a total of ten 24-inch diameter pipe piles, with wall thickness of $\frac{3}{4}$ inch were tested. Each pile was filled with 8#9 rebar, spiral ties and concrete.

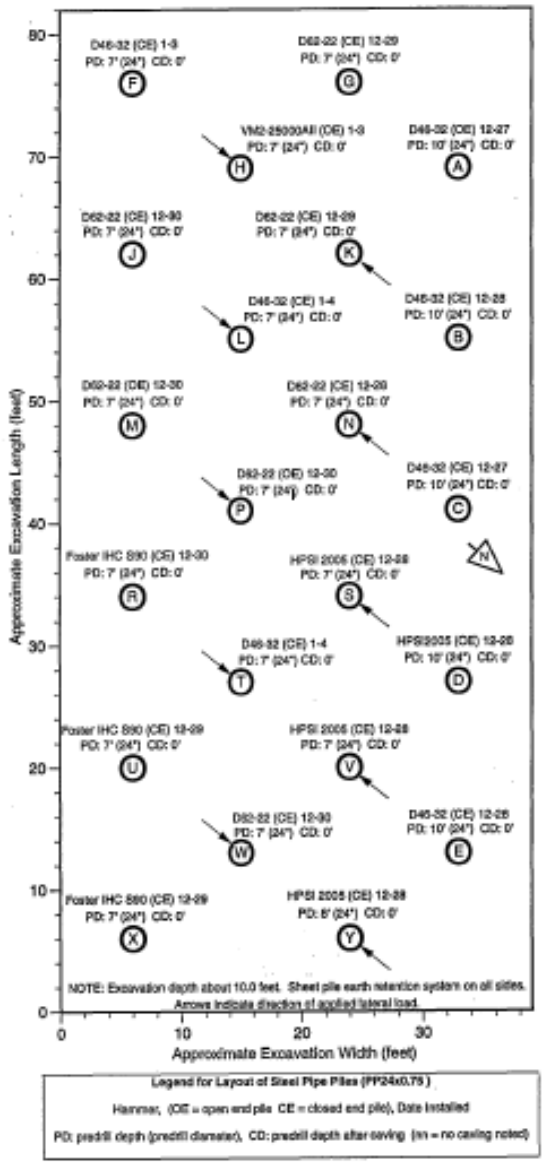

Figure 4.13: *Plan View of Test Pile Layout- Site 2 (Lemke, 1997)*

Piles were tested in general accordance with ASTM D 3966-81, "Standard Method of Testing Piles under Lateral Loads." The loading procedure was in general compliance with Section 6.4.2 of the mentioned standard. Load applied to each pile was measured using a pressure gauge on the hydraulic pump operating the jacks and two donut load cells mounted on each pile co-axially with each high strength threadbars. The load cells had a 200 kip capacity and were

calibrated. Horizontal displacements at each pile top were measured using a total of four displacement transducers mounted on reference beams about 1 to 2 feet above the ground surface.

Load increment of about 7 to 20 kips were applied to each test pile and held for a period of about 10 minutes. Generally, from 5 to 10 load cycles were applied to each test pile. Lateral loads were applied to the top of the pile at a rate of about 5 to 10 kips per minute during load applications. The loading condition for the test piles was free-ended with shear applied at the pile top without moment.

Lateral deflection of the pile along its length was measured by using slope inclinometer instrument, which measures slope changes inside a plastic casing cast within concrete at the approximate center of each test pile. Slope changes were measured in two orthogonal directions. One direction was chosen to be in line with the direction of the applied lateral load. Horizontal displacements can be calculated from the measured slope over the length of the slope inclinometer instrument. As stated in the report (Lemke, 1997), the accuracy of measured horizontal displacements is within about $\frac{1}{4}$ inch over 100 feet of casing assuming that no operational errors occur. Corrections were applied to all slope inclinometer readings in order to reduce various types of errors. Each reading was multiplied by the ratio of the horizontal deflection at the pile top as measured by displacement transducers divided by the slope inclinometer deflection at the pile top. The clear horizontal spacing between each pair of test piles pulled together was about 9 feet. This distance is less than the horizontal distance recommended by ASTM D 3966-81 and may have influenced the measured load and displacement characteristics of the test piles.

4.1.3. Input Parameters for Analysis

Pile properties, as well as soils strength parameters are to be utilized to the integrated model. The pile properties include; B (pile diameter), L (pile length), E_p(pile material modulus of elasticity), E_y (yield modulus of pile material), A (pile cross section area), I (pile section moment of inertia), and M_{y-pile} (pile section yield moment). Also pile head constraint condition will be introduced into the model.

The only soils information to be uploaded to the model is CPT data file and the depth of ground water. The Matchad script in the model determines the basic soils parameters required to be utilized into a "ticle" file, which feeds the "OpenSees" program to solve the model.

The basic soil input parameters the Matchad script calculates are K_{max}, P_u, C and y_{50}. These parameters are determined as explained in chapter 3. The profiles of input parameters for this site along the depth of the soft clay layer are depicted in the following Figure 4.14. The value of C, the soils constant, is determined from equation 3.39, and for the soft clay layer at this site varies between 0.018 and 0.022.

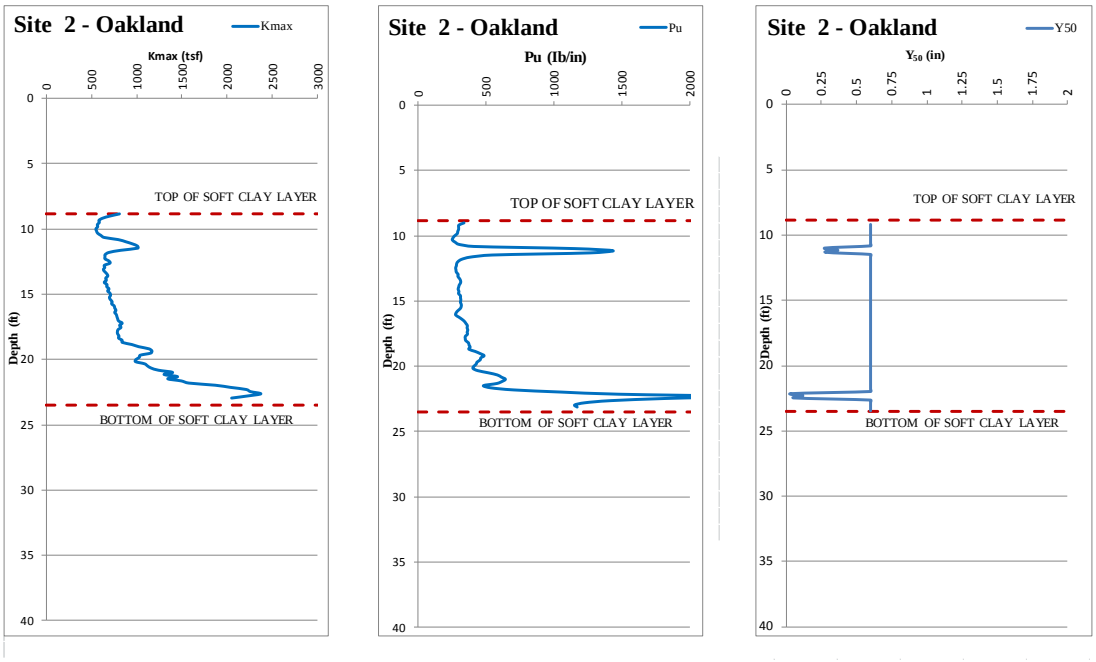

Figure 4.14: *Input Parameters profiles for Site 2, Oakland*

4.1.4. Measured and Predicted Results

By utilizing the CPT data into the "Model", the values warranted to plot *p-y* curves were obtained. The values for each depth necessary to plot *p-y* curve are; initial stiffness, *K*, ultimate resistance, p_u, and parameter *C* which defines the curve's shape. The *p*-y curves are plotted for four different depths where the curves resulted from field measurements were available (Lemke, 1997). On Figures 4.15 to 4.18, the p-y curves from the "Model" are plotted over the field results. The determined *p-y* curves show a reasonable agreement comparing to the *p-y* data resulted from field measurements. For each plot, values of p_u, K_{max} and *C* are shown. Shear wave Velocity, V_s, is being determined using Robertson (2009).

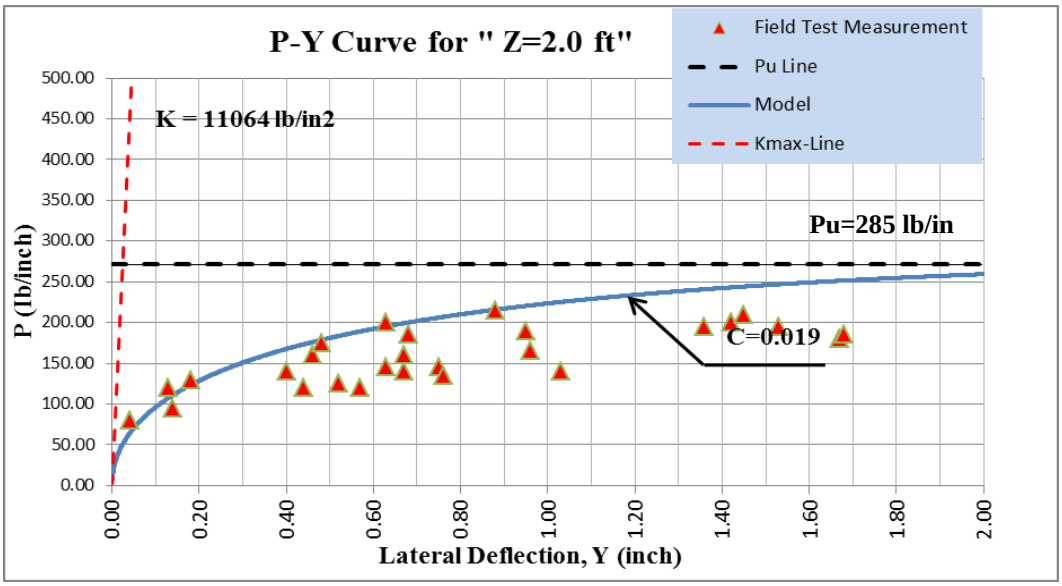

Figure 4.15: *Resulted p-y curve from the "Model" vs. field measurements at 2 feet*

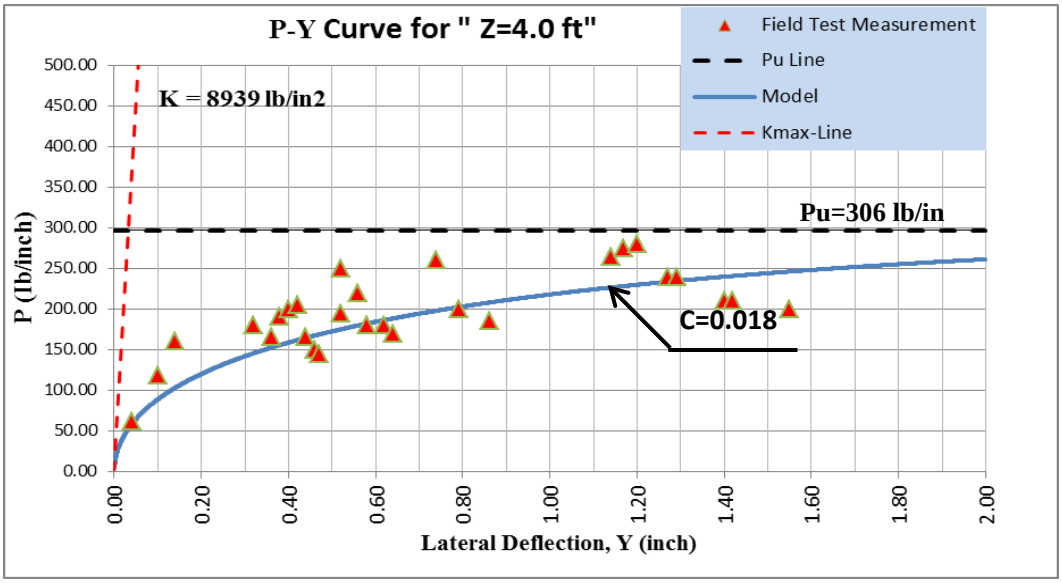

Figure 4.16: *Resulted p-y curve from the "Model" vs. field measurements at 4 feet*

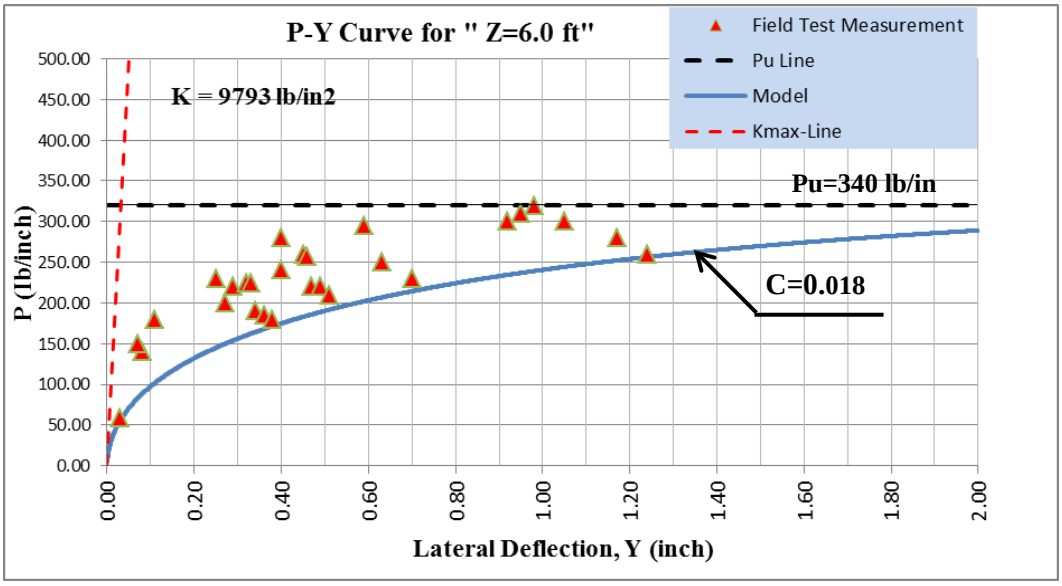

Figure 4.17: *Resulted p-y curve from the "Model" vs. field measurements at 6 feet*

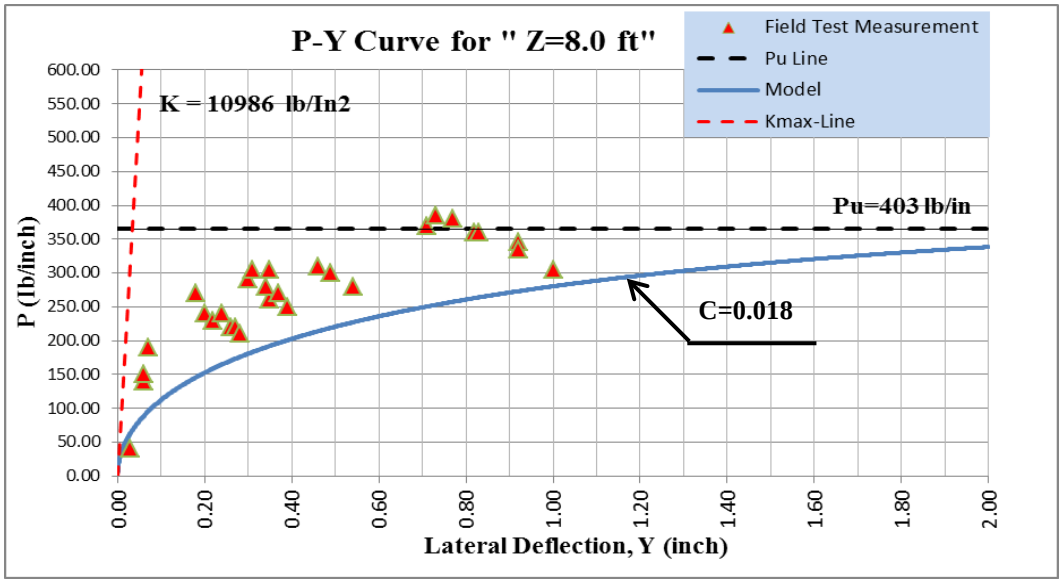

Figure 4.18: *Resulted p-y curve from the "Model" vs. field measurements at 8 feet*

Pile head load-displacement was measured for nine piles at Site 2, Oakland. The results of pile head measurements are retrieved from Lemke (1997), report and are re-plotted on Figure 4.19. Using CPT data and the "Model", head force-displacement relation is determined, and is plotted

in on the same Figure 4.19. Also the solution from LPILE program is depicted on the same Figure 4.19.

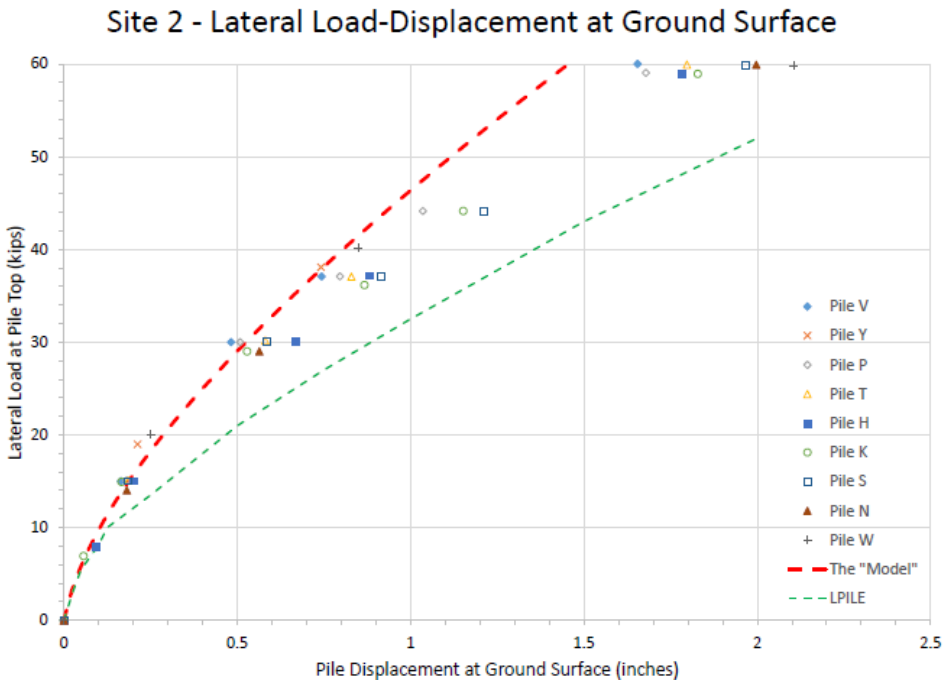

Figure 4.19: *Pile head Load-Displacement curves measured at Site 2 versus resulted curve from the model and LPILE results*

Due to lack of site specific V_s data, CPT-based correlations embedded in the "Model" were activated in the analysis. As shown on Figures 4.15 to 4.18, the value of initial stiffness, *K*, is approximately 9 to 11 Kips/in^2. As discussed in Chapter 3, the accurate measurement of V_s is an important factor affecting the shape of the *p-y* curves. For a selected depth of 4 feet, *p-y* curves are plotted in Figure 4.20, using different V_s values from Robertson, 2009 and Mayne, 2007. The *K* value from Robertson (2009) is 8939 lb/in2, about 44% higher than the value from Mayne (2007). Referring to the analysis from the "Model", determined V_s values for this depth from Robertson (2009) and Mayne (2007), are 234 and 290 ft/sec, respectively. Although the difference in V_s using these two correlations is about 20%, the initial stiffness values differ about 44%, which is because

of initial stiffness's relation to the squared value of V_s. This amplifies the importance of using site specific/measured V_s. The enlarged part of the initial zone on Figure 4.20 is shown as Figure 4.21.

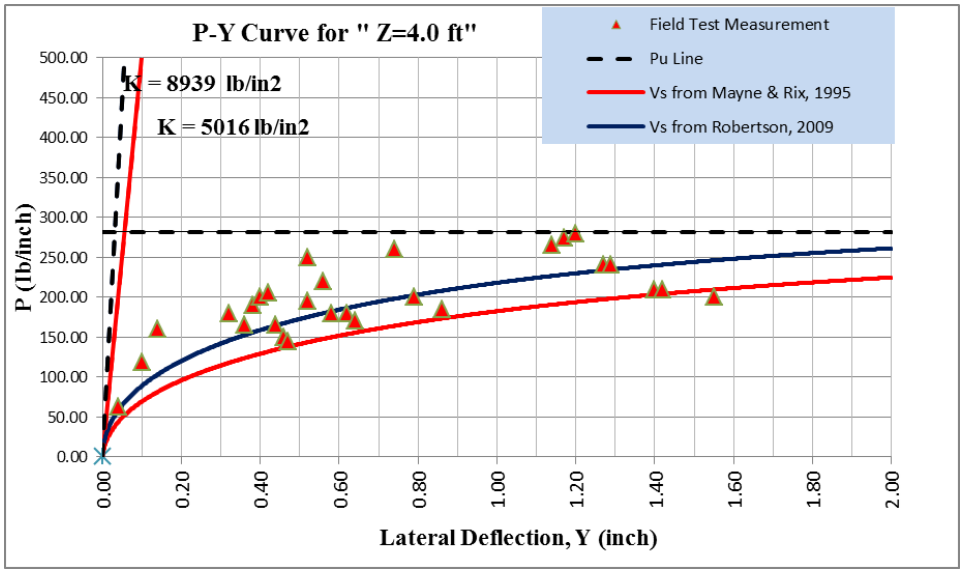

Figure 4.20: *Effect of choosing V_s correlation on resultant p-y curve; Comparison between using Mayne et al (1995) and Robertson (2009) suggested correlations for V_s*

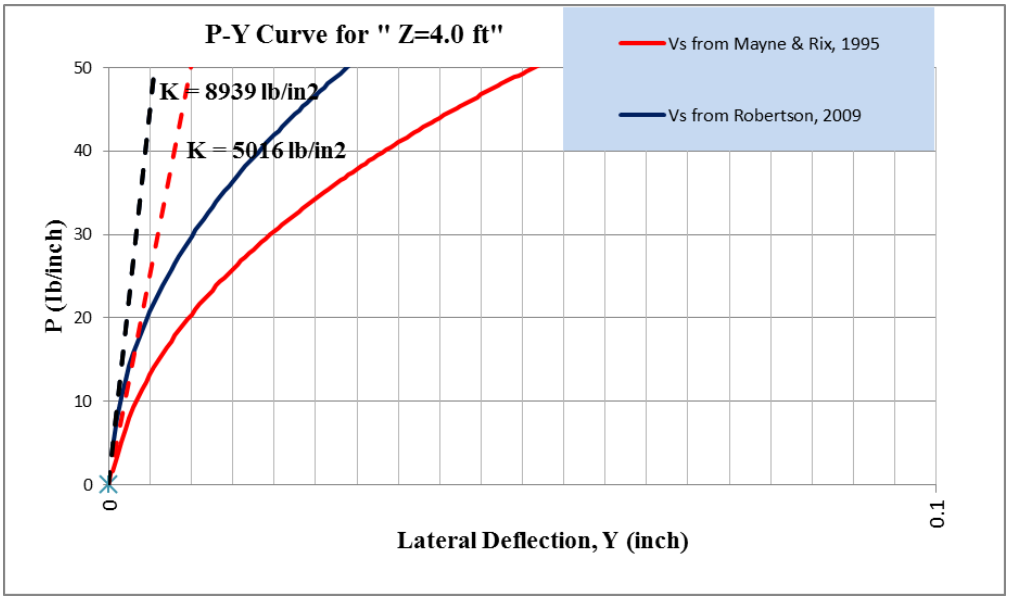

Figure 4.21: *Effect of choosing V_s correlation on initial stiffness of p-y curve; Comparison between using Mayne et al. (1995) and Robertson (2009) suggested correlations for V_s*

4.1.5. Discussion on the Results

As mentioned, during the test, ground water level was at top of the clay layer, and the soft clay layer was saturated, representing an undrained behavior in shear. Within the depth range of concern, i.e. the upper 15 feet of the soft clay layer, I_c varies between 2.9 to 3.3, with exception of a few limited Points where I_c values are around 2.5 to 2.7. The clay layer will behave undrained in shearing, and values of I_c compared to the criteria suggested by Robertson (2010), shown as Figure 2.41, results in the same behavior for the clay layer.

The most credible field measurement during pile lateral testing is displacement at pile head. For this case, pile head Load-Displacement resulted from the "Model" shows a very good agreement with the field measurements, as compared in Figure 4.19.

The *p-y* curve from the "Model" at the depth of 2.0 feet is depicted on Figure 4.15. As it is seen, the "Model" curve is slightly higher than the trends of the field-resulted data points. This might be because of softening in the shallow clay occurred due to driving operation of the pile, which resulted in decreased resistance for the clay. The "Model" curve at 4 feet, i.e. Figure 4.16, has a very reasonable fit, and the curves for 6 and 8 feet shown in Figures 4.17 and 4.18, fall slightly below the data points. When comparing the model driven *p-y* curves with the *p*-y curves from field measurements at this site, the followings might be considered as main reasons for some mismatches encountered:

- Data points for *p-y* curves shown as field measurements were determined in a conventional way of measuring the pile's slope/curvature at different depths, and determining p and y accordingly. However, the change in slope through the pile was measured by inclinometers installed at center of the piles. This method of measuring

curvature is not as accurate as other means such as use of *LVDTs* (Linear Variable Differential Transformers).

- Shear wave velocity was not measured at the site. The V_s values obtained using correlations suggested by Robertson (2009) and Mayne (2007) have resulted in relatively low values for V_s. However, if the real V_s for the subject site is higher than the values used in the analysis ("Model"), the curves from the "Model" will shift upward, resulting in a better match with the field measurements.

- In very soft clays, there may be some uncertainty with the accuracy of in q_t values. In these cases, it would be better to estimate s_u from correlations based on excess pore water pressure $\mathbf{(}\Delta u_2\mathbf{)}$ measured behind the cone. This will result in a more accurate value for s_u when in very soft clay soils.

- The values obtained for the soil ultimate resistance p_u at different depths from the "Model" varies between about 285 lb/in to 403 lb/in for the depths between 2 to 8 feet, as shown in Figures 4.15 to 4.19. However, for the same depths, the values for p_u reported by Lemke (1997) vary between 180 to 360 lb/in. The undrained shear strengths are derived from CPT data, and the profile was calibrated to best fit to the filed specific values from laboratory tests. However, the s_u values for the site were determined from unconfined compression tests on the samples. The preciseness of s_u values obtained from unconfined compression tests is a matter of concern and may be a relatively important factor in explaining some differences in the results.

- Field measured head force-displacement for nine tested piles at this site are shown on Figure 4.19. The head force-displacement curve from both the proposed model and

LPILE are depicted as well. The curve from the model shows a better agreement with the field test data than output from LPILE. Especially, initial stiffness of the curve, i.e. initial slope, from the model seems to be more reasonable.

4.2. Site 4 – Oakland, California

The following information is from a Caltrans report explaining a lateral pile load testing program conducted in the 1990's (Lemke, 1997). "Site 4" is located to the northwest of Wood Street in the Southern Pacific Railroad Desert Yard as shown on Figure 4.22. The results of pile lateral testing including load and displacement values at different depths were measured and have been provided in the report for Caltrans by prepared by Lemke (1997) during the tests. The pile testing at this site was accomplished as a part of previously mentioned pile testing program for the I-880 Replacement Project.

Figure 4.22: *Site 4, Oakland - Location Map (Caltrans, Lemke, 1997)*

4.2.1. Soil Condition

Similar to the Site 2, pile load tests at Site 4 were conducted in an excavation with a planar dimension of about 39 by 82 feet. A plan view of the pile load test layout is shown on Figure 4.33. One boring, B-15, was completed by Caltrans on July 29, 1993 within the area of the performed excavation at Site 4. The boring log and summary of field and laboratory tests performed are shown as Figure 4.24 and 4.25.

In addition, three CPT soundings were completed in the vicinity of Site 4. Prior to installation of the test piles, soil was excavated to an elevation of about -3.3 feet. A 1- foot thick layer of gravel was placed across the bottom of the excavation bringing the final elevation up to -2.3 feet. The schematic profile shown in Figure 4.23 demonstrates the excavated pit for the test area, and the ground surface prior to excavation.

From boring B-15, it is concluded that the upper subsurface soil consisted of dense clayey sand with gravel fill material extending from the ground surface at elevation of +7.0 feet down to an elevation of about -3 feet. The clayey sand was underlain by soft clay extending to an elevation of about -32 feet. Based on the results of Atterberg limits tests on the samples obtained from soft clay layer, the liquid limit ranged from 80% to 101% and plasticity index values ranged from 45 to 60 and both generally decreased with depth. Also, five unconfined compression tests were performed on samples obtained from this layer, and the results indicate undrained shear strengths varying between 430 and 710 psf,. From about -32.0, a stiff clay layer started, and extended to an elevation of about -56 feet. Results of Atterberg limits tests performed on the samples retrieved from stiff clay layer indicate liquid limit ranged from 33% to 65%, and plasticity index ranged from 18 to 38, and both generally decreased with depth. Also three unconfined compression tests and three unconsolidated undrained triaxial compression tests were

performed on samples obtained from this layer, and the results indicate undrained shear strengths between 500 and 2860 psf. The stiff clay layer was underlain by very dense sand with gravel extending to the maximum depth explored in boring B-15 at elevation -64 feet. Groundwater level was established in boring B-15 at an elevation of about -0.4 feet on July 30, 1993.

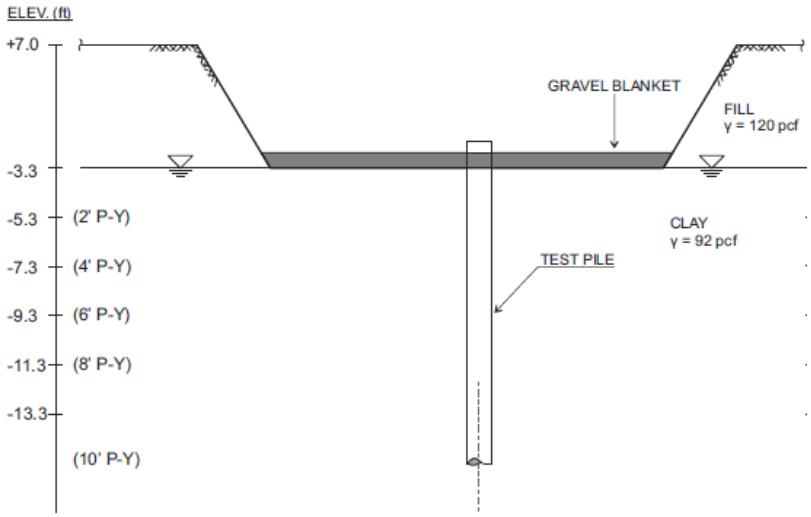

Figure 4.23: *Schematic Cross Section of piles test pit at Site 2, Oakland*

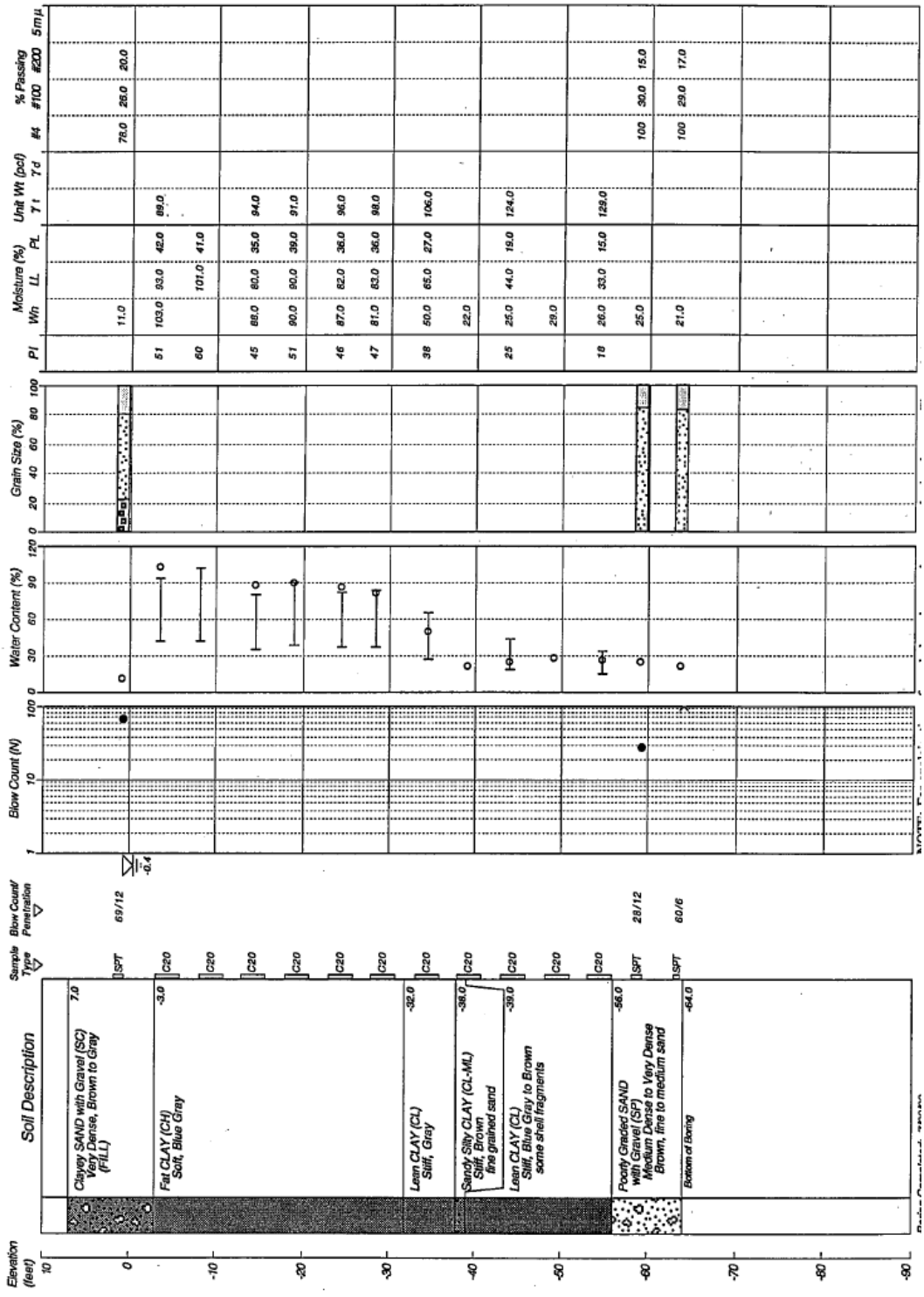

Figure 4.24: *Boring B-15, Site 4 (Lemke, 1997)*

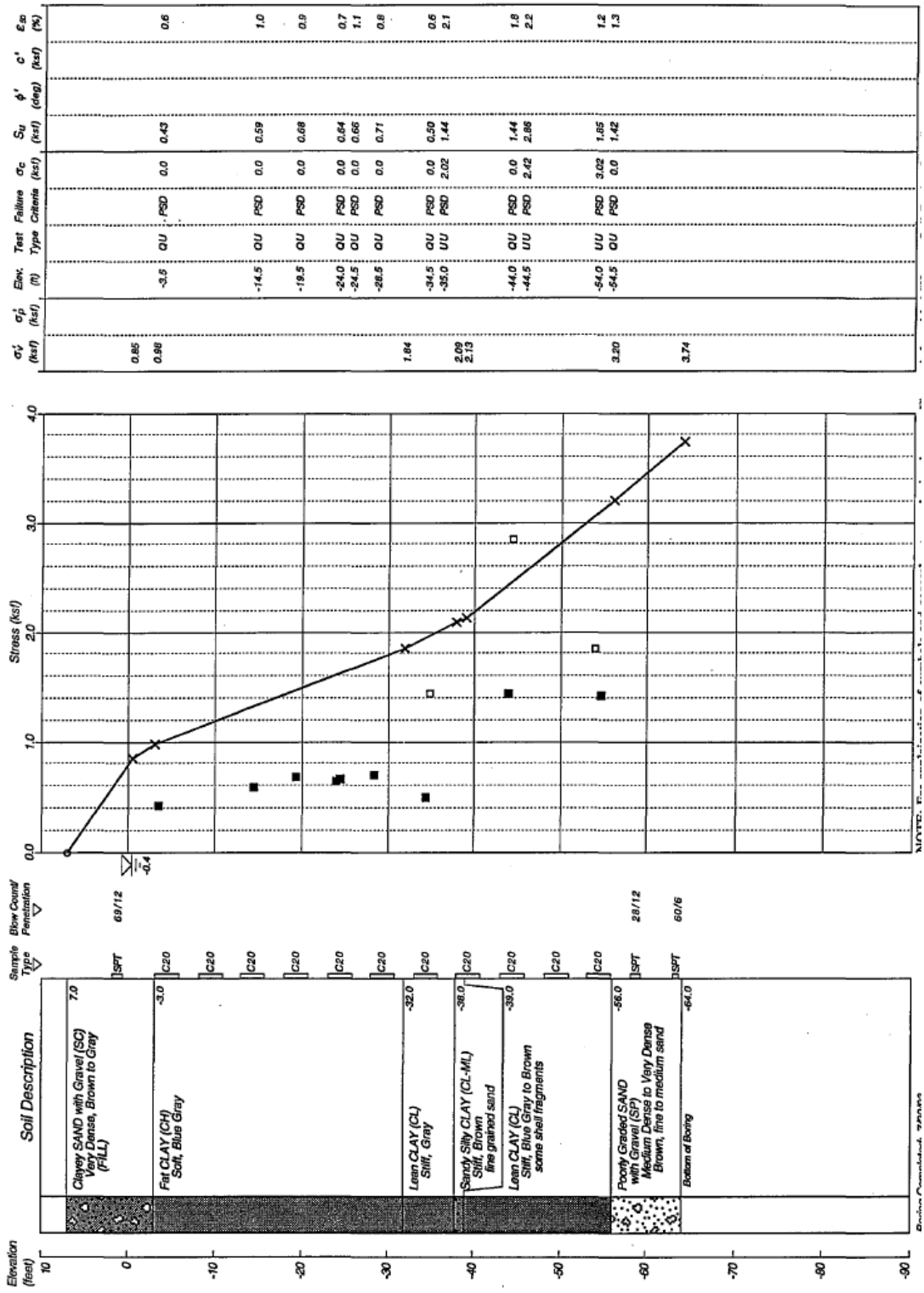

Figure 4.25: *Boring B-15, Site 4 (Lemke, 1997)*

By utilizing the available CPT field data into the" CPTeT-IT" software, the regular and normalized plots of cone resistance, friction ratio, Soil Behavior Type index (SBT) and stratification of the site at test location are obtained and depicted as Figures 4.26 and 4.27. As shown on Figure 4.23, ground elevation of ground prior to test was about +7.0 feet, and top of the clay layer and the bottom of the test pit excavation was at about -3.3 feet. The CPT plots presented in Figures 4.26 and 4.27 conclude the same elevation for the soft clay layer, extending from elevation of about -4.0 to about –35.0 feet. Within the soft clay layer, I_c is higher than 3, indicating that the undrained/Clay-Like behavior of the soft clay layer prevails.

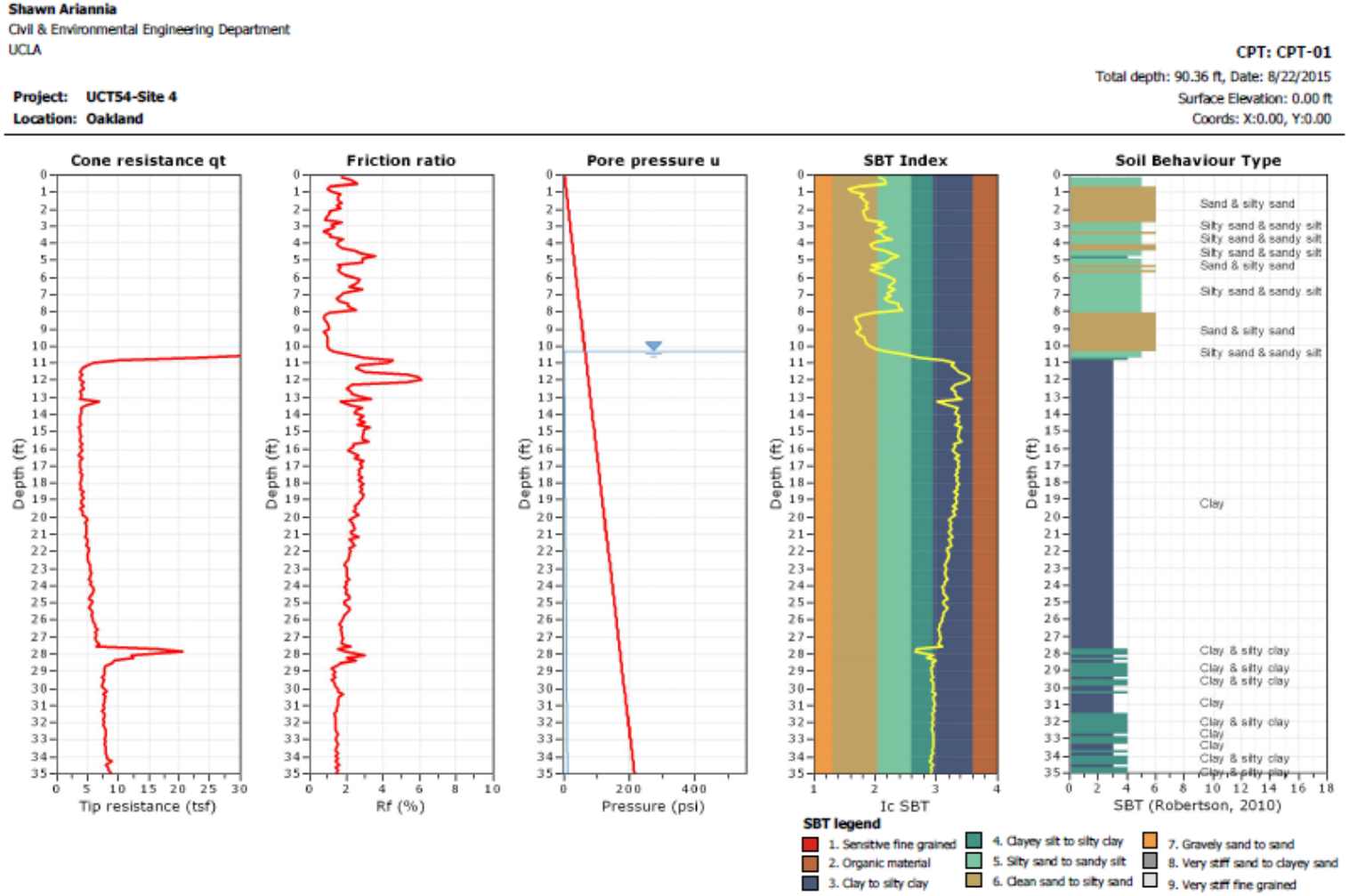

Figure 4.26: *CPT basic plots for Site 4*

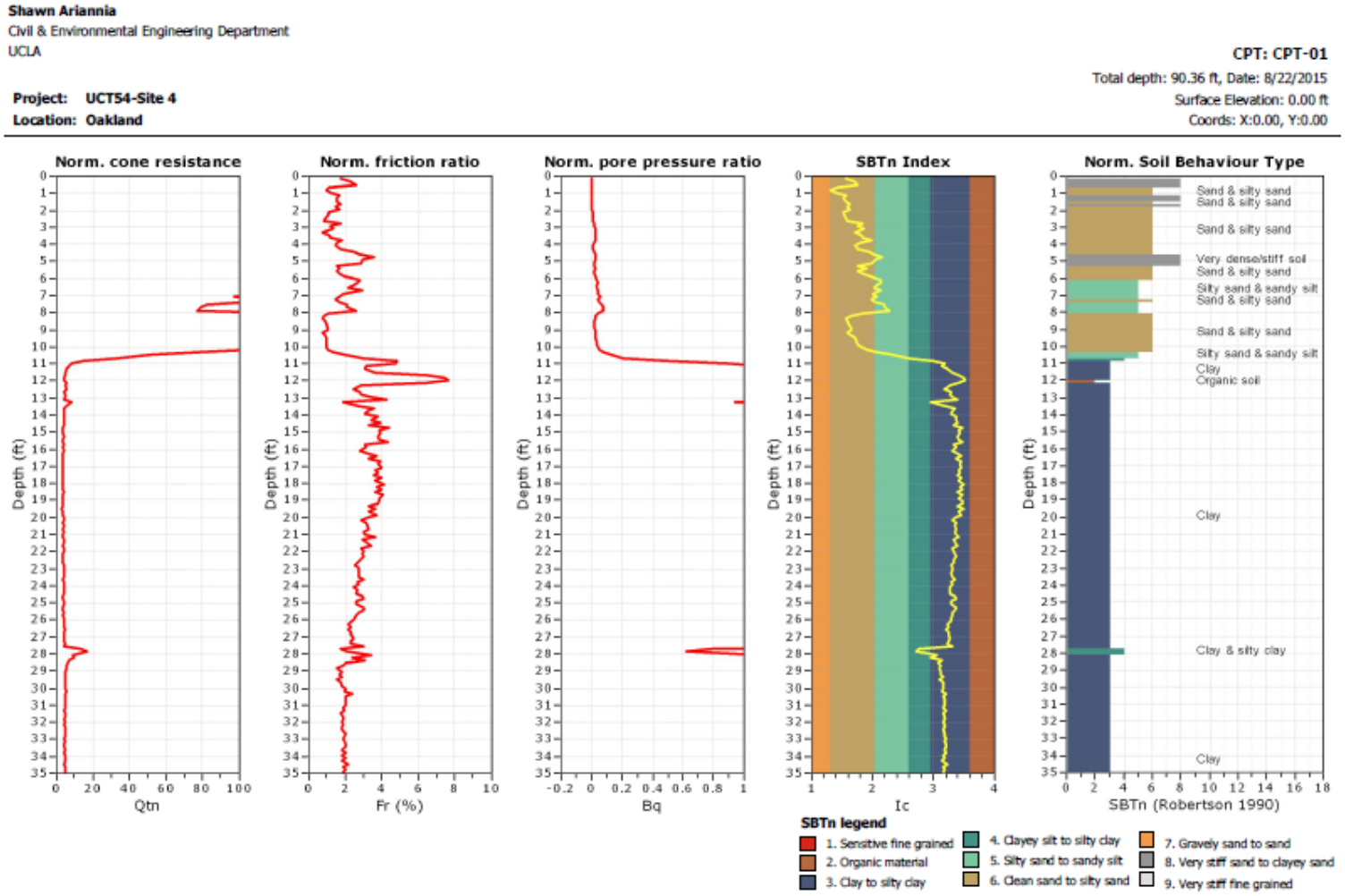

Figure 4.27: *CPT normalized plots for Site 4*

As mentioned, five unconfined compression tests were performed on samples obtained from the soft clay layer, and the results indicate undrained shear strengths varying between 430 and 710 psf. The following undrained shear strength profile in Figure 4.28 is obtained by using equation $s_u = \frac{(q_t - \sigma_v)}{N_{kt}}$, and utilizing the field specific calibrated value of N_{kt}=8.

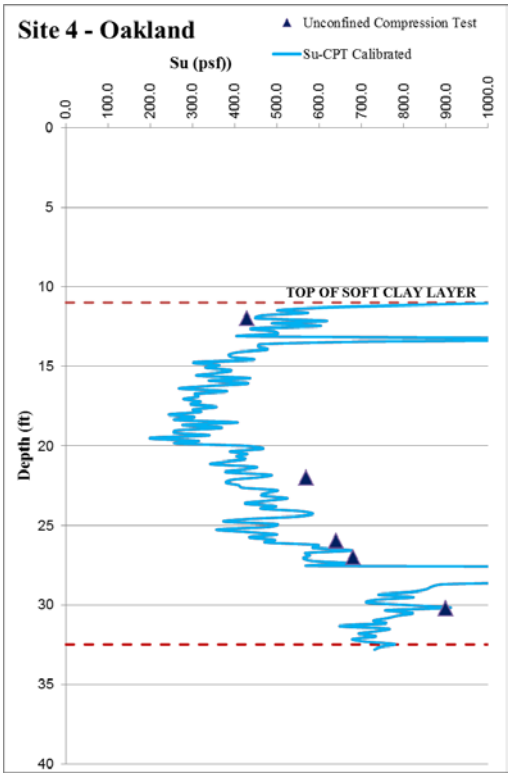

Figure 4.28: *Calibrated S_u profile for the site*

The value of N_{kt}=8 is in the lower part of the usual/expected range for N_{kt}. Values around 10 for N_{kt} are for very soft clays, and when the clay is sensitive, values less than 10 are expected.

Similar to previously discussed for site 2, the effect of shear strength decrease at test time due to excavation, was considered and implemented into the model. Figure 4.29 summarizes plots for overburden pressure during test time and CPT time, and shows s_u profiles for the CPT and pile test time.

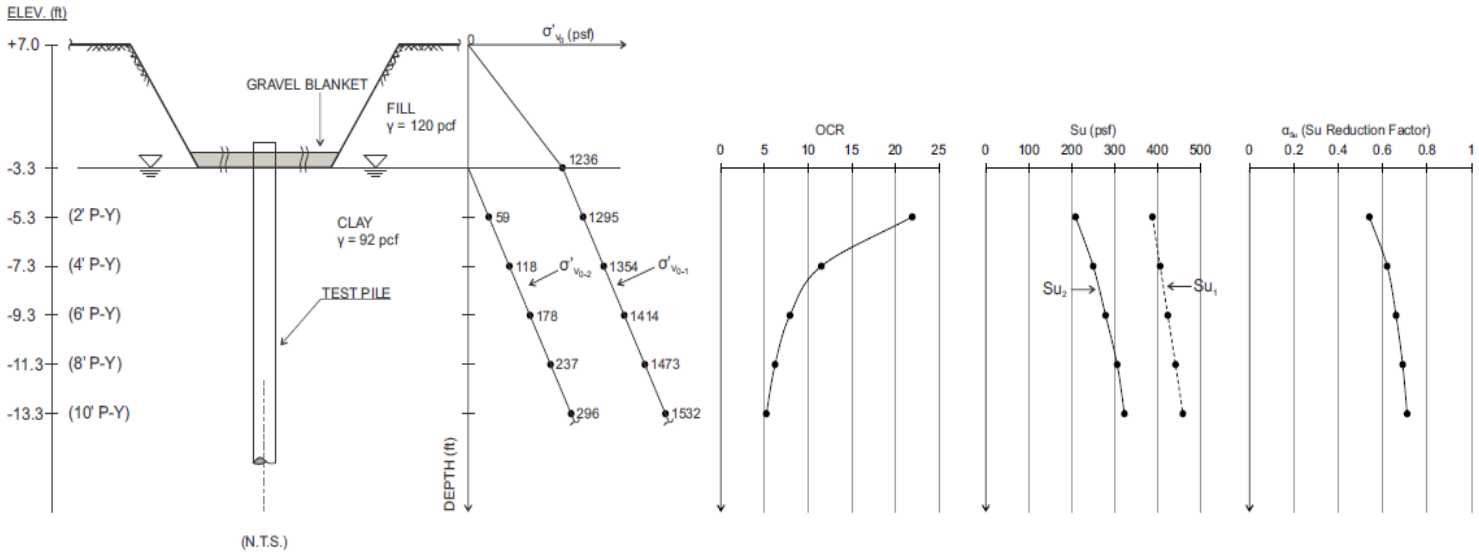

PILE TEST PROFILE FOR OAKLAND - SITE 4

σ'_{v0-1}: EFFECTIVE OVERBURDEN STRESS (CPT TIME)
σ'_{v0-2}: EFFECTIVE OVERBURDEN STRESS (PILE TEST TIME)
Su_1: UNDRAINED SHEAR STRENGTH (CPT TIME)
Su_2: UNDRAINED SHEAR STRENGTH (PILE TEST TIME)

Figure 4.29: *Effect of excavation on shear strength - Site 2, Oakland*

Therefore, and because of the decrease in shear strength due to the heave resulted from excavation during test time, another adjustment should be implemented to the calibrated profile shown in Figure 4.28. As presented in Figure 4.29, at each depth, a reduction factor shall be multiplied to the s_u values. The resulted profile will then be calibrated for the specific strength parameters of the site soils, and includes the effect of testing specific layout, i.e. heave of the clay due to the excavation. This final profile is shown on Figure 4.30.

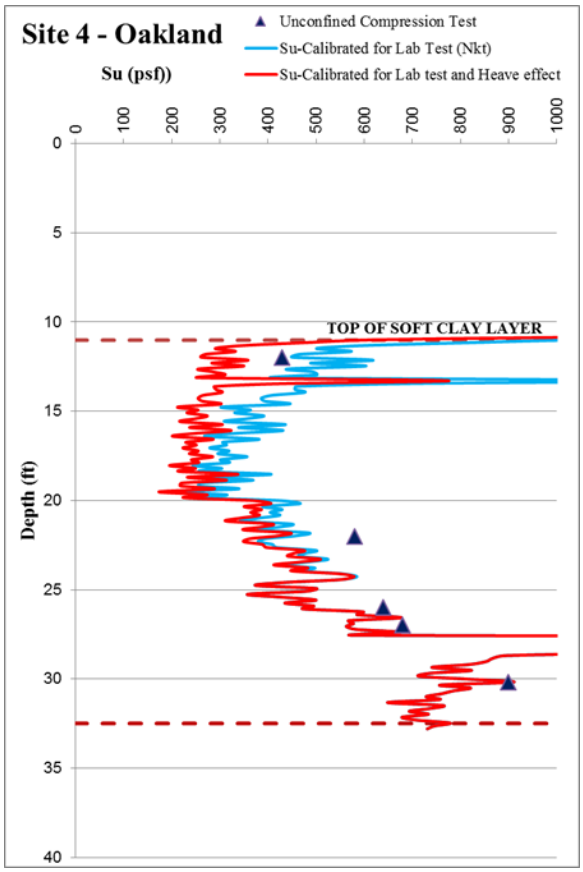

Figure 4.30: *Final calibrated S_u profile for the site*

Sensitivity of clays could be calculated using the following equation, suggested by Schmertmann (1978):

$$St = \frac{N_s}{R_f} \tag{4.2}$$

Where N_s is a constant. Rad and Lunne (1986) found that N_s is between 5 to 10, while Robertson and Campanella (1988) suggested an average value of 6 for N_s. By selecting N_s=6, the sensitivity of the clay layer is obtained and plotted in Figure 4.31. As it could be observed, the sensitivity within the range of concern, i.e. top of the clay layer to elevation of -20.0 feet is less than 1.0 and the clay most likely is sensitive. This somehow explains the value of N_{kt}=8 used for site calibration.

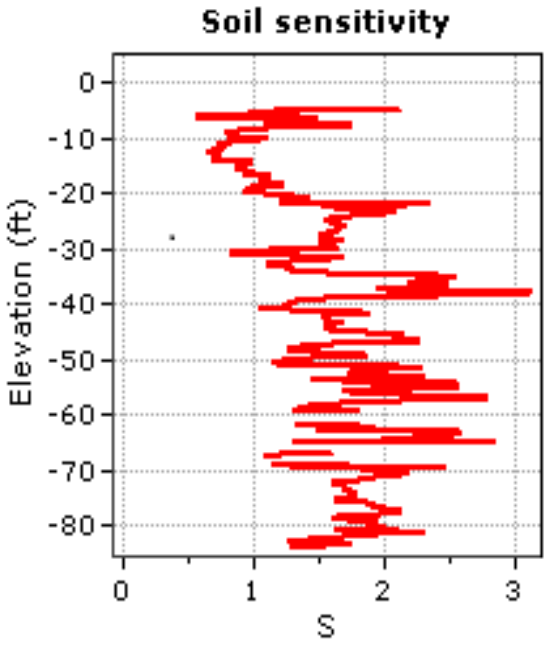

Figure 4.31: *Sensitivity profile for the clay layer using CPT data-based correlations*

Shear wave velocity was not measured at this site. Therefore, CPT-based correlations have been used to determine shear wave velocity profile. Shear wave velocity profile is determined by using equations 3.91 and 3.92 (Robertson, 2009) and equations 3.93 (Mayne, 1995). The profiles

plotted on Figure 4.32 indicate that the V_s within the first 10 feet of the soft clay layer obtained from (Mayne, 1995) is about 200 ft/sec, while by using Roberson, 2009, the determined shear wave velocity is about 280 to 300 ft/sec.

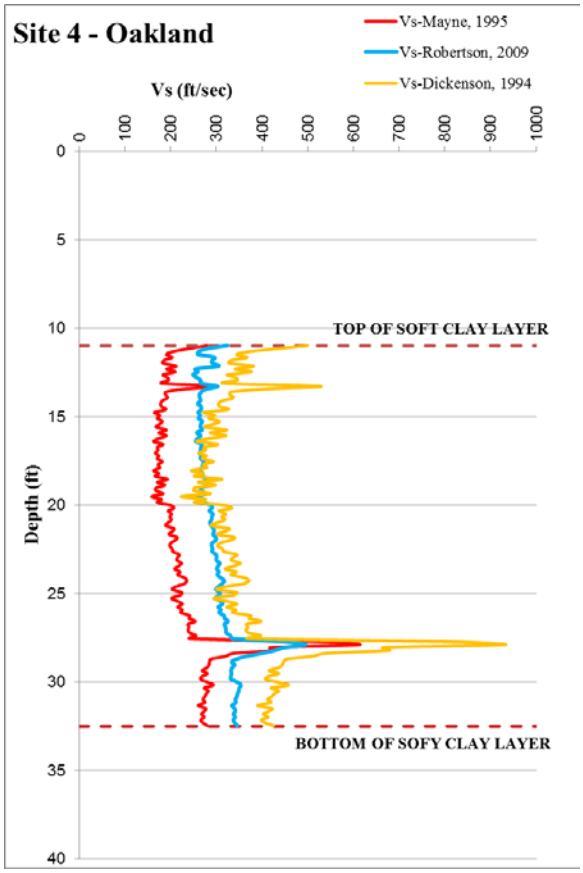

Figure 4.32: *Comparison of shear wave velocity obtained from CPT data using different correlations - Site 4*

Dickenson, S.E. and Seed, R.B. (1992) studied response of soft clay sites during the 1989 Loma Prieta Earthquake. In their study, they published the following Figure 4.33, which depicts the relations between shear wave velocity, V_S, and undrained shear strength, s_u for cohesive deposits in San Francisco Bay Area region. The suggested curve is $Vs=18\ (s_u)^{0.475}$.

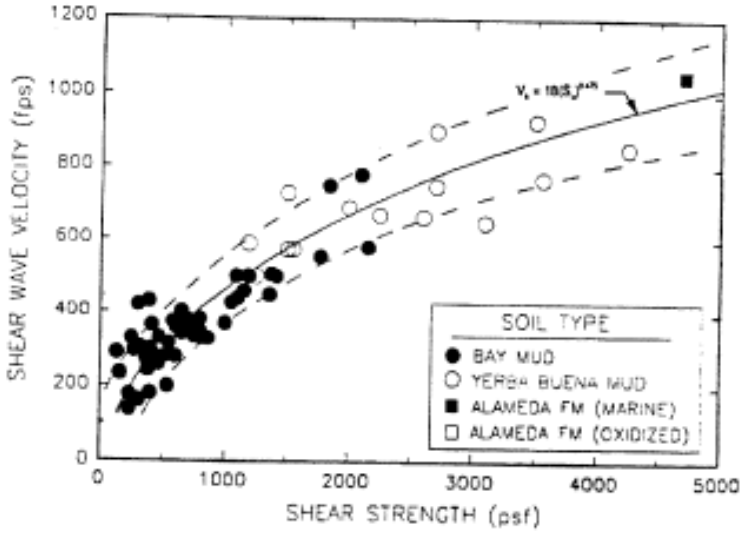

Figure 4.33: *Variation of V_s with s_u (monotonic) for SF Bay Area soft clay (Dickenson, 1994)*

For the site 4, the profile of shear wave velocity from the suggested correlation by Dickenson is shown on Figure 4.31. The two correlations by Robertson (2009) and Dickenson (1994) show a reasonable agreement.

4.2.2. Pile Properties and Load Test Description

Lateral pile load tests were conducted by simultaneously forcing of piles in pairs by jacking two piles together with two high strength threadbars connected to the piles and two hydraulic jacks. Figure 4.34 depicts plan and profile view of test set up for 4, in Oakland.

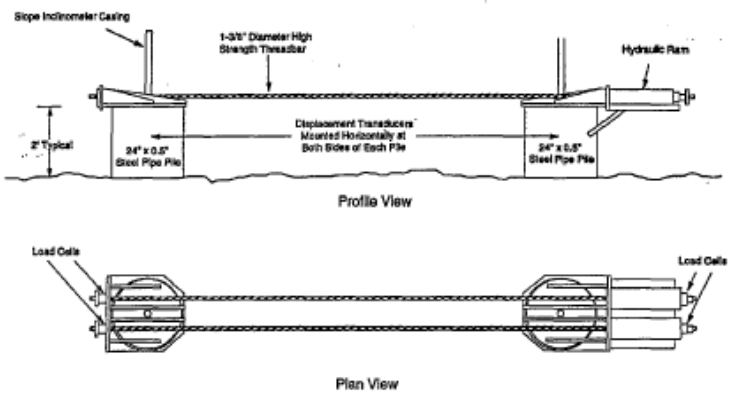

Figure 4.34: *Lateral Load Application set-up for the Oakland Site tests (Lemke, 1997)*

Pile load tests at Site 4 were conducted in an excavation with a planar dimension of about 39 by 82 feet. A planar layout of the pile load test area is shown on Figure 4.35.

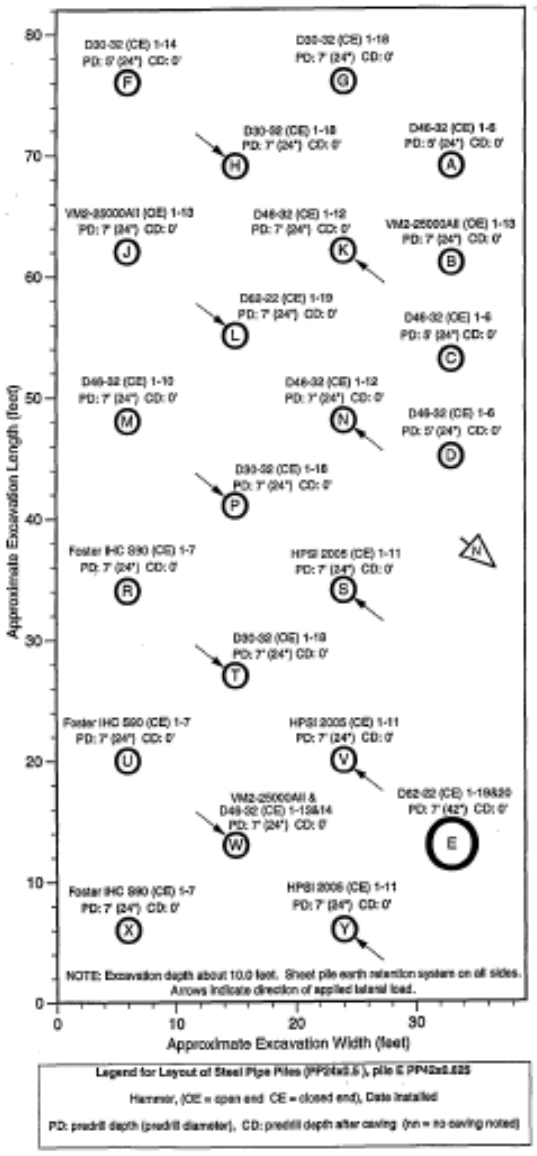

Figure 4.35: *Plan View of Test Pile Layout- Site 4 (Lemke, 1997)*

Prior to installation of the test piles, soil was excavated to an elevation of about -3.3 feet. An about one foot thick layer of gravel was placed across the bottom of the excavation bringing the final elevation up to -2.3 feet. The schematic profile shown as Figure 4.23 demonstrates the elevation of the excavated pit for the test area, and the ground surface prior to excavation. At Site

4, a total of ten 24-inch diameter pipe piles, with wall thickness of $\frac{1}{2}$ inch were tested. Each pile was filled with 8#9 rebar, spiral ties, and concrete.

Piles were tested in general accordance with ASTM D 3966-81, "Standard Method of Testing Piles under Lateral Loads." The loading procedure was in general compliance with Section 6.4.2 of the mentioned standard. Load applied to each pile was measured using a pressure gauge on the hydraulic pump operating the jacks and two donut load cells mounted on each pile co-axially with each high strength threadbar. The load cells had a 200 kip capacity and were calibrated. Horizontal displacements at each pile top were measured using a total of four displacement transducers mounted on reference beams about 1 to 2 feet above the ground surface. Two displacement transducers on each side of each pile were recorded electronically while two manual displacement transducers on each side of the pile were used.

Loads increments of about 7 to 20 kip were applied to each test pile and held for a period of about 10 minutes. Generally, from 5 to 10 load cycles were applied to each test pile. Lateral loads were applied to the top of the pile at a rate of about 5 to 10 kips per minute during load applications. The loading condition for the test piles was free-ended with shear applied at the pile top without moment.

During each hold period, slope inclinometer readings were typically taken in each pile in order to measure horizontal deflection along the pile length. All slope inclinometer readings were recorded by a digital computer.

The lateral deflection of the pile along its length was measured by using slope inclinometer instrument, which measures slope changes inside a plastic casing cast within concrete at the approximate center of each test pile. Slope changes were measured in two orthogonal directions.

One direction was chosen to be in line with the direction of the applied lateral load. Horizontal displacements may be calculated using the measured slope over the length of the slope inclinometer instrument. As stated in the report (Lemke, 1997), the accuracy of measured horizontal displacements is within about 1/4 inch over 100 feet of casing assuming that no operational errors occur. Corrections were applied to all slope inclinometer readings in order to reduce various types of errors. Each reading was multiplied by the ratio of the horizontal deflection at the pile top as measured by displacement transducers divided by the slope inclinometer deflection at the pile top. The clear horizontal spacing between each pair of test piles pulled together was about 9 feet. This distance is less than the horizontal distance recommended by ASTM D 3966-81 and may have influenced the measured load and displacement characteristics of the test piles.

4.2.3. Input Parameters for Analysis

Pile properties, as well as soils strength parameters shall be utilized to the integrated model. The pile properties include; B (pile diameter), L (pile length), E_p(pile material modulus of elasticity), E_y (yield modulus of pile material), A (pile cross section area), I (pile section moment of inertia), and M_{y-pile} (pile section yield moment). Also pile head constraint condition will be utilized into the model.

The only soils information to be uploaded to the model is CPT data file and the depth of ground water. The Matchad script in the model determines the basic soils parameters required to be utilized into a “ticle” file, which feeds the “OpenSees” program to solve the model.

The basic soil input parameters the Matchad script calculates are K_{max}, p_u, C and $y_{50.}$ These parameters are determined as explained in chapter 3. The profiles of input parameters for this site

along the depth of the soft clay layer are depicted in the following Figure 4.36. The value of C, the soils constant, is determined from equation 3.35, and for the soft clay layer at this site varied between 0.029 and 0.035

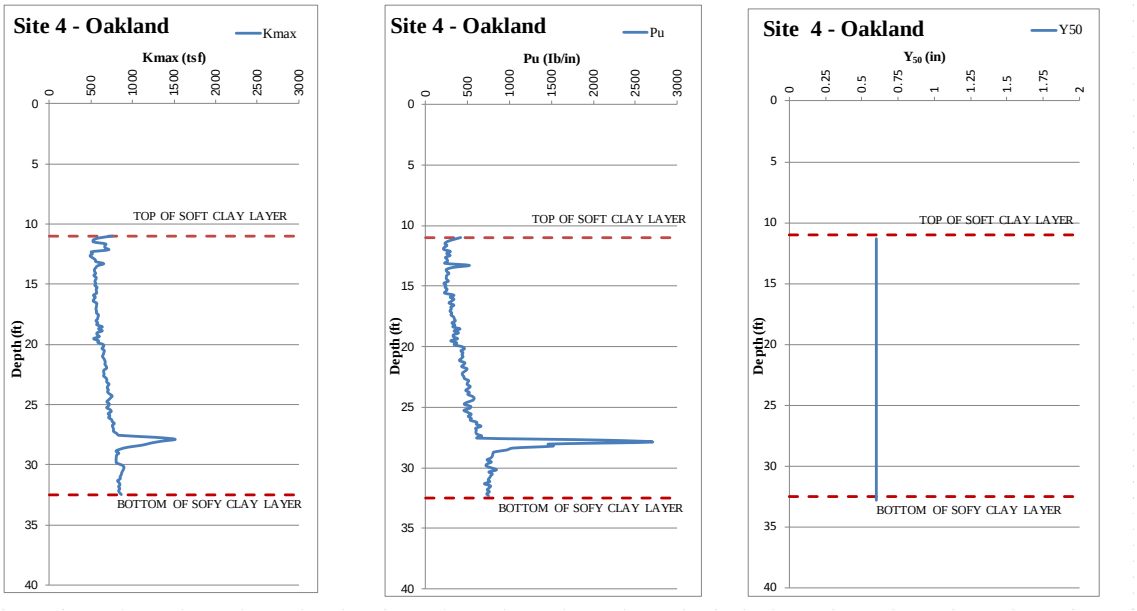

Figure 4.36: *Input Parameters profiles for Site 4, Oakland*

4.2.4. Measured and Predicted Results

By utilizing the CPT data into the "Model", the *p-y* curves for different depths were obtained. In the model, the values for each depth necessary to plot *p*-y curve are; initial stiffness, K_{max}, ultimate resistance, p_u, and parameter C which defines the curve's shape. The *p*-y curves are plotted for four different depths where the field resulted measurements were available. Field measurements are extracted from Lemke, 1997, and re-plotted on Figures 4.37 to 4.40. The *p-y* curves from the "Model" are plotted over the field results. The determined *p-y* curves show a reasonable agreement comparing to the field measurements. For each plot, values of *Pu*, K_{max} and *C* are shown. Shear wave Velocity, V_s is determined using Robertson (2009).

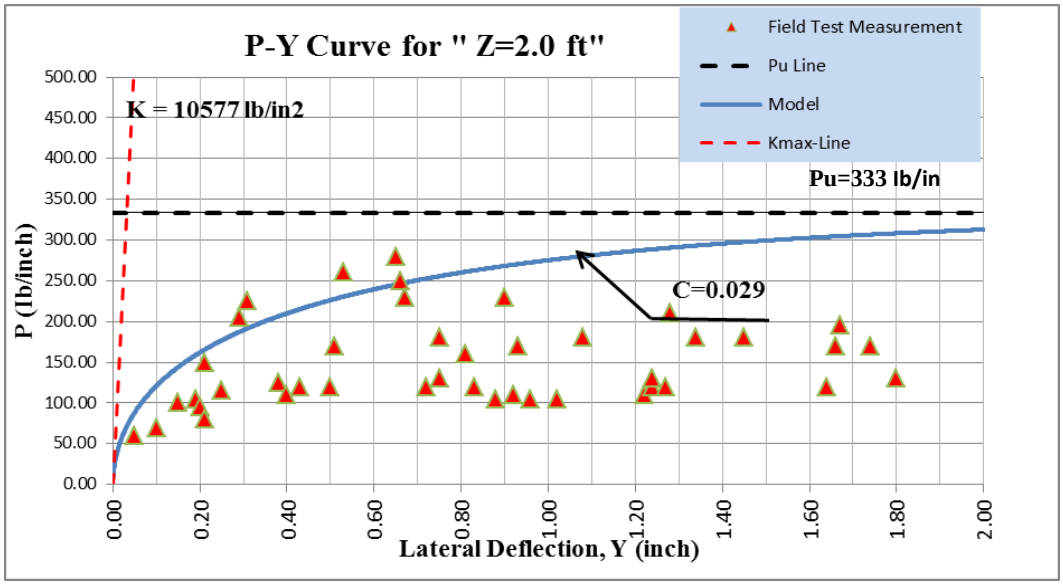

Figure 4.37: *Resulted p-y curve from the "Model" vs. field measurements at 2 feet*

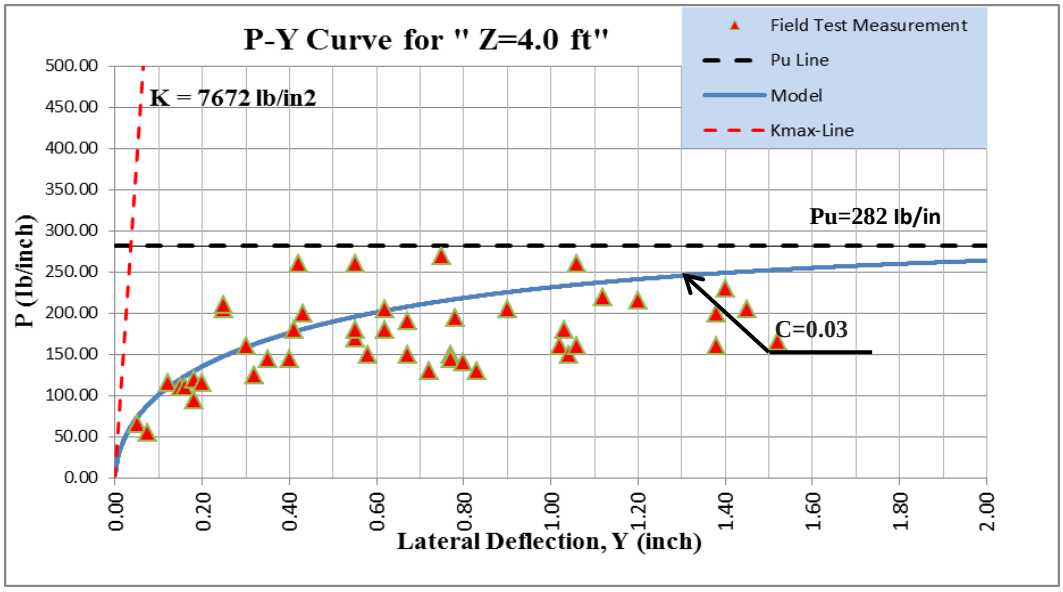

Figure 4.38: *Resulted p-y curve from the "Model" vs. field measurements at 4 feet*

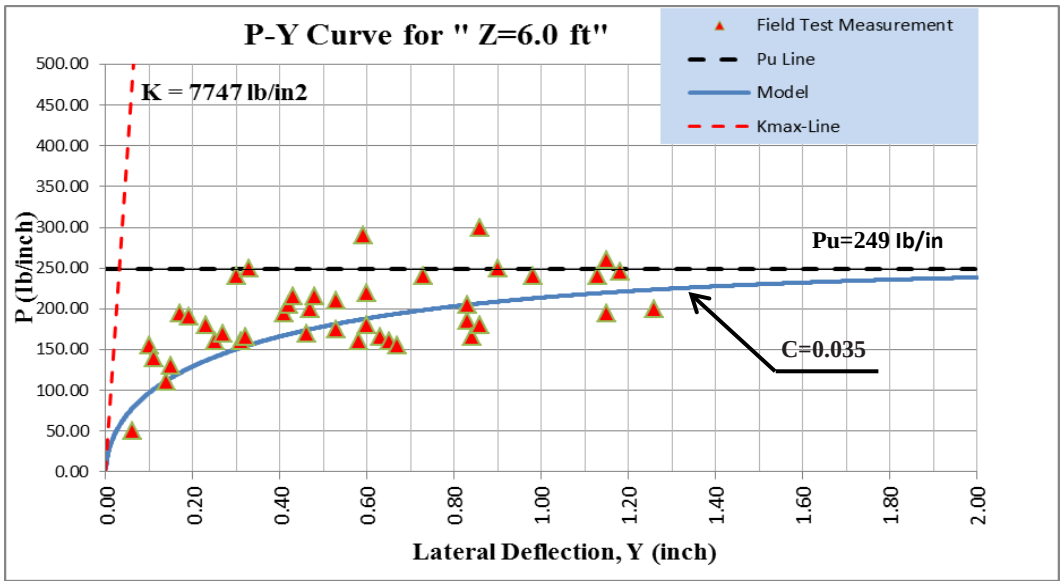

Figure 4.39: *Resulted p-y curve from the "Model" vs. field measurements at 6 feet*

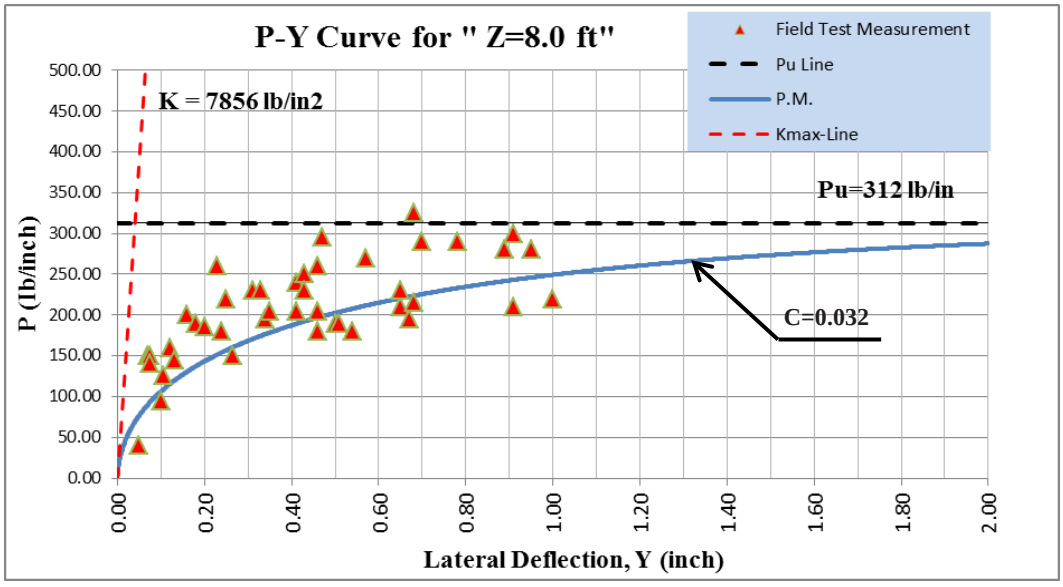

Figure 4.40: *Resulted p-y curve from the "Model" vs. field measurements at 8 feet*

Lateral load tests were performed on nine piles at Site 4, Oakland. The provided pile head force-displacement plots in the report (Lemke, 1997) have been digitized and re-plotted in Figure 4.41. Using CPT data and the "Model", p-y head force-displacement relation was determined, and is

plotted in red on Figure 4.41. For comparison, the force-displacement relationship resulted from LPILE program is plotted as well.

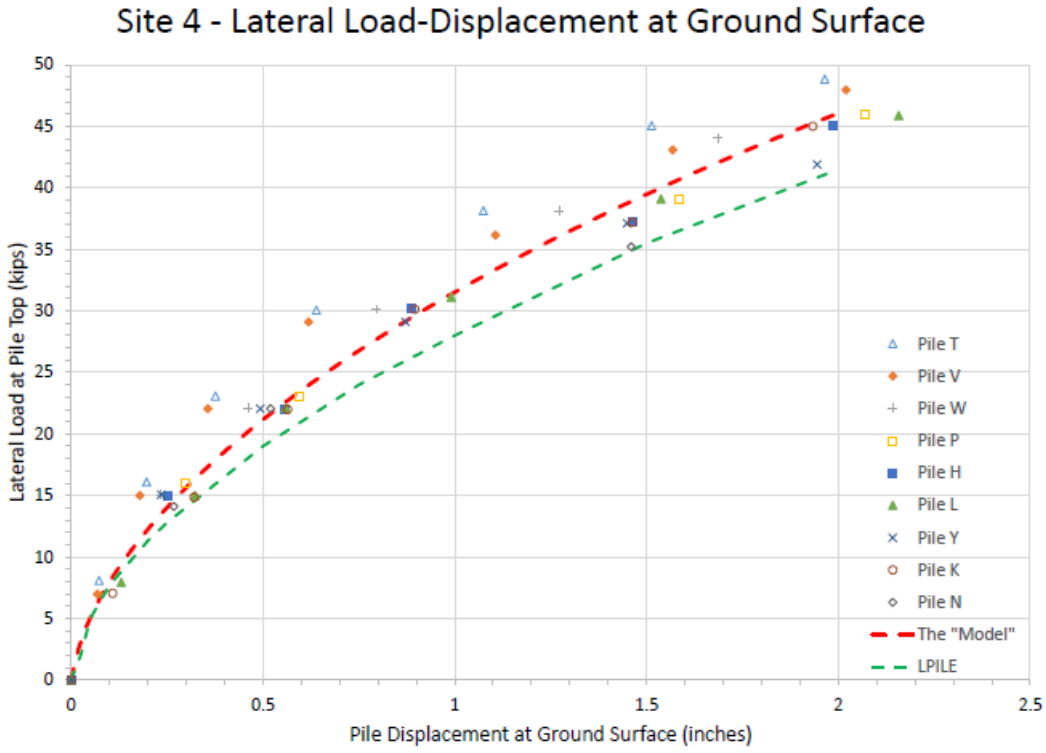

Figure 4.41*: Pile head Load-Displacement curves measured at Site 4 versus resulted curve from the Model and LPILE*

Due to lack of site specific V_s data for the site, CPT-based correlations embedded in the "Model" were activated in the analysis. As shown on Figures 4.37 to 4.40, the value of initial stiffness, K_{max}, is from 7.5 to 10.5 Kips/in^2. As discussed in Chapter 3, the accurate measurement of V_s is an important factor affecting the shape of the *p-y* curve. For a selected depth of 4 feet, *p-y* curves were plotted using different V_s values from Robertson (2009) and Mayne (1995). The *K* value from Robertson (2009) is 7,672 lb/in2, about 55% higher than the value from Mayne (1995). Referring to the analysis from the "Model", the determined V_s from Robertson (2009) and Mayne (1995), are 266 and 195 ft/sec, respectively. Although the difference in V_s using these two correlations is about 27%, the initial stiffness values differ about 55%, which is because of initial

stiffness's relation to the squared value of V_s. This amplifies the importance of using site specific/measured V_s. The enlarged part of the initial zone on Figure 4.42 is shown as Figure 4.43.

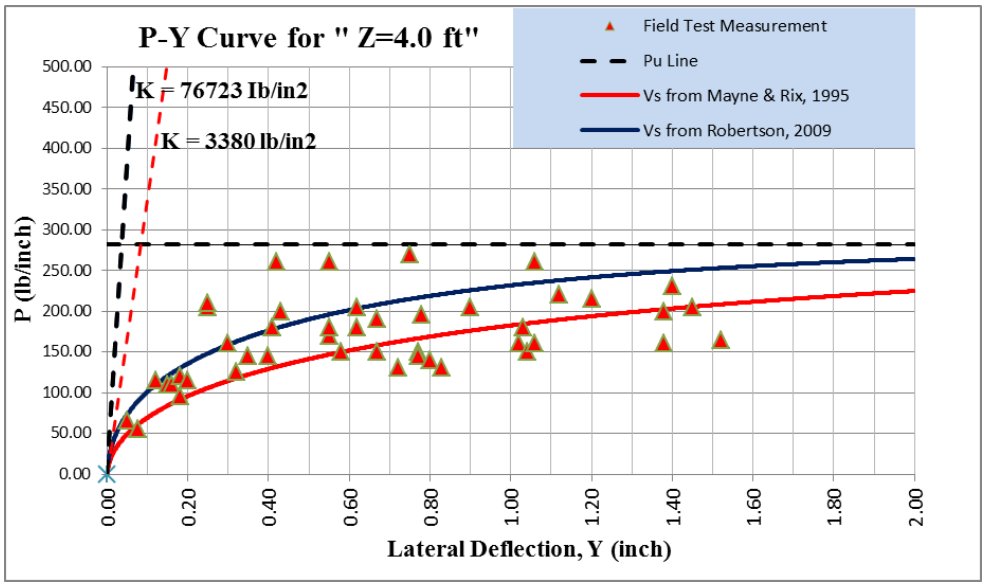

Figure 4.42: *Effect of choosing V_s correlation on resultant p-y curve; Comparison between using Mayne et al (1995) and Robertson (2009) suggested correlations for V_s*

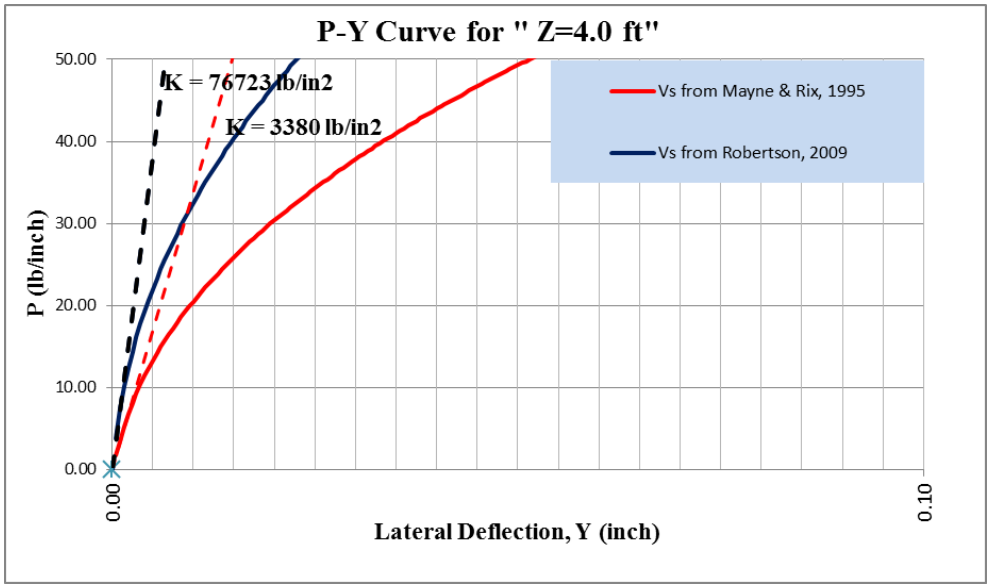

Figure 4.43: *Effect of choosing V_s correlation on initial stiffness of p-y curve; Comparison between using Mayne et al (1995) and Robertson (2009) suggested correlations for V_s*

One of the recent models presented is Lehane and Truong (2014). The model was developed based on numerical analysis 3D finite element, as mentioned in section 2.3.7. In their suggested model, a new parameter named I_r, shall be calculated and entered as an input parameter. For a specific depth of Z= 4 feet, the p-y curves obtained by using Lehane and Truong (2014) are plotted on the same Figure 4.38, and presented in the following Figure 4.44. The curves are plotted for two values of I_r equal to 33 and 67, respectively corresponding to clays with values of *Ec* equal to 0.01 and 0.005.

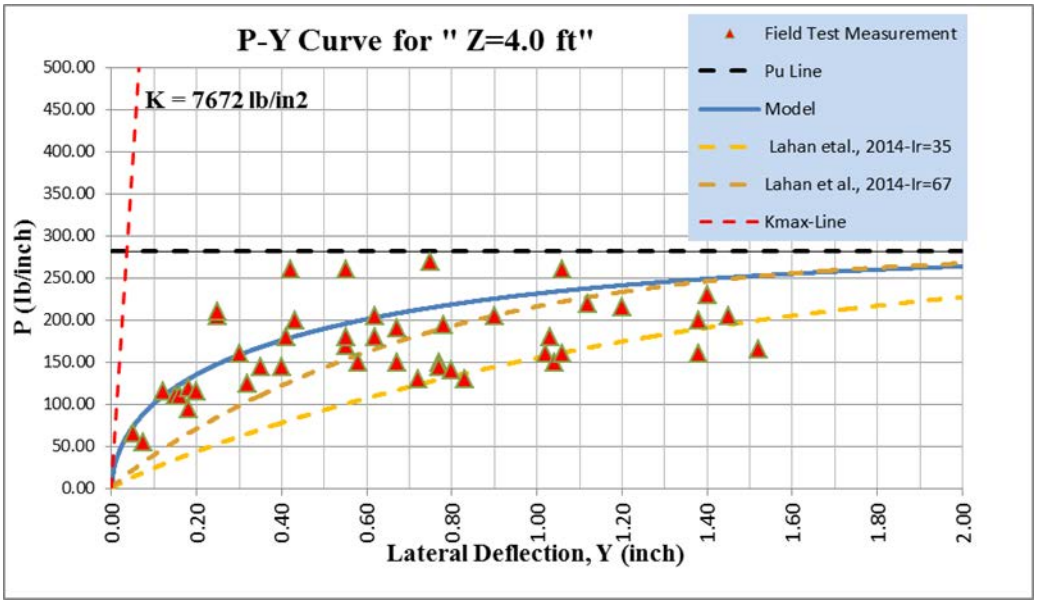

Figure 4.44: *Resulted p-y curve from the "Model" vs. field measurement, and p-y curve from Lehane et al. (2014)*

4.2.5. The Model Sensitivity to Input Parameters

The soil input parameters for the model are K_e (K_{max}) $P_{u,}$ C and $y_{50.}$ Also the soil yield force, P_y, as defined in the aforementioned section 3, is another input parameter. In this section, sensitivity of the model's outputs, i.e. analysis results, to variation of some of input parameters such as $P_{u,}$ K_e and P_y are studied and the sensitivity plots are presented. Also sensitivity plots for pile head force-displacement are presented.

Figure 4.45 depicts the sensitivity plots of pile reaction to variation of P_u, the soil ultimate resistance. The plots of pile displacement, moment, shear and mobilized soils resistance are shown for the original analysis, when the soil resistance is Pu, and pile responses for two conditions of soils resistance, i.e. $2P_{\mathrm{u}}$ and $0.5P_u$ are plotted. Figure 4.46 depicts the sensitivity plots of pile reaction to variation of K_e, the initial stiffness of the soil. The plots of pile displacement, moment, shear and mobilized soils resistance are shown for the original analysis, when the soil initial stiffness is K_e, and pile responses for two conditions, i.e. $2\ K_e$ and $0.5\ K_e$ are plotted. Figure 4.47 includes the sensitivity plots of pile reaction to variation of P_y, the soil yield force. The plots of pile displacement, moment, shear and mobilized soils resistance are shown for the original analysis, when the soil yield force is P_y, and pile responses for two conditions of soils resistance, i.e. $2P_y$ and $0.5P_y$ are plotted. Figure 4.48 is a similar sensitivity plot of the soil/pile responses to variation of $\varepsilon_{50,}$ the strain corresponding one-half of the maximum stress on a laboratory stress-strain curve resulted from triaxial test on the soil.

It can be concluded that the analysis results, i.e. pile responses, are more sensitive to variation of soil ultimate resistance, P_u and less sensitive to variation of soil yield force.

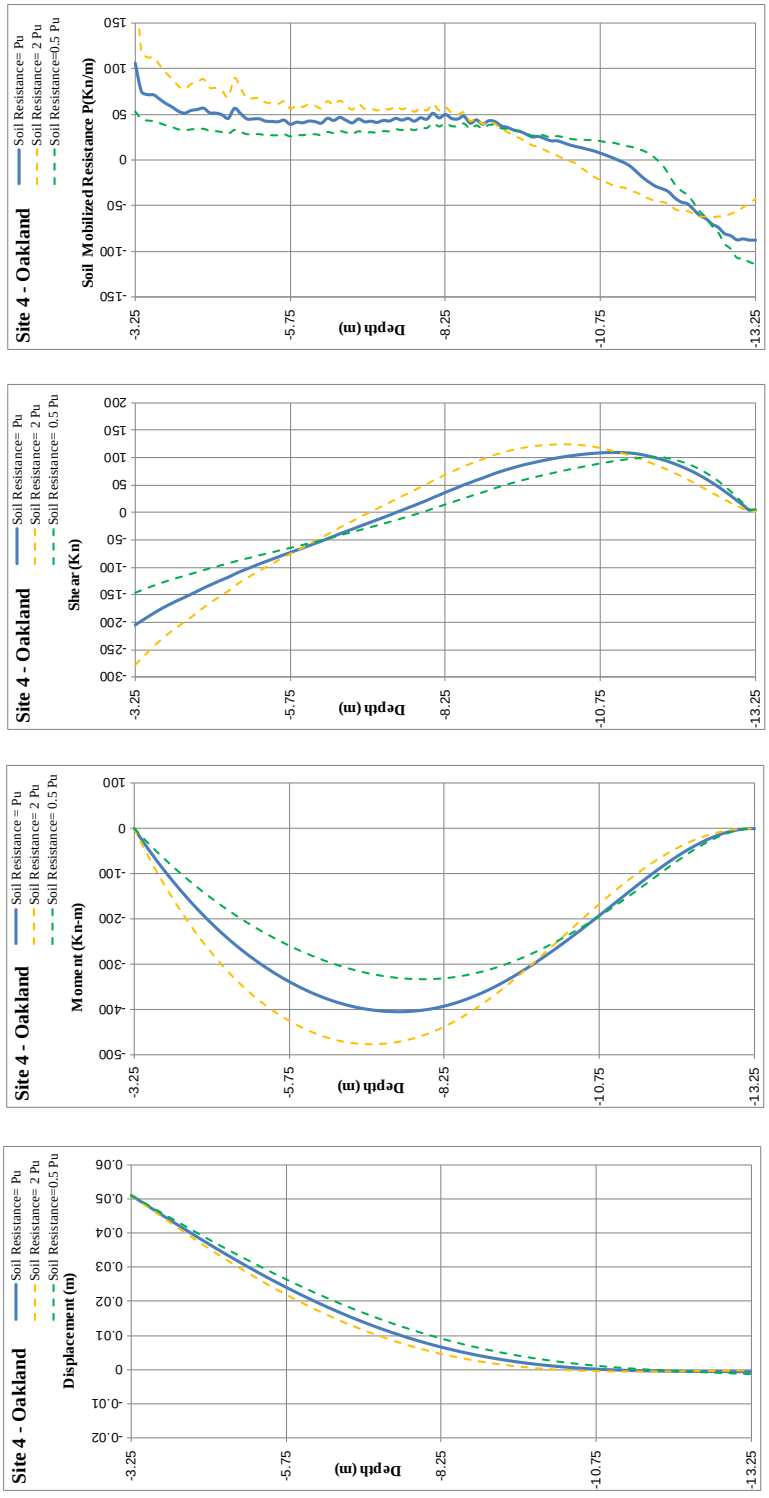

Figure 4.45: *Sensitivity plots of pile responses to variation of soil ultimate resistance, Pu*

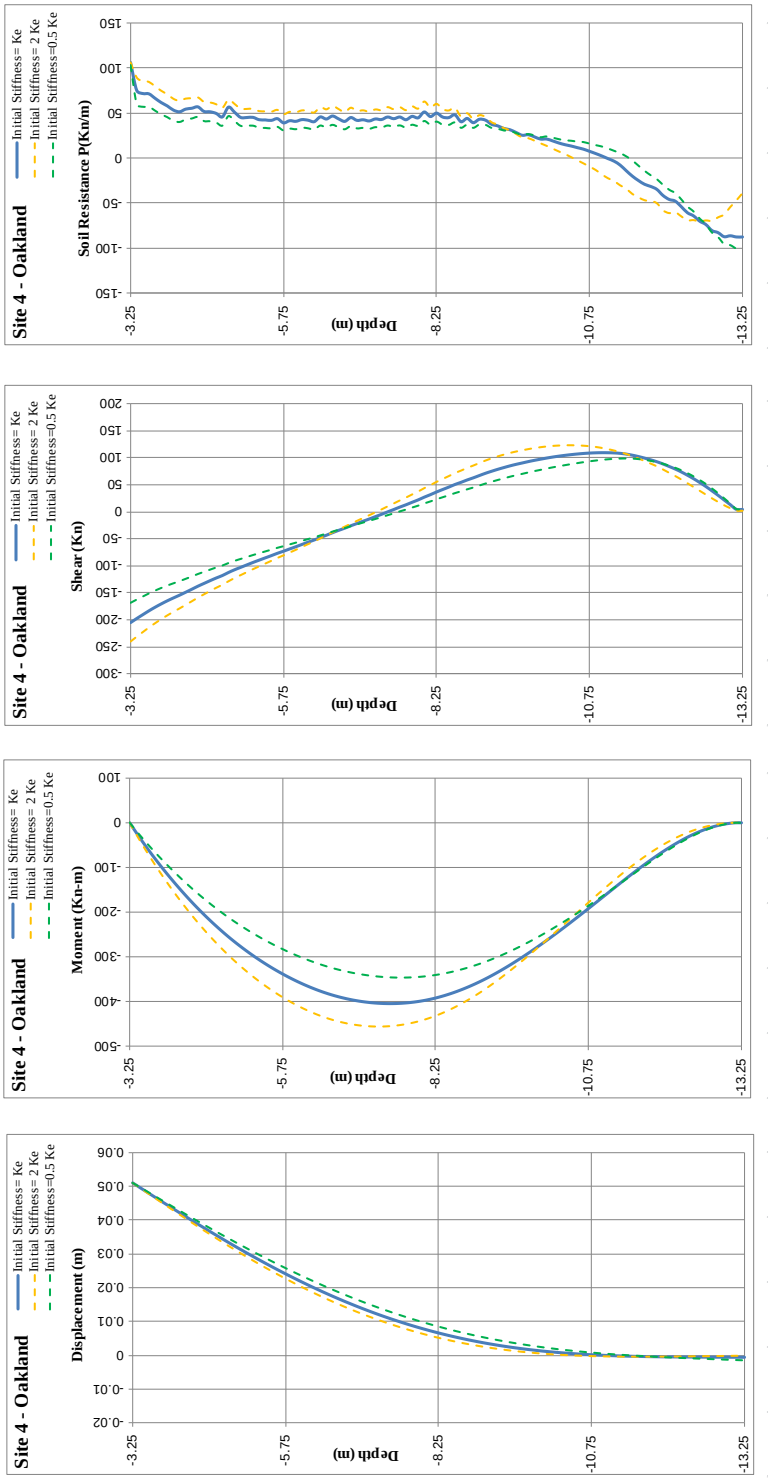

Figure 4.46: *Sensitivity plots of pile responses to variation of initial stiffness, Ke*

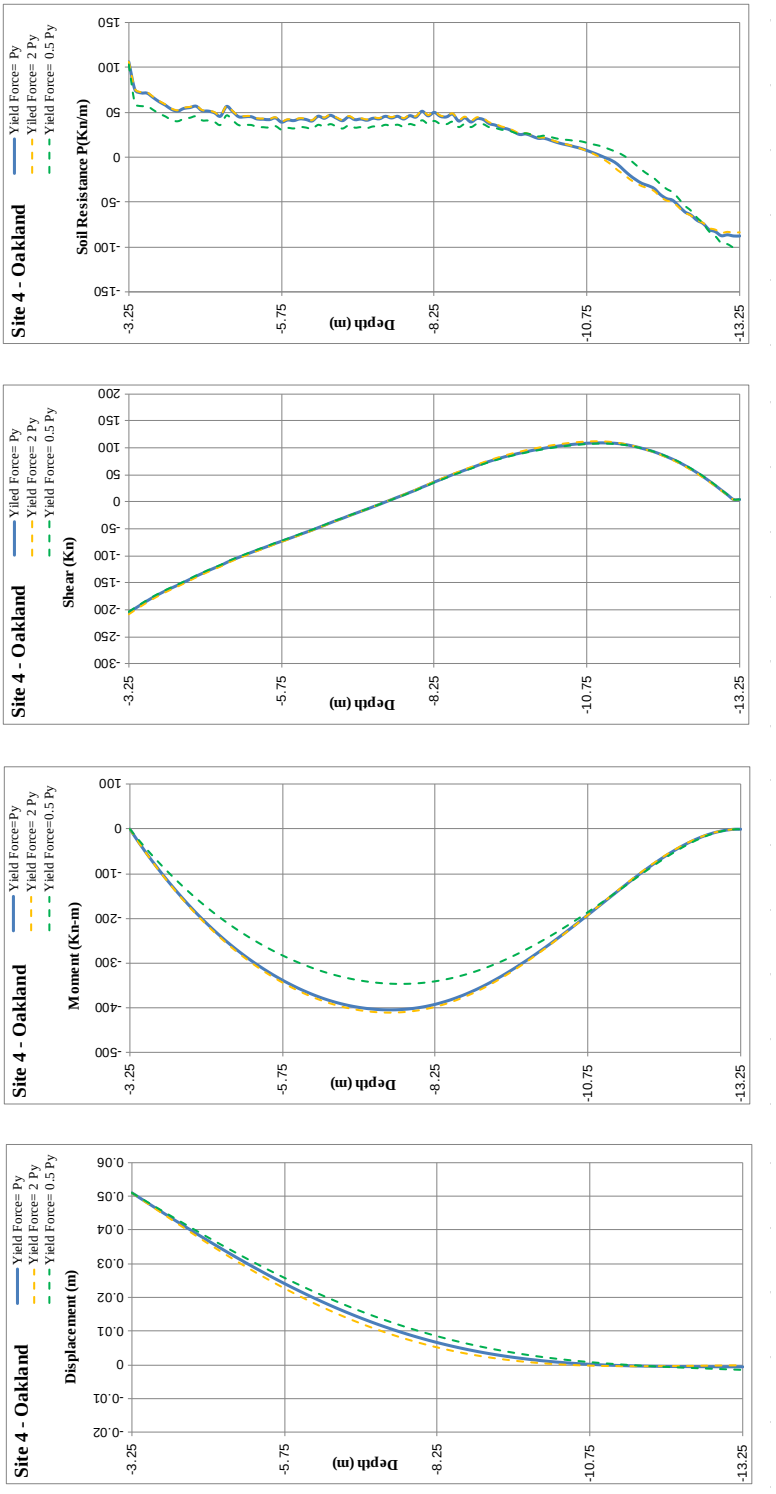

Figure 4.47: *Sensitivity plots of pile responses to variation of yield force, Py*

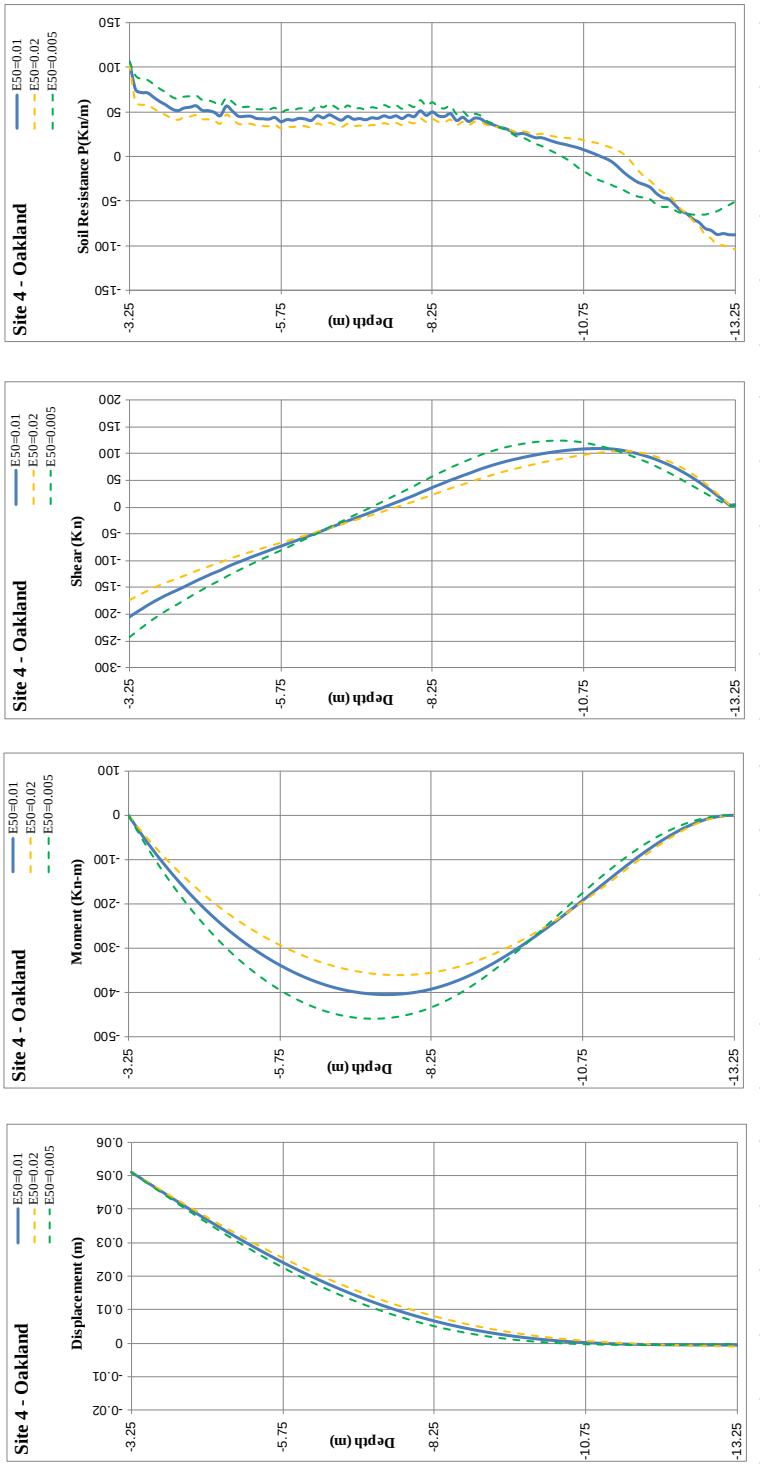

Figure 4.48: *Sensitivity plots of pile responses to variation of* ϵ_{50}

Figures 4.49 to 4.52 show sensitivity of pile head force-displacement to variation of the said input parameters. Variation in P_u results in larger changes in pile head force-displacement, while variation of the initial stiffness has less effect on the pile response. Figure 4.51 indicates that change in soil yield force, P_y, has a negligible effect on the pile response.

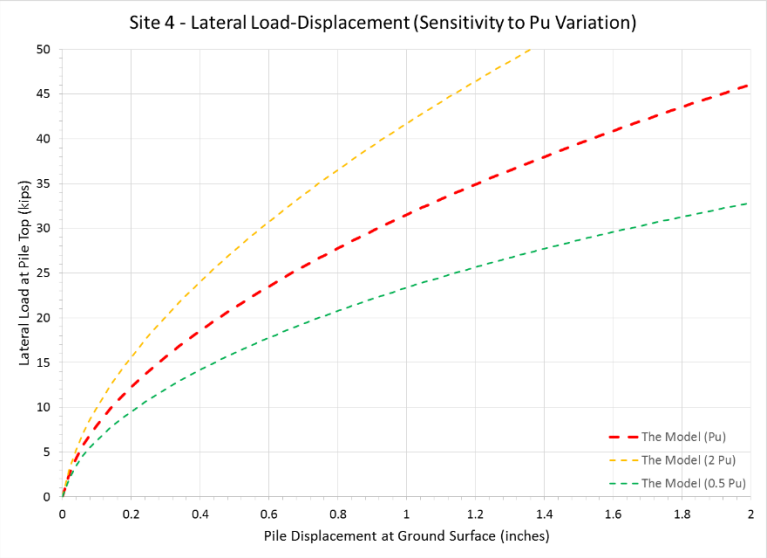

Figure 4.49: *Pile head Force-Displacement Sensitivity to variation of* P_u

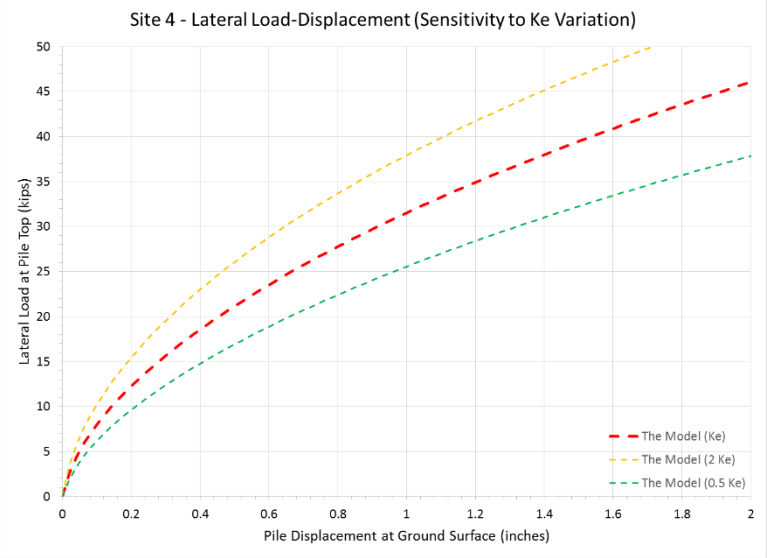

Figure 4.50: *Pile head Force-Displacement Sensitivity to variation of* K_e

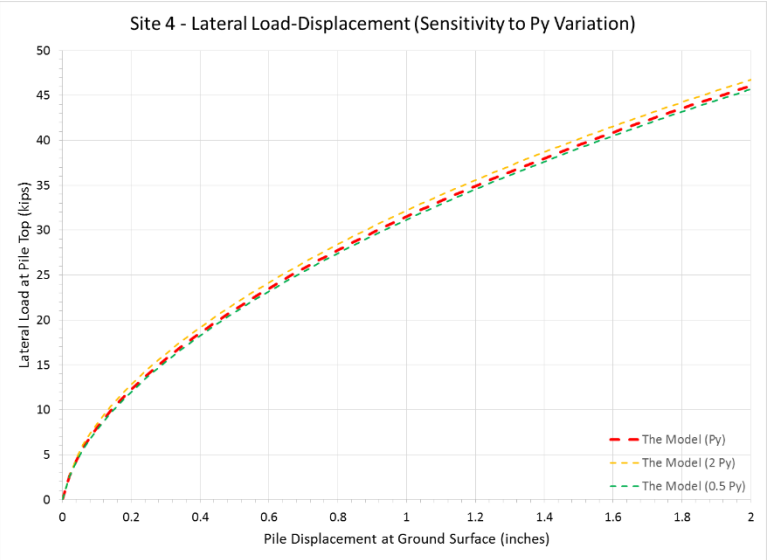

Figure 4.51: *Pile head Force-Displacement Sensitivity to variation of* P_y

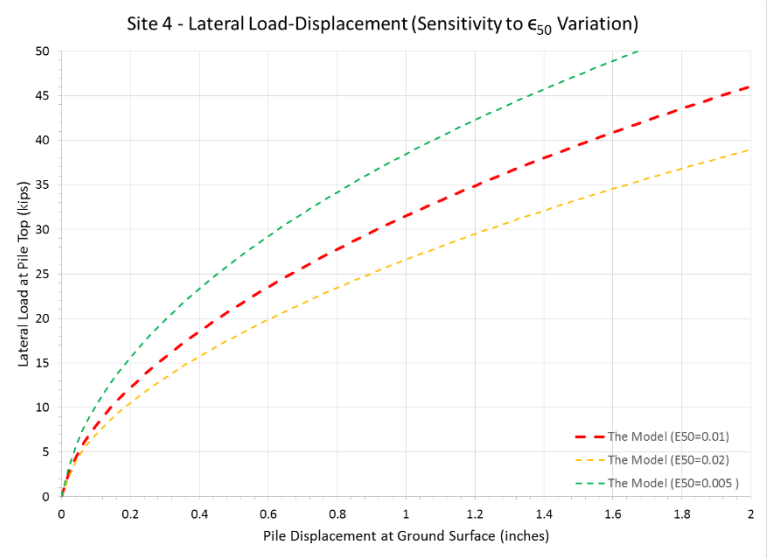

Figure 4.52: *Pile head Force-Displacement Sensitivity to variation of* ε_{50}

4.2.6. Discussion on Results

During the test, ground water level was at top of the clay layer, and the soft clay layer was saturated, representing an undrained behavior in shear. Within the depth range of concern, i.e. the upper 15 feet of the soft clay layer, I_c varies between 2.9 to 3.8. The clay layer will behave

undrained in shearing, and values of I_c compared to the criteria suggested by Robertson (2010), as shown as Figure 2.41, concludes the same behavior for the clay layer.

The most credible field measurement during pile lateral testing is displacements at pile head. For this case, pile head Load-Displacement obtained from the "Model" shows a very good match with the field measurements, as compared in Figure 4.41. The *p-y* curve from the "Model" at depth of 2.0 feet is depicted on Figure 4.37. Similar to the "Site 2" case, as it is seen, the "Model" curve is slightly higher than the trends of the data points. This might be because of softening in the shallow clay occurred due to driving operation of the pile, which resulted in decreased resistance values for the clay. The "Model" curve at 4 and 6 feet, i.e. Figure 4.38 and Figure 4.39, have a reasonable fit, and the curve at 8 feet shown in Figures 4.40, falls slightly below the data points.

As discussed for the "Site 2" case, when comparing the model driven *p-y* curves with field measurements at this site, the followings might be considered as main reasons for some mismatches encountered:

- Data points for *p-y* curves shown as field measurements were determined in a conventional way of measuring the pile's slope/curvature at different depths, and determining *p* and *y* accordingly. However, the change in slope through the pile was measured by inclinometers installed at center of the piles. This method of measuring curvature is not as accurate as other means such as use of LVDTs.
- Shear wave velocity was not measured at the site. The V_s values obtained using correlations suggested by Robertson (2009) and Mayne (1995) have resulted in relatively low values for V_s However, if the real V_s for the subject site is higher than the values used in analysis by the "Model", the curves from the "Model" will shift upward, resulting in a better match with the field measurements.

- In very soft clays, there may be some uncertainty with the accuracy of in q_t values. In these cases, it would be better to estimate s_u from correlations based on excess pore water pressure (Δu_2) measured behind the cone. This will result in a more accurate value for s_u when in very soft clay soils.
- The values obtained for the soil ultimate resistance P_u at different depths from the "Model" varies between 249 lb/in to 333 lb/in for the depths between 2 to 8 feet, as shown in Figures 4.37 to 4.40. However, for the same depths, the values for P_u reported in Lemke (1997) vary between 170 to 280 lb/in. The undrained shear strengths used in the "Model" are derived from CPT data, and the profile was calibrated to best fit to the filed specific values from laboratory tests. However, the s_u values for the site were determined from unconfined compression tests on the samples. The preciseness of s_u values obtained from unconfined compression tests is a matter of concern and may be a relatively important factor in explaining some differences in the results.
- Field measured head force-displacement for nine tested piles at this site are shown on Figure 4.41. The head force-displacement curve from both the proposed model and LPILE are depicted as well. The curve from the model shows a better agreement with the field test data than output from LPILE. Especially, initial stiffness of the curve, i.e. initial slope, from the model seems to be more reasonable.

Considering the factors discussed, the results of *p-y* curves from the "Model" are reasonably satisfactory, and the pile head Load-Displacement results are in a very good agreement with the field measurements.

4.3. Caltrans Test Site, Hawthorne, California

The Hawthorne site is located in Los Angeles, California. The site belongs to the California Department of Transportation (Caltrans) and in a collaborative project between Caltrans and UCLA, a series of field tests were conducted at the said site. The purpose of test program was to assess the influence of pile diameter, boundary condition and group effects on the lateral load behavior of CIDH piles. The test program on single pile and group piles are part of tests conducted on bridge foundation components between 1998 and 2006 (Janoyan et al. 2006; Stewart et al. 2007).

4.3.1. Soil Condition

The test site is located near the intersection of Interstate Highways 105 and 405 in Hawthorne, California. The mapped local geology is Quaternary alluvium. According to the exploratory boring conducted at the site, a shallow layer of undocumented fill exists at the site. The artificial fill layer is 1.2 m-thick and is underlain by partially saturated over-consolidated clay, with some occasional thin sand interbedded layers, which extends to about 7.3 meters below the surface. A layer of silty sand soil was encountered between 7.3 to 8.8 meters, and was underlain by a layer of slightly silty clay, extended to about 15 meters.

Field in-situ and laboratory testing was performed to characterize the soil conditions at the site. The field testing included conducting seismic cone penetration testing (SCPT), rotary-wash borings with standard penetration testing (SPT), down-hole suspension logging of shear wave velocities, pressuremeter testing (PMT). Thin-walled Pitcher tubes were obtained from the borings and were hand-carved from the walls of the test pit. Laboratory tests including particle size distribution, Atterberg limits, shear strength, and consolidation characteristics were

performed. In the native soils layer underlying the surficial artificial fill Laboratory testing indicates a fines content of approximately 60%, LL = 34%, and PL = 19, leading to a soil classification of CL by the Unified Soil Classification System, extending to about 7.3 meters. A relatively thin lens of silty sand/sandy silt soils was encountered between 3.8 to 4.2 meters within the said clay layer. A medium- to fine-grained silty sand/sandy silt layer was encountered at 7.3, and extended down to about 8.8 meters below the ground surface. This layer was underlain by a slightly silty clay layer, extending to about 15 meters below the ground. The 0.6 meter shafts bases were located into the silty sand/sandy silt layer located between 7.3 to 8.8 meters. Figure 4.53 presents profiles of soils, cone tip resistance, friction ratio, CPT- based calibrated undrained shear strength, as well as moisture content test results at the site.

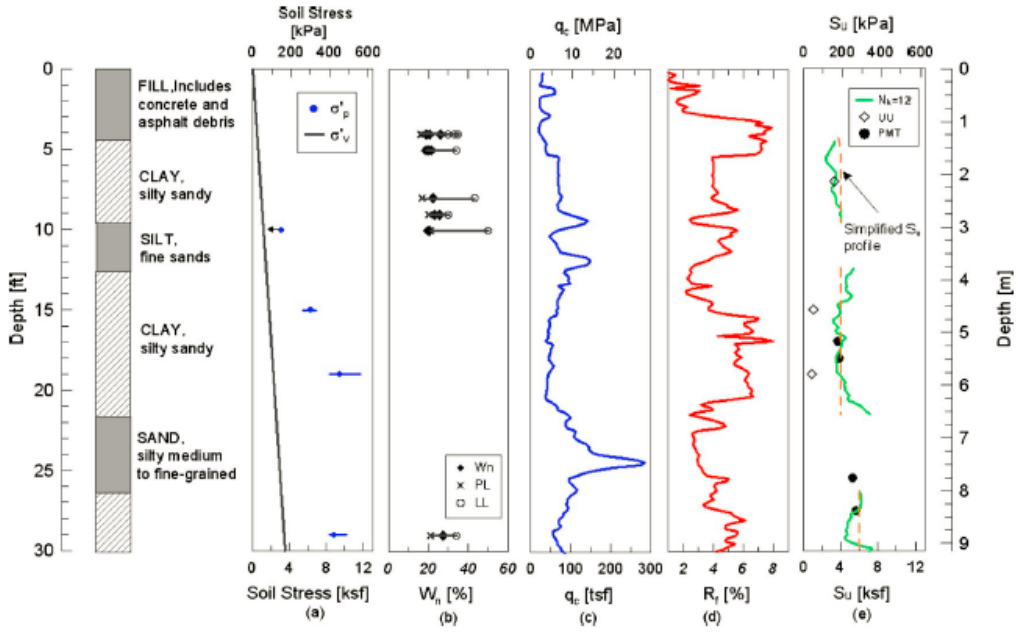

Figure 4.53: *Site Stratigraphy and soil condition at the Hawthorne test site (Lemnitzer et al, 2010)*

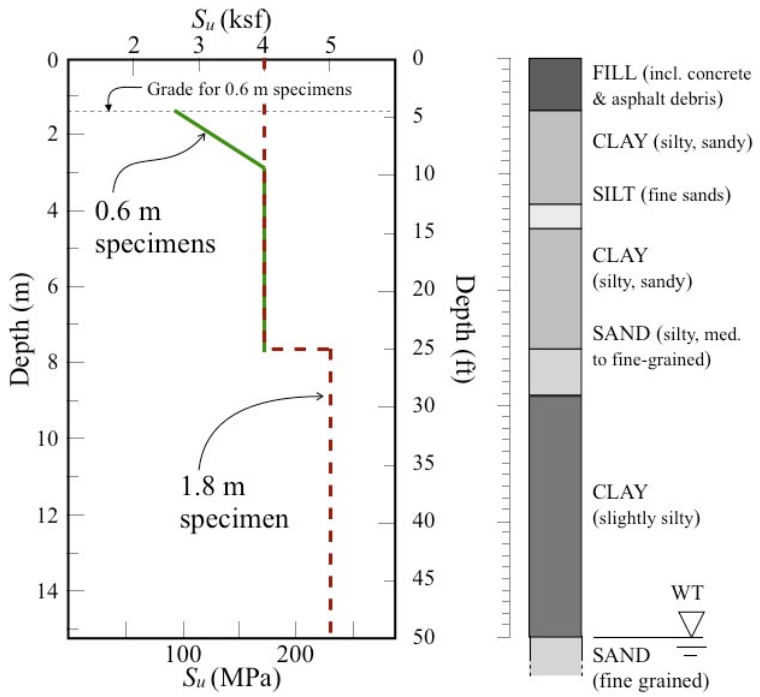

Figure 4.54: *Simplified representation of soil undrained shear strength (S_u) profile and stratigraphy at site (Khalili Tehrani et al., 2012)*

Within the stiff clay layer, three laboratory unconsolidated-undrained (UU) tests performed on the collected samples using Pitcher tube samples. The samples were tested under confining pressure corresponding to in-situ condition and at their in-situ water content. Shear strength was taken equal to 50% of the peak deviatoric stress. Also in-situ pressuremeter test (PMT) was performed and the results were used to determine undrained shear strength (Menard 1975; Briaud 1986, 1992). The determined undrained shear strengths are shown on Figure 4.53 (e). Figure 4.54 depicts the simplified shear strength profile at the site.

By utilizing the available CPT field data into the" CPTeT-IT" software, the regular and normalized plots of cone resistance, friction ratio, Soil Behavior Type index (SBT) and stratification of the site at the test location are obtained and depicted as Figures 4.55 and 4.56 The CPT plots conclude that within the first 22 feet from the ground surface, the earth materials

consist of silty clay and clay soils. Also a relatively thin lens of silty sand/sandy silt soils was encountered at around 3.8 to 4.0 meters within the said clay layer. This CPT-based stratification is in agreement with the boring log shown in Figures 4.53 and 4.54. Within the stiff clay layer, i.e. 1.2 to 7.3 meters deep, I_c is varying between 2.3 to 2.8, being predominantly between 2.4 to 2.6.

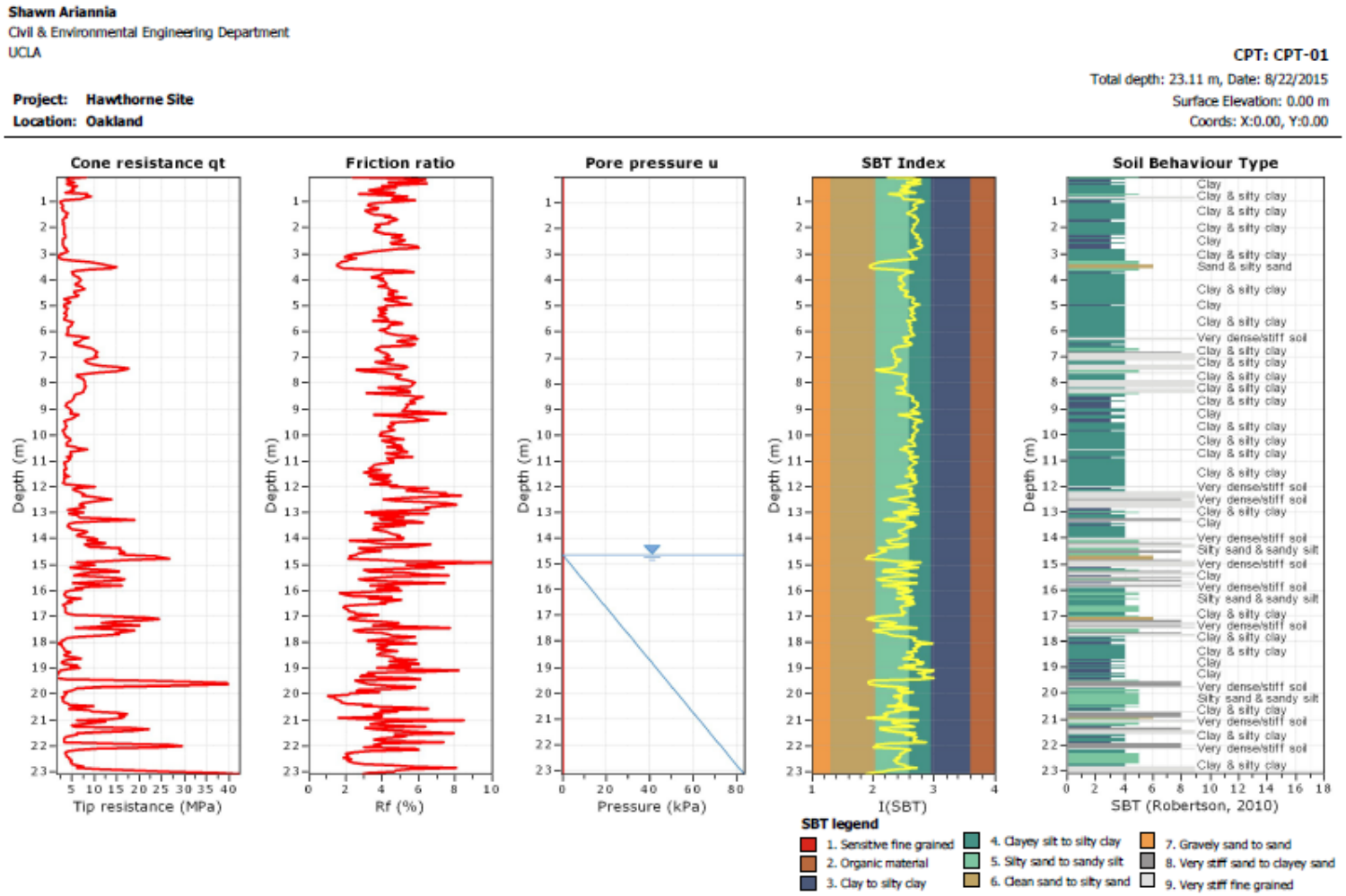

Figure 4.55: *CPT basic plots for Hawthorne Site*

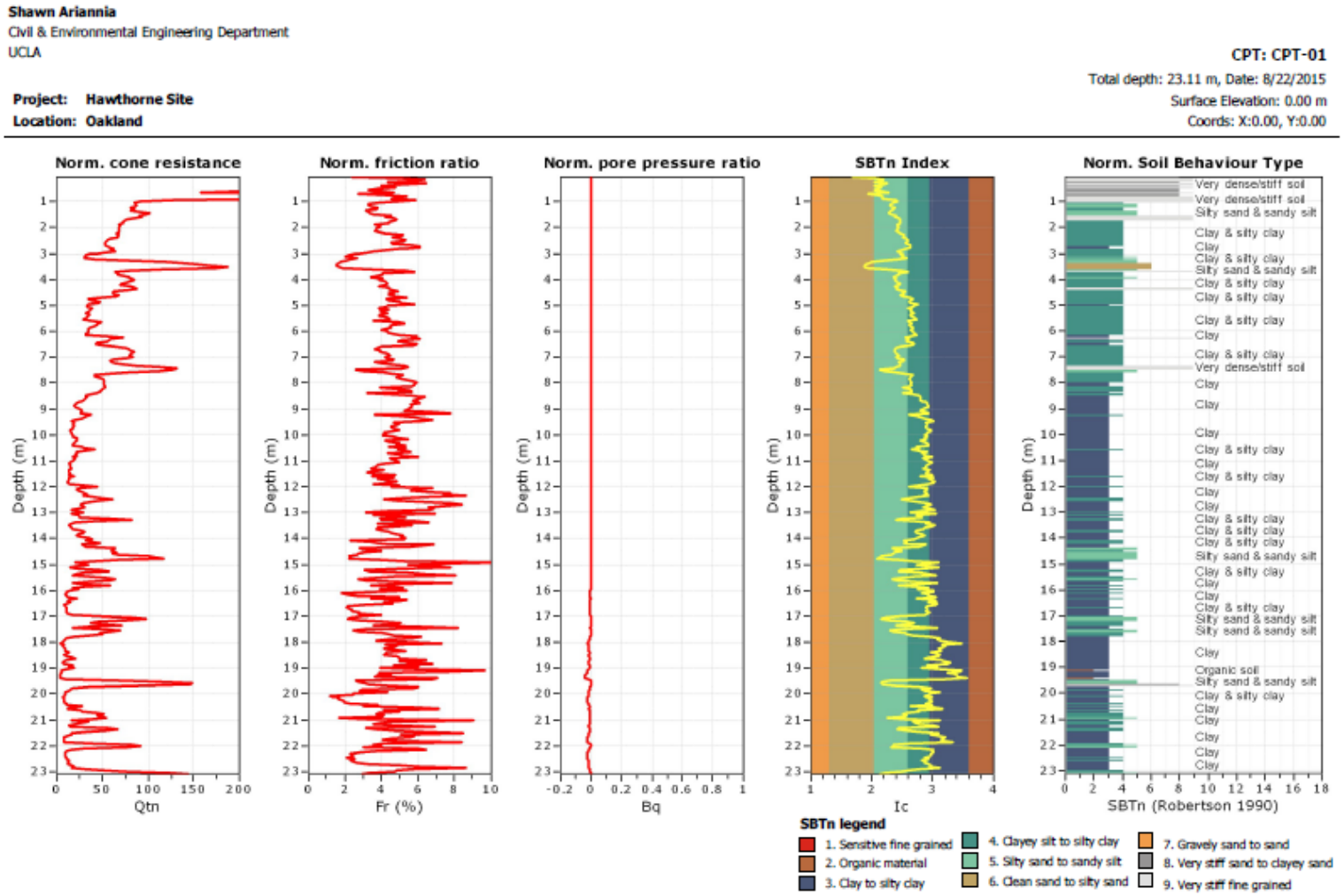

Figure 4.56: *CPT basic plots for Hawthorne Site*

Referring to Figure 4.53(e), undrained shear strengths were obtained from laboratory tests, i.e. unconsolidated-undrained (UU) test, and using the results of in-situ pressuremeter tests. In the study by Lemnitzer et al, (2010), the CPT cone resistance was site-calibrated giving preference to undrained shear strength values resulted from pressuremeter test (PMT). In this study, the following undrained shear strength profile in Figure 4.57, is being determined by initially using CPT data and equation $s_u = \frac{(q_t - \sigma_v)}{N_{kt}}$, and utilizing a field specific calibrated value of N_{kt}=17.

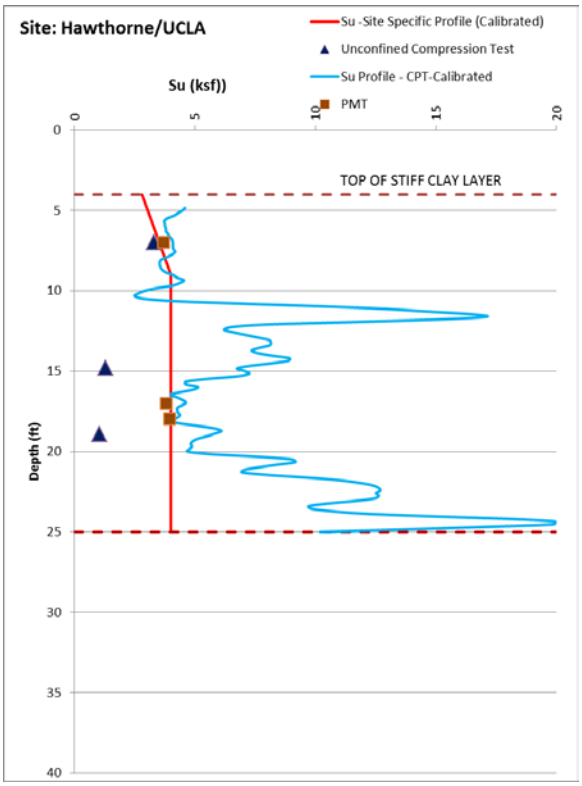

Figure 4.57: *Calibrated S_u profile for the site*

By performing seismic cone penetration test (SCPT), shear wave velocity was measured at this site. The measurement performed at 5 feet (1.52 m) vertical intervals through the clay layer and the results are plotted on Figure 4.58. Within the first 12 feet of the clay layer, V_s was measured and varies between about 800 to 1200 ft/sec. Also, shear wave velocity profile determined by

using Robertson correlations (2009) is plotted on the same figure. The V_s profile from Robertson (2009) is calibrated to fit the site measurements and is being utilized into the "Model".

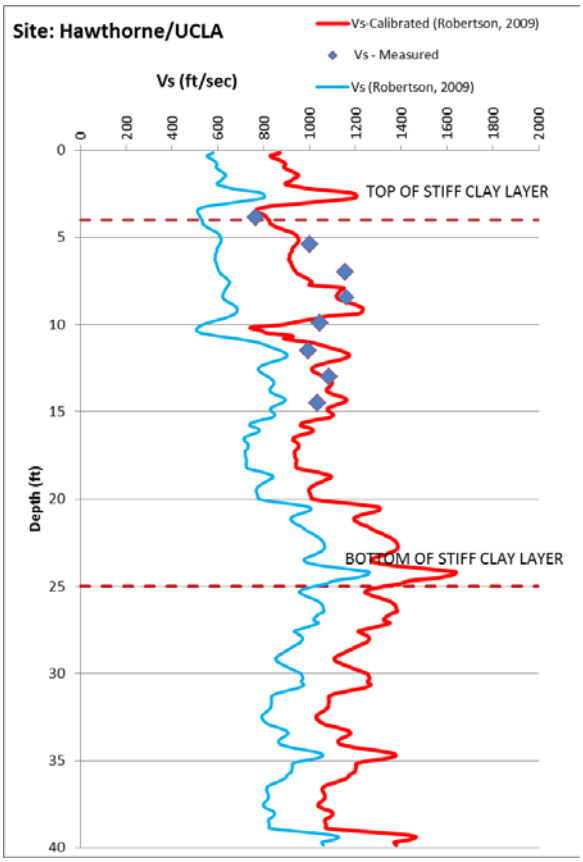

Figure 4.58 *Comparison of shear wave velocity obtained from Robertson, 2009 and site-calibrated V_s profile*

4.3.2. Pile Properties and Load Test Description

The test piles in this program included two free-head flagpole piles, 0.6-m diameter and 1.8-m shaft diameter, a single 0.61-m fixed-head pile, a pile group consisting of nine 0.61-m diameter shafts. Details of the testing program, and measured responses have been presented in Janoyan et al. (2006) and in Lemnitzer et al. (2010). As a part of the program, pile head Load-Displacement were measured at ground and pile head level. Also *p-y* curves from the filed measurement were determined. Figure 4.59 depicts the schematic set-up of the pile test for the 0.6 m diameter free-head flagpole and 0.6 m diameter fixed-head CIDH concrete piles. The single pile was extended

7.6 m below the ground level. Longitudinal reinforcement extended over the full height of the pile consisted of eight #9 (29 mm) bars. Spiral ties of #5(16 mm) with 11.4 cm pitch were installed around the longitudinal bars. The rebar yield stress, *fy*, was tested to be 483 MPa. The concrete compressive strength tested to be between 30.3 to 35.9 MPa. The cap was installed with a 9-cm gap above the ground surface to avoid base friction.

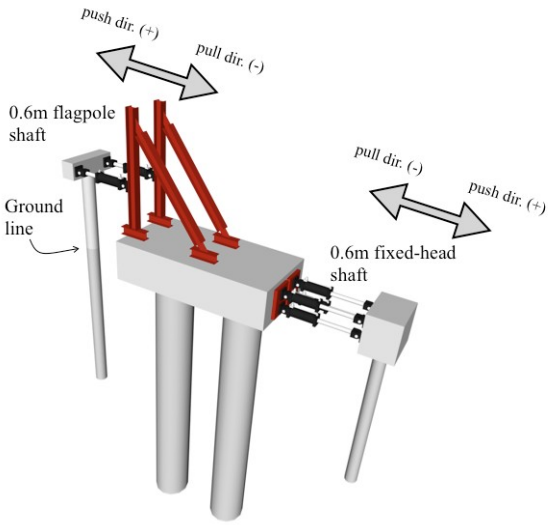

Figure 4.59: *The reaction block and the configuration of 0.6m diameter specimens (Khalili Tehrani et al., 2012)*

The concrete reaction block with planar dimension of 24 by 12 feet and depth of 5 feet was cast integrally with two 1.8-m diameter, 14.6-m long piles. Loads were applied using hydraulic actuators placed between pile caps and a reaction block. The load cells were installed between the actuators and specimen to record applied loads. To record above-ground displacements LVDTs (linear variable differential transformer) were used for all piles other than the 1.8 m flagpole, for which a total station was used to measure and stablish the displacement. Also inclinometers were placed down in the middle of the pile to record slope.

To conduct the lateral loading test on the 0.6 meter diameter flagpole and fixed-head piles, a reaction system as shown in Figure 4.59 was constructed. For the 0.6 m flagpole, quasi-static

loading was applied. The loads were applied using two 1.8 MN, servo-hydraulic controlled actuators that were connected between the top of the column/pile head an installed steel frame reaction. The lateral load was imposed on the fixed-head pile using two pairs of actuators located one above the other on the pile cap as shown in Figure 4.59. Additional details on the instrumentation are described in Janoyan et al. (2006), Stewart et al. (2007), and Lemnitzer et al (2010).

4.3.3. Input Parameters for Analysis

Pile properties, as well as soils strength parameters shall be utilized to the integrated model. The pile properties include; B (pile diameter), L (pile length), E_p(pile material modulus of elasticity), E_y (yield modulus of pile material), A (pile cross section area), I (pile section moment of inertia), and M_{y-pile} (pile section yield moment). Also pile head constraint condition will be utilized into the model.

The site soils information, i.e. CPT data file and the depth of ground water, were uploaded into the model. The Matchad script in the model determines the basic soils parameters required to be utilized into a “ticle” file, which feeds the “OpenSees” program to solve the model.

The basic soil input parameters the Matchad script calculates are K_{max}, P_u, C and y_{50}. These parameters are determined as explained in chapter 3. The profiles of input parameters for this site along the depth of the soft clay layer are depicted in the following Figure 4.60. The value of C, the soils constant, is determined from equation 3.35, and for the soft clay layer at this site varied between 0.03 and 0.06.

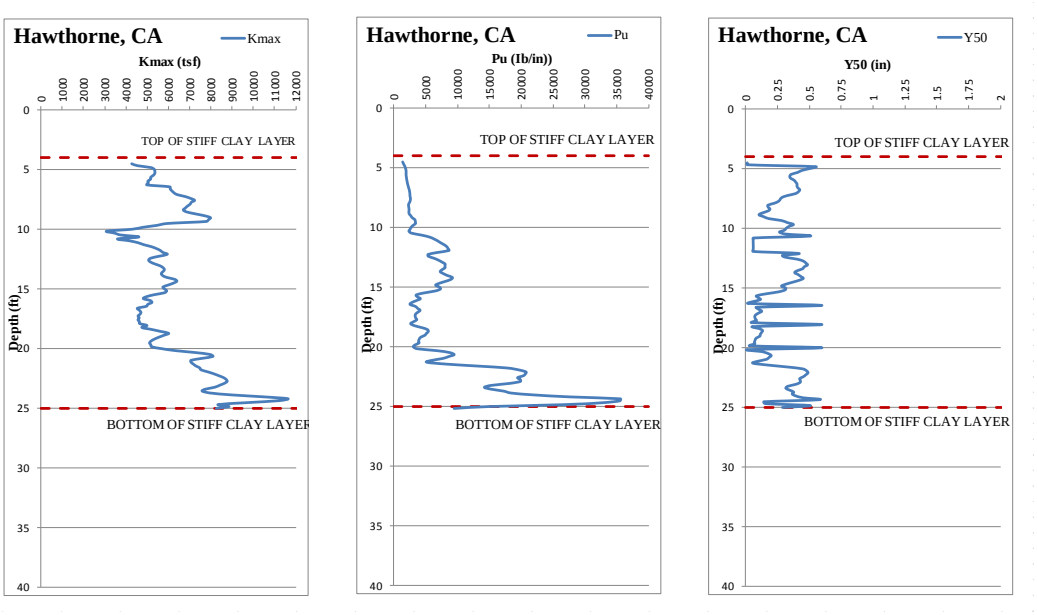

Figure 4.60: *Input Parameters profiles for Lawndale site, California*

4.3.4. Measured and Predicted Results

The lateral load-displacement measurements of the 0.6 m fixed-head pile is depicted on Figure 4.61. The data points plotted in red circle present the real field measurements and are being used for comparison and verification of the results from the suggested model in this research.

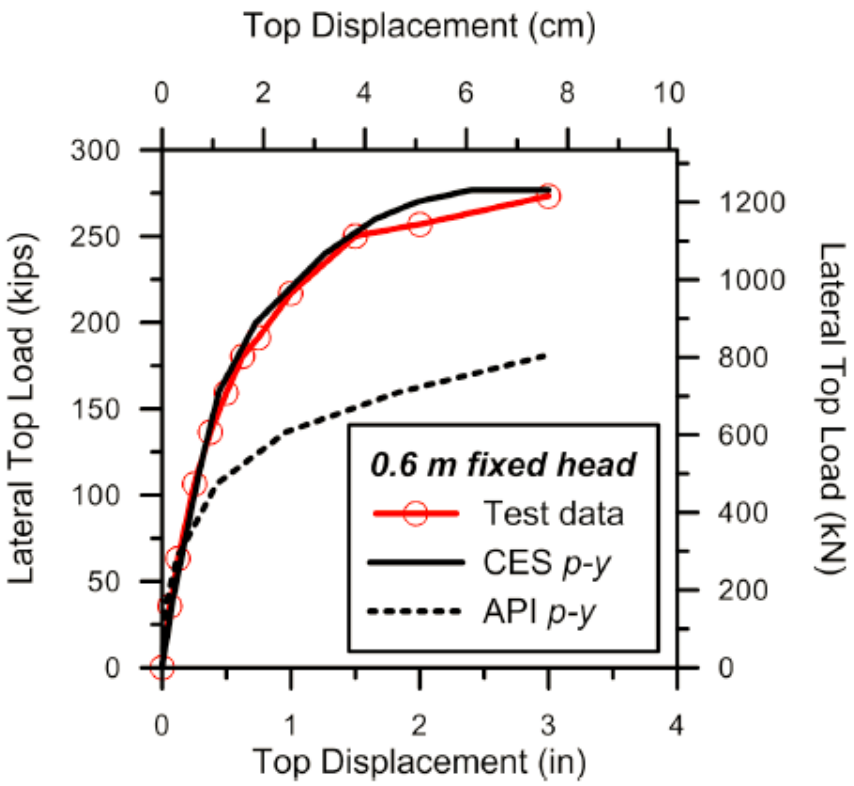

Figure 4.61: *0.6 m fixed- head pile top Force-Displacement response from field measurement (Khalili Tehrani et al., 2012)*

As a conventional and standard approach in determining *p-y* curves, values of pile curvature at various displacement levels are evaluated from pile instrumentation. For a given level of lateral loading a fit curve through curvature-depth data points is determined. By using a moment-curvature relationship for the pile section, and the curvature known at each depth, the moments at discrete depths are determined and a moment-depth plot is obtained. By double differentiating the moment profile, *p* values were obtained. Double integration of the moment-depth profile results in the values of y. By repeating the same process for different lateral loads and plotting *p* and *y* values for each depth, the *p-y* curve for the intended depth may be obtained. Lumnitzer et al (2010), describes that utilization of the mentioned procedure for obtaining p-y curves is unstable, due to the extreme sensitivity of the *p* profile to tenuous features of the curvature profile and the non-linear moment-curvature relationship. Stewart et al. (2007) reported similar features and

instability. Therefore, Khalili et al. (2014) utilized an alternative approach called “Calculation of *p-y* Curves by Constrained Exhaustive Search (CES)”. Details of their approach is discussed in Khalili et al. (2012) and resulted *p-y* curves for the 0.6 m fixed-head condition at two depths equal to *0.5D* and *1.5D*, where *D* is pile diameter equal to 24 inches, is presented in their paper, as shown in the following Figure 4.62.

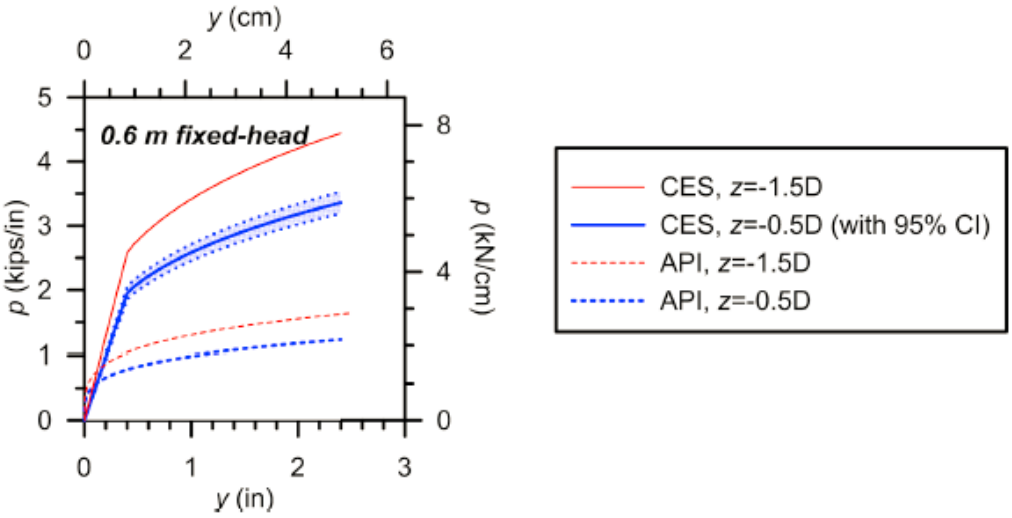

Figure 4.62: Comparison of API and CES p-y curves for *0.6 m fixed-head pile, p-y curves (Khalili Tehrani et al, 2014)*

Details of Constrained Exhaustive Search method applied in their study to obtain p-y curves are provided in Khalili Tehrani et al. (2014). For the depth equal to $z = 0.5D$, equal to 12 inches, the limits for 95% confidence intervals are plotted as well.

There is an important and unique point in their study that differentiates this study from the previous ones. At this site, the test piles were instrumented by multiple devices such as fiber-optic, rebar strain gauge, LVDTs and inclinometers, enabling to calculate curvatures at multiple depths/points using different sets of data. Curvature profile was generated using the following approaches:

1- By using axial strain measurements, as:

$$\varphi(z) = \frac{d^2y}{dz^2} = [\varepsilon_1(z) - \varepsilon_2(z)]/\Delta y$$

where $\varepsilon_1(z)$ and$\varepsilon_1(z)$ are axial strain measurements on opposite sides of the shaft at elevation z and Δy is horizontal distance between the relevant sensors.

2- By using inclinometer slope readings, and:

$$\varphi(z) = [s(z_1) - s(z_2)]/(z_1 - z_2)$$

where *S* is the slope and Z_1 and Z_2 are adjacent depths where slopes are measured.

Model Predictions: The CPT were utilized to compute *p-y* curves, and the following quantities were compared: (1) load versus displacement, (2) p-y curves at various depths computed using the CES method and using the "Model", and (3) curvature versus depth.

The degree of saturation of the clay at the Hawthorne site was approximately 86 to 100%. Matric suction is anticipated to be significant at this site because the soil is either unsaturated, or saturated above the phreatic surface (in which case matric suction would be negative due to the large depth to the water table). This is important because knowledge of effective stress is essential for interpreting the CPT data, and therefore for computing the p-y material properties. The relation between degree of saturation and matric suction is not known for the clay soil at the Hawthorne site, so guidance is sought in the literature to understand in a crude sense the range of matric suction to anticipate. Fig. 4.63 shows a typical soil-water characteristic curve for four different soils (Fredlund, 1995). For a given degree of saturation, matric suction is significantly higher for clay than for sand or silt, approaching hundreds or thousands of kPa at a degree of saturation of 80%.

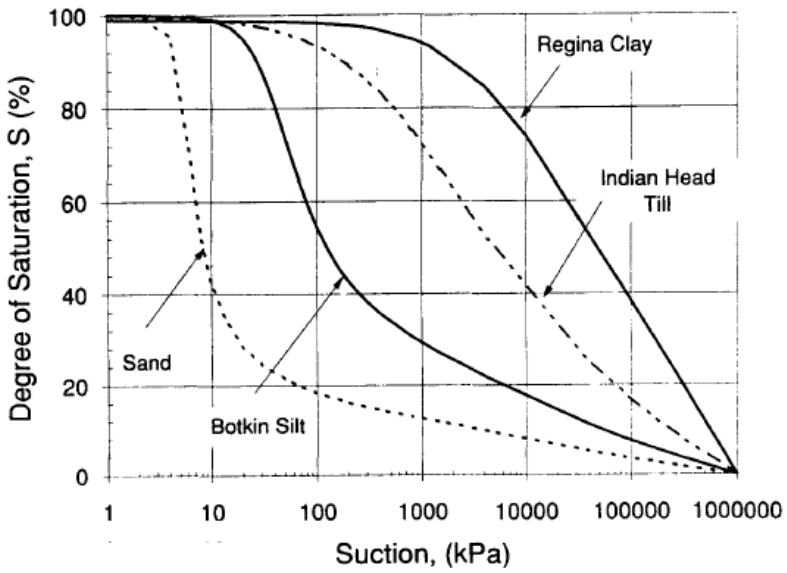

Figure 4.63: *Typical Soil-Water Characteristic curves for four soils from Saskatchewan, Canada (Fredlund, D.G., 1995)*

The influence of matric suction on the soil behavior type index is shown in Fig. 4.70(b). As matric suction increases, the value of I_c increases as well. When matric suction is assumed to be zero, I_c is close to 2.3, indicating that the soil is behaving in a sand-like manner. As I_c increases to only 40 kPa, I_c increases to being larger than 2.7 in the clay, indicating a clay-like material. The actual amount of matric suction is likely much larger than 40 kPa, therefore the soil at this site should be interpreted as being clay-like, controlled by undrained loading conditions. This is consistent with the assumption by Lemnitzer et al. (2010).

Computed *p-y* curves assuming matric suction is at least 40 kPa (5.8 lb/in^2) are plotted for four different depths, presented in Figures 4.64 to 4.67. Shear wave velocity, V_s, is computed by calibrating the functional form by Robertson (2009)) to match the field values and shown on Figure 4.58.

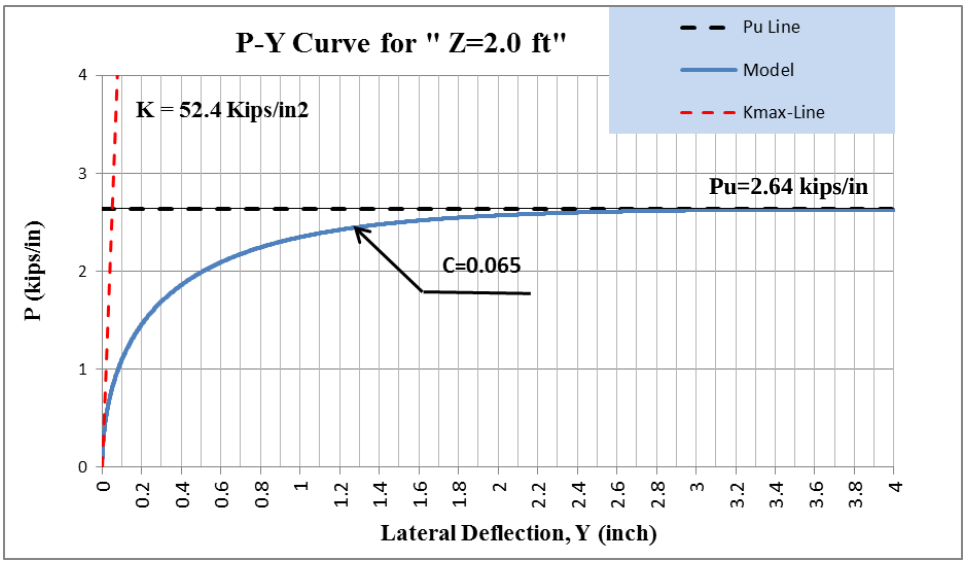

Figure 4.64: *Resulted p-y curve from the "Model" at 2 feet*

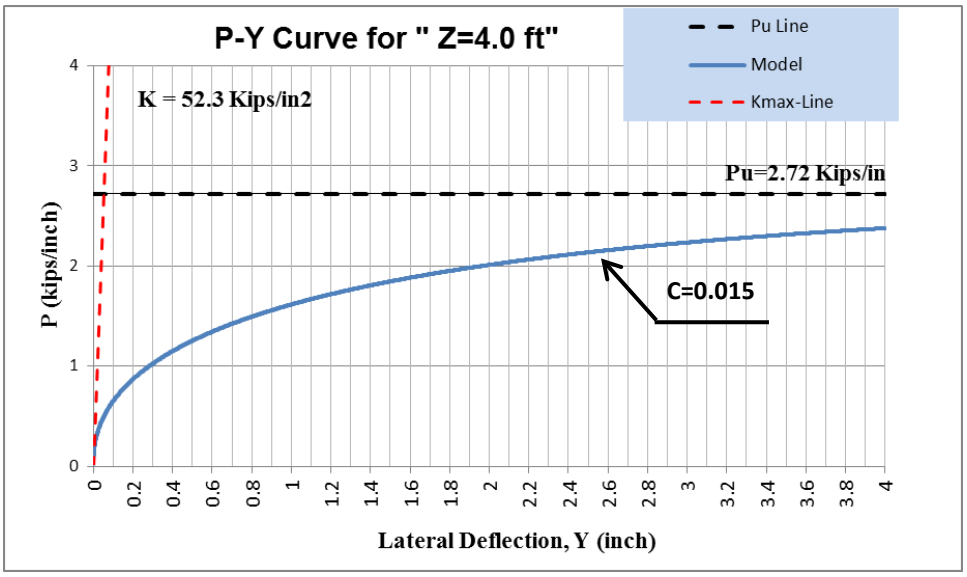

Figure 4.65: *Resulted p-y curve from the "Model" at 4 feet*

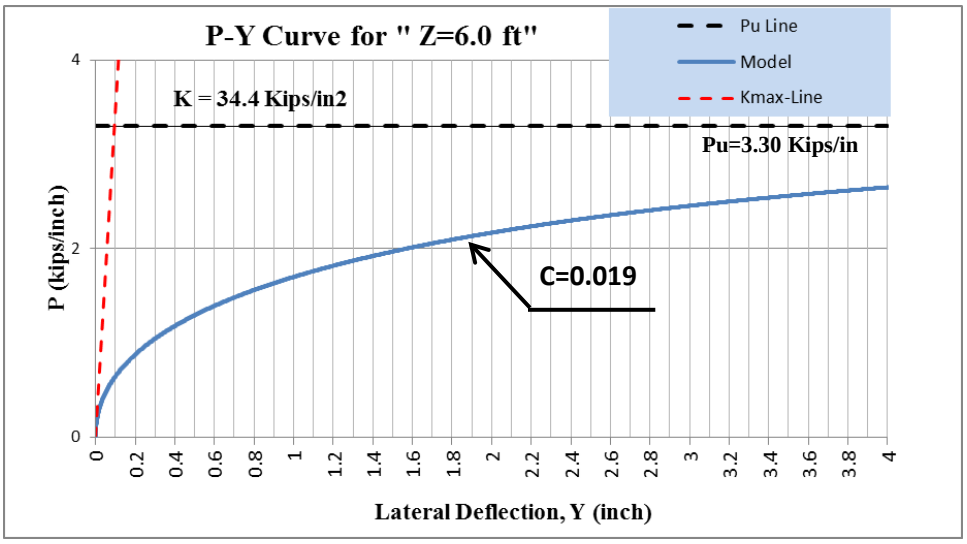

Figure 4.66: *Resulted p-y curve from the "Model" at 6 feet*

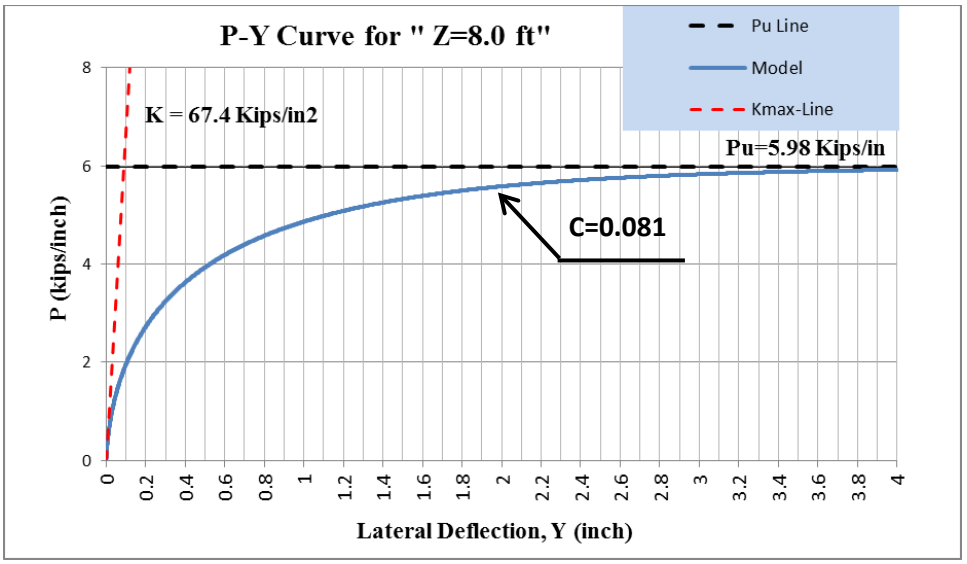

Figure 4.67: *Resulted p-y curve from the "Model" at 8 feet*

Khalili Tehrani et al. (2014) presented a comparison between *p-y* curves determined by utilizing their CES approach and API method. This is presented in Figure 4.62. To compare the results from our model and their work, a *p-y* curve obtained using the "Model" for a comparable depth of 3 feet, corresponding to 1.5 times pile diameter is determined and plotted on the following Figure

4.68. The CPT-based model predicts that the p-y behavior is significantly stiffer at small displacements, and also weaker than the CES curve.

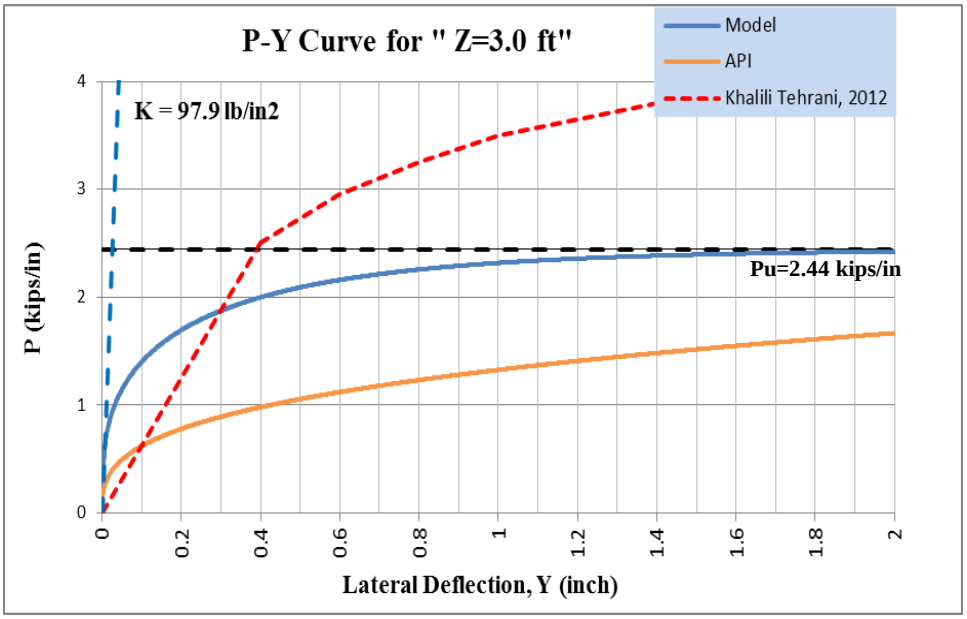

Figure 4.68: *Comparison of p-y curve from the "Model", API and CES approach (Khalili Tehrani et al, 2012) at depth of* $z = 1.5D = 3\ feet$

Using CPT data and the "Model", head force-deflection for fixed-head 0.6 m diameter pile is determined and plotted on Figure 4.69. Also the measured field data from Figures 4.61 are re-plotted on the same figure.

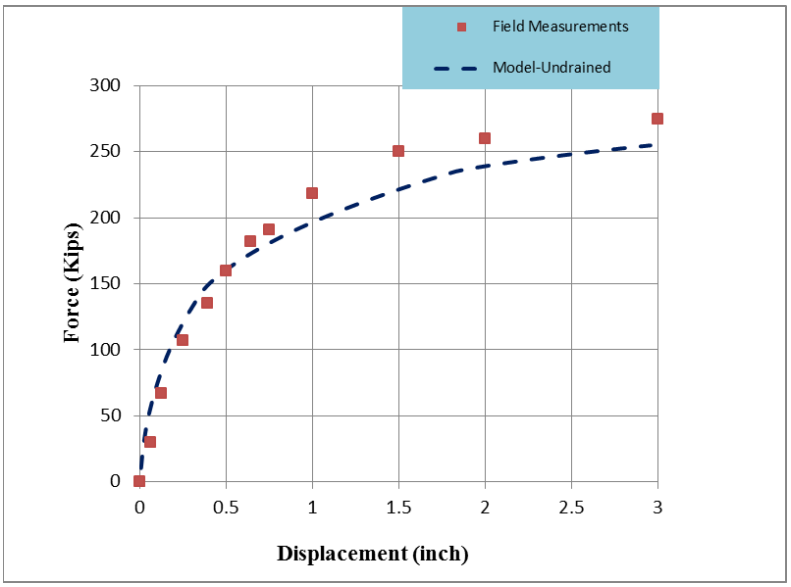

Figure 4.69: *Comparison of pile head Force-Displacement between the proposed "Model", field measurements, and LPILE for fixed-head 0.6 m pile at Hawthorne Site*

The profile of curvature versus depth for a head displacement of 3.8 cm is compared with the profile provided by Lemnitzer et al. (2010) in Figure 4.70.(a). The measured peak curvature is smaller, and occurs shallower than the predicted values. This indicates that the soil stiffness and/or strength is under-predicted at a pile head displacement of 3.8 cm.

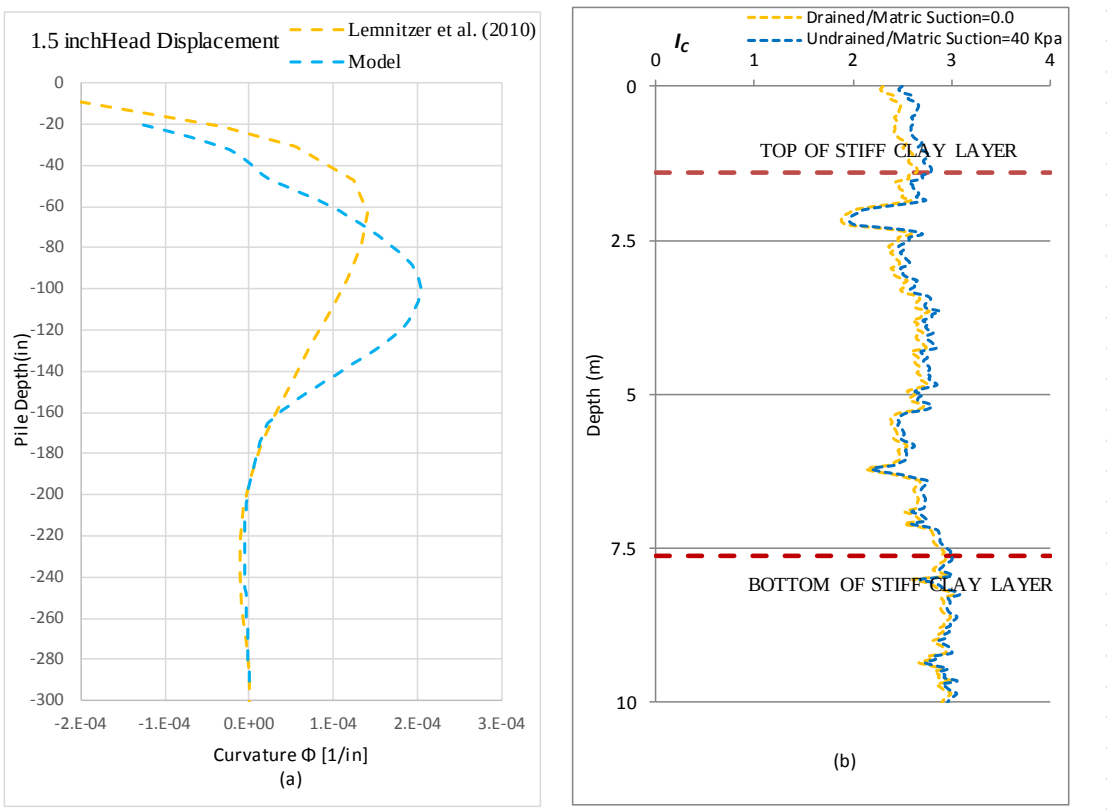

4.70. *(a): Comparison of curvature along the pile length between the model and Lemintzer et al. (2010) (b):Ic profile for no matric suction and matric suction equal to 40KPa*

4.3.5. Discussion on Results

By advancing seismic cone (SCPT), shear wave velocity, V_s was measured for this site. The site specific V_s was utilized into the "Model". The values for initial stiffness *K*, as shown on Figures 4.63 to 4.66, are based on using site specific V_s in the analysis. The values of *K* in different depths vary from 52 to 98 Kips/in^2. At 3 feet deep, as depicted on Figure 4.67, the initial stiffness from the "Model" is 97.9 Kips/in^2 and is higher than initial stiffness for the *p-y* curve from Khalili Tehrani et al.(2014).

- Ground water level was at about 48 feet below the ground surface at the site. Based on the tests performed on the samples, the degree of saturation in the clay layer was from 86% to

100%, and in their work (Khalili Tehrani et al., 2014) reasonably assumed that undrained shear condition will prevail. Prior knowledge or assumption about the way the soil will shear, i.e. drained or undrained", is an important piece of information, needed before performing analysis and determining *p-y* curves using conventional methods. The known common in-practice criteria such as Matlock (1970), Reese and Welch (1975), and API are based on the condition when the clay during shearing completely behaves undrained and no volume change during shearing occurs.

- The CPT data confirm that the I_c value is higher than 2.7 when matric suction is set to 40 kPa or higher. However, I_c values as low as 2.3 are computed when matric suction is set to 0. Including matric suction is very important for interpreting soil behavior type in unsaturated soils.

- Pile head Load-Displacement obtained from the "Model" and field measurements for 0.6 meter diameter fixed-head pile are both plotted in Figure 4.68. In smaller head displacements, i.e. less than 0.6 inches the "Model" fits closely the filed measurements, while in larger than 0.6 inches head displacement, the head-displacement resulted from the "model" falls about 15% to 20% below the field measured values. The load-displacement obtained from LPILE program is being plotted for comparison. The model resulted curve is in a better agreement with the field results than LPIE curve.

- The obtained *p-y* curve from the "Model" at the depths of 2.0, 4.0, 6.0 and 8.0 feet are depicted as Figures 4.63 to 4.66. Khalili Tehrani et al. (2014) provided *p-y* curves for certain depths, shown in Figure 4.62. To compare between the "Model" and their work, *p-y* curve a comparable depth of 3 feet, corresponding to 1.5 times pile diameter is being

determined and plotted on Figure 4.67. The API curve for the same depth is also depicted on the same Figure. As it is observed, the “Model” curve falls between two other curves. Also the initial slope of the “Model” curve is based on the site specific shear wave velocity and intents to be realistically reflective of small strain stiffness of the soil.

4.4. Los Angeles International Airport (LAX) Site

As a part of ongoing modernization and expansion in the Los Angeles International Airport (LAX), a pile test program was conducted in 2014 and 2015. Based on the information provided by Diaz Yourman & Associates (DYA), the project site is split into two parts, i.e. airside and landside. The airside is located at elevation 116 feet MSL, and the landside is closer to elevation 103 feet MSL. A ReMi survey was performed on the airside of the project, and the shear wave velocity at the site was determined. Load test on Test Pile No. 1 was performed within the airside, on the east side of Terminal 1, as shown on Figure 4.68. The pile test performed adjacent to the location of a previously performed boring DYB-13-T1-09. Also a CPT was performed at the vicinity of pile test, close to Boring DYB-13-T1-09. The area of test pile 1 is depicted on the site plan, Figure 4.71.

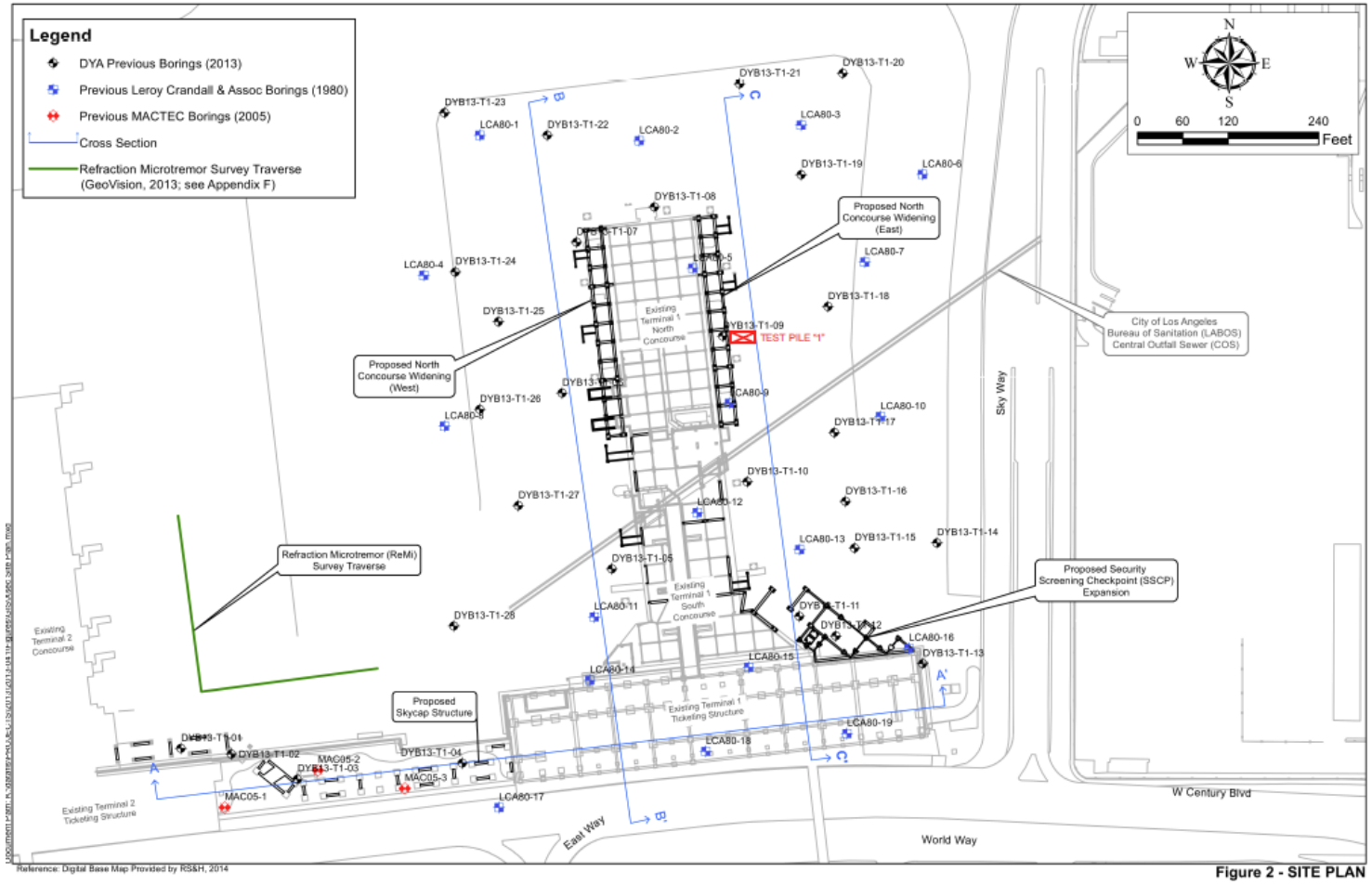

Figure 2 - SITE PLAN

Figure 4.71: *Site Plan and Location of Test pile 1 (Courtesy of DYA)*

4.4.1. Soil Condition

The airside soil profile, as shown on Figure 4.72, generally consists of 15-20 feet of dense sandy artificial fill (SP-SM, SM), underlain by dense to very dense natural sands (SP, SP-SM). The in-place fill was determined to be in very dense condition, with high blow counts averaging about 50 within the fill layer as shown on boring logs, Figure 4.72. For clarity purpose, an enlarged depiction of boring DYB-13-TI-09 located in the vicinity of test pile No.1 is presented as Figure 4.73.

A CPT sounding was conducted close to the location of Test Pile 1. The readings of CPT data was utilized into the" CPTeT-IT" program, and regular and normalized plots of cone resistance, friction ratio, Soil Behavior Type index (SBT) and stratification of the site at the test location are obtained and are presented in Figures 4.74 and 4.75. For performing lateral testing on the pile, a test pit with about 4 feet depth was excavated so the ground surface for pile testing was at about -4 feet below the pre-test finished grade. The CPT test plots are truncated to start from the zero level for pile testing, i.e. 4 feet below the finished grade. The CPT plots conclude that within the depth explored, the earth materials consist of relatively dense layers of sand and silty sands. The CPT-based stratification is in agreement with the boring log shown in Figure 4.73, indicating presence of 15-20 feet of dense sandy soils (SP-SM, SM), underlain by dense to very dense natural sands (SP, SP-SM). The purpose of performing lateral testing on the pile at the site was to respond to the City of Los Angeles concerns about competency of the artificial in-place fill.

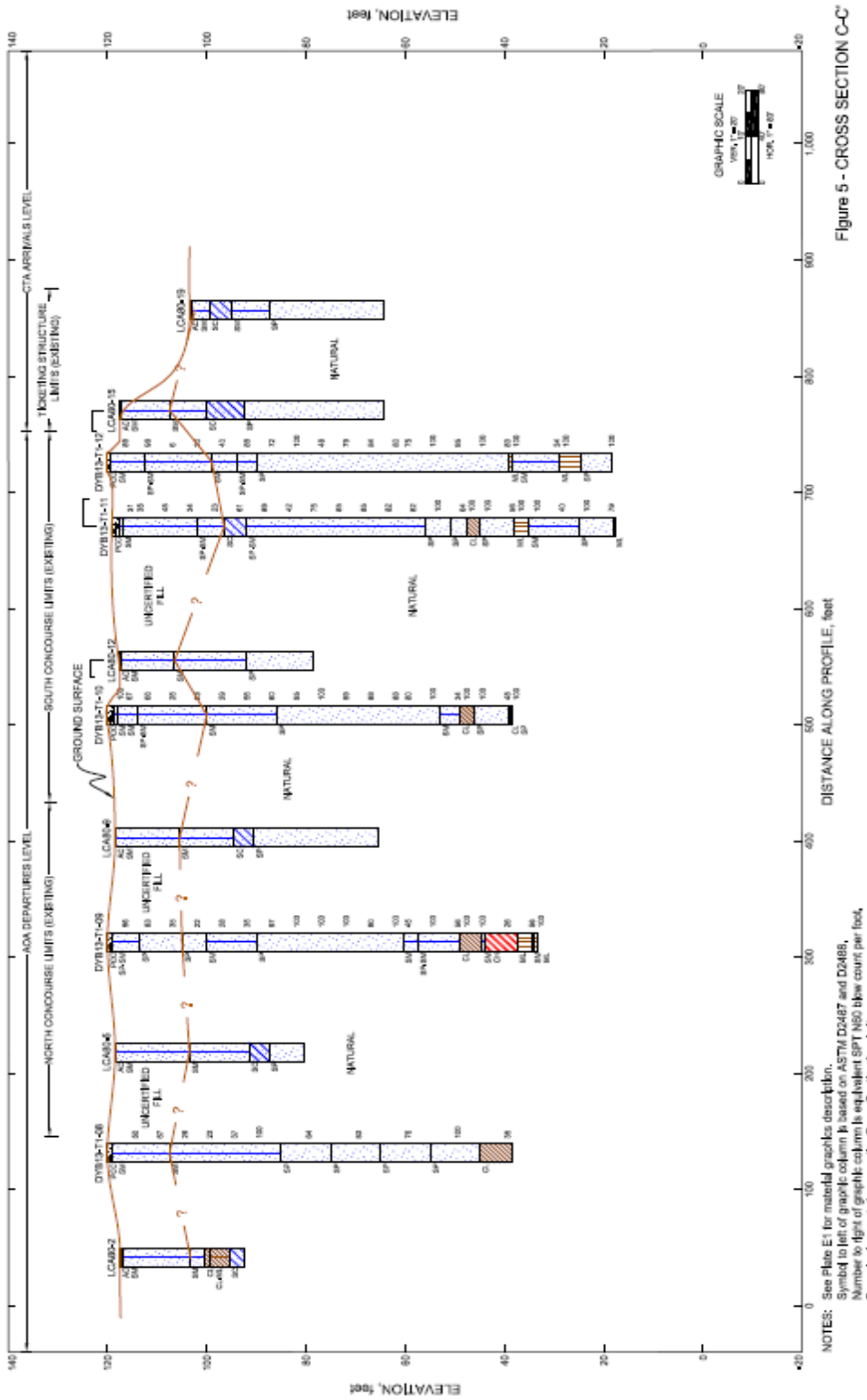

Figure 5 - CROSS SECTION C-C'

Figure 4.72: *Boring logs profile and soils stratification (Courtesy of DYA)*

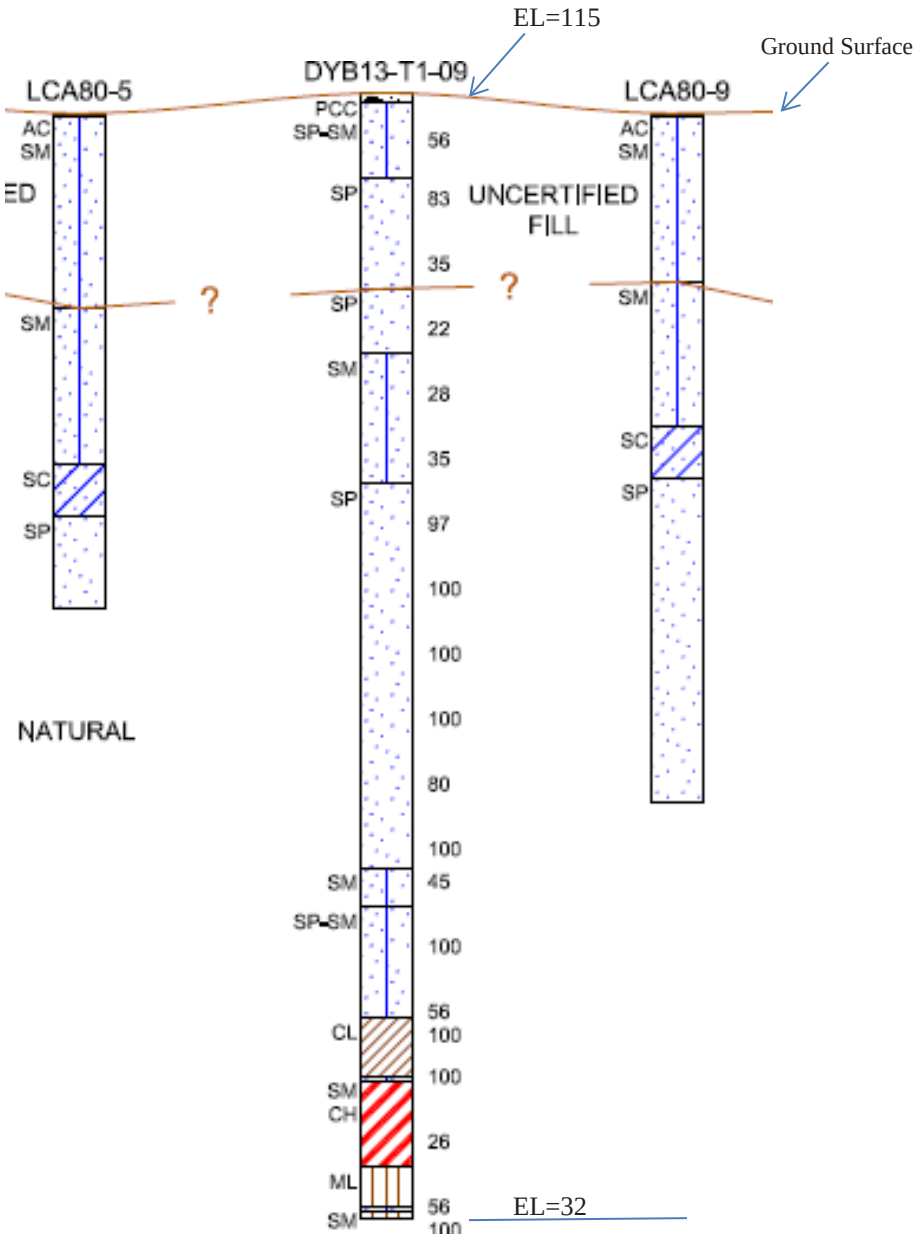

Figure 4.73: *Log of boring TI-09 adjacent to the test location*

Shawn Ariannia
Civil & Environmental Engineering Department
UCLA

Project: **LAX PILE TEST PROGRAM**
Location: **Los Angeles International Airport**

CPT: CPT-01
Total depth: 35.43 ft, Date: 2/7/2015
Surface Elevation: 0.00 ft
Coords: X:0.00, Y:0.00

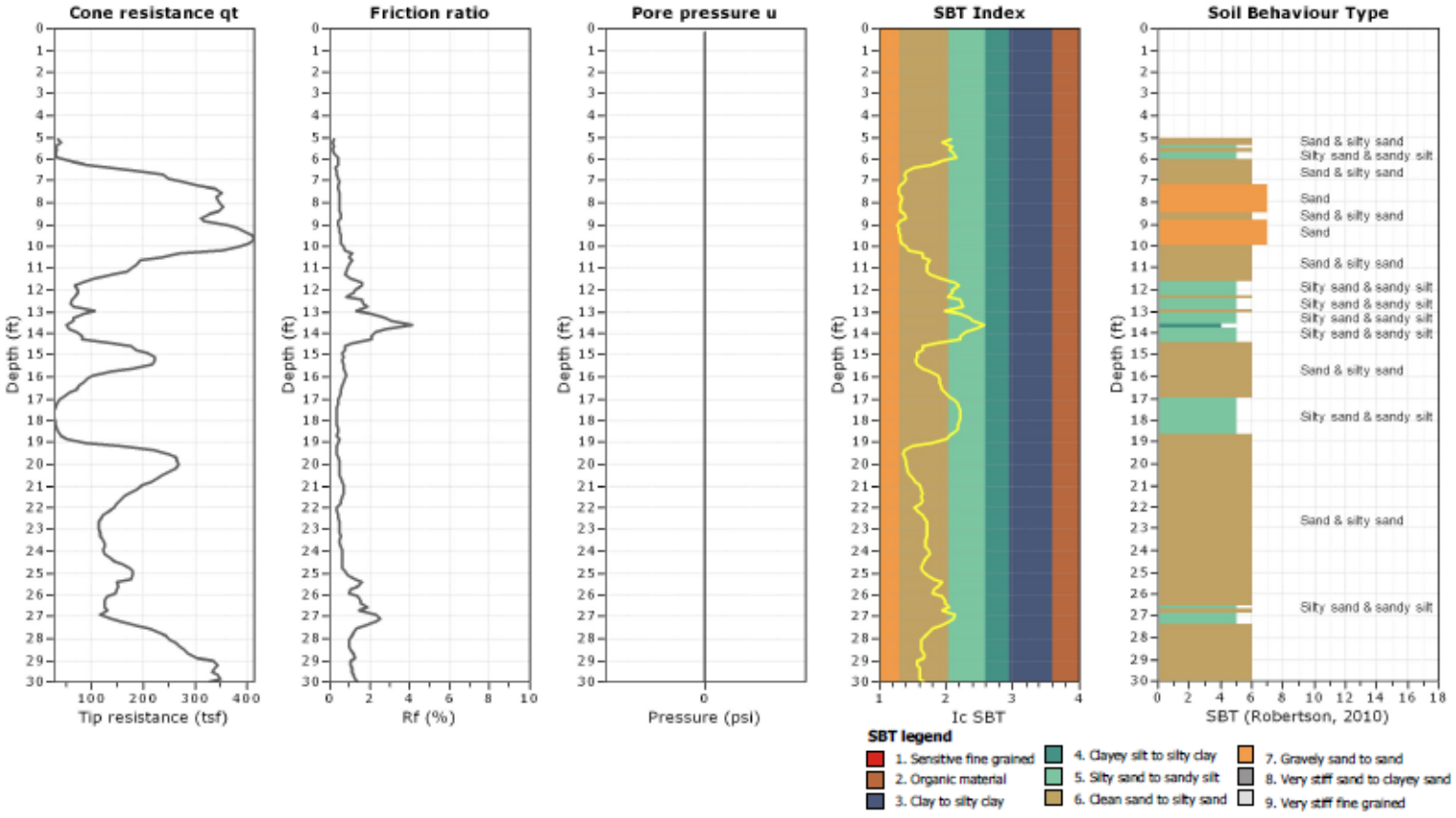

Figure 4.74: *CPT basic plots for Pile Test 1 at LAX Site*

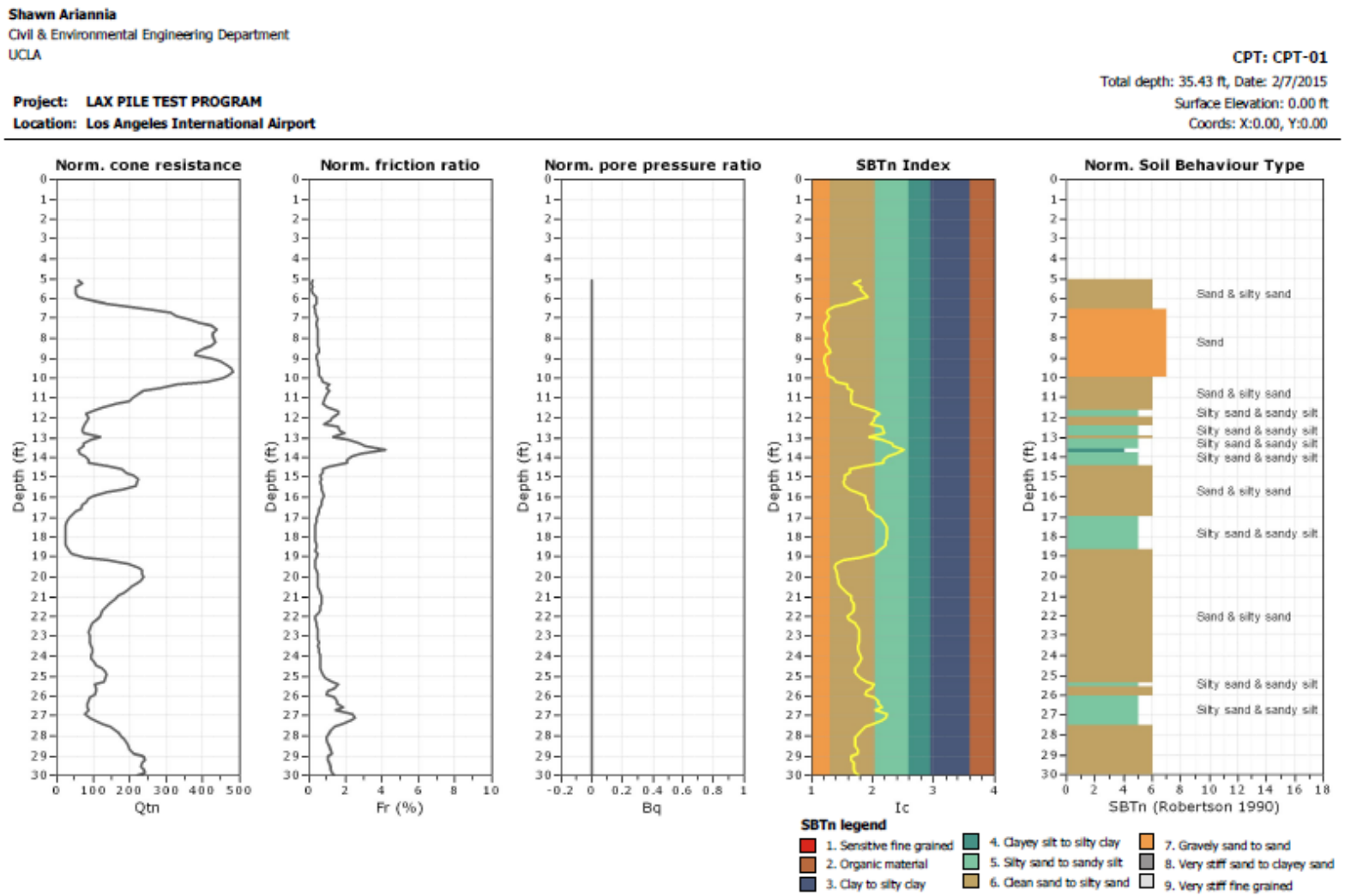

Figure 4.75: *CPT normalized plots for Pile Test 1 at LAX Site*

As mentioned, a ReMi survey was conducted at the site and shear wave velocity was measured. The results of ReMi measurement are provided in the following Table 4.3. Shear wave velocity profile determined by using equations 3.27 and 3.28 (Robertson, 2009), as well as the field measurement values are plotted in Figure 4.76. In this sandy profile, the shape of V_s obtained from correlations is reasonably following the trend of V_s measured at the site.

Depth to		Layer		S-Wave	
m	ft	m	ft	m/s	ft/s
0	0.0	1	3.3	160	525
1	3.3	2	6.6	210	689
3	9.8	3	9.8	260	853
6	19.7	4	13.1	300	984
10	32.8	5	16.4	350	1148
15	49.2	7	23.0	400	1312
22	72.2	19	62.3	450	1476
41	134.5	12	39.4	475	1558
53	173.9	>7	>23	500	1640

Table 4.3: *Field measured shear wave velocity at LAX Site*

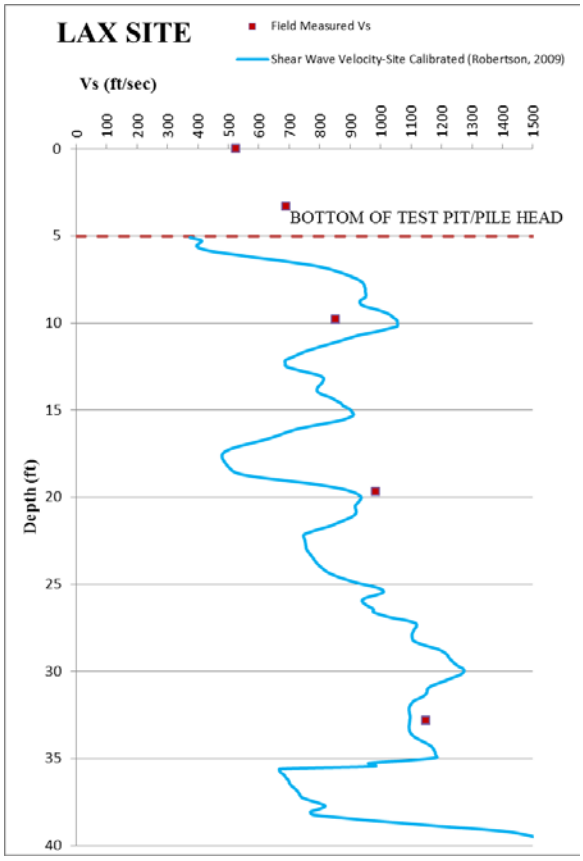

Figure 4.76: *Comparison of shear wave velocity obtained from CPT data using Robertson (2009) correlations vs. Site Measured Vs- LAX Site*

4.4.2. Pile Properties and Load Test Description

The pile test program included installation of a steel pipe pile. The pile's outside diameter and wall thickness were $12\frac{3}{4}$ and $\frac{3}{8}$ inches, respectively. Test pile 1 was driven 33.7 feet below the original grade. An about five feet wide square shape test pit was excavated at the test location. The pile steel was Grade 50 (f_y = 50 Ksi).

The pile was installed using Torque-Down technique, by utilizing a hydraulic rotary rig (Model SR-90). Torque-Down Piles (TDP) are full-displacement, concrete-filled, steel pipe piles. Tip of TDP consists of a special patented closed-end conical tip. By utilizing the right proportions of torque and crowd (downward pressure), TDPs are driven such as screwing them into the ground

with a large drill rig. As a result, the screw-driven method of the TDP provides several unique benefits when compared to other conventional driven-pile methods, such as no vibration and less noise during installation, fast advancing and installment of piles, and cost effectiveness.

The installed test pile 1, with 29.7 feet embedment length below the bottom of the test pit is shown in Figure 4.77. The pile tested for axial downward, axial upward and lateral capacity, which the latter test is the matter of concern for this research, and will be discussed. Lateral force to the top of the pile was imposed by utilizing a hydraulic jack.

As shown in Figures 4.77 and 4.78, three dial gauges were installed to measure the lateral displacement. The gauges were located at the bottom level of the test pit, 14.25 inches and 32 inches above the bottom of the test pit**.** The gauges were fixed against a reference beam structure supported at distant from the test pit.

Figure 4.77: *Lateral load testing set up for pile test 1 at LAX*

Figure 4.78: *Lateral load testing set up for pile test 1 at LAX*

4.4.3. Input Parameters for Analysis

Pile properties including; B (pile diameter), L (pile length), E_p (pile material modulus of elasticity), E_y (yield modulus of pile material), A (pile cross section area), I (pile section moment of inertia), and M_{y-pile} (pile section yield moment), as well as pile head constraint condition were introduced to the model.

The site soils information, i.e. CPT data file and the depth of ground water, were uploaded into the model. The Matchad script in the model determines the basic soils parameters required to be utilized into a “ticle” file, which feeds the “OpenSees” program to solve the model.

The profiles of input parameters for this site within the first 40 feet depth of the sandy layer underlying the site are depicted in the following Figure 4.79.

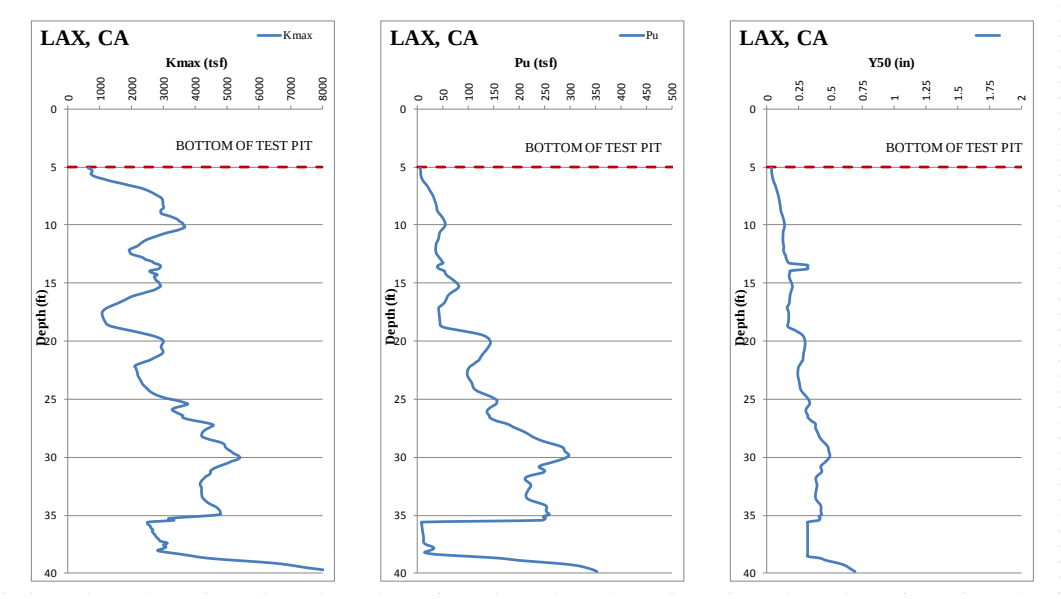

Figure 4.79: *Input Parameters profiles for LAX site, California*

4.4.4. Measured and Predicted Results

In Section 4.4.2 and Figures 4.77 and 4.78, the set-up for lateral load testing of the steel pipe torqued down pile was presented. As the first trial, and using CPT data and the "Model", head force-displacement was determined and is plotted on Figure 4.80. Also the measured field data for test pile 1, is shown on the same Figure.

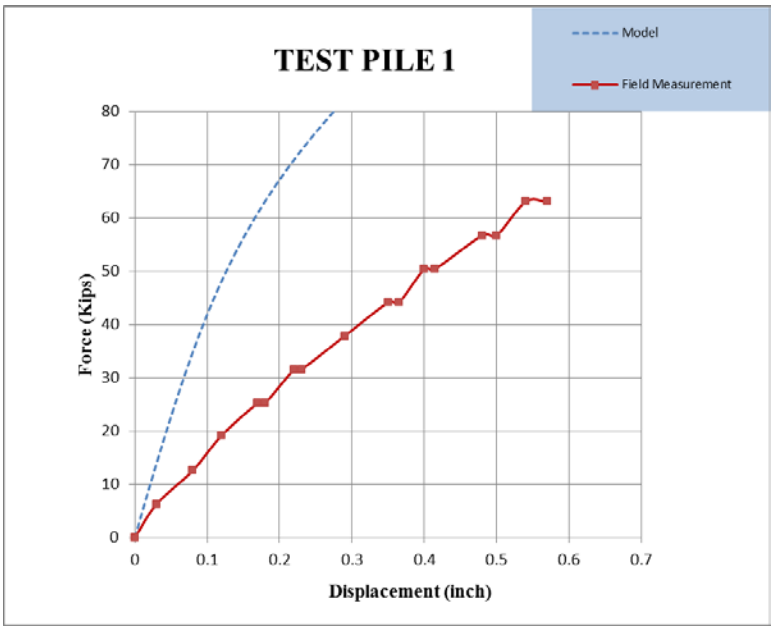

Figure 4.80: *Comparison of pile head Force-Displacement between the proposed "Model" and field measurements for "Test Pile 1 " at LAX Site*

As it is observed, the pile head force-displacement curve by the "Model" is higher than the field measured curve. Therefore, more in depth consideration of the test situation and more rigorous and detail analysis was performed to find out the reason for this considerable difference. The main reason for the differences observed in the pile head force-displacement response is believed to be the pile set-up and effect of the excavated test pit on the lateral resistance of the pile. This will be explained in the forthcoming paragraphs.

As depicted in Figure 4.77, the test set-up comprises of excavation of a 4 feet deep test pit. The planar dimension of the test pit is approximately 5 by 5 feet. The pile was torqued down into the ground and the wall of the test pit has been used to provide support to utilize lateral loads to the pile head. Pile head movement was measured by using the gauges installed at the pile head elevation, in the test pit. The CPT test was performed from the finished grade. The main thing to be noticed in this set up is that the existence of side walls/soils blocks above the level of the

bottom of test pit, i.e. pile head, will increase lateral resistance of the soil and a larger soil wedge will resist in front of the pile. This could be observed by comparing the conditions (a) and (b) shown in Figure 4.81, where condition (a) is a test scheme as if the pile is tested at ground level, not in the test pit/excavation.

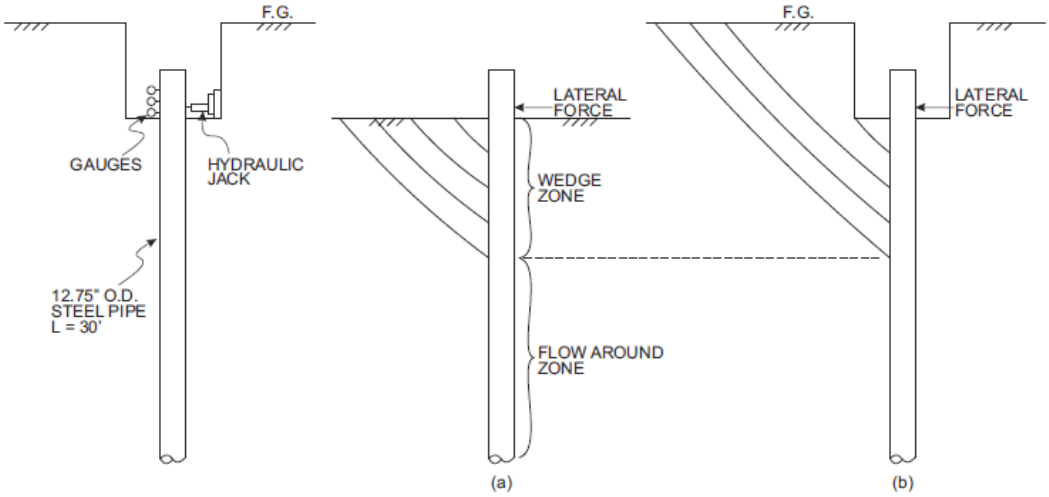

Figure 4.81: *Pile lateral test at LAX site: Effect of test set up on lateral resistance*

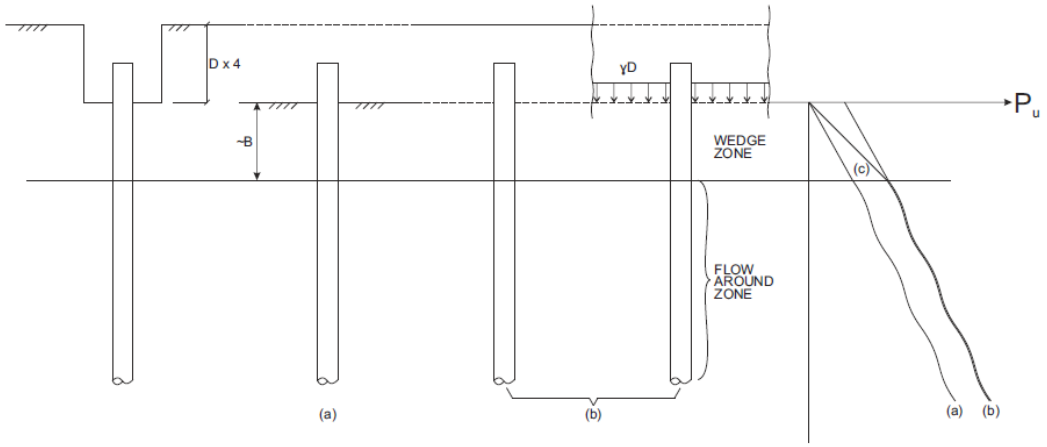

Figure 4.82: *Pile lateral test at LAX site: Effect of test set up on lateral resistance*

Therefore, to determine the effect of the used set up and its influence on the pile response, i.e. lateral capacity, the following approach was utilized;

Referring to Figures 4.81 and 4.82, two boundary conditions for the test are assumed:

(a): The free ground level corresponding to the pile head elevation is at the level of the bottom of the test pit.

(b): The ground level is at the level of the finished grade, i.e. pre-excavation grade.

The schematic profile of soils resistance, P_u, for the two conditions are shown and compared in Figure 4.78. Intuitively, the soil resistance corresponding to the performed test condition which includes testing inside the excavated test pit, will be between these two conditions, starting from the zero point for case (a) and intersecting to the (b) profile at the depth of start of the flow mechanism around the pile.

To simulate the described condition into the "Model", the following was performed;

1. The model was run for condition (a), and the pile head force-displacement relation was obtained. This results in lower boundary condition, as shown in Figure 4.80.
2. The model was run for condition (b). To do so, an overburden pressure equal to the pressure for the depth of the test pit, *D*, was utilized into the model. This results in the upper boundary curve for the pile head force-displacement relation, shown as case (b) in Figure 4.83.
3. The simulated condition to the test condition at LAX, i.e. performing test in the pit, is expected to be between these two limits, curves (a) and (b), in Figure 4.82. A linear

increase for *Pu*, from zero at ground (test pit) level for case (a) to the value corresponding to depth B on the (b) curve was considered and utilized to the model.

4. Pile head force-displacement for the simulated condition was determined and is depicted as curve (c) on the following Figure 4.83. This curve represents the simulated model to the condition how the test was performed at the site. As it is seen, the resulted curve from the model is in a very good agreement with the filed measurements.

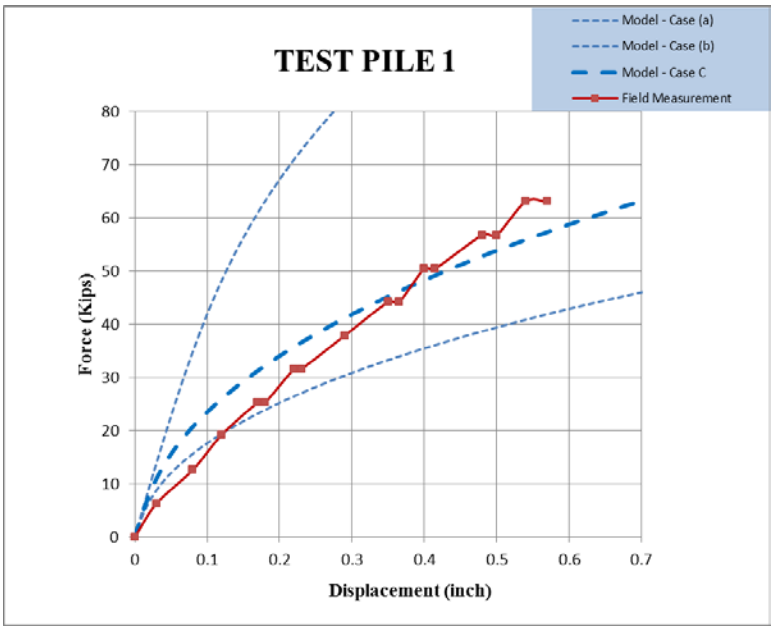

Figure 4.83: *Comparison of pile head Force-Displacement between the proposed "Model" and field measurements for "Test Pile 1 at LAX Site*

By tricking LPile program, the real condition, i.e. case (c) can be simulated. Doing so, the outputs of LPILE for the discussed cases are plotted on the same previous Figure 4.83 and is presented as Figure 4.84 below:

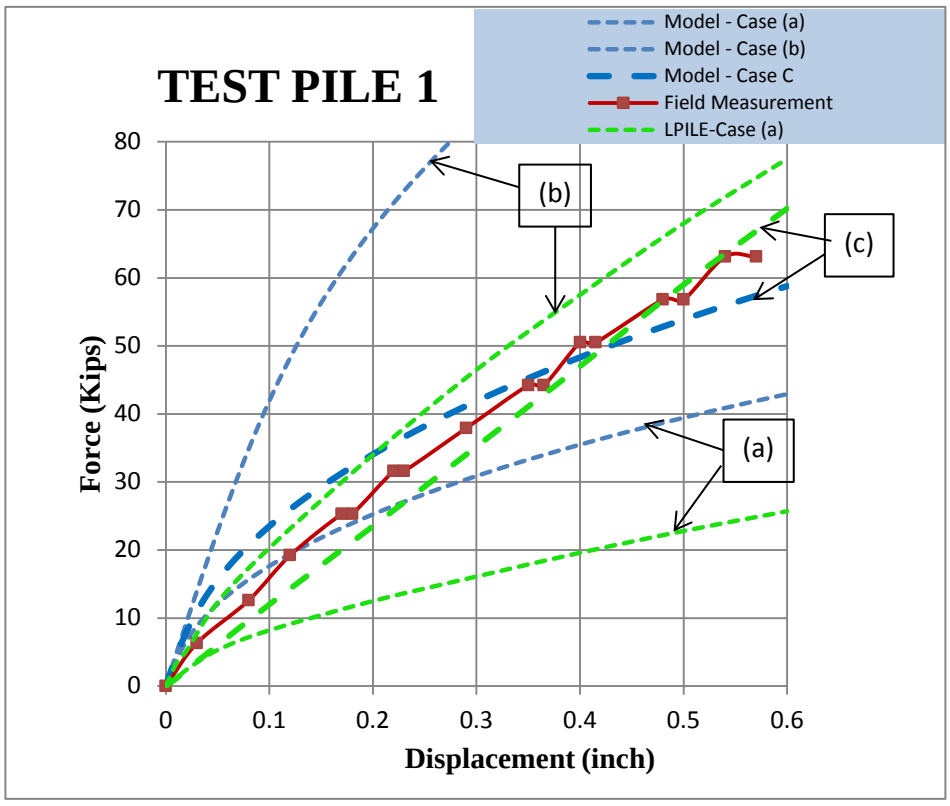

Figure 4.84: *Comparison of pile head Force-Displacement between the proposed "Model", field measurements and LPILE for "Test Pile 1 at LAX Site*

Also by utilizing the CPT data into the "Model", *p-y* curve for the depth of 4 feet below the pile head is determined. Two different *p-y* curves are plotted in Figure 4.85, by determining shear wave velocity from CPT data, using correlations by Robertson (2009) and Baldi et al. (1989), and the resulted initial stiffness are 40.9 and 34.1 Kips/in^2 , respectively. For this case and in absence of any field resulted *p-y* curves**,** and for comparison purpose, the curves resulted from the "Model" are plotted against API curve and are presented on the same Figure 4.85.

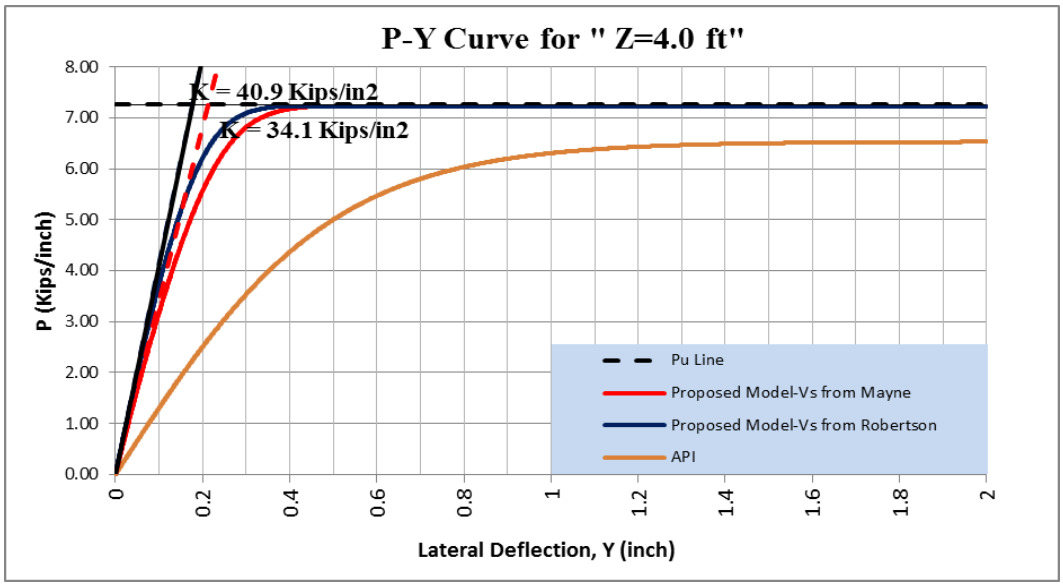

Figure 4.85: *Effect of choosing V_s correlation on resultant p-y curve; Comparison between using Robertson (2009) and Baldi (1989) suggested Correlations for Vs, and API curve "Test Pile 1" at LAX*

The enlarged part of the initial zone on Figure 4.85 is shown as Figure 4.86. The initial stiffness from API curve is considerably lower than the ones from the "Model", which are resulted by utilizing the field-specific V_S.

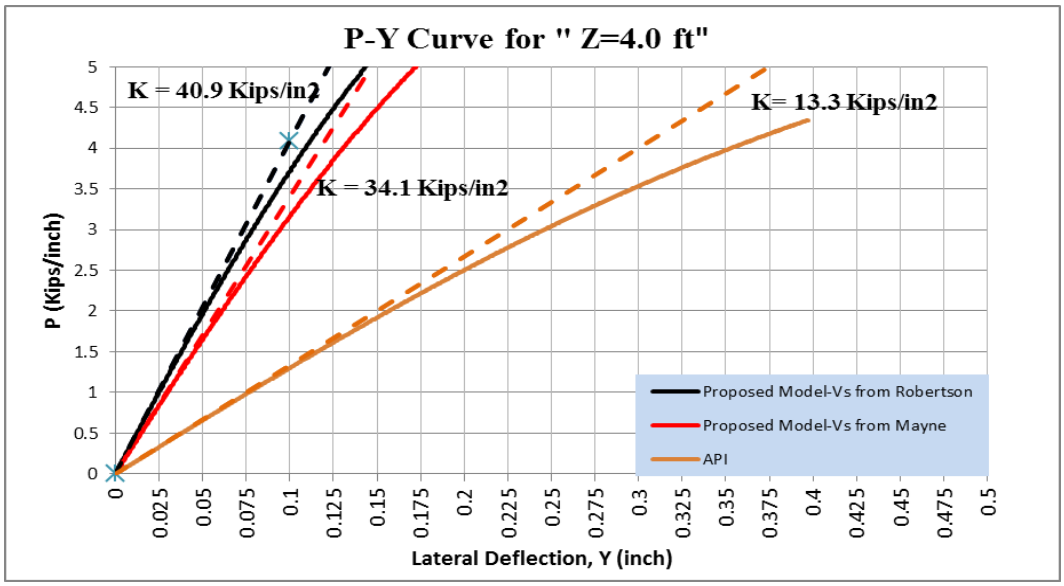

Figure 4.86: *Effect of choosing V_s on initial stiffness of p-y curve; Comparison between using Robertson (2009) and Baldi (1989) suggested correlation for V_s and API curve (Test Pile 1 - LAX)*

4.4.5. Discussion on Results

By Calibrating the Robertson (2009) equation, the site specific V_s was utilized into the "Model". The value for initial stiffness k, as shown on Figures 4.85 and 4.86, obtained by using site calibrated Robertson (2009) correlation is based on using site specific V_s in the analysis. At 4 feet deep, as depicted on Figure 4.86, the initial stiffness from the "Model" is 40.9 Kips/in^2 and is considerably higher than initial stiffness for the p-y curve from API.

By utilizing CPT data into the "Model", it was observed that within the depth of concern, i.e. from about 5 feet below the finished elevation to about 20 feet deep, I_c varies from 1.2 to 2.0, which based on the criteria defined in the "Model", corresponds to sand-like behavior. From top of the pile to about 12 feet below the grade, the cone tip resistance q_t varies from about 100 to 400 tsf. The SPT blow counts for the same depth range varies from 35 to 83. Both cone resistance and SPT blow counts indicate presence of a dense to very dense layer of sand.

Pile head Load-Displacement obtained from the "Model" and field measurements are both plotted in Figure 4.83. The curve from the "Model" labeled as curve (c), is in very good agreement with the field measurements. As discussed, the real condition of the test set-up, which is performing the test inside an excavated pit, was modeled and implemented to the model.

4.5. The University of British Columbia Site

University of British Columbia in Vancouver Canada owns a site for full scale pile testing. Figure 4.87 depicts the site vicinity map. The site is located in south of Vancouver, on the north side of the Annacis Channel within the south arm of the Fraser River. Over the entire site, 2 to 4 meters of heterogeneous fill exists at the surface. To facilitate pile testing, the fill material was removed at the site and was replaced with clean river sand.

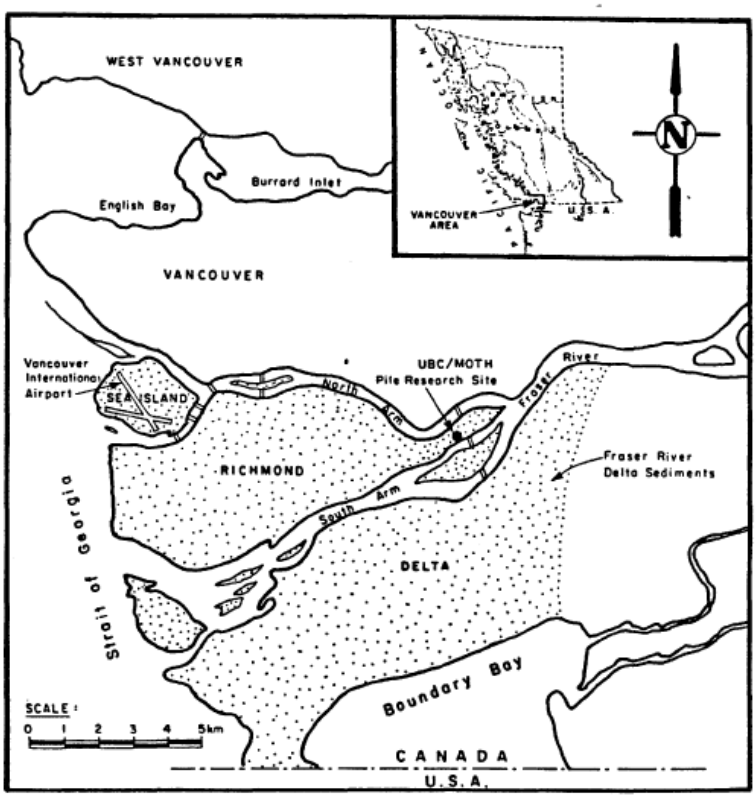

Figure 4.87: *General location of the UBC Research Site (M.P. Davies, 1987)*

4.5.1. Soil Condition

Figure 4.88 shows soils stratification at the site. The upper 2 to 4 meter is placed river sand, underlain by soft organic silty clay extending down to about 17 meters below the ground surface. The said silty clay layer is underlain by medium dense sands, down to about 28 to 30 meters below the ground surface. Starting from 28 to 30 meters deep to somewhere deeper than 150 meters, a layer of clayey silt, interbedded with sand layers, exist.

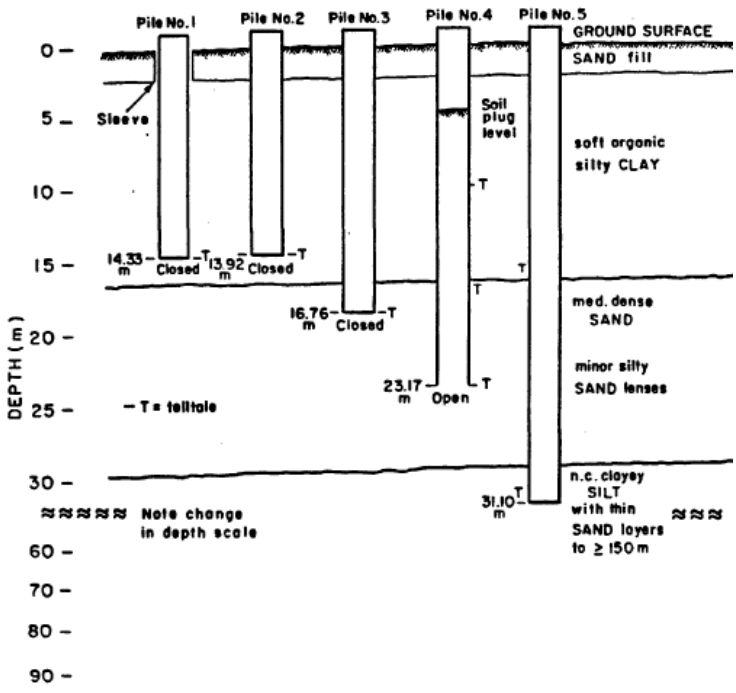

Figure 4.88: *Soil stratification and embedment depth for tested piles (M.P. Davies, 1987)*

Raw data/excel file of a CPT data conducted at the UBC pile test site was available. The location of the CPT sounding with respect to the location of the laterally tested “Pile 5” is not known to us, but considering the uniform stratification of the underlying soils at the site, the available CPT data was used in the analysis, and the outcome is compared with the field measured pile head force-displacement. The readings of CPT was utilized into the” CPTeT-IT” software, and regular and normalized plots of cone resistance, friction ratio, Soil Behavior Type index (SBT) and stratification of the site at the test location are obtained and depicted as Figures 4.89 and 4.90. This CPT-based stratification is in agreement with the soils profile shown in Figure 4.85, indicating presence of about 16 meters of clay, underlain by about 14 meters of sands with interbedded silty sand layers extending to the depth of about 30 meters below the grade.

Shawn Ariannia
Civil & Environmental Engineering Department
UCLA

Project: **Pile Lateral Loading Test**
Location: **UBC Site - Canada**

CPT: CPT-01
Total depth: 41.21 m, Date: 3/28/2015
Surface Elevation: 0.00 m
Coords: X:0.00, Y:0.00
Cone Type: Uknown
Cone Operator: Uknown

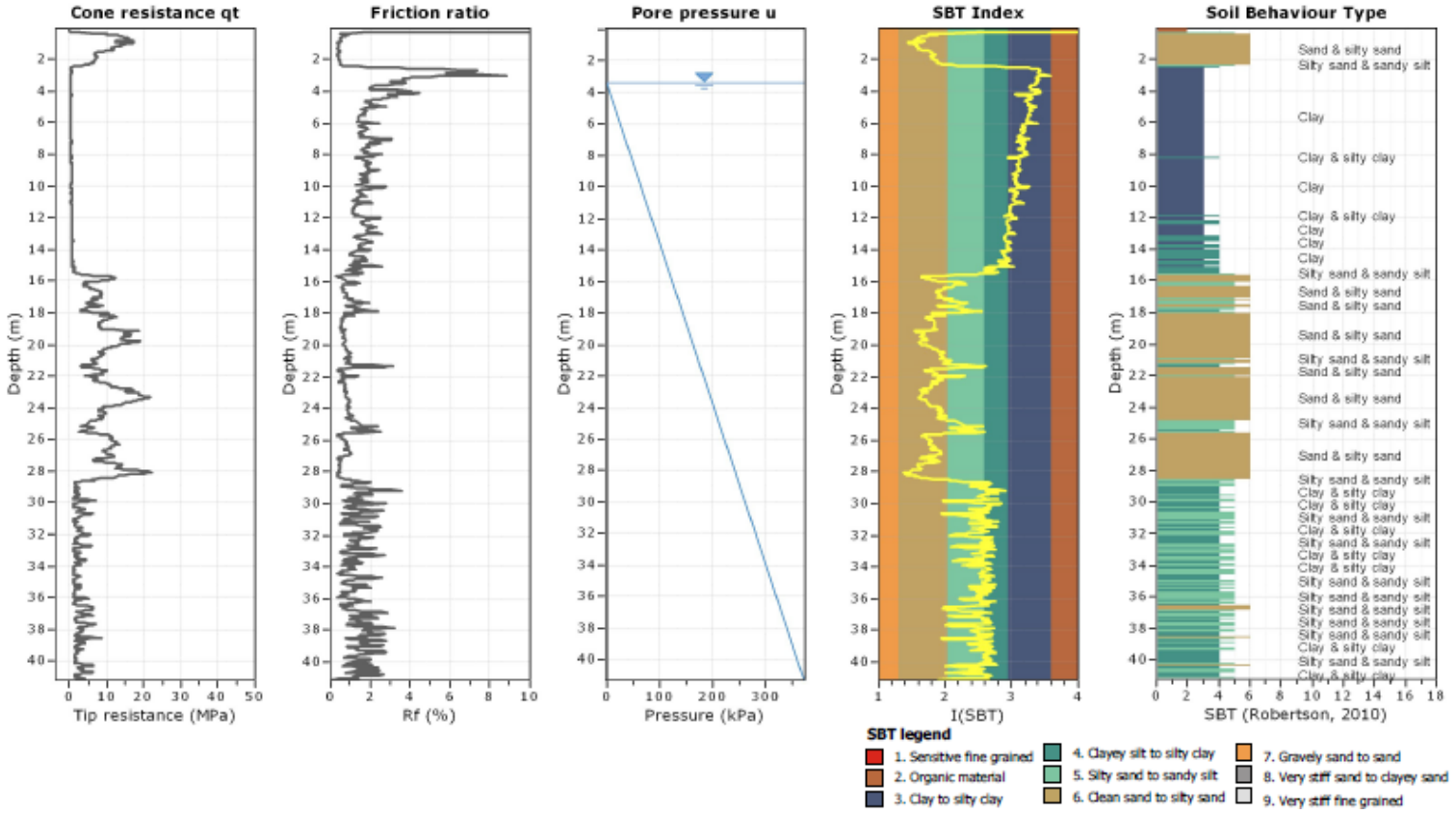

Figure 4.89: *CPT basic plots for UBC Site*

Shawn Ariannia
Civil & Environmental Engineering Department
UCLA

Project: **Pile Lateral Loading Test**
Location: **UBC Site - Canada**

CPT: CPT-01
Total depth: 41.21 m, Date: 3/28/2015
Surface Elevation: 0.00 m
Coords: X:0.00, Y:0.00
Cone Type: Uknown
Cone Operator: Uknown

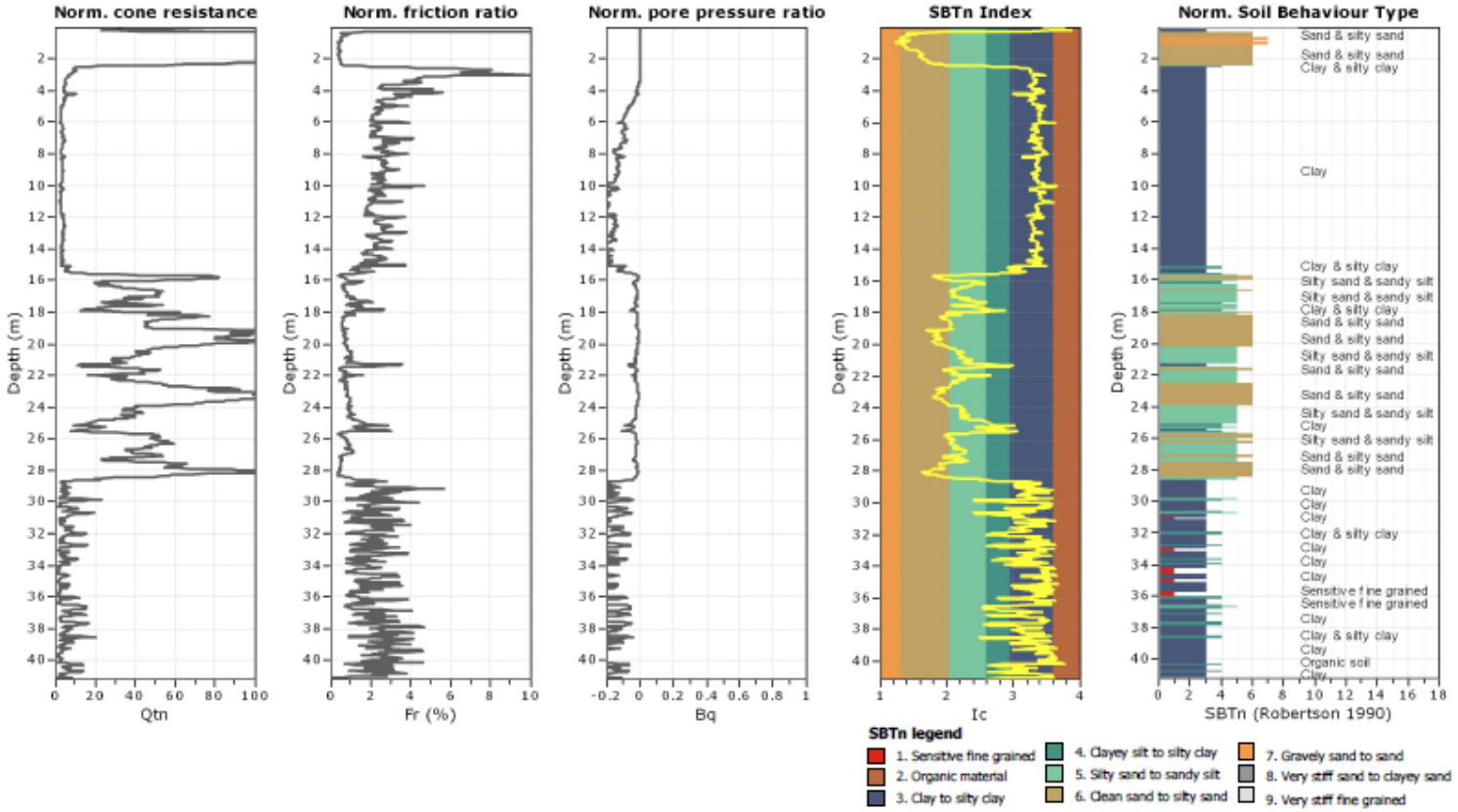

Figure 4.90: *CPT normalized plots for UBC Site*

4.5.2. Pile Properties and Load Test Description

As a part of a research program, five piles were driven (four 324 mm dia., 9.5 mm wall thickness; one 324 mm dia., 11.5 mm wall thickness) at the UBC site. The piles were driven to the ground by using a steel drop hammer, a metal helmet and plywood cushion. The piles were tested for axial and lateral capacity determination. All piles were tested for axial load condition, while pile 5 was tested to determine lateral load-displacement behavior.

Pile 5 is a close ended, fully displacement pile with 31.1 meter length. The profile of the site at the test locations as well as for pile 5 is depicted on Figure 4.88. Pile 5 was 324 mm in diameter, with a 11.5 mm thick walls. The lateral loads were applied in increments of 20 KN and held for approximately 15 minutes to allow time for readings to be taken. These readings consisted of dial gauge and inclinometer readings. The dial gauge readings were checked by the use of LVDTs on the test pile. A schematic of the load set up is shown in Fig. 4.91.

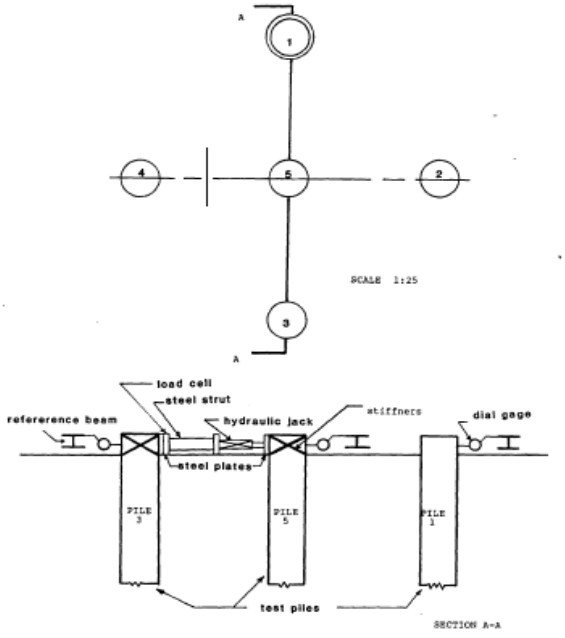

Figure 4.91: *Lateral load test set-up (M.P. Davies, 1987)*

4.5.3. Input Parameters for Analysis

Pile properties, as well as soils strength parameters shall be utilized to the integrated model. The pile properties include; B (pile diameter), L (pile length), E_p(pile material modulus of elasticity), E_y (yield modulus of pile material), A (pile cross section area), I (pile section moment of inertia), and M_{y-pile} (pile section yield moment). Also pile head constraint condition will be utilized into the model. The site soils information, i.e. CPT data file and the depth of ground water were uploaded into the model. The Matchad script in the model determines the basic soils parameters required to be utilized into a "ticle" file, which feeds the "OpenSees" program to solve the model.

The basic soil input parameters the Matchad script calculates are K_{max}, P_u, C and y_{50}. The profiles of input parameters for this site along the depth of the soft clay layer are depicted in the following Figure 4.92.

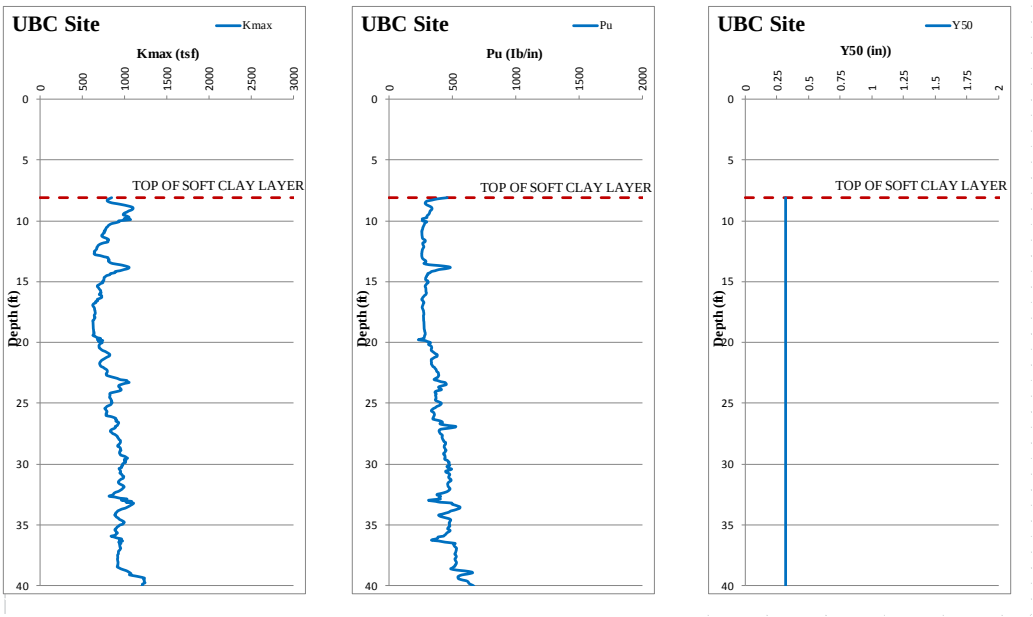

Figure 4.92: *Input Parameters profiles for UBC site, Canada*

4.5.4. Measured and Predicted Results

In Section 4.5.2., the set-up for lateral load testing was depicted. Using CPT data and the "Model", head force-displacement is determined and is plotted on Figure 4.93 below. Also the measured field data for test pile 5 are shown.

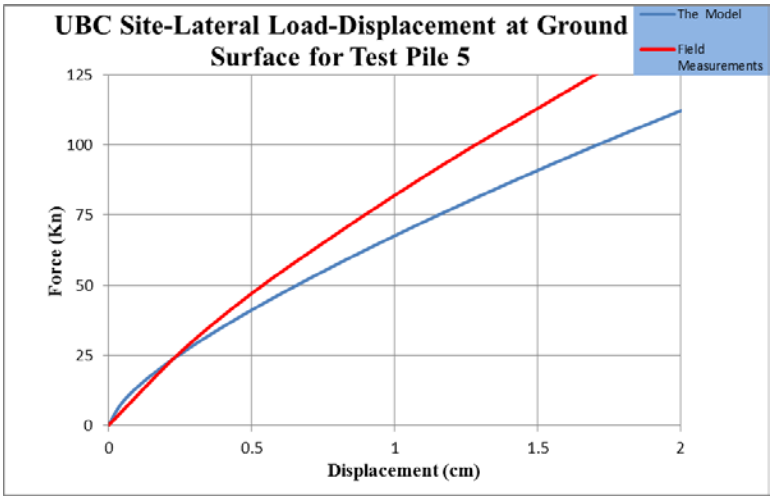

Figure 4.93: *Comparison of pile head Force-Displacement between the proposed model and field measurements for "Pile 5"at UBC Site*

4.5.5. Discussion on Results

By utilizing CPT data into the "Model", it is observed that within the depth of concern, i.e. from ground level to about 2 m below the surface, I_c is less than 2.0, while from about 2 m to the depth of 16 m, I_c varies between about 3 to 4, which based on the criteria defined in the "Model", corresponds to clay-like behavior. Within the clay layer, the cone tip resistance q_t varies from about 2 to 8 tsf.

Pile head Load-Displacement obtained from the "Model" and field measurements are both plotted on Figure 4.93. The load-displacement curve from the model plots lower than the filed measured values. In absence of more detailed information such as proximity of the CPT location to the tested pile, or more information about test set-up, it is not possible to explain the reason for the

difference. In general, both field measurement/data and the ”Model” curve are less different for lateral displacements smaller than about 0.6 inches, and the difference becomes larger for larger displacements. Distance of the CPT sounding performed for the UBC site used in the model calculations was not known with respect to the location of pile testing. This might be one of the reasons for the observed differences in the results. However, the pile head response from the model is reasonably matching the field measurements.

5. Conclusions and Future Works

This study formalized a method for determining p-y curves directly from CPT data. The model computes p-y curves at every CPT measurement location, interpolates the p-y curve properties at desired nodal depths over the length of the pile, the p-y curves are implemented into the OpenSees, and pile-soil response is determined based on specified boundary conditions. In addition to CPT measurements, site specific values for shear wave velocity and undrained shear strength of the soil may be incorporated into the model by implementing proper calibration on V_s and s_u.

Utilizing CPT data to infer soil properties as inputs for analysis of laterally loaded piles is not new; others have estimated friction angle and/or undrained shear strength, along with other properties, from CPT data in many past applications. These prior applications typically identify distinct strata, and assign soil properties to those strata based on average CPT measurements. This approach does not fully utilize the high resolution in the stratigraphic detail of a CPT sounding. The novel aspect of this dissertation is that the soil properties are estimated *for every point in the CPT sounding*, and subsequently mapped to the p-y elements in a manner that preserves stratigraphic detail. Furthermore, the mapping algorithm involves smoothing windows that reproduce the weakening/softening influence that weak layers exert on soft layers observed in past numerical modeling studies. These stratigraphic details were important for predicting the behavior of several laterally loaded piles in the case histories studied herein.

The PySimple3 material model in OpenSees utilized in this dissertation provides certain benefits compared with published p-y curves used in commercial codes such as LPile. Inputs to the PySimple3 model include the elastic stiffness, ultimate capacity, yield force, and a shape

parameter that can be set to achieve a desired value of y_{50}. The yield force can be set very small so that small-strain nonlinear behavior is captured. This contrasts with the API sand model, which is very linear at small displacements, and does not adequately capture small-strain nonlinearity. Furthermore, the initial stiffness can be set to the small-strain stiffness, based on measured or inferred shear wave velocity, rather than having to select a strain-compatible value of elastic stiffness as is commonly done with the API sand equation. Matlock's equations for p-y curves for clay exhibit an infinite initial stiffness, which is also known to be unrealistic. The PySimple3 material model solves this problem. Finally, the initial stiffness of p-y curves is often assumed to either be constant or increase linearly with depth. However, the shear modulus of soil is known to increase in a nonlinear manner with effective stress. By directly utilizing measured shear wave velocity values to set the elastic stiffness, the PySimple3 model overcomes the limitations of these previous methods.

A significant benefit of the methodology applied in this dissertation is that an assessment of soil type is not required in order to formulate the p-y curve material parameters. For example, in LPile, users must first decide whether to use p-y curves for sand, clay, silt, or rock, then specify input parameters required by these different types of p-y curves. In this dissertation, the p-y material properties are consistent with undrained loading conditions when the soil behavior type index is higher than 2.7, and for drained loading conditions when it is less than 2.3. Values of the PySimple3 material input parameters are interpolated for intermediate soils that may be partially drained during CPT testing. These soils are precisely the ones for which selecting a soil type for p-y curve determination is difficult. More research is required to ascertain whether the linear interpolation procedure adopted herein is accurate, and future adjustments may be necessary.

Five field pile lateral load tests, selected from a much large list of available case histories, were analyzed using the proposed methodology. The five case histories were chosen because CPT data from the pile test site were available in each case, relevant structural details were available, and the recorded data were of high quality. The CPT data recorded at each site was used to compute p-y curves from the field tests, and the piles were analyzed in OpenSees under boundary conditions consistent with field loading conditions. Predicted pile head load versus displacement curves were compared with the measured ones in each case. For some of the field cases, p-y curves were computed based on measurements of curvature or rotation along the pile length, and the computed p-y curves were compared with those predicted from the CPT data. No attempt was made to fine-tune the proposed procedure on a site-specific basis; rather the case histories were analyzed using a common procedure. Agreement was good in all cases, and generally better than predictions made using LPile.

An important consideration in analyzing the case histories was the influence of any changes made to the site between the time the CPT testing was conducted and the pile load test was conducted. At two sites in Oakland, CPT testing was performed, then a surficial layer of fill was removed from the site prior to installation and testing of the piles. The soft Bay Mud had adequate time to swell after removal of the fill, and the undrained shear strength of the clay decreased as a result. Corrections to the undrained shear strength inferred from CPT measurements were required to obtain accurate p-y results. At the LAX site, a hole approximately 4 ft by 4 ft square, and 5 ft deep was excavated around the pile to facilitate installation of the loading apparatus. The vertical effective stress profile in the soil beneath the bottom of the excavation was between the initial effective stress prior to excavation and γz due to vertical stress attenuation. Corrections to the effective stress profile were required to accurately reproduce the p-y response of the piles at LAX.

The initial stiffness of the measured load-displacement behavior was softer than the predicted behavior at the LAX site, though the measurements and predictions were in better accord at higher levels of displacement. This mismatch is attributed to disturbance of the soil around the pile during the "torque-down" installation. A hole was pre-drilled, then the piles were torqued into place using a helical bit near the bottom of the pile. The helix was no larger than the pile diameter, but disturbance between the pile and soil still occurred. In general, it makes sense that lateral stiffness would be more influenced by soil disturbance than ultimate capacity because the zone of influence is initially small, enveloping the soil only very close to the pile. As displacement increases, more soil is mobilized, rendering the influence of pile disturbance less important.

In some of the field case histories, shear wave velocity measurements and laboratory undrained shear strength measurements were available. These measurements were incorporated into the lateral pile analysis by calibrating site-specific correlations that matched the independent measurements. It is also possible to use a correlation between CPT tip resistance and shear wave velocity, or undrained shear strength. However, these correlations are based on a wide range of different soil conditions, and contain significant uncertainty. Calibrating site-specific input parameters is recommended, and crude calibrations should never be used as a substitute for measuring important input parameters.

Future Work

Although this dissertation is considered a self-contained, complete study, there are several areas in which the research can go in the future to improve its technical content and dissemination within the engineering community.

The procedure used to run the simulations was not particularly user-friendly, and needs to be improved to facilitate use by engineers. The procedure involved a Mathcad script to generate input, OpenSees to run the finite element simulations, and another Mathcad script to visualize the simulation output. In the future, developing an integrated computer code that permits users to enter a CPT sounding, pile properties, and loading conditions, and subsequently runs the simulation and post-processes the results is desirable. Absent such a code, it is highly unlikely that the effort required to run the simulations presented herein would be justified for all but the most important Civil Engineering projects.

The proposed methodology has provided reasonable agreement with five case histories covering a range of soil types and pile properties. However, more validation would be valuable to identify any areas in which the proposed procedure results in biased predictions and could be improved. Developing the aforementioned integrated computer code would improve the opportunity for such studies to be performed.

The primary technical issue that should be addressed in the future is interpolation of the p-y behavior for intermediate soils with soil behavior type index between 2.3 and 2.7. It is possible that variable rate cone penetration testing could be used to more thoroughly characterize the drained and undrained properties of the soil. However, such testing is highly specialized and not common or practical for ordinary projects. Numerical simulations and physical modeling studies (field and/or lab/centrifuge) could potentially be utilized to shed light on this important topic. Note that this issue is not limited to use of the proposed methodology. Intermediate soils are perhaps even more difficult to handle in traditional p-y programs because a decision must be made at the outset whether to treat such soils as sands or as clays.

REFERENCES

Atkinson, J. (2006) “The Mechanics of Soils and Foundations”. Taylor and Francis

Anoyatis G, Di Laora R, Mandolini A, Mylonakis G (2013) “Kinematic response of single piles for different boundary conditions: Analytical solutions and normalization schemes” *Soil Dynamics and Earthquake Engineering*, 44: 183-195.

API (2011) “ANSI/API Recommended Practice 2GEO”. First Edition, Part 4: Geotechnical and Foundation Design Considerations.

API (1982) “Recommended Practice for Planning, Designing, and Constructing Fixed Offshore Platforms “. American Petroleum Institute, Washington, D.C.

Baldi, G, R Bellotti, VN Ghionna, M Jamiolkowski, and DCF LoPresti (1989) “Modulus of sands from CPTs and DMTs” *Proc*., 12th Inter. Conf. Soil Mech. and Foundation Eng., Vol. 1, Rio de Janeiro, pp. 165–170.

Bogard, D., Matlock, H. (1980) “Simplified Calculation of *p-y* Curves for Laterally Loaded Piles in Sand”. Unpublished Report-The Earth Technology Corporation, Inc., Huston, Texas).

Bolton, M.D., (1986) “The strength and dilatancy of sands”. Geotechnicque 36, No.1, p65-78

Brandenberg, S., J., Jung In Choi, Myoung Mo Kim (2013) “Modeling the Dynamic Behavior of a Single Pile in Dry Sand using a new p-y Material Model.”. eScholarship University of California.

Brandenberg, S., J., Naresh, B., Shantz, T., (2010) “Shear Wave Velocity as a Statistical Function of Standard Penetration Test Resistance and Vertical Effective Stress at Caltrans Bridge Sites”. Pacific Earthquake Engineering Research Center.

Briaud, J.L., Smith, T.D., Mayer, B. J., (1983) “Using the Pressuremeter Curve to Design Laterally Loaded Piles”. Proceedings, 15th Offshore Technology Conference.

Briaud, J. L., (1986) “Pressuremeter and foundation design.” Proc., ASCE Specialty Conf. on Use of In Situ Tests in Geotech. Eng., Blacksburg, Va.

Briaud, J. L., (1992) “The pressuremeter”. Balkema, Rotterdam, The Netherlands.
Broms, B. B. (1965) "Design of laterally loaded piles". *Journal of Soil Mechanics and Foundations Division*, ASCE, 91(SM3), 79-99.

Broms B. B., (1964a) “Lateral Resistance of Piles in Cohesive Soils”. ASCE, Vol. 90, SM2: 27-63.

Broms B. B., (1964b) “Lateral Resistance of Piles in Cohesionless Soils”. ASCE, Vol. 90, SM3:123-156

Bustamante, M., Gianeselli, L. (1982) “Pile bearing capacity predictions by means of static penetrometer CPT”. Proceedings of the Second European symposium on penetration testing, ESOPT-II, Amsterdam, The Netherlands, vol.2. pp.493-500.

Casagrande, A., (1936) "Characteristics of Cohesionless Soils Affecting the Stability of Earth Fills", Journal of the Boston Society of Civil Engineers. Reprinted in "CONTRIBUTIONS TO SOIL I MECHANICS, 1925-1940", Boston. Society of Civil Engineers, October 1940.

Choi, J., and Brandenberg, S. J., (2015) “Cyclic *p-y* Plasticity Model Applied to Pile Foundations In Sand” Journal of Geotechnical and Environmental Engineering, 141 (5).

Dobry, R., Ladd, R. S., Yokel, F.Y., Chung, R.M., Powell, D., (1982) “Prediction of pore water pressure buildup and liquefaction of sands during earthquakes by the cyclic strain method”. .NBS Building Science Series 138, Nat. Bureau of Standards, Gaithersburg, MD.

Dodds, A., (2005) “A numerical study of pile behavior in large groups under lateral loading”. A dissertation report, University of Southern California.

Douglas, D.J., Olsen, R.S., (1981) “Soil classification using electric cone penetrometer”. *I*n Proceedings of Symposium on Cone Penetration Testing and Experience, Geotechnical Engineering Division, ASCE. St. Louis, Missouri, pp. 209-227.

Douglas, D.J., Davis, E.H. (1964) “The movement of buried footings due to moment and horizontal load and the movement of anchor plates”. *Geotechnique*, Vol. 14).

Davies, M.P. (1987), “Predicting axially and laterally loaded pile behavior using in-situ testing methods” Master Degree Thesis, University of British Columbia, Vancouver, Canada.

Fleming, W.G.K., Weltman, A.J., Randolph, M.F., and Elson, W.K., (1985) “Piling Engineering”. Surrey University Press.

Fredlund, D.G., (1995) “Unsaturated soil functions using the Soil-Water Characteristic Curve”. Bengt B. Broms Symposium In Geotechnical Engineering, December 1995, Singapore

Gazetas, G., Gerolymos, N., (2005), “Development of Winkler model for static and dynamic response of caisson foundations with soil and interface nonlinearities”. Soil Dynamics and Earthquake Engineering.

Gazetas, G., Dobry, R., (1984)”Horizontal Response of Piles in Layered Soils.” Journal of Geotechnical and Environmental Engineering, Vol 110, No.1, pp. 20-40.

Gazioglu, S.M., O'Neill, M.W., (1984) "Evaluation of P-Y Relationships in Cohesive Soils" Proceedings, ASCE National Convention, San Francisco, California.

Gazetas, G., et al (1983) "Lateral Dynamic Response of Constrained Head Piles".

ASCE Journal of Geotechnical Engineering, Vol. 109, No. 8, August, 1983.
Georgiadis, M. (1983) "Development of p-y curves for layered soils". ASCE, Proceedings of the conference on Geotechnical Practice in Offshore Engineering, Austin Texas.

Hegazy, Y.A, Mayne, P.W., (1995) "Statistical Correlation Between V_s and CPT Data for Different Soil Types" Proceeding, Symposium of Cone Penetration Testing, Vol.2, Swedish Geotechnical Society, Linkopin, Sweden, pp. 173-178.

Hetenyi, M., (1946) "Beams on Elastic Foundation". University of Michigan Press.

Hwang, J.-H., Liang, N., and Chen, C.-H. (2001) "Ground response during pile driving." Journal of Geotechnical and Geo-environmental Engineering, ASCE 127(11), November, 939-949.

Ishibashi, I. (1992) "Discussion to "Effect of soil plasticity on cyclic response" by M. Vucetic and R. Dobry, Journal of Geotechnical Engineering, ASCE, VOL. 118, No.5, pp. 830-832.

Jaeger, R.A., DeJong, J.T., Boulanger, R.W., Low, H.E., and Randolph, M.F (2010) "Variable penetration rate CPT in an intermediate soil". 2nd International Symposium on Cone Penetration Testing, 2010, 15 pp.

Jamiolkowski, M., Lancellotta, R., LoPresti, D.C.F., and Pallara, O. (1994) "Stiffness of Toyoura sand at small and intermediate strain. Proceedings, 13th International Conference on Soil Mechanics and Foundation Engineering (1), New Delhi, 169-172

Jamiolkowski, M., Garassino, A. (1977) "Soil modulus for laterally loaded piles". In Proceedings of the Specialty Session 10, Ninth International Conference on Soil Mechanics and Foundation Engineering, 14th July, IX ICSMFE Publications Committee (ed.), ICSMFE, Tokyo, 43-58.

Janoyan, K. D., Wallace, J. W., and Stewart, J. P., (2006) "Full-scale cyclic lateral load test of reinforced concrete pier-column". ACI Structural Journal, 103(2), 178–187.

Jefferies M., Been K., "Soil Liquefaction, A critical state approach" (2006-Taylor & Francis)
Jefferies, M.G., and Davies, M.P., (1993) "Use of CPTU to estimate equivalent SPT N60". Geotechnical Testing Journal, ASTM, **16**(4): 458-468.

Khalili Tehrani P., Stewart J.P., Taciroglu, E., et al., (2014) "Nonlinear Deflection Behavior of Reinforced Concrete Drilled Piles in Stiff Clay". ASCE Journal of Geotechnical and Geoenvironmental engineering, Vol 140, No.3.

Kagawa, T., and Kraft, L.M. (1980) “Seismic p-y response of flexible piles” J. Geotechnical Eng. Division, 106 (GT*), pp 899-918.

Kavvadas, M., Gazetas, G., (1993) “Kinematic seismic response and bending of free-head piles in layered soils”. *Geotechnique* 43, No 2, 207-222.

Ladd, C.C., and DeGroot, D.J., (2003) “Recommended practice for soft ground site characterization” Proceeding of 12th PanAmerican Conference, MIT.

Ladd, C.C., (1991) “Stability evaluation during staged construction”. ASCE Journal of Geotechnical Engineering, Vol. 117, No.4.

Ladd, C.c., and Foott, R, (1974) “New design procedure for stability of soft clays”. Journal of Geotechnical Division.

Lehane, B.M., Suryasentana, S. (2014a) “Verification of numerically drived CPT based p-y curves for piles in sand”. 3rd international Symposium on Penetration Testing, Las Vegas, Nevada.

Lehane, B.M., Guo, F. (2014b) “Experimentally derived CPT-based p-y curves for soft clay”. 3rd international Symposium on Penetration Testing, Las Vegas, Nevada.

Lemke, J., (1997)”Lateral Pile Load Test Report I-880 Replacement Project Sites 1 through 4 Oakland, California”. Report Prepared for Caltrans, by Delta Geotechnical Services.

Lemnitzer, A., et al. (2010), “Nonlinear Efficiency of Bored Pile Group under Lateral Loading”, ASCE Journal of the Geotechnical Engineering Division, December 2010, pp. 1673-1685.

Lunne, T., Eidsmoen, T., Gillespie, D., and Howland, J.D., (1986) “Laboratory and field evaluation on cone penetrometers”. Proceedings of ASCE Specialty Conference, In Situ’86: Use of In Situ Tests in Geotechnical Engineering. Blacksburg, ASCE, GSP 6 714-729.

Matlock, H., (1970) “Correlations for Design of Laterally Loaded Piles in Soft Clay”. Offshore Technology Conference.

Mayne, P.W. et al. (2009) “Proceeding of the 17th International Conference on Soil Mechanics and Geotechnical Engineering”.

Mayne, P. W. (2007) “Cone Penetration Testing, A Synthesis of Highway Practice”. National Cooperative Highway Research Program, NCHRP Synthesis 368.

Mayne, P. W. (2000) “Enhanced Geotechnical Site Characterization By Seismic Piezocone Penetration Tests”. Fourth International Geotechnical Conference, Cairo University.

Mayne, PW, and GJ Rix (1995). “Correlations Between Shear Wave Velocity and Cone Tip Resistance in Natural Clays”. *Soils and Foundations*, 35(2):107–110.

Mayne, P.W., (1991), “Determination of OCR in clays by Piezocone tests using cavity expansion and critical state concepts”. Soils and Foundation, 31(2), 65-76.

Mayne, P.W. Kulhawy, F.H., and Mayne P.W., (1990). "Direct and Indirect Measurements of In-Situ K_o in Clays", Transportation Research Record 1278, Washington, D.C., pp. 141-149.
Menard, L., (1975), “The Menard pressuremeter: Interpretation and application of the pressuremeter test results to foundations design.” Sols-Soils, Vol. 26, Paris.

Meyerhof, G.G. (1976) “Bearing capacity and settlement of pile foundations”. J. Geotech. Eng. Div. 102(GT3), 195-228.

Mitchell, J.K., (2012) “Interpretation of in-situ Tests – Some Insights”. Proceeding of ISC’4, Recife, Brazil.

Murchison, M., O’Neill, M.W. (1984) “Evaluation of p-y Relationship in Cohesionless Soils”. Proceeding ASCE Codes and Standards Conference in San Francisco.

Murchison, M., O’Neill, M.W. (1984) “An Evaluation of p-y Relationships is Sands”. University of Huston, Texas.

Mylonakis, G., (2001) “Simplified Model for seismic pile bending at soil layer interfaces”. Soils and Foundation, Japanese Geotechnical Society, Vol. 41, No.4, p47-58.

Nottingham, L.C. (1975) “Use of quasi-static friction cone penetrometer data to predict load capacity of displacement piles”. PhD thesis, University of Florida.

Paker, F., Jr., Reese, L.C., (1970) “Experimental and Analytical Study of Behavior of Single Piles in Sand Under Lateral and Axial Loading”. Research Report No. 117-2, Center of Highway Research, The University of Texas, Austin, Texas.

Poulos, H.G., Davis, E.H., (1980) “Pile Foundation Analysis and Design”. John Wiley & Sons, Inc.

Poulos, H.G., (1971) “Behavior of Laterally Loaded Piles-Single Piles”. ASCE, Journal of soils mechanics and Foundation Division.

Price, G., Wardle, I.F., (1982) “A comparison between cone penetration test results and the performance of small diameter instrumented piles in stiff clay”. Proceedings of the second European symposium on penetration testing, ESOPT-II, Amsterdam, The Netherlands, vol.2. pp.151-158.

Rad, N.S., Lunne, T., (1988) “Direct correlations between piezocone test results and undrained shear strength of clay”. Proceedings of International Symposium on Penetration Testing, ISOPT-1, Orlando, 2, 911-17, Balkema Publications, Rotterdam.

Reese, L.C., Isenhower, W.M., Wang, ST., (2006) “Shallow and Deep Foundations”. John Wiley & Sons, Inc.).

Reese, L. C. (1986) “Behavior of Piles and Pile Groups Under Lateral Load”. Report No. FHWA/RD-85/106, Federal Highway Administration, Washington, D.C.
Reese, L.C., Cox, W.R., Koop, F.D., (1975) “Field Testing and Analysis of Laterally Loaded Piles in Stiff Clay” .Offshore Technology Conference.

Reese, L.C., Cox, W.R., Koop, F.D., (1974) “Analysis of Laterally Loaded Piles in Sand”. 6th Offshore Technology Conference, Huston, Texas.

Reese, L.C., Matlock, H. (1956) “Non-dimensional solutions for Lateral loaded piles with soil modulus assumed proportional to depth”. Proceedings of the 8th Texas Conference on Soil Mechanics and Foundation Engineering, Austin, Texas, pp. 1-41.

Reese, L.C., Welch, R.C. (1975) “Lateral Loading of Deep Foundations in Stiff Clay”. ASCE Journal of the Geotechnical Engineering Division, pp. 633-649.

Robertson P.K., (2012) “Interpretation of in-situ tests-some insights”. Proceedings of ISC’4 Recife, Brazil.

Robertson P.K., (2010) “Estimating in-situ state parameters and friction angle in sandy soils from CPT”. 2nd international symposium on Cone Penetration Testing, Huntington Beach, CA).

Robertson, P.K., (2009) “Interpretation of cone penetration tests – a unified approach”. Canadian Geotechnical Journal, 46:1337-1355.

Robertson, P.K., Wride, C.E., (1998) “Evaluating cyclic liquefaction potential using the cone penetration test”. Canadian Geotechnical Journal, Ottawa, 35(3): 442-459.

Robertson, P.K., Lunnel, T., Powell J.J.M., (1997) “Cone Penetration Testing in Geotechnical Practice”. Spon Press, Taylor & Francis Group.

Robertson, P.K., (1990) “Soil classification using the cone penetration test”. Canadian Geotechnical Journal, **27**(1): 151-158.

Robertson, P.K., Campanella, R.G. (1988)”Guidelines for geotechnical design using CPT and CPTU”. University of British Columbia, Vancouver.

Robertson, P.K., Campanella, R.G., Davies, M.G., and Sy, A. (1988)"Axial Capacity of driven piles in detail soils using CPT". Proceedings of the International Symposium on Penetration Testing, ISOPT-1, Orlando, 2, 919-28, Balkema Pub., Rotterdam.

Robertson, P.K., (1986) "In situ testing and its application to foundation engineering". Canadian Geotechnical Journal, 23:573-594.

Robertson. P.K., Campanella, R.G., Gillespie, D., and Greig, J., (1986) "Use of Piezometer Cone data". In-Situ'86 Use of In-situ testing in Geotechnical Engineering, GSP 6, ASCE, Reston, VA, Specialty Publication, SM 92, pp 1263-1280.

Roesset, J.M., (1980) "The use of simple models in soils Structures Interaction". Second ASCE Conference on Civil Engineering and Nuclear Power, September 15-17 1980- Vol II, Geotechnical Topics.

Schmertmann, J.H. (1978) "Guidelines for Cone Penetration Test, performance and design". U.S. Department of Transportation, Washington, D.C., p.145. Rep. No. FHWA-TS-78-209.

Schofield, A. and Worth, C.P., (1968) "Critical State Soil Mechanics". McGraw Hill..

Scott, R. F. (1981) "Foundation Analysis". Prentice-Hall.

Scott, R.F., (1980) "Analysis of Centrifuge Pile Tests: Simulation of Pile Driving". Research Report, American Petroleum Institute OSAPR Project 13, California Institute of Technology, Pasadena, California.

Stevens, J.B., Audibert, J.M.E., (1979) "Re-examination of p-y curve formulations". Offshore Technology Conference.

Stewart, J. P., et al. (2007), "Full scale cyclic large deflection testing of foundation support systems for highway bridges. I: Drilled shaft foundations", Rep. No. UCLA SGEL-01, Univ. of California, Los Angeles.

Syngros C (2004) "Seismic response of piles and pile-supported bridge piers evaluated through case histories". PhD Dissertation, City College of New York.

Tatsuoka, F., and Shibuya, S. (1992) "Deformation characteristics of soils and rocks from filed and laboratory tests". Report of the Inst. Of Industrial Science, Vol. 37, No.1, University of Tokyo

Terzaghi, K. (1955) "Evaluation of coefficients of subgrade reaction." *Géotechnique*, 5, 297-326.

Terzaghi, K. (1943) "Theoretical Soil Mechanics". John Wiley & Sons, Inc., New York.

Tomlinson, M., Woodward, J., (2008) "Pile Design and Construction Practice". Taylor & Fra.

Vucetic, M. and Dobry, R. (1991) “Effect of soil plasticity on cyclic response”. Journal of Geotechnical Engineering (ASCE). Vol. 117, No. 1, pp. 89-117.

Varun, V. (2010). “A nonlinear dynamic macroelement for soil structure interaction analyses in liquefiable sites.” Ph.D. thesis, School of Civil and Environmental Engineering, Georgia Institute of Technology, Atlanta.

Wair B.R., Shantz, T., (2012) “Guidelines for Estimating of Shear Wave Velocity Profiles”. PEER 2012/08.

Winkler, E., (1867) “Die Lehre Von Elasticitaet Und Festigkeit”. 1st Edn., H. Dominicus, Prague
Yang, Z., Jeremic, B. (2002), “Numerical Analysis of Pile Behavior under Lateral Loads in Layered Elastic-Plastic Soils”. International Journal for Numerical and Analytical Methods in Geomechanics.

Zhang, G., Robertson, P.K. and Brachman, R.W.I., (2002) “Estimating Liquefaction induced Ground Settlements from CPT for Level Ground”. Canadian Geotechnical Journal, 39(5): 1168-1180